NOVEL CAMBINOL ANALOGUES AS POTENTIAL ANTICANCER AGENTS : AN IMPROVED UNDERSTANDING OF SIRTUIN ISOFORM SELECTIVITY

Federico Medda

A Thesis Submitted for the Degree of PhD
at the
University of St Andrews

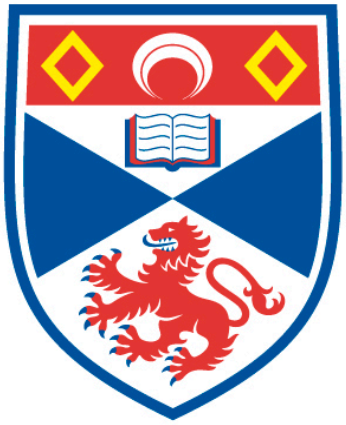

2010

Novel Cambinol Analogues as Potential Anticancer Agents: An Improved Understanding of Sirtuin Isoform Selectivity

Thesis presented for the degree of Doctor of Philosophy

Federico Medda

September 2010

School of Chemistry

University of St Andrews

1. Candidate's declarations:

I, Federico Medda, hereby certify that this thesis, which is approximately 70000 words in length, has been written by me, that it is the record of work carried out by me and that it has not been submitted in any previous application for a higher degree.

I was admitted as a research student in September 2007 and as a candidate for the degree of PhD in September 2010; the higher study for which this is a record was carried out in the University of St Andrews between 2007 and 2010.

Date 30th of September 2010 signature of candidate

2. Supervisor's declaration:

I hereby certify that the candidate has fulfilled the conditions of the Resolution and Regulations appropriate for the degree of PhD in the University of St Andrews and that the candidate is qualified to submit this thesis in application for that degree.

Date 30th of September 2010 signature of supervisor

3. Permission for electronic publication:

In submitting this thesis to the University of St Andrews I understand that I am giving permission for it to be made available for use in accordance with the regulations of the University Library for the time being in force, subject to any copyright vested in the work not being affected thereby. I also understand that the title and the abstract will be published, and that a copy of the work may be made and supplied to any bona fide library or research worker, that my thesis will be electronically accessible for personal or research use unless exempt by award of an embargo as requested below, and that the library has the right to migrate my thesis into new electronic forms as required to ensure continued access to the thesis. I have obtained any third-party copyright permissions that may be required in order to allow such access and migration, or have requested the appropriate embargo below.

The following is an agreed request by candidate and supervisor regarding the electronic publication of this thesis:

(iii) Embargo on both of printed copy and electronic copy for the same fixed period of 2 years on the following ground:

publication may be commercially damaging to the University.

Date 30th of September 2010

signature of candidate signature of supervisor

ABSTRACT

SIRT1 and SIRT2 are two NAD^+-dependent deacetylases which negatively modulate the activity of p53, a protein which is involved in cell cycle arrest, senescence and apoptosis following genotoxic stress. **Part I** of the thesis describes the exploration of the chemical space around a reported unselective and modest inhibitor of SIRT1 and SIRT2, with the aim of improving the selectivity and potency of the inhibitor against the two isoforms. Particular emphasis is placed upon understanding the mode of binding of the novel analogues within the active site of the enzymes.

Chapter 1 reviews the physiological roles of class III NAD^+-dependent deacetylases, also known as sirtuins. In particular, the application of SIRT1 and SIRT2 inhibitors as potential anticancer agents is described. Amongst these, only cambinol and the tenovins showed *in vivo* activity in a mouse xenograft model. Previously only one analogue of cambinol had been reported in the literature.

Chapter 2 describes the development of a small collection of novel cambinol analogues (First Generation Studies). The role played by different substituents at the phenyl group and at the *N*-1 of the thiouracil core is discussed. Along with the synthesis and structure activity relationship (SAR) associated with the core structure, in-cell experiments intended to confirm the activity of the most active compounds are reported.

Chapter 3 provides a rationalisation for the SAR discussed in Chapter 2. Based on computational molecular modelling studies (GOLD), the activity of the most potent and selective SIRT2 inhibitors is explained. Two series of novel cambinol analogues were designed (Second and Third Generation Analogues) in order to assess further the proposed binding mode.

Chapter 4 focuses on the development of the "Second Generation" analogues, characterised by the presence of lipophilic substituents at the sulfur atom and at the *N*-3 position of the thiouracil core. The synthesis, biological evaluation and SAR are discussed in detail.

Chapter 5 reports the development of the "Third Generation" analogues, characterised by either a benzyl group or *para*-alkoxy-substituted benzyl group at the *N*-1 position of cambinol. Once again, the synthesis, biological evaluation and SAR data are presented. An improved

understanding of the mode of binding of the novel compounds is proposed based on molecular dynamics (MD) studies.

Indole-based alkaloids, such as Vincristine and Vinblastine, are well known for their anticancer activity. Recently, the anticancer activity of members of the *calycanthaceous* family of alkaloids has been discovered. **Part II** of the thesis focuses on model studies aimed at developing the total synthesis of one of these compounds, perophoramidine.

Chapter 7 provides an overview of the *calycanthaceous* alkaloid family of natural products, including their biological properties. The structural features of perophoramidine, along with the previously reported synthetic studies are outlined.

Chapter 8 describes the synthesis of an advanced intermediate in the total synthesis of dehaloperophoramidine, a structural analogue of perophoramidine Problems encountered, optimisation studies and the synthesis of a re-designed intermediate are also reported in this chapter.

ACKNOWLEDGEMENTS

Firstly, I would like to thank Dr Nick Westwood for the opportunity to work in his lab and for his constant supervision and guidance over the past three years. I always felt fully supported by Nick and I feel privileged to have been trained by him. I am also particularly thankful to him for having enrolled me in the 4-year CRUK medicinal chemistry training program shared between the Universities of Edinburgh and St Andrews (EaStChem).

I would also like to thank all the members of the Westwood group, both past and present, for their help and support. In particular I would like to thank Dr Anna R. McCarthy and Ms Lisa Pirrie (*in vitro* biological evaluation), Mr Paul Brear (docking analysis training), Dr Chris Lawson (HPLC training), Mr Craig Jonston (LC-MS and Endnote training) and Dr Edward (Ted) Makiyi for his precious chemistry teaching and friendship over the first two years of my PhD.

I am particularly grateful to all the members of staff in School of Chemistry and CBMS who have helped me with analysis and structural determination: Mrs Caroline Horsburgh (mass spectrometry), Mrs Sylvia Williamson (elemental analysis), Prof. Alexandra Slawin (X-ray crystallography), and Dr Tomas "Tom" Lebl and Mrs Melanja Smith (NMR spectroscopy). A kind acknowledgement goes to Dr Rupert Russell for the first generation of docking studies.

I would like to thank Prof David Lane and Dr Sonia Lain for their co-supervision and the fructuous collaboration in the medicinal chemistry project. A kind acknowledgement goes to Miss Joanna Campbell and Mrs Maureen Higgins for the *in vivo* biological evaluation of the most active compounds, and to Dr Chandra Verma and Thomas Joseph for the molecular dynamic experiments which have helped to increase my understanding of the SAR data presented in this thesis.

Many people outside the department have constantly been close to me over the last three years, supporting me with their friendship and company. I will be eternally grateful to my "Friends of All Three Years" – Laura, Flavio, Serena and her flatmates, Ingrid "the warden", Alberto, Ronan, Vikash, Damiano, Stefano, Cesarino, Silvano, Diego, Armando, Marco "Lino", Nikos "Saki Raheem", the agencies Tito and Dan, the big catalysts Gary and Scott and many others... to list everybody would be impossible: if you read this you know who you are!!!

I kind thank you also goes to the members (past and present) of the Italian Society of the University of St Andrews “ItalSoc” and of the Chemistry Society “ChemSoc” for the entertainment provided and the unforgettable nights out spent together. I can’t forget the big friends Aldo and Rachid of “Le Rendezvous” for cooking me their tasty lasagne and wrappas when there was no time to cook my own meals.

Finally, but certainly not in terms of importance, I am always grateful to my parents Rosella and Rinaldo and to my brother Nicola for their continuous encouragement and support from one extreme to another of Europe. If I am where I am is certainly because they taught me never to give up and aspire always to the maximum!!!

(Italian: infine, ma non certamente in ordine di importanza, saro’ sempre grato ai miei genitori Rosella e Rinaldo ed a mio fratello Nicola per il loro continuo incoraggiamento e supporto da un estremo all’ altro dell’ Europa. Se sono dove sono e’ certamente perche’ mi hanno insegnato a non arrendermi mai e ad apirare sempre al massimo)

Once again, thanks to all of you guys for these three years spent at the maximum form both at a professional and a human point of view....unforgettable!!!

ABBREVIATIONS AND ACRONYMS

Å	Ångstrom
Ac	Acetyl group (-$COCH_3$)
AcOH	Acetic acid (CH_3CO_2H)
ADP	Adenosine diphosphate
AKT	Serine/threonine-specific protein kinase family
BAIB	[Bis(acetoxy)iodo]benzene
BCA	Bicinchoninic acid
BCL2	B-cell lymphoma 2 gene (Burkitt lymphoma)
br	Broad (spectral)
Bn	Benzyl group (-$CH_2C_6H_5$)
Boc	*tert*-Butyloxycarbonyl (-CO*t*C_4H_9)
Boc_2O	Boc anhydride ((CO*t*C_4H_9)$_2$O)
n-Bu	Primary butyl group
t-Bu	Tertiary butyl group
t-BuOH	*tert*-butanol
t-BuOK	Potassium *tert*-butoxide
°C	Degrees centigrade/celcius, temperature unit
calcd	Calculated
cf.	*Confer impe*r, (Latin), compared to
CI	Chemical ionisation, ionisation technique (mass spectrometry)
cm^{-1}	Wavenumber(s)
Comp.	Compound
Conc.	Concentrated
Cop1	Constitutive photomorphogenic 1
COSY	Correlation spectroscopy (NMR)
d	Day(s); doublet (spectral)
dba	Dibenzylideneacetone
DBC1	Deleted in breast cancer 1 gene
DBU	1,8-Diazabicyclo[5.4.0]undec-7-ene
DCM	Dichloromethane
Decomp.	Decomposition (melting point measurement)
δ	Chemical shift in ppm (NMR)
DMA	*N*,*N*-Dimethylacetamide
DMF	*N*,*N*-Dimethylformamide
DMP	*N*,*'N*-Dimethylpiperazine
DMSO	Dimethyl sulfoxide
DNA	Deoxyribonucleic acid
ECL	Enhanced chemiluminescence
EI	Electron impact, ionisation technique (mass spectrometry)
en route	French, on the way or along the way
Equiv./eq.	Equivalents
ES	Electrospray (mass spectrometry)
Et	Ethyl group (-CH_2CH_3)
et al	*Et alia* (Latin), and others
Et_2O	Diethyl ether
EtOAc	Ethyl acetate
EtOH	Ethanol
FT	Fourier transform
g	Gram(s)

Glu	Glutamic acid, amino acid
GOLD	Molecular docking program
h	Hour(s)
HAT	Histon acetyltransferase enzyme
HCT116	Colon carcinoma cell line
HDAC	Histone deacetylase enzyme
His	Histidine, amino acid
HIV	Human immunodeficiency virus
HMBC	Heteronuclear Multiple Bond Correlation (NMR)
HPLC	High performance liquid chromatography
HRMS	High resolution mass spectrometry
HRP	Horse radish peroxidase
HSQC	Heteronuclear Single Quantum Coherence (NMR)
HT299	Colorectal cancer cells
HUVE	Human umbilical vein endothelial cells
Hz	Hertz
i-Bu	*iso*-Butyl group ($-CH_2CH(CH_3)_2$)
IBX	2-Iodoxybenzoic acid
IC_{50}	Half maximal inhibitory concentration
IgG	Immunoglobulin G
Ile	*Iso*-leucine, amino acid
in silico	Performed on computer or *via* computer simulation
in vitro	Latin, within the glass
in vivo	Latin, within the living
i-Pr	*iso*-Propyl group ($-CH(CH_3)_2$)
IR	Infrared
J	Coupling constant (NMR)
K	Kelvin, temperature unit
KO*t*Bu	Potassium *tert*-butoxide
L	Litre(s)
LC-MS	Liquid chromatography mass spectrometry
LDS	Lithium dodecyl sulfate
Leu	Leucine, amino acid
Lit.	Literature
LRMS	Low resolution mass spectrometry
m	Multiplet (spectral); metre(s); milli
M	Concentration, molar, mol l^{-1}; molecular ion (mass spectrometry)
MCF-7	Human breast adenocarcinoma cell line
MD	Molecular dynamics
Mdm 2/4	Murine double minute 2/4 oncoprotein (negative regulator of p53)
Me	Methyl group ($-CH_3$)
MeOH	Methanol
mg	Milligram(s)
MHz	MegaHertz
min	Minute(s)
mL	Millilitre(s)
mm	Millimetre(s)
mmol/mM	Concentration, millimolar, mmol l^{-1}
mol	Mole(s)
MOM	Methoxymethyl ($-CH_2OCH_3$)
Mp	Melting point
MS	Mass spectrometry
Ms	Mesyl group, methylsulfonyl (CH_3SO_2-)

m/z	Mass over charge ratio (mass spectrometry)
NAD^+	Nicotinamide adenine dinucleotide
n-Bu	*n*-Butyl group ($-(CH_2)_3CH_3$)
NCS	*N*-chlorosuccinimide, or isothiocyanate
nM	Concentration, nanomolar
NMO	*N*-Methylmorpholine-*N*-oxide
NMR	Nuclear magnetic resonance
nOe	Nucear overhauser effect (NMR)
n-Pr	*n*-Propyl group ($-CH_2CH_2CH_3$)
ns	Nano second(s)
P	Generic protecting group
PBS	Phosphate buffered saline
PCNA	Proliferating cell nuclear antigen
PDC	Pyridinium dichromate
PENDANT	Polarisation enhancement during attached nucleus testing (NMR)
p53	Protein 53 or tumour protein 53 – tumour suppressor protein (TP53)
Phe	Phenylalanine, amino acid
pK_a	Acid dissociation constant
PENDANT	Polarisation enhancement nurtured during attached nucleus testing (NMR)
Ph	Phenyl group ($-C_6H_5$)
Pirh2	p53-induced ring-H2 domain protein or gene
PMB	*para*-methoxybenzyl
pRb	Retinoblastoma gene
prod.	Product
ppm	Parts per million
q	Quartet (spectral)
R	Generic group
R_f	Retention factor (chromatography)
RP-HPLC	Reverse phase HPLC
RPD3	Yeast protein related to histone deacetylase
RPMI	Cell culture medium
Rt	Retention time
rt	Room temperature
s	Singlet (spectral); second(s)
SAR	Structure activity relationship (medicinal chemistry)
Sir	Silent information regulator
SIRT	Sirtuins, class III histon deacetylases
sm	Starting material
S_N1	Unimolecular nucleophilic substitution
S_N2	Bimolecular nucleophilic substitution
t	Triplet (spectral)
TBAF	Tetrabutylammonium fluoride
TBDMS	*tert*-Butyldimethylsilyl
t-Bu	*tert*-butyl group ($-C(CH_3)_3$)
TCA	Trichloroacetic acid
TEA	Triethylamine
TEMPO	2,2,6,6-Tetramethylpiperidine-1-oxyl, $(CH_2)_3(CMe_2)_2NO$
Tf	Triflate group, trifluoromethanesulfonate ($-OSO_2CF_3$)
TFA	Trifluoroacetic acid
THF	Tetrahydrofuran
TLC	Thin layer chromatography
TMS	Trimethylsilyl group ($-Si(CH_3)_3$)
TMSNCS	Trimethylsilyl isothiocyanate

TOF	Time of flight (mass spectrometry)
TosMIC	Toluenesulfonylmethyl isocyanide
TPAP	Tetrapropylammonium perruthenate, $(N(C_3H_7)_4RuO_4$
Tyr	Tyrosine, amino acid
TP53	Protein 53 or tumour protein 53 – tumour suppressor protein (p53)
μL	Microlitre(s)
μM	Micrometre(s)
UV	Ultraviolet
vs	Versus
υ	Wavenumbers (IR spectroscopy)

CONTENTS

SUPPLEMENTARY MATERIAL (CD):

1. Selected ^{1}H NMR and [^{1}H, ^{13}C] HMBC Spectra
2. HPLC Analysis of Purity
3. Molecular Dynamics Simulations
4. Attempted Oxidation of **238** to **243**: Experimental Procedures

1. INTRODUCTION

1.1 Cancer and p53

1.1.1 Cancer

Cancer is a complex pathology which strongly affects our society through both elevated social and healthcare costs. In the UK in 2007, almost 300,000 people were diagnosed with cancer. The following year, it was the cause of 156,723 deaths.[1] In the USA, according to the American Society for Cancer Studies, only cardiovascular diseases causes more deaths per year than cancer.[2]

It is difficult to find a precise definition of cancer, which is often also referred to as a tumour or neoplasm. The British oncologist R.A. Willis defined it as *"an abnormal mass of tissue, the growth of which exceeds and is uncoordinated with that of the normal tissues, and persists in the same excessive manner after cessation of the stimulus which evoked the change."*[3] Tumours can be divided into two main categories – malignant or benign. The new mass of tumour tissue lacks a physiological function and grows autonomously. When malignant, it often leads to increasing amounts of damage to the host organism due to the fact that cancer cells compete with the normal cells for both energetic and nutritional supplies. For this reason, the growth of tumours is often associated with the progressive wasting of the host organism.

Over the past few decades, major biological discoveries have clarified many molecular pathways involved in carcinogenesis. In particular, the identification of mutations in genes encoding for proteins associated with the control of important preventive processes (oncosuppressors), such as apoptosis, cell-cycle arrest and senescence, have represented an important advancement in this area. Along with pRb, the p53 gene is the oncosuppressor which has been studied in the greatest detail.[4] p53 was discovered in 1979 and is also known as "*the guardian of the genome"*. [5] Twenty years later, in 1989, a mutation in p53 was identified as the cause of colerectal cancer.[6] Since its discovery as an oncosuppressor, p53 has become one of the major areas of investigation in cancer research as it has been found to be the most commonly mutated gene in human tumours.[7]

1.1.2 Role of p53 in Cancer Therapy

p53 is a protein involved in ceasing cell proliferation, activating apoptosis and arresting the cell cycle in response to different oncogenic stresses. It does this by acting as a transcriptional regulator inducing the expression of different anti-proliferative target genes.[8] Furthermore, a new role for p53 in controlling development, longevity and overall fitness of an organism is now emerging.[9]

More than 50% of adult human tumours are characterised by inactivating mutations or deletions of the TP53 gene. In addition to these inactivating mutations and deletions, there are several other tumour types in which p53 is wild-type but errors in the control mechanisms that lead to p53 activation occur.[8] It is thought that in these types of cancer, activation of the p53 tumor suppressor protein may lead to therapeutically beneficial responses.[10] In this context, new non-genotoxic small molecule activators of wild-type p53 may play a crucial role in providing novel therapeutic treatments for cancer.[10]

Recently, our group has been actively involved in screening for non-genotoxic small molecules activators of p53.[10] This has led to the discovery of a new class of molecules, named the tenovins (see **Figure 1.3.11** later), which act as non-genotoxic activators of p53.[11]

1.1.3 Regulation of p53 Levels and Activity

Acting as a transcription factor, p53 can bind to almost 300 different promoter elements in DNA and is able to regulate the expression of a wide range of genes. In the absence of genotoxic stress, p53 undergoes a rapid turnover which keeps it at a low level. The levels of p53 are mainly regulated by ubiquitin ligases, such as Mdm2, Mdm4, Pirh2 and Cop1. Under normal conditions, p53 itself acts as a transcriptional activator of the Mdm2 gene.[12] The derived Mdm2 protein binds to p53, forming a complex which is transported to the cytoplasm where p53 is subsequently degraded by the proteasome pathway.[13]

In the presence of different genotoxic stresses, such as UV and ionising radiation, DNA damage, oxidation or hypoxia, p53 is activated through a series of post-translational modifications, mainly comprised of acetylations and phosphorylations. After dissociation

from Mdm2, p53 activation leads to increased transcription of the downstream target genes, resulting in cell cycle arrest, apoptosis and senescence.[14]

Another mechanism by which wild-type p53 is inactivated is by the action of a nuclear protein called SIRT1. SIRT1 belongs to a family of enzymes called sirtuins and catalyses the deacetylation of the ε-*N*-acetyl-lysine 382 of p53 (**Figure 1.1.3**).[15,16]

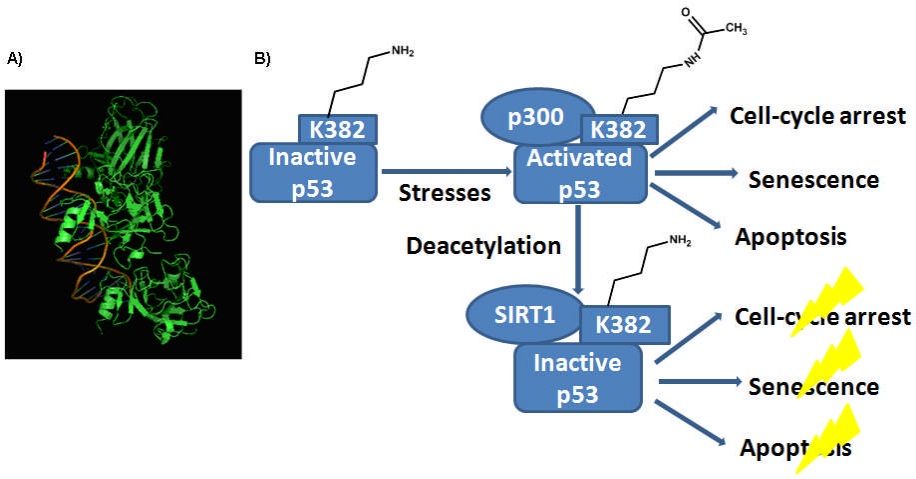

Figure 1.1.3 - A. Crystal structure of p53 bound to DNA (PDB 1TUP).[17] **B.** SIRT1 is involved in the regulation of p53 activity. Deacetylation of p53 by SIRT1 leads to cell survival during stress conditions. Acetylated p53 is more active and restricts cell growth by triggering cell-cycle arrest, senescence and apoptosis.[14]

Oncogenic stresses cause acetylation of p53 on lysine 382 by p300/CPB (**Figure 1.1.3**). Once acetylated, p53 is more active and limits cell growth through cell cycle arrest, senescence or apoptosis. It has been shown that SIRT1 prevents p53 activation through the deacetylation of Lys382, relieving the block to cell cycle progression. The result of p53 SIRT1-mediated deacetylation is the progression of cell growth driven by the oncogenic stresses.[14,15] Thus, inhibition of SIRT1 and its isoforms, particularly SIRT2, is thought to represent an important target for p53 activation and cancer therapy.[18]

More generally, SIRT1 and the sirtuin class of enzymes belong to a wider family of enzymes, known as the histone deacetylases (HDACs). This class of enzymes counteracts the acetylation of histones and non-histone proteins (such as p53) carried out by different histone acetyltransferases (HATs), such as *p300*, *CBP* and *pCAF*.[14] The reversible acetylation-deacetylation of histones is also known as post-translational histone modification and belongs to a series of modifications involved in the regulation of gene expression in a manner that is independent from the DNA sequence.[19] In general, histone deacetylation

causes transcriptional silencing, whereas histone hyperacetylation induces the transcriptional activation of genes, such as *p21*, *Gadd 45*, *FAS* and *caspase-3*, which are all associated with growth arrest and apoptosis in tumour cells.[19]

Before describing the specific roles which SIRT1 and SIRT2 play in inactivating p53, a brief introduction to the HDAC family of enzymes will be provided.

1.2 HDACs

To date, eighteen HDAC family members have been identified in humans (**Table 1.2**). They are divided into two categories: zinc-dependent enzymes (Class I, II and IV) and NAD^+-dependent enzymes (Class III, also known as sirtuins).[20]

1.2.1 Zinc-Dependent HDACs

Class I HDACs, characterised by their homology to the yeast protein RPD3, include HDAC1, HDAC2, HDAC3 and HDAC8 (**Table 1.2**). These enzymes are localised mainly in the nucleus, except for HDACs 3 and 8, which can also be found in the cytoplasm. They are all involved in transcriptional repression and HDAC8[21] is also involved in smooth muscle cell contraction.[20]

Class II HDACs include HDAC4, HDAC5, HDAC6, HDAC7, HDAC9 and HDAC10 (**Table 1.2**). Based on their sequence homology and domain organisation, this class is usually divided into two subclasses, IIa (HDAC4, HDAC5, HDAC7 and HDAC9) and IIb (HDAC6 and 10). They are all co-localised both in the nucleus and in the cytoplasm, except for HDACs 6 and 10, which are found only in the cytoplasm. All components of this class are involved in transcriptional repression and in the blockage of muscle differentiation. HDAC6 also seems to be involved in both the regulation of microtubule stability and in the regulation of molecular chaperone functions.[20]

HDAC Class IV includes only one member – the nuclear HDAC11 – which is the most recently identified HDAC member, and is believed to be involved in transcriptional repression.[20]

1.2.2 NAD^+-Dependent HDACs (The Sirtuins)

The members of the Class III HDACs (SIRTs 1-7), also known as the sirtuins, show distinct homology with the yeast enzyme Sir2 (**Table 1.2**). In yeast there are five sirtuin homologs identified to date: Sir2 (silent information regulator 2) and HSTs1-4.[21] In these organisms, Sir2 is involved in transcriptional silencing of different parts of the yeast genome, especially the silent mating loci, the ribosomal DNA and the telomere.[22]

Table 1.2 - HDAC family of enzymes: classification, localisation and functions.[20]

	Localisation	Function
Zinc-Dependent Enzymes		
Class I (RDP3 Homologues)		
HDAC1	Nucleus	Transcriptional repression
HDAC2	Nucleus	Transcriptional repression
HDAC3	Nucleus, cytoplasm	Transcriptional repression
HDAC8	Nucleus, cytoplasm	Smooth muscle cell contractility
Class II (HDA1 Homologues)		
HDAC4 (IIa)	Nucleus, cytoplasm	Transcriptional repression
HDAC5 (IIa)	Nucleus, cytoplasm	Transcriptional repression
HDAC7 (IIa)	Nucleus, cytoplasm	Transcriptional repression
HDAC9 (IIa)	Nucleus, cytoplasm	Transcriptional repression
HDAC6 (IIb)	Cytoplasm	Various functions
HDAC10 (IIb)	Cytoplasm	Unknown
Class IV		
HDAC11	Nucleus	Transcriptional repression
Class III (Sir2 Homologue)		
SIRT1	Nucleus	Regulation of p53 transcriptional repression
SIRT2	Nucleus, cytoplasm	Cell cycle regulation
SIRT3	Mitochondria	Various mitochondrial functions
SIRT4	Mitochondria	Insulin secretion
SIRT5	Mitochondria	Unknown
SIRT6	Nucleus	DNA repair, genomic stability
SIRT7	Nucleus	Activation of RNA polymerase transcription

There are seven known human sirtuins (SIRT1-7). Sirtuins differ from Class I and Class II HDACs (classic HDACs) by the lack of a Zn^{2+} ion in the catalytic site of the enzyme.[18]

SIRTs 1-3 and SIRTs 5-7 have been shown to deacetylate histone and non-histone proteins, whereas SIRT4 does not possess *in vitro* deacetylase activity. SIRTs 4 and 6 are characterised as ADP-ribosyl-transferases, whereas the role of SIRT7 is still not clear.[18] The sirtuins are found in a variety of locations within cells: SIRTs 1, 6 and 7 are localised in the nucleus, whereas SIRTs 3, 4 and 5 are mainly found in the mitochondria. Only SIRT2 is localised in the cytoplasm.[23]

As discussed previously, these enzymes catalyse the deacetylation of a lysine residue in different proteins within mammalian cells. In addition to the deacetylation of histones, sirtuins can also remove acetyl groups from transcription factors, such as p53 (SIRT1 and SIRT2), α-tubulin (SIRT2) and acetyl-CoA synthase (SIRT3).[21] Furthermore, in mammals, sirtuins are implicated in a wide range of biological functions, such as development, aging, longevity under calorie restriction, adipogenesis and metabolism.[23]

1.2.3 Sirtuins: Chemical Mechanism

The deacetylation reaction carried out by sirtuins is coupled to NAD^+ (**1**) hydrolysis. Nicotinamide **2**, deacetylated protein **3** and the unique metabolite 2'-*O*-acetyl-ADP-ribose (2'-*O*AADPr, **4**) are generated in this reaction (**Figure 1.2.3.1**).[15]

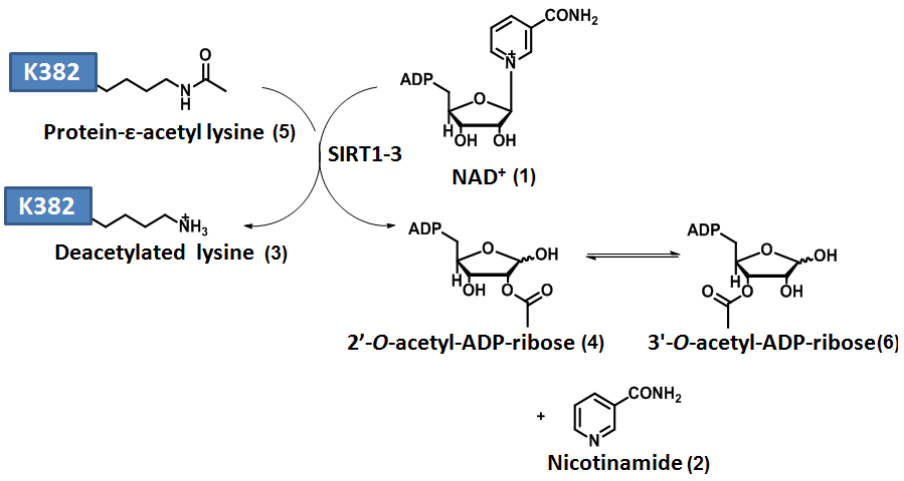

Figure 1.2.3.1 - An overview of the deacetylation reaction catalysed by the sirtuins.[15]

One equivalent of water is also consumed in the process. Thus, the acetyl group is finally transferred from the protein **5** to the 2'-OH of the nicotinamide ribose. After release, 2'-

*O*AADPr has been found to equilibrate spontaneously with its 3'-*O*AADPr isomer **6**, although the role of these two compounds in cells is still poorly understood.[24-26]

Overall, this reaction produces an ester from an amide in an energetically disfavoured transformation where the energetic cost is paid by NAD^+ hydrolysis.[15]

Regarding the mechanism of the deacetylation, the so called "ADPR-peptidyl-imidate mechanism" currently best fits the available experimental data (**Figure 1.2.3.1-1.2.3.2**).[27] Various structural, kinetic, isotope labelling and computational studies support this mechanism. However, the description of these studies is not within the scope of this section. Further details can be found in recently published review articles.[21,27]

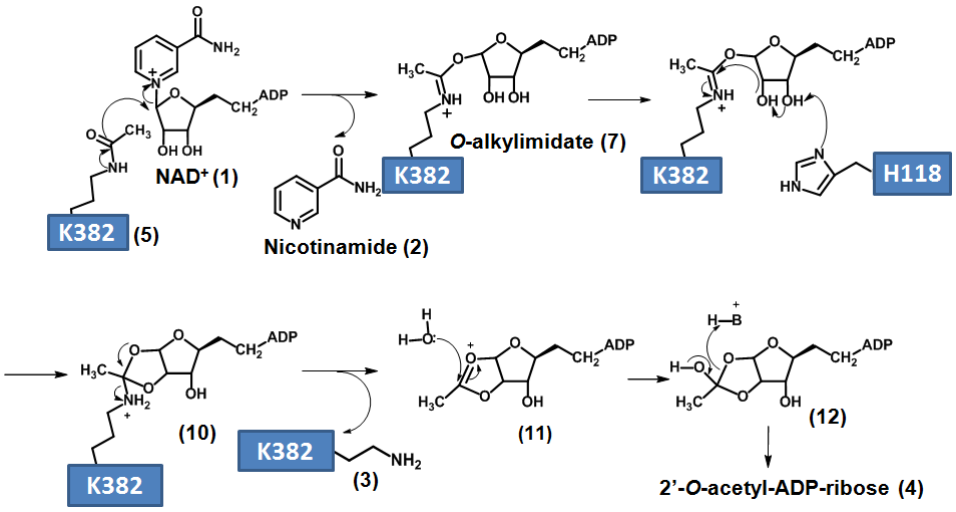

Figure 1.2.3.2 - Proposed mechanism for the deacetylation reaction catalysed by SIRTs1-3 and 5-7. They catalyse the deacetylation of a lysine residue of a variety of targets. NAD^+ **1** and acetylated protein **5** are converted *via* sirtuins to nicotinamide **2**, free lysine side chain **3** and 2'-*O*-acetyl-ADP-ribose **4.**[27 21]

The deacetylation process is proposed to start with the reaction between acetylated peptide **5** and NAD^+ **1**. Support for the formation of the bond between the acetyl oxygen and the C-1' atom of the ADP-ribose moiety comes from the use of ^{18}O-isotopically labelled substates.[24,28] This reaction forms the new peptidylimidate intermediate **7**. Three different possible mechanisms have been proposed for the first step (**Figure 1.2.3.3**), all of which lead to the final imidate **7**:[27]

1. In a "stepwise dissociative" mechanism (S_N1), an oxicarbenium ion **8** is proposed to form after release of nicotinamide **2**. This same ion is thought to react with acetyl-lysine to form **7**.

2. In a "dissociative asynchronous" mechanism, the oxicarbenium ion can form at the transition state **9**. In particular, this transition state is characterised by partial bond cleavage with the leaving group nicotinamide **2** and weak bond formation with the nucleophile acetyl-lysine **5.**

3. The third mechanism involves a concerted S_N2 reaction, and the transition state is equally coordinated to both the leaving group **2** and the nucleophile **5**.

To date, experimental data has been provided for all of the above-described mechanisms. It therefore remains unclear which best explains the first step of the sirtuin catalysed reaction.[27]

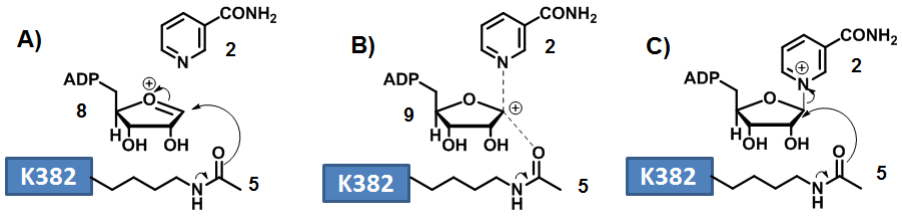

Figure 1.2.3.3 - First step of the deacetylation reaction catalysed by the sirtuins: **A**. Stepwise S_N1 mechanism; **B**. Dissociative asynchronous mechanism; **C**. Concerted S_N2 mechanism.[27]

Once formed, intermediate **7** can equilibrate with nicotinamide **2** that is bound in the nicotinamide C pocket thus reforming NAD^+ **1**. This reversible step is also known as the "base exchange" reaction and is important for the regulation of sirtuin activity. In fact, the activity of a range of sirtuins has been reported to be dependent on the physiological levels of nicotinamide.[29,30] Furthermore, there is growing evidence to support the role of nicotinamide as an endogenous negative regulator of sirtuins.[27]

The imidate **7** is proposed to undergo nucleophilic attack by the 2'-hydroxyl group forming the cyclic intermediate **10**. A conserved histidine residue in the active site of the enzyme deprotonates the 3'-OH group during this step, thus activating this reaction. Mutation of this residue leads to a consistent decrease in the rate of the catalytic process.[24,28,31] Intermediate **10** subsequently undergoes spontaneous elimination of the deacetylated peptide **3** forming an

oxonium species. At this point, attack from water on **11** is proposed to form a second tetrahedral species **12** which, after elimination of the C-1 hydroxyl group generates 2'-*O*-AADPR **4** (**Figure 1.2.3.2**).

A second reaction catalysed by the sirtuins, known as ADP-ribosylation, has also been reported. At this point there is still uncertainty regarding the mechanism, and the products of this process have not yet been fully characterised.[32,33]

1.2.4 Sirtuins: Structure and Active Site

Crystallisation of a range of archeal sirtuins and yeast Sir2Af1, Sir2Af2 and Hst2 in the presence of different ligands has provided a clear view of the structure of the active site.[31,34,35] Amongst the human sirtuins, at present only the crystal structures of SIRT2, SIRT3 and SIRT5 have been determined.[36-39] Whilst SIRT2 was crystallised in its apo-form, SIRT3 was crystallised bound to its acetyl-lysine substrate. Furthermore, two SIRT3 crystal structures containing a reaction intermediate trapped by a thioacetyl peptide and a bound dethioacetylated peptide, were reported in the same work. Finally, SIRT5 was crystallised as a dimer and in the presence of the inhibitor suramin (see **Section 1.3.7**).[39]

All of the sirtuins contain a highly-conserved catalytic core of approximately 275 amino acids. The structure is completed by the N- and C-terminal regions, which are variable in terms of sequence.[40] Overall, the sirtuin structure can be divided into two charateristic domains (**Figure 1.2.4.1**):

1. An NAD^+ binding domain that can be envisaged as a variant of the Rossmann fold. It is composed of six parallel β-strands which form a central β-sheet surrounded by α-helices. This domain contains several amino acid sequences (such as Gly-X-Gly) which are usually found in NAD-binding sites.

2. A smaller subdomain composed of a helical module and a zinc-binding domain. The Zn^{2+} ion is bound to two conserved cysteine residues. Despite not being involved directly in the catalytic activity, this ion is essential for the deacetylase reaction.[31,39,40]

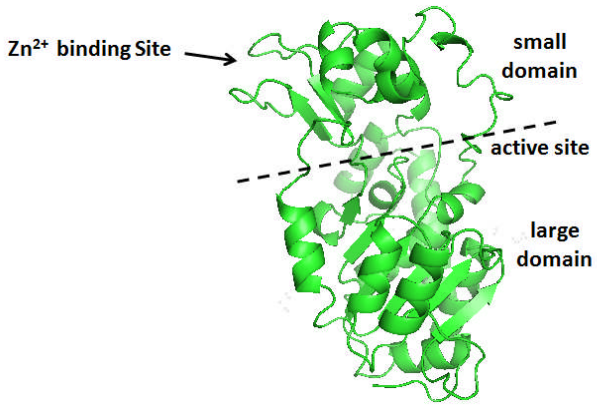

Figure 1.2.4.1 – Crystal structure of human SIRT2 (PDB 1j8F).[36]

While the large domain is characterised by structural similarities amongst the different isoforms, the smaller domain exhibits structural diversities. The variability of this smaller domain is proposed to play an important role in protein-protein interactions, substrate specificity and enzyme localisation.[39,41,42]

Several loops connect the two domains. The active site of the proteins is localised in the cleft between the two domains, in the area around the loops. The substrate **5** and the cofactor **1** have both been found to bind in this area, which exhibits the highest sequence homology amongst the protein family. The active site is usually divided into three parts, according to the different areas where the NAD^+ co-factor binds: site A (adenine-ribose), site B (nicotinamide-ribose) and site C (nicotinamide).[31] A fourth site, site D has been also reported.[43] This controversial site is proposed to be the binding site of the inhibitory nicotinamide molecule and is distinct from the nicotinamide moiety of the NAD^+ cofactor **1**. The exsistence of this binding site has been adversed by Wolberger.[44]

NAD^+ **1** binds in an extended conformation to the cleft between the large and small domains, in close proximity to the acetyl-lysine binding site. Interestingly, **1** binds in an inverted orientation in comparison to other NAD^+ dependent dehydrogenases.[31] The nicotinamide moiety of the cofactor is flexible and can adopt different positions depending on the presence of the peptide. Importantly, when the acetyl-lysine channel is occupied by the substrate, the nicotinamide is buried inside site C. This conformation of the NAD^+ co-factor is known as the "productive conformation." The main aspect of this conformational change is that the co-planarity of the nicotinamide with the glycosidic bond is altered, leading to destabilisation compared to the ground state of the cofactor. The fact that the positive charge of the

nicotinamide moiety is now buried in a largely hydrophobic pocket further contributes to this destabilisation (**Figure 1.2.4.2**).[42,45-47]

The acetylated peptide binds along the same enzyme cleft and forms an enzyme-substrate β-sheet with two flanking strands from the enzyme. The position of the acetyl-lysine side chain is important, as it protrudes into an hydrophobic tunnel that terminates close to the nicotinamide ribose of NAD^+ (**Figure 1.2.4.2**).[34,48]

Recent studies suggest that sirtuins first bind to the substrate (acetylated peptide, **5**) followed by NAD^+ **1** in order to form a ternary complex. It has been suggested that at this point a rearrangement of the NAD^+ binding pocket occurs, bringing the substrate **5** and the NAD^+ cofactor **1** into close proximity, therefore allowing the reaction to take place (**Figure 1.2.4.2**).[37]

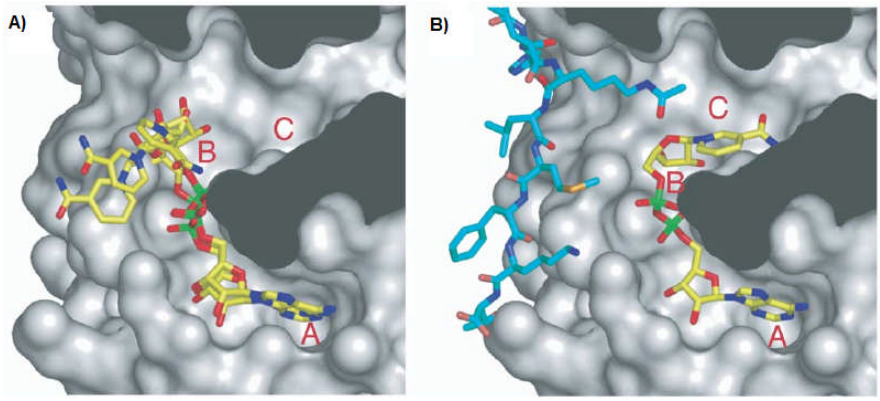

Figure 1.2.4.2 - Overview of the mode of binding of the acetylated-peptide substrate and the NAD^+ co-factor in the sirtuin active site. **A**. In the absence of substrate, NAD^+ **1** (yellow) can bind in the A and B pockets of the active site in alternative non-productive conformations. **B**. In the presence of the peptide substrate **5** (blue), the cofactor **1** binds in a defined conformation, with the nicotinamide moiety buried in the highly conserved C pocket of the active site.[47] (Figure reproduced with the kind authorisation of Elsevier Inc).

1.2.5 Role of SIRT1 and SIRT2 in the Activation of p53 and Cell Cycle Control

Amongst the sirtuin family of enzymes, we are particularly interested in SIRT1 and SIRT2. Indeed, roles for SIRTs 1 and 2 are now emerging in the regulation of cell survival during stress conditions.[14,49,50]

Besides having deacetylase activity on histone proteins, SIRT1 has also been implicated in the deacetylation of different proteins which regulate the cell cycle and apoptosis. To date,

p53, Foxo3a and Ku70 are thought to be the main targets of SIRT1. Acetylation of these proteins leads to cell death during stress.[51-54] Inhibition of SIRT1 also seems to suppress the tumour promoter BCL6 in B-cell lymphomas, including Burkitt lymphoma cells.[55] In line with the reported activity of SIRT1 as a tumour promoter, SIRT1 knockout mice have higher levels of acetylated p53 and show increased levels of radiation-induced apoptosis.[56] Inhibition of SIRT1 results in the suppression of senescence and cell growth arrest in human cancer cells.[57] Inhibition of SIRT1 activity by the protein DBC1 (deleted in breast cancer 1) results in the upregulation of p53 functions, with higher levels of acetylated p53 being observed.[58] Consistent with these observations, higher levels of SIRT1 have been detected in many cancers, such as leukemia, prostate, skin and colon cancers.[59-62]

SIRT2, which is usually found in the cytoplasm, can move into the nucleus during mitosis, where it deacetylates Lys16 of histone H4.[63] It has been found associated with chromatin during the G2/M transition and has been shown to act as a mitotic checkpoint protein, interacting with the homeobox transcription factor HOXA10.[64] Its levels have been found to increase during mitosis, leading to delays in this phase of the cell cycle.[65] Furthermore, SIRT2 has been shown to regulate the mammalian cell cycle.[66] SIRT2 is inactivated through phosphorylation (CDK complexes) and acetylation (p300).[65,67,68] It is involved in controlling the dynamics of microtubules through acetylation of lysine-40 of α-tubulin, its main intracellular target.[69] Tumours characterised by overexpression of SIRT2 show a poor response to chemotherapy, particularly when microtubule poisons are used.[69,70] Furthermore, SIRT2 has been linked to glioma tumorigenesis.[71]

In a recent report, SIRT2 has been proposed for the first time to down-regulate the activity of p53.[72] This isoform interacts with 14-3-3 β/γ proteins in an AKT dependent manner, causing negative modulation of the transcriptional activity of p53 (**Figure 1.2.5**). 14-3-3 β/γ Proteins bind to SIRT2 only when it is phosphorylated at specific serine-threonone residues by the corresponding kinases. After phosphorylation of SIRT2 by AKT, the protein is capable of interacting with 14-3-3 β/γ leading to deacetylation of p53 and subsequent down-regulation of p53. This finding supports the application of SIRT2 inhibitors as potential anticancer agents.[72]

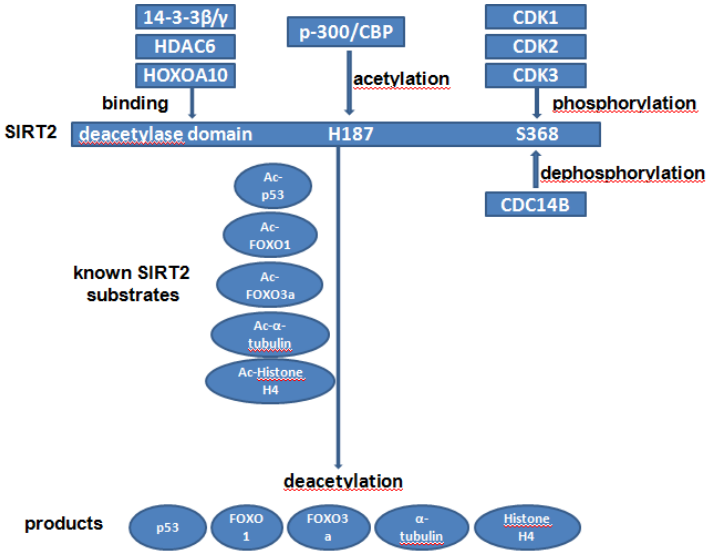

Figure 1.2.5 - The SIRT2 regulatory network.[73]

The potential application of SIRT2 inhibition in the treatment of neurodegenerative diseases is now emerging. This aspect will be discussed in more detail in the next section (see **Section 1.3.9**)

1.3 Inhibitors of SIRT1 and SIRT2

Due to the potential application of SIRT1 and SIRT2 inhibition in the treatment of cancer, several inhibitors of sirtuins have been reported in the literature over the last ten years. Despite the fact that this area is still relatively new, there has been a constant increase in interest, as can be seen in **Figure 1.3** which outlines the number of publications in the area since 2001 to May 2010. All the data discussed in this section are summarised in **Table 1.3**.

Due to the large number of compounds reported, the aim of this section is to detail only the most potent sirtuin inhibitors. For a more complete overview of this subject, recently published reviews articles should be consulted.[74-77] For simplicity, the inhibitors will be divided according to their structures.

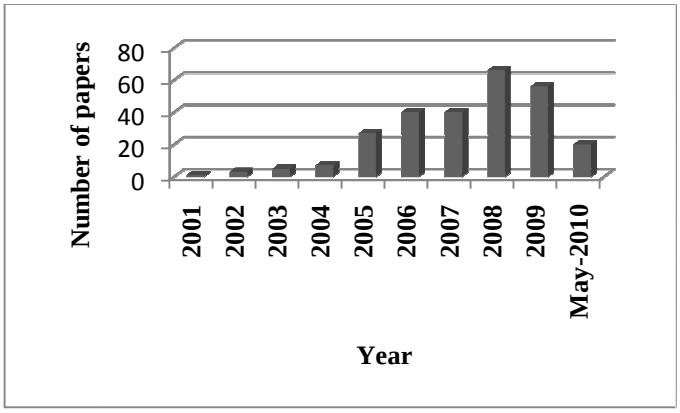

Figure 1.3 - The increasing interest in sirtuins inhibitors over the last nine years. (Source: SciFinder, Accessed May 2010).

1.3.1 Nicotinamide and its Analogues

Nicotinamide **2** (**Figure 1.3.1**) is the physiological inhibitor of the sirtuins. As a co-product of the deacetylation reaction, this molecule inhibits the same reaction by reacting with the *O*-alkyl-imidate intermediate **7** in a process known as the nicotinamide base exchange reaction. K_i values for nicotinamide inhibition of bacterial, yeast and mouse sirtuins are usually in the range of 26-160 μM.[78] Nicotinamide has recently been reported to inhibit *Plasmodium falciparum* Sir2 *in vivo*.[79]

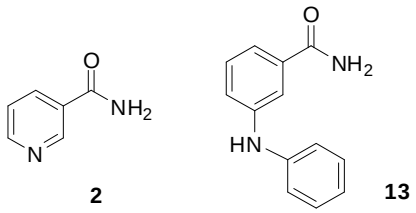

Figure 1.3.1 - Structure of nicotinamide **2** and 2-anilinobenzamide **13.**

A class of nicotinamide analogues, the 2-anilinobenzamides (**Figure 1.3.1**), were described as selective inhibitors of SIRT1.[80] Compound **13** was the most potent molecule, with an IC_{50} of 4.1 μM. No data are reported regarding the activity of **13** against SIRT2. Lineweaver-Burke competition experiments suggested that the anilinobenzamides are non-competitive with respect to NAD^+ and competitive with the acetyl-lysine substrate. When docked into the active site of Hst2, **13** showed key interactions with Ala 227 and Tyr 229. Compound **13** was also shown to increase the levels of acetylated p53 in HCT116 cells in the presence of the genotoxic agent etoposide.[80]

1.3.2 Thioacetyl-lysine-based Inhibitors

Thioacetyl-lysine peptides have been recently reported as "mechanism-based" inhibitors (**Figure 1.3.2**).[81,82] The main advantage of this class of compounds is the high selectivity and potency *in vitro.* Due to their structural similarity, these compounds mimic the acetyl-lysine substrate **5**, leading to the formation of a stalled thiomidate intermediate during the catalytic cycle. Compound **14** was found to inhibit SIRT1 with IC_{50} values of 0.9 nM.[81] This peptide was not tested against SIRT2. In related work, a series of thio peptides were designed based on the human p53 and α-tubulin sequences.[82] Peptide **15** was reported as a potent and selective SIRT1 inhibitor, with an IC_{50} of 180 nM. The same peptide **15** was a less potent inhibitor of SIRT2 (IC_{50} 3.8 μM). The observed selectivity and potency was rationalised based on the different side chains used in the peptide sequence.

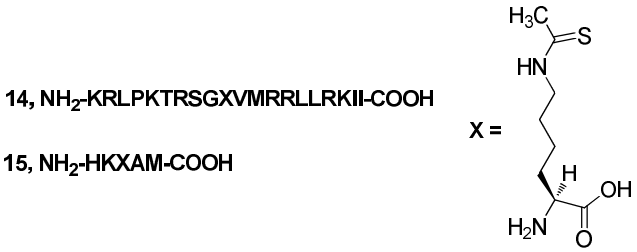

Figure 1.3.2 - Structure of thioacetyl-lysine substrates **14** and **15.**

1.3.3 Sirtinol and Analogues

Sirtinol (**16**, IC_{50} = 38 μM against SIRT2, **Figure 1.3.3**) was the first sirtuin inhibitor identified after nicotinamide **2**. The discovery was made during a high-throughput phenotype screen for small molecule inhibitors of yeast Sir2p.[83] The 2-hydroxy-1-naphthaldehyde moiety present in **16** has been proposed to be the pharmacophore. Despite the fact that **16** was not tested against SIRT1 in the original work, in a series of following reports it was described as a poor SIRT1 inhibitor (IC_{50} = 131μM).[84] A series of structural analogues of sirtinol **16** have been reported. One such analogue, *para*-sirtinol (**17**, **Figure 1.3.3**) showed a good inhibitory activity against SIRT1 (IC_{50} = 13 μM) over SIRT2 (IC_{50} = 26 μM). The observed selectivity was not rationalised by the authors.[84] Another analogue, Salermide (**18**, **Figure 1.3.3**) induced apoptosis in cancer cells in a SIRT1 dependent manner. A precise evaluation of **18** as a sirtuin inhibitor is limited by the fact that the activity is reported as a percentage of inhibition at different concentrations. IC_{50} values against SIRT1 and SIRT2 were not determined.[85]

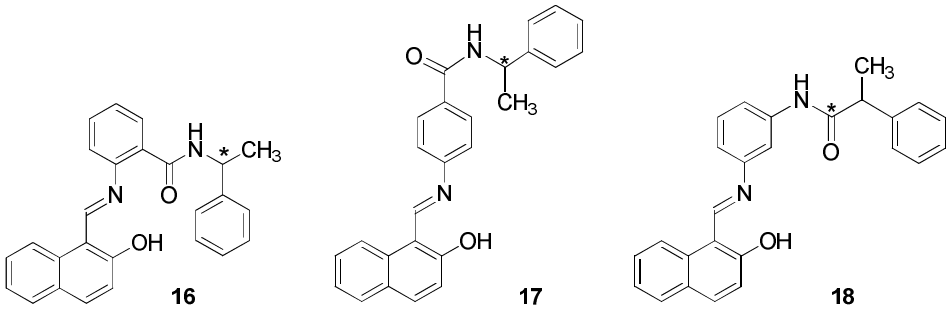

Figure 1.3.3 - Structures of sirtinol (**16**)**,** *para*-sirtinol (**17**) and salermide (**18**). *: compounds tested as racemates.

1.3.4 Indole-based Inhibitors

Indole-based compounds represent the most potent SIRT1 inhibitors described so far. Racemic EX527 (**19**, **Figure 1.3.4**) exhibited an IC_{50} of 9.8 nM against SIRT1.[86] When the same compound was used by other authors as a control, the IC_{50} was found to be slightly higher (0.28 μM).[87] The *S* enantiomer of **19** was the most potent, with an IC_{50} of 123 nM. The *R* enantiomer shows an inhibitory activity greater than 100 μM. Racemic **19** was less potent against SIRT2 (IC_{50} = 19.6 μM). Enzymatic kinetic studies performed using a fluorimetric assay suggested that this molecule binds after the release of nicotinamide **2** from the enzyme, and prevents the release of the two products of the enzyme catalysed reaction, namely deacetylated peptide **3** and 2'-*O*-acetyl-ADP-ribose **4**. SAR studies further clarified a range of structural requirements for high potency. The presence of the carboxamide moiety in the 1-position is necessary for potent activity, as well as the seven-membered carbocycle C ring. Insertion of a nitrogen atom in the C ring resulted in loss of activity. [86]

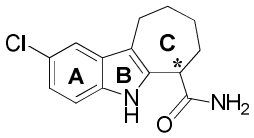

Figure 1.3.4 - Structure of EX-527 **19**. *: compound initially tested as racemate.

Huhtiniemi and co-workers further investigated the mode of binding of EX527 **19**.[88] Due to the lack of a crystal structure for SIRT1, they generated a three-dimensional comparison model of the SIRT1 catalytic core. EX527 **19** was found to bind in the C pocket, in the very extensively conserved region of residues from Thr344 to Asp348. The amidic NH_2 was found to donate an H-bond to the carbonyl group of Asp348. The NH of the indole ring was involved in a further

hydrogen bond to the backbone carbonyl oxygen of Gln345. Another key interaction was present between the carbonyl oxygen of **19** and the NH of either Asp348 or Ile347.

1.3.5 Bisindolyl-maleimides

As kinase inhibitors have also been reported to target NAD^+-dependent enzymes, a library of kinase inhibitors was tested for SIRT2 inhibitory activity.[89] Compound **20** (**Figure 1.3.5**) composed of the bisindolyl-maleimide scaffold was a potent and selective inhibitor of SIRT2, with an IC_{50} of 0.8 μM. The same compound was a less potent inhibitor of SIRT1 (IC_{50} = 3.5 μM). In agreement with molecular modelling studies, biochemical assays suggested that **20** is competitive with NAD^+. Docking studies showed that **20** occupies the region were the adenine ring of NAD^+ binds. In particular, the isothiourea moiety of **20** binds in the area around Ile93 and Asp95.

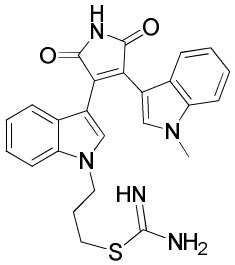

Figure 1.3.5 - Structure of **20.**

1.3.6 Splitomicin and Analogues

As a result of screening a 6000-compound library, splitomicin (**21**, **Figure 1.3.6**) was reported as a selective inhibitor of yeast Sir2 (IC_{50} = 60 μM).[90, 91] Further studies by Posakony on a small collection of splitomicin analogues led to the establishment of structure activity relationships (SARs) for this class of molecules.[92] No activity on human sirtuins was observed for **21** and the initial analogues.

Following a series of SAR studies, Jung and co-workers discovered HR73 (**22**, **Figure 1.3.6**) was a selective SIRT1 inhibitor (IC_{50} < 5 μM), with the IC_{50} value against SIRT2 being higher than 100 μM. An increase in the p53 acetylation level was detected *in vivo* after treatment with this compound.[93]

As HR73 is an inhibitor of HIV Tat protein deacetylation and HIV transcription, this molecule may also represent the starting point for the development of new anti-HIV drugs.[93]

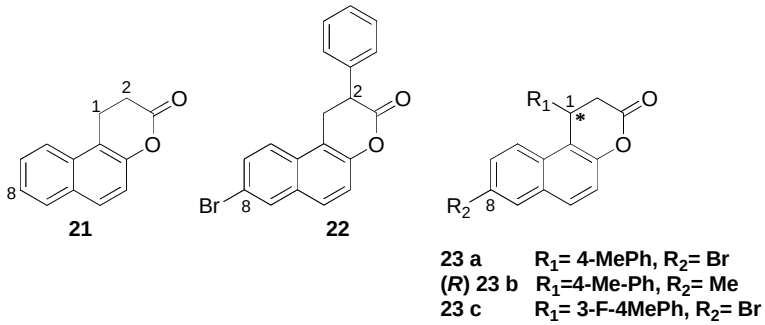

Figure 1.3.6 - Structures of splitomicin **21**, HR73 **22** and *β*-splitomicins **23a-c**.

A new group of splitomicin analogues, *β*-splitomicins (**23 a-d**, **Figure 1.3.6**), was synthesised and their biological properties against SIRT2 evaluated.[94] No data are reported regarding SIRT1 inhibition. A range of substitutions at the C-1 position of the lactone ring and at the C-8 position of the naphthalene moiety led to a consistent improvement of the inhibitory activity against SIRT2, with IC_{50} values in the low micromolar range. The (*R*)-enantiomers were approximately 12 times more potent than the (*S*)-enantiomers. Rationalisation of the experimental results was carried out using ligand docking studies and Poisson-Boltzmann/surface area (MM-PBSA) calculations. These molecules were found to bind in the nicotinamide C subpocket. The higher activity of the *β*-isomer is due to the orientation of the *β*-phenyl substituent, as the interaction with the substrate binding channel (Phe119 and His187) was observed only for the (*R*)-enantiomers. Consistent with this, competition experiments revealed that the *β*-splitomicins are non-competitive with the NAD^+ co-factor. Some of the best inhibitors (**23a-b**) showed antiproliferative activity and led to increased α-tubulin acetylation in MCF-7 breast cancer cells, thus representing promising candidates as anticancer drugs. At present, a rationalisation for the selectivity observed amongst splitomicin analogues **22** and **23a-d** against SIRT1 and SIRT2 upon changing the position of the phenyl substituent is still missing.

1.3.7 Suramin and its Analogues

The symmetrical polyanionic naphthylurea suramin (**24**, **Figure 1.3.7.1**) was reported to inhibit both SIRT1 (IC_{50} = 297 nM) and SIRT2 (IC_{50} = 1.15μM).[95] Furthermore, suramin was co-

crystallised with SIRT5, and to date it is the only sirtuin inhibitor co-crystallised in the active site of one of these proteins. The binding site of suramin to SIRT5 was identified in a region between the nicotinamide binding pocket (C site) and the cleft that binds the acetylated peptide.[39]

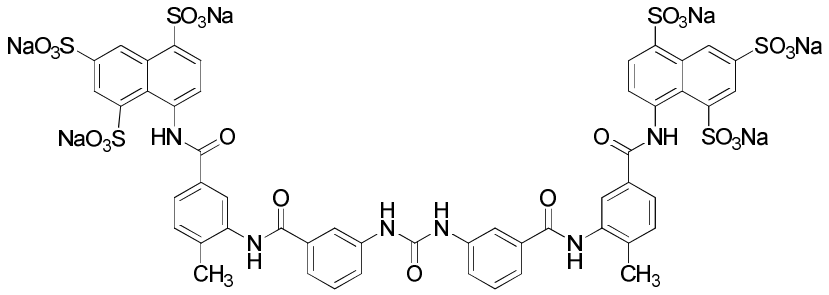

Figure 1.3.7.1 - Structure of Suramin **24**.

In a subsequent study, a group of suramin derivatives was described by Jung and co-workers (**Figure 1.3.7.2**).[96] NF675 **25,** NF259 **26** and NF154 **27** were found to inhibit SIRT1 to a greater extent than SIRT2, with IC_{50} values in the two digit nanomolar range. Competition experiments indicated that suramin **24** and its analogues are non-competitive with respect to the NAD^+ cofactor. Docking studies performed using the reported SIRT2 structure showed that these molecules interact in a mode similar to that observed for suramin with SIRT5. The naphthyl rings bearing the sulfonic acid groups are positioned in a polar pocket between Arg97, Phe119 and Phe235, Arg97, Phe96. The backbone NH group of Phe70 acts as a hydrogen bond donor to the sulfonyl groups of the inhibitors. At present, the possibility of employing these inhibitors as therapeutic agents is unclear. Despite the high inhibitory activity observed, some limitations exist due to the limited cellular uptake of these highly-polar poly-sulfonic acids.

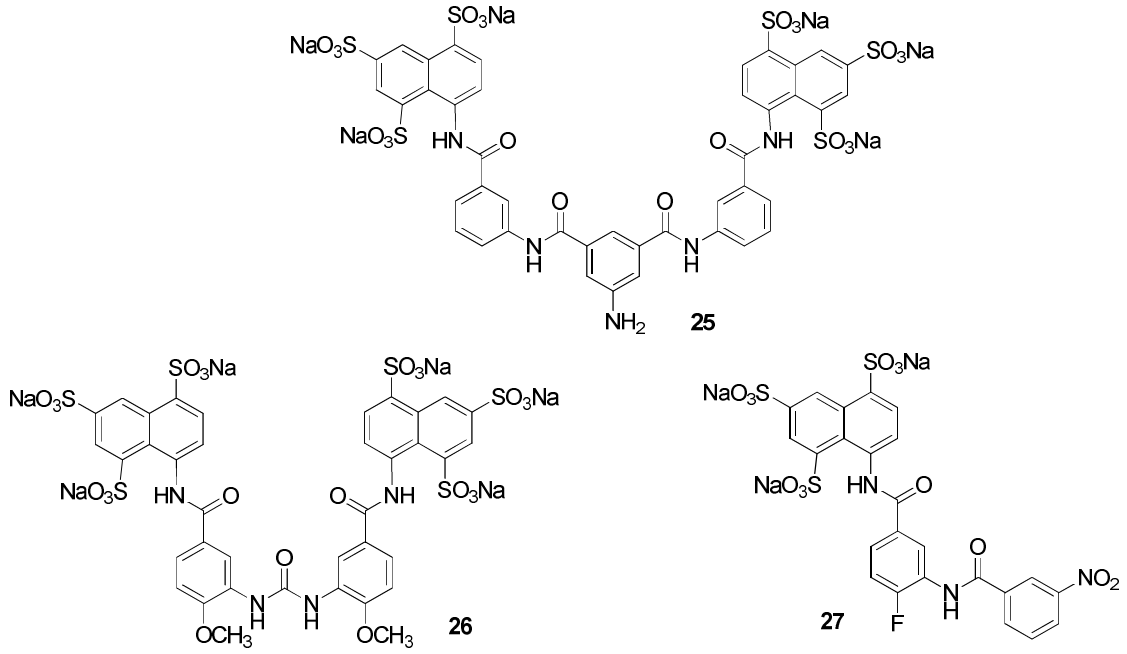

Figure 1.3.7.2 - Structures of NF675 **25**, NF259 **26** and NF154 **27**.

1.3.8 Thiobarbiturates

Thiobarbiturates were discovered as sirtuin inhibitors by a virtual screening of compounds belonging to the ChemBridge database. Initially, the most potent compound, **28** (**Figure 1.3.8**) exhibited IC_{50} values of 13.2 μM (SIRT1) and 9.1 μM (SIRT2) and was proposed to interact with the nicotinamide binding pocket.[97]

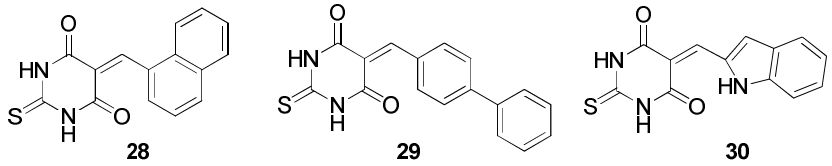

Figure 1.3.8 - Structure of thioubarbiturates **28, 29** and **30**.

Interestingly, π-stacking interactions between the aromatic component of **28-30** and the substrate binding channel stabilises the binding to the protein. Further molecular mechanics Poisson-Boltzmann/surface area (MM-PBSA) studies led to the synthesis of analogues **29** and **30** (**Figure 1.3.8**). Biphenyl derivative **29** was a selective SIRT2 inhibitor (IC_{50} = 8.7 μM) SIRT1 (IC_{50} = 50.5 μM). **30** exhibited a slight selectivity to SIRT1 over SIRT2 (IC_{50} = 5.9 μM and 20.3 μM, respectively). The selectivity observed with analogues **29** and **30** was not explained by the authors.[97]

1.3.9 AGK-2

AGK-2 (**31**, **Figure 1.3.9**) is one of the most potent and selective SIRT2 inhibitors reported to date, with an IC_{50} value of 3.5 μM.[98] The inhibitory values recorded against SIRT1 were poor (IC_{50} > 50 μM). Docking simulations indicated that the C-subpocket of the SIRT2 active site is the optimal binding site for **31**. No docking analysis was carried out in the SIRT1 active site and no rationale has been proposed for the observed selectivity. Interestingly, this compound showed different activities in cells. Hyperacetylation of tubulin was observed in cells after treatment with **31**.[98] In a Parkinson's disease model, **31** diminished α-synuclein toxicity in dopamine neurons in a dose dependent manner.[98] These interesting observations are likely mediated by α-synuclein stabilisation and microtubule aggregation derived from α-tubulin acetylation in the cytoplasm. Inhibition of SIRT2 by AGK-2 **31** also resulted in neuroprotection in a cellular and invertebrate model of Huntington's Disease (HD).[99] This was rationalised by a decreased synthesis of sterols, probably mediated by reduced nuclear trafficking of SREBP-2. This last effect was likely due to alteration of microtubule-mediated trafficking after SIRT2 inhibition.[99]

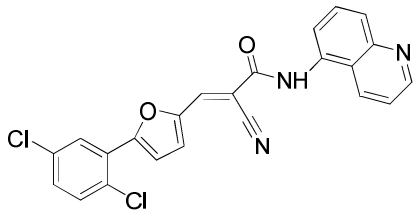

Figure 1.3.9 - Structure of AGK-2 (**31**).

1.3.10 Natural Product Inhibitors

Sirtuin inhibitors have also been identified from natural sources. In 2007 Gey reported two natural products as good inhibitors of SIRT1 and SIRT2.[100] The phloroglucinol derivatives (+)-guttiferone G **32** and hyperforin **33** were isolated from *Garcinia cochinchinensis* and *Hypericum perforatum* respectively. A third compound, synthetically derived from hyperforin **33**, called aristoforin (**34**, **Figure 1.3.10.1**) was also tested in the same study. Guttiferone G **32** was found to inhibit recombinant human SIRT1 and SIRT2 at micromolar concentrations (IC_{50} = 9 μM and 22 μM respectively). Hyperforin **33** and aristoforin **34** were also good inhibitors of both SIRT1 and SIRT2 (28 μM and 21 μM, respectively). Furthermore, inhibition

of cell proliferation was observed with HUVEc cells for all three compounds. The phloroglucinol scaffold of these molecules was considered to be the pharmacophore.[100]

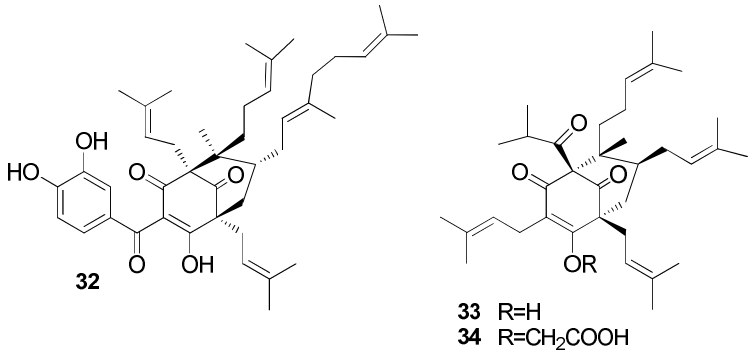

Figure 1.3.10.1 - Structures of (+)-guttiferone **32**, hyperforin **33** and aristoforin **34**.

Tanikolide dimer stereoisomers **35** and **36** were recently isolated from the Madagascar marine cyanobacterium *Lyngbya majuscule* (**Figure 1.3.10.2**).[101] Tanikolide dimer **35** inhibited SIRT2 with an IC_{50} value of 176 nM in one assay and 2.4 µM in another assay. They were proposed to block the entrance to a narrow channel in the active site of the enzyme, adjacent to Ile169 and Asp170.

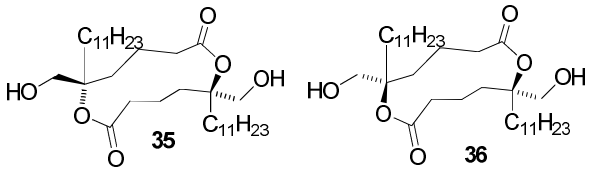

Figure 1.3.10.2 - Structure of tanikolide seco-acid **35** and tanikolide dimer **36**.

Table 1.3 – Summary of the most active SIRT1 and SIRT2 inhibitors.[77]

Inhibitor	Type of Inhibition		IC_{50} (μM)			
	NAD^+	Substrate	SIRT1	SIRT2	Fold selectivity[f]	Others
2	**Noncompetitive**	**Noncompetitive**	**25**	**100**	**0.25**	**130 (HST2)**
13	**Noncompetitive**	**Competitive**	**17**	**74**	**0.22**	**235 (SIRT3)**
14	**-**	**Competitive**	**0.9**	**4.3**	**0.20**	**4.5 (SIRT3)**
15	**-**	**Competitive**	**0.18**	**3.8**	**0.05**	**-**
16	**-**	**-**	**131**	**38**	**3.44**	**66 (sir2p)**
17	**-**	**-**	**13**	**25.9**	**0.4**	**33 (sir2p)**
18	**-**	**-**	**80%[d]**	**80%[d]**	**-**	**-**
19[a]	**-**	**-**	**0.098**	**-**	**-**	**-**
20	**Competitive**	**-**	**3.5**	**0.8**	**1.25**	**-**
21	**-**	**-**	**-**	**-**	**-**	**74 (sir2p)**
22	**-**	**-**	**5**	**-**	**-**	**-**
23a-c	**-**	**-**	**-**	**1.5-2.0**	**-**	**-**
24	**Noncompetitive**	**-**	**0.297**	**1.15**	**0.25**	**22 (SIRT5)**
25	**Noncompetitive**	**-**	**0.093**	**2.26**	**0.041**	**-**
26	**-**	**-**	**0.46**	**44%[e]**	**-**	**-**
27	**-**	**-**	**0.52**	**15.5**	**0.03**	**-**
28	**-**	**-**	**13.2**	**9.1**	**1.45**	**-**
29	**-**	**-**	**50.5**	**8.7**	**5.80**	**-**
30	**-**	**-**	**5.9**	**20.3**	**0.29**	**-**
31	**-**	**-**	**> 50**	**3.5**	**-**	**> 50 (SIRT3)**
32	**-**	**-**	**9**	**22**	**0.40**	**-**
33	**-**	**-**	**15**	**28**	**0.53**	**-**
34	**-**	**-**	**7**	**21**	**0.33**	**-**
35	**-**	**-**	**29**	**2**	**14.5**	**-**
36	**-**	**-**	**34**	**3**	**11.3**	**-**
37	**-**	**-**	**-[b]**	**-[b]**	**-**	**-**
38[c]	**-**	**-**	**21**	**10**	**2.1**	**67 (SIRT3)**
39[c]	**Noncompetitive**	**competitive**	**56**	**59**	**0.9**	**-**
41	**-**	**-**	**8.4**	**191**	**0.04**	**-**
42	**-**	**-**	**4.2**	**NI**	**-**	**-**
43	**-**	**-**	**5.3**	**NI**	**-**	**-**

[a] racemic; [b] not determined for solubility problems; at 10 μM concentration **37** was equipotent as **38**. [c] compounds which showed *in vivo* activity in mouse xenograph models. [d] at 90μM. [e] at 80 μM.
[f] Determined as IC_{50} SIRT1/IC_{50} SIRT2. - Not determined. NI, no inhibition.

1.3.11 The Tenovins

Our group has been involved in the synthesis of a new series of sirtuin inhibitors. In collaboration with Dr Sonia Lain and Prof. Sir David P. Lane, the tenovins (**37 and 38**) have recently been reported as a new class of sirtuin inhibitors (**Figure 1.3.11**).[11] The most active compound **38** exhibited IC_{50} values of 21 μM and 10 μM against SIRT1 and SIRT2, respectively. From cell-based screening, it was found that this class of molecules activates p53 and decreases the growth of ARN8-derived tumours *in vivo* as single agents.

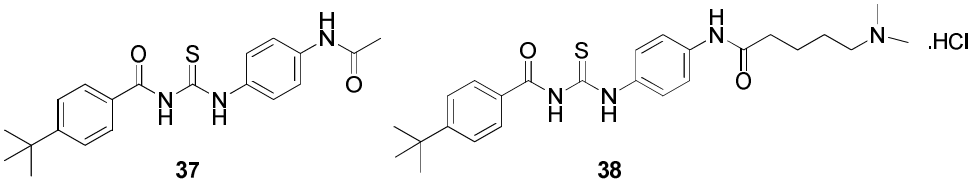

Figure 1.3.11 - Structures of tenovin-1 **37** and tenovin-6 **38**.

1.4 Cambinol

1.4.1 A SIRT 1 and SIRT2 Inhibitor with *in vivo* Anticancer Activity

Before the tenovins were discovered, in 2006 Heltweg and co-workers described cambinol (**39, Figure 1.4.1**) as the first sirtuin inhibitor with *in vivo* activity against Burkitt lymphoma derived xenografts.[18] This activity was consistent with the observation that cambinol **39** as a single agent induced apoptosis of BCL-6-expressing Burkitt lymphoma cells, with concomittant hyperacetylation of p53 and BCL6. As hyperacetylation inactivates the onco-promoter BCL6 and activates the onco-suppressor p53, this antitumor activity was explained by the combined effect on BCL-6 and p53.[18]

The *in vitro* inhibitory activity of **39** against SIRT1 and SIRT2 was modest (IC_{50} = 56 μM and 59 μM respectively). Despite the moderate and non-selective activity, cambinol-induced inhibition of SIRT1 during etoposide-induced genotoxic stress did indeed cause hyperacetylation of key stress response proteins, such as p53, resulting in cell cycle arrest and apoptosis. Acetylation of α-tubulin was also observed in cells, presumably as a result of SIRT2 inhibition. These results also suggest that cambinol inhibits both enzymes in cells. No activity against SIRT3, SIRT5 and the HDAC 6 was observed. These data strongly support the possible application of cambinol **39** as a novel anticancer agent.[18]

The mode of action of cambinol is still unclear. Lineweaver-Burke experiments carried out with SIRT2 suggest that cambinol is competitive with the substrate (Acetyl-H4 peptide) and non-competitive with respect to the NAD^+ co-factor.[18] In agreement with this, after molecular docking studies Neugebauer and co-workers proposed that cambinol binds in the nicotinamide subpocket (C). In particular, the interactions with the polar residues of Gln167, Asn168 and water molecules are important for the interaction of **39** with the C pocket of the enzyme.[94] As for other known inhibitors, the *β*-naphthol moiety was considered to be the pharmacophore. It was observed that replacement of this group with a phenol moiety (ADS012, **40**, **Figure 1.4.1**) resulted in loss of the inhibitory activity against the two enzymes (IC_{50} not reported).[18]

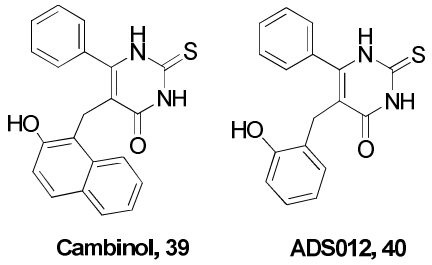

Figure 1.4.1.1 - Structures of cambinol **39** and its analogue ADS012 **40**.

Only recently have new cambinol analogues been reported.[102] Tetracyclic pyrimidinediones **41**, **42** and **43** can be considered as ring constrained versions of **39** (**Figure 1.4.1.2**). They exhibited a better inhibitory activity against SIRT1 in comparison to cambinol **39** (IC_{50} = 8.4, 4.2 and 5.3 μM, respectively). In cell activity of **41**-**43** was detected through increased levels of Ac-p53 in MCF7 cells. Moreover, U937 leukemia cells treated with **41**-**43** exhibited cell-cycle arrest in the G1 phase as well as programmed cell death.[102]

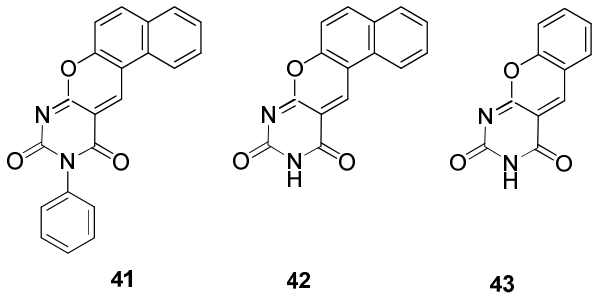

Figure 1.4.1.2. The new cambinol analogues recently reported by Rotili and co-workers.

1.4.2 Preliminary SAR Studies in the Westwood group

Our interest in cambinol **39** arises from the fact that inhibitors of SIRT1 and SIRT2 have been reported as potential therapeutic agents for the treatment of cancer.[18] Additional interest came from the *in vivo* antitumour activity observed for **39**. Furthermore, only one analogue of cambinol **39**, ADS012 (**40**, **Figure 1.4.1**), had been synthesised and tested for its selective inhibitory activity against the two isoforms.[18] Thus, due to the lack of cambinol **39** analogues in the literature, a series of synthetic and biological studies were carried out in the Westwood and Lane groups in order to establish a series of preliminary structure activity relationships (SARs) for cambinol.[103] These studies were carried out by the candidate during his MSc final project in the Westwood group.

Five compounds (**44-48**, **Figure 1.4.2**) were synthesised using a previously reported synthetic route (**Scheme 1.4.2**).[104] This synthesis consisted of three steps. Firstly, the Knoevenagel condensation of 2-hydroxy-1-naphthaldehyde **49** with various ethyl benzoylacetates **50a-c** in the presence of piperidine resulted in the formation of different ketocoumarins **51a-c**. Subsequent reduction of the conjugated double bond with $NaBH_4$ in pyridine led to the formation of 1,2-dihydro ketocoumarins **52a-c**, which were then condensed with thiourea **53** in the presence of NaOEt to give cambinol **39** and analogues **44-46.** Analogue **44** was obtained from the reaction between **52a** and urea **54**, whereas **47** came from condensation of ketocoumarin **52a** with *N*-methylthiourea **55**.[103]

The regiochemistry observed in the synthesis of **47** was established by means of [^{1}H-^{13}C] HMBC spectroscopy experiments. In the HMBC spectrum, the singlet derived from the three protons of the new methyl substituent at *N*-1 exhibited only two cross peaks: the first with the signal corresponding to the carbon of the thiocarbonyl group and the second with the quaternary carbon C-6.[103]

The approach used to access analogue **48** involved the initial preparation of the starting material **56** through a Suzuki-coupling reaction between phenyl boronic acid **57** and 5-bromo-2-hydroxybenzaldehyde **58**. **56** was then condensed with **50a** (R_1 = H) to yield **59**. The final product **48** was then obtained through the previously described two-step sequence.[103]

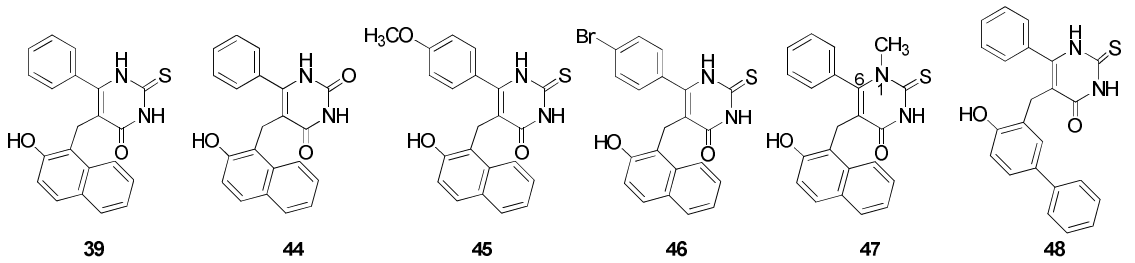

Figure 1.4.2 - Structures of cambinol **39** and of the 5 new analogues synthesised **44-48**.[103]

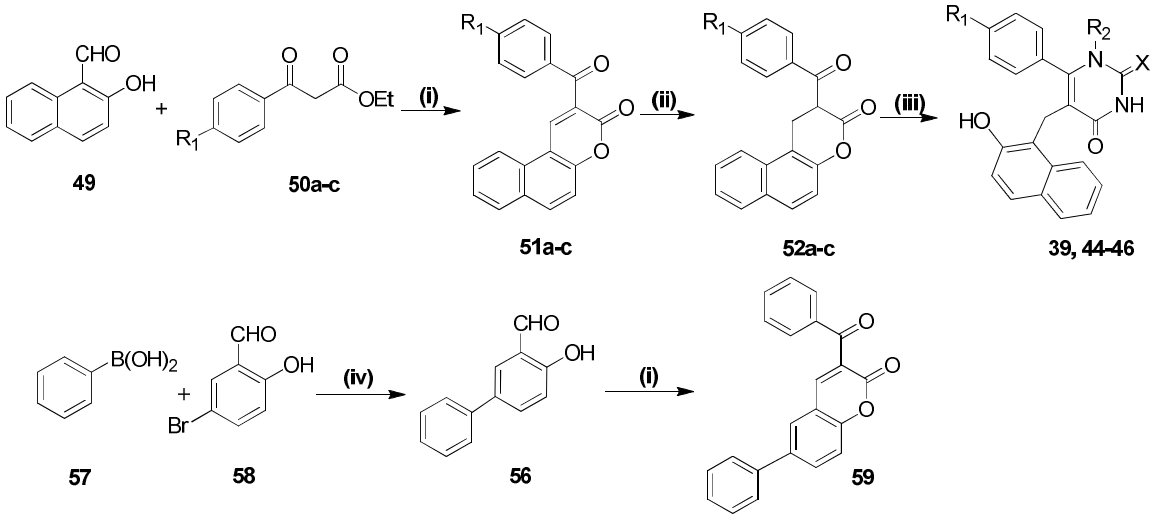

Scheme 1.4.2 - Synthesis of cambinol **39** and of its new analogues **44-48**. *Reagents and conditions:* (i) **50a** (R_1 = H), **50b** (R_1 = CH_3O) or **50c** (R_1 = Br), piperidine, ethanol, reflux, 2 h; (ii) $NaBH_4$, pyridine, rt, 2 h; (iii) Na, ethanol, thiourea (**53**), or urea (**54,** X = O), or *N*-methylthiourea (**55,** R_2 = Me), reflux, 18 h; (iv) $Pd(dppf)Cl_2.CH_2Cl_2$, K_2CO_3, DME:H_2O (3:1), reflux, 4 h.[103]

The yields observed in the three steps of the synthesis of **39** and **44-48** are summarised in **Table 1.4.2.1**. The first two steps proved to be high-yielding but disappointingly, a decrease in the yield was observed for the last step. In all the reactions pure products were obtained following straightforward procedures. These mainly consisted of direct precipitation of the product after formation (**Step (i)**) or precipitation of the product after acidification of the reaction mixture (**Step (ii)**). For **Step (iii)**, the final analogues were obtained by precipitation after acidification of the aqueous solution of the crude reaction mixture. Thus, this synthetic pathway was believed to be applicable to the synthesis of a larger number of cambinol analogues, in particular those characterised by a range of substituents at the phenyl ring and at the *N*-1 of the thiouracil core.[103]

Table 1.4.2.1 – Yields observed in previous synthetic studies run in the Westwood group.[103]

	Yield (%)		
Analogue	**Step (i)**	**Step (ii)**	**Step (iii)**
39	86	95	51
44	86	95	20
45	95	76	42
46	87	93	43
47	86	95	16
48	66	95	40

Cambinol **39** plus the five new analogues **44-48** were tested for their *in vitro* inhibitory activity against SIRT1 and SIRT2 (**Table 1.4.2.2**).[103] Cambinol **39** gave results in line with the literature. [18] Analogue **46** was found to be a relatively active and selective inhibitor of SIRT1 ($IC_{50} = 12.7 \pm 2\ \mu M$). This represents a 4-fold improvement with respect to the inhibitory activity of cambinol **39** itself against SIRT1. Similarly, analogue **47** showed a relatively strong and selective inhibitory activity against SIRT2 ($IC_{50} = 20.1 \pm 5\ \mu M$), leading to an inhibition 3 times better than cambinol **39**.[103]

Table 1.4.2.2 - SIRT1 and SIRT2 inhibitory activity of compounds **39** and **44-48** are shown.[103]

	SIRT1		SIRT2	
Compound	**Inhibitory activity**[a]	**IC_{50} (μM)**[b]	**Inhibitory activity**[a]	**IC_{50} (μM)**[b]
39	91.4 ± 8	40.7 ± 8	55.5 ± 11	47.9 ± 11
44	14.7 ± 3	> 90	30.9 ± 19	> 90
45	20.5 ± 20	> 90	9.2 ± 2	> 90
46	92.5 ± 10	12.7 ± 2	34.2 ± 0	> 90
47	36.2 ± 6	> 90	88.2 ± 2	20.1 ± 5
48	48.2 ± 13	61.7 ± 13	35.9 ± 5	> 90

[a] The results are the average of testing in duplicate and are expressed as % of inhibition at 60 μM concentration ± SE (standard error, n =2). [b] IC_{50} values were determined for all compounds and were repeated at least twice.

These preliminary studies therefore demonstrated that it was possible to take the modest and non-selective SIRT1 and SIRT2 inhibitor cambinol **39** and convert it into a more potent and selective inhibitor of the two isoforms through a series of structural modifications. Thus, as the synthesis of further cambinol **39** analogues offers scope for finding more potent and

selective inhibitors of SIRT1 and SIRT2 and hence for the development of novel anticancer agents, it was decided to continue these studies during the PhD.

1.5 Aims of This Study

Encouraged by the results obtained from our previous synthetic and *in vitro* biological studies, it was decided to further explore the SARs associated with cambinol **39**. Initially, two main modifications to the structure of cambinol **39** were planned:

1. Due to the encouraging *in vitro* activity obtained for **46** (IC_{50} = 12.7 μM, SIRT1), the synthesis of a series of analogues characterised by a range of substituents at different positions of the phenyl ring, bearing both electron-withdrawing and electron-donating properties, was planned.

2. After observing the selective and potent inhibitory activity of analogue **47** for SIRT2 (IC_{50} = 20.1 μM), it was decided to prepare a second group of analogues characterised by different substituents, both aromatic and aliphatic, at the *N*-1 position of the thiouracil core.

Due to the good yields and easy work-up procedures observed in the previous conventional synthesis of **44-48**, application of the 3-step synthetic pathway to the parallel synthesis of these "first generation" analogues was planned.

Subsequent *in vitro* biological evaluation of this collection of compounds for their inhibitory activity against SIRT1 and SIRT2 was also planned using a fluorescence-based assay kit (*Fluor de Lys*™).[105] Finally, it was decided that the most potent inhibitors would be tested for their capacity to inhibit selectively SIRT1 and SIRT2 in cells, leading to an increase in the levels of *in vivo* sirtuin targets, such as p53 (SIRT1) and α-tubulin (SIRT2).

Potential rationalisation of the observed SAR by means of computational techniques, such as automated molecular docking and molecular dynamics, was also envisaged. The second objective of these *in silico* studies was the rational design and synthesis of new potent and selective "second generation" cambinol analogues.

2. PARALLEL SYNTHESIS AND BIOLOGICAL EVALUATION OF NEW CAMBINOL ANALOGUES

This chapter describes the parallel synthesis of eleven new cambinol analogues characterised by different mono-substitutions in the phenyl ring of the molecule. Furthermore, the synthesis of four other cambinol analogues bearing different alkyl chains at the *N*-1 position of the thiouracil core will be described. The parallel synthesis approach was based on the synthesis of cambinol previously reported in the literature and successfully applied in the Westwood group.[103] This chapter finishes with a description of the *in vitro* biological evaluation of all fifteen new analogues as SIRT1 and SIRT2 inhibitors, followed by in cell testing of the most potent inhibitors. This work was published as a full article in the *Journal of Medicinal Chemistry*.[106] Spectroscopic and analytical data for all compounds, along with the biology protocols, are reported in **Chapter 6**, part 1.

2.1. Parallel Synthesis of Cambinol Analogues, Preliminary Studies

The synthesis of cambinol **39** was previously reported by Wamhoff and co-workers (**Scheme 2.1**).[104] This synthetic route was successfully applied to the synthesis of five analogues in order to investigate the SAR of cambinol **39** (**Table 1.4.2.1, Introduction**).[103]

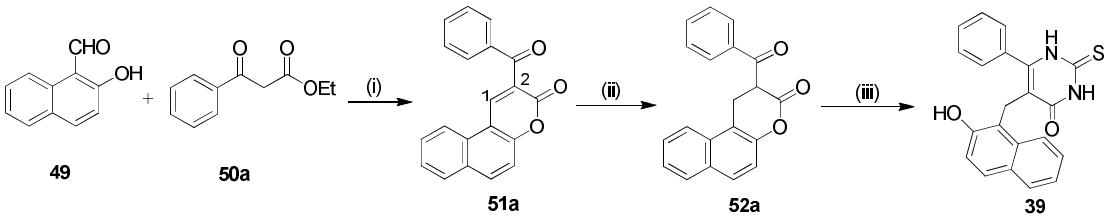

Scheme 2.1 - General procedure applied to the synthesis of five new cambinol analogues **44-48**. *Reagents and conditions*: (i) piperidine (cat.), ethanol, reflux, 2 h; (ii) $NaBH_4$ (1.1 eq.), pyridine, rt, 2 h; (iii) Na, ethanol, thiourea**,** reflux, 18 h. [103,104,106]

Inspired by the results from the analysis of analogues **44-48**, it was decided to apply this three-step procedure to the synthesis of a small collection of new cambinol analogues.

The parallel synthesis was run using a Radleys parallel synthesis apparatus (**Picture 2.1, A**). This apparatus is composed of a classic hot plate stirrer equipped with a chamber which houses 24 vessels. The chamber is closed at the top with a system of 24 small condensers. This allows

24 parallel reactions to be run both at reflux and also at room temperature. The use of an inert atmosphere is also possible through connection of the sealed chamber to a nitrogen line. Furthermore, filtration of the reaction products could be run in parallel using the available Fish Tank (**Picture 2.1, B**).

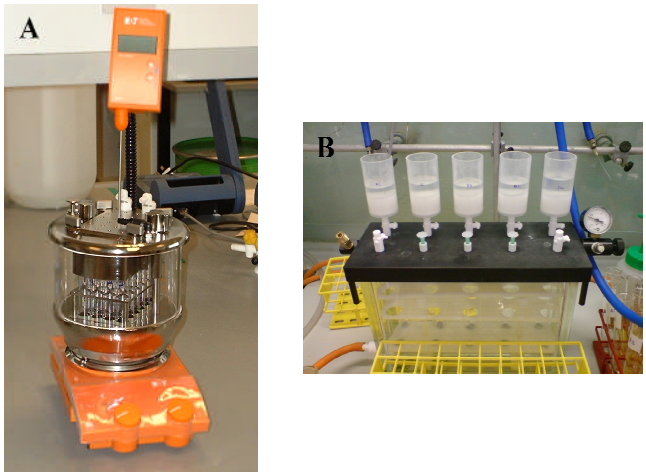

Picture 2.1. An overview of the instruments used for the parallel synthesis of a small collection of new cambinol analogues. **A**, Radleys parallel synthesis apparatus; **B**. Fish tank parallel filtration apparatus.

Before the parallel synthesis reactions were carried out, their feasibility in the Radleys apparatus was tested. In order to do this, four parallel syntheses of cambinol **39** were run in four different vessels of the apparatus. The aim of these preliminary synthetic studies was to determine the reproducibility of the set-up and to assess whether the yield of the same reaction could be influenced by differences in the stirring and/or in the heating at different positions of the chamber.

2.1.1 Step 1: Knoevenagel Condensation

The first step was performed with minimal changes to the original protocol in normal glassware (**Scheme 2.1**). Equimolar amounts of 2-hydroxy-1-naphthaldehyde (**49**) and ethyl benzoylacetate (**50a**) were loaded into different vessels of the parallel synthesis apparatus. The reactants were dissolved in ethanol (4 mL) and piperidine (catalytic, 5 drops) was added. The desired 3-benzoylbenzocoumarin **51a** formed as a yellow precipitate after a few minutes at reflux. All four reactions afforded the desired product **51a** in high yields (**Table 2.1.3**). The yields were similar to those observed in the previous synthetic studies (**Table 2.1.3**).

The purification procedure involved washing the crude precipitates with ethanol after a parallel filtration on the Fish Tank. ^{1}H NMR analysis of the four precipitates suggested that the products obtained from the four reactions were highly pure and could be used in the following step without further purification.

2.1.2 Step 2: Sodium Borohydride Reduction of the 1,2-Conjugated Double Bond

Compound **51a** was then reduced to the corresponding 1,2-dihydro-ketocoumarin **52a** in four different vessels of the parallel synthesis apparatus. The starting material **51a** was dissolved in pyridine (4 mL) and 1.1 equivalents of $NaBH_4$ added. After 2 hours at room temperature, each reaction mixture was poured directly into cold (0 °C) 2M hydrochloric acid which resulted in the formation of the product as a white precipitate. The precipitates were filtered in parallel on the Fish Tank and pyridine was removed by washing with further aliquots of 2M hydrochloric acid. Further purification was carried out by recrystallisation from ethanol.

^{1}H NMR analysis of these products indicated that they were highly pure and could be used in the following step without further purification. However, the yields were lower than those observed in the previous synthetic studies (**Table 2.1.3**). This aspect still remains difficult to rationalise. It may be possible that the recrystallisation procedure was less efficient on the smaller scale adopted in the parallel synthesis.

2.1.3 Step 3: Condensation with Thiourea

It was necessary to make significant changes to the protocol adopted in the last step of the parallel synthesis. Thiourea **53** was first added to the vessels of the parallel synthesis apparatus and NaOEt (2M) in ethanol (prepared previously as a stock solution) was added using a syringe to each of the four vessels employed. The other reactant, ketocoumarin **52a** was then added as a solid and the reaction stirred at reflux for 18 hours. This methodology differed from the previous protocol in that the solution of NaOEt was created as a stock solution in a separate flask and transferred to the four different reaction vessels. Previously, the NaOEt solution was prepared directly in the reaction flask. This change in methodology reflected a desire to minimise the exposure of Na metal to moisture in the air, which could lead to the formation of NaOH.

After 18 hours heating at reflux, the solvent was removed and the residue of each reaction re-dissolved in distilled water. Acidification of the aqueous solutions afforded four different batches of impure cambinol **39** as a white precipitate. Higher levels of purity were obtained after recrystallisation from hot ethanol. The yields (**Table 2.1.3**) were slightly lower than those observed in the synthesis carried out in normal glassware. This fact may be explained by difficulties in stirring and variations in temperature across the plate of the parallel synthesis apparatus, as well as the scale of the recrystallisation.

Table 2.1.3 - Comparison of the yields observed in the three steps of the synthesis of cambinol **39** in the parallel synthesis apparatus (positions A6, B5, C2 and D1 of the Radleys apparatus) with those observed in the previous synthetic studies (normal glassware).

Position	Step i (51a)	Step ii (52a)	Step iii (39)
A6	79	55	32
B5	75	61	46
C2	76	56	43
D1	80	58	42
normal glassware	86	95	51

To further confirm the successful synthesis of cambinol **39**, one of the four new batches obtained in these preliminary studies was recrystallised by slow evaporation from ethanol. The new crystals were suitable for X-ray analysis and structure determination. **Figure 2.1.3** shows the crystal structure of cambinol **39** obtained.

A molecule of ethanol was present in the unit cell. Interestingly, this crystal structure was characterised by a pseudo-eight member ring formed by an intramolecular bond between the phenolic hydrogen bonded to *O*-15 and the ketone functionality of the thiouracil core (*O*-4). Furthermore, the phenyl ring at C6 was twisted out of the plane of the thiouracil core of **39**.[106]

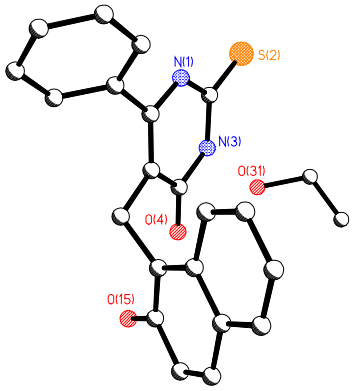

Figure 2.1.3 - Structure of cambinol **39** determined by X-ray crystallography. Crystallisation was carried out by slow evaporation from ethanol and the unit cell contains one molecule of ethanol.[106]

It was concluded that, despite a small decrease in the average yield observed in steps 2 and 3 of the parallel synthesis of cambinol **39**, this approach was applicable to the parallel synthesis of a small collection of cambinol analogues.

2.2 Parallel Synthesis

Encouraged by the relatively high yields observed and the manageable work-up over the three steps, it was decided to attempt the parallel synthesis. Based on the initial SARs (**Introduction, Table 1.4.2.2**) and the commercial availability and prices of the ethyl benzoyl acetate starting materials **50**, it was decided to focus our efforts on introducing different substituents, both with electron-withdrawing and electron-donating properties, at the different positions of the phenyl ring of cambinol **39**. Secondly, based on known SAR data (**Chapter 1, Section 4.2**) and the commercial availability of different *N*-substituted thioureas, the synthesis of a series of *N*-1 substituted cambinol analogues was planned.

2.2.1 First Step: Knoevenagel Condensation

In the first step, 23 analogues of ethyl benzoyl acetate (**R_1, 50 c-y**), differently substituted at the various positions of the phenyl ring, were mixed with 2-hydroxy-napthaldehyde **49** in different vessels of the parallel synthesis apparatus (**Scheme 2.2.1**).[106] Ethanol was added, followed by

piperidine, and the reaction stirred under reflux for 2 hours (METHOD A). Twenty-two reactions out of twenty-three afforded the desired products in a wide range of yields (45-98%, **Table 2.2.1**). The products were obtained in high purity after filtering and washing with ethanol. A low yield was observed for the furyl substituted ketocoumarin **51x**, whereas the only product which was not observed was the pyridyl-ketocoumarin **51y**.

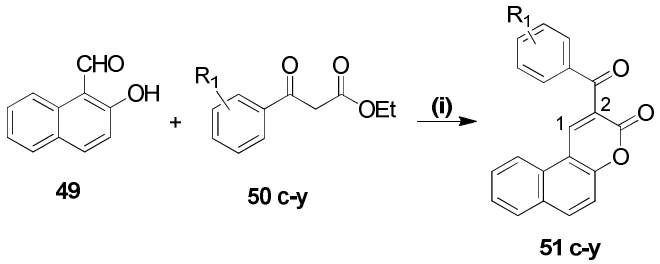

Scheme 2.2.1 - Step 1 of the parallel synthesis of new cambinol analogues. *Reagents and Conditions*: (i) ethanol (4 mL), piperidine (5 drops), reflux, 2 h.[106]

The variability in the observed yields can possibly be explained by the differences in solubility of the products in ethanol. Thus, during the parallel filtration and ethanol washing, different amounts of the products may have dissolved in the ethanol aliquots depending on their solubility. This could be particularly true for the furyl ketocoumarin **51y**. Furthermore, it seems likely that the differences in the yields also reflect the different reactivity of the ethyl benzoylacetate starting materials **50c-y** employed.

Analysis of the ^{1}H NMR spectra associated with the products formed from all the reactions clearly showed the presence of ten aromatic protons as expected when mono-substituted ethyl benzoyl acetate starting materials were being used. In addition, and of importance for confirming the formation of the desired ketocoumarins, was the presence in all the ^{1}H NMR spectra of a singlet which integrated as one proton corresponding to the H-1 proton of the lactone ring. The chemical shifts observed for this signal were between 8.89 (**51w**) and 9.64 ppm (**51r**) (**Table 2.2.1**).

Further characterisation by ^{13}C NMR, [^{1}H-^{1}H] COSY, [^{1}H-^{13}C] HSQC and HMBC, and IR spectroscopy was carried out on five of the new ketocoumarins in order to assign all proton and carbon signals. Although most of the other products had not been previously reported in the literature, they were characterised only by Mp, ^{1}H NMR and LRMS. Due to the library nature of our synthesis, this choice was based on the *Journal of Combinatorial Chemistry* instructions for authors.[107]

Table 2.2.1 - Yields observed for products **51d-y** in the first step of the parallel synthesis. Compound **51c** was resynthesised as control. Chemical shift values for the diagnostic singlet derived from the H-1 proton are listed.[106]

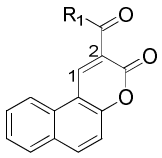

51 c-y

Compound	R_1	Yield (%)	Chemical shift H-1 (ppm)
51c	*p*-Br-Ph	93	8.98
51d	*o*-F-Ph	86	9.08
51e	*m*-F-Ph	79	8.98
51f	*p*-F-Ph	84	8.95
51g	*o*-Cl-Ph	83	9.23
51h	*m*-Cl-Ph	87	8.98
51i	*p*-Cl-Ph	74	8.97
51j	*o*-Br-Ph	76	9.27
51k	*m*-Br-Ph	83	8.98
51l	*o*-I-Ph	80	9.29
51m	*m*-I-Ph	80	8.97
51n	*p*-I-Ph	98	8.97
51o	*o*-CF_3-Ph	70	9.34
51p	*m*-CF_3-Ph	83	9.06
51q	*p*-CF_3-Ph	77	9.00
51r	*o*-NO_2-Ph	98	9.64
51s	*m*-NO_2-Ph	80	9.15
51t	*p*-NO_2-Ph	80	9.15
51u	*o*-CH_3-Ph	79	9.02
51v	*m*-CH_3-Ph	66	8.91
51w	*p*-CH_3-Ph	62	8.89
51x	2-Furyl-	45	8.95
51y	2-Pyridyl-	Failed	-

2.2.2 Second Step: Reduction at the C1-C2-Double Bond of 51c-x

In the second step of the parallel synthesis, selective reduction of the 1,2-conjugated double bond of the twenty two ketocoumarins (**51c-x**) afforded sixteen new 1,2-dihydroketocoumarins (**52c-f, h-i, k, m-n, p-q, s-w**) in a range of different yields (35-95%, **Table 2.2.2**).[106] The starting materials (**51c-x**) were loaded into the different vessels and dissolved in pyridine (4 mL). $NaBH_4$ was added in one portion and the reactions stirred at room temperature for

2 hours (METHOD B, **Scheme 2.2.2.1**). The products precipitated after pouring the reaction mixtures into cold 2M hydrochloric acid solution. After filtration of the crude precipitates, the products were obtained in high purity (as assessed by ^{1}H NMR analysis) after recrystallisation from hot ethanol.

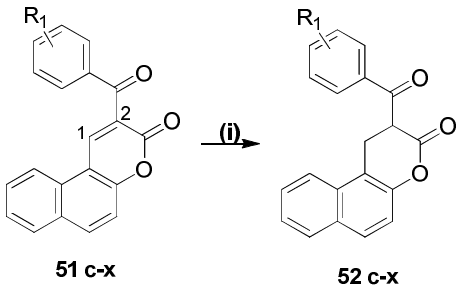

Scheme 2.2.2.1 - Step 2 of the parallel synthesis of new cambinol analogues. *Reagents and Conditions*: (i) $NaBH_4$ (1.1 eq), pyridine (4 mL), 2 h, rt.[106]

As with the starting materials (**51d-x**), all spectra of the new products were characterised by the presence of ten aromatic protons. Two doublets of doublets, each integrating as one proton, corresponding to the new diastereotopic protons at the H-1 position, were now observed between 4.00 and 3.50 ppm (**Table 2.2.2**). In the ^{1}H NMR spectra of the products, the H-2 proton was found at approximately 4.70 ppm (**Table 2.2.2**). The rules of the *Journal of Combinatorial Chemistry* were again applied to the characterisation of the new compounds.[107]

The wide range of yields observed in this reaction (**Table 2.2.2**) can possibly be rationalised with the parallel recrystallisation adopted for the purification. It is possible that the different products exhibit variations in solubility in the solvent used for the recrystallisation (ethanol).

The selective reduction of the conjugated double bond (1,4-reduction) over the ketone functionality (1,2-reduction) can be rationalised by the presence of two electron-withdrawing groups attached to C-2 in **51**. This structural aspect renders the C-1 position particularly activated to attack by the hydride reducing species **60** and makes it competitive with attack at the highly electrophilic ketone functionality (**Scheme 2.2.2.2.A**). The absence of an over-reduced product resulting from additional reduction of the C-2 ketone can be explained by the use of pyridine as the solvent (**Scheme 2.2.2.2.B**). After reduction of the 1,4-conjugated double bond of **51**, the aprotic solvent pyridine is proposed to preserve the resulting enolate **51'**. The acidic work up provides a source of protons to convert enolate **51'** to the ketone **52**. Thus the ketone functionality is regenerated when the reaction is quenched, without any further possibility for this group to be reduced to an alcohol. In the presence of a protic solvent

(**Scheme 2.2.2.2.C**), it would be possible for the solvent to act as a source of protons (**51'**), generating the ketone **52,** which would subsequently be reduced to the alcohol **61**.

Table 2.2.2 - Yields observed for the products of the second step of the parallel synthesis. Chemical shift values for protons H-1 and H-2 are listed.[106] Compound **52c** was resynthesised as a control.

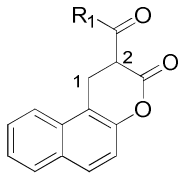

52 c-x

			Chemical Shift (ppm)		
Compound	**R_1**	**Yield (%)**	**H-2**	**1 × H-1**	**1 × H-1**
52c	*p*-Br-Ph	93	4.74	3.83	3.72
52d	*o*-F-Ph	40	4.74	3.76	3.64
52e	*m*-F-Ph	62	4.75	3.84	3.62
52f	*p*-F-Ph	71	4.80	3.78	3.59
52g	*o*-Cl-Ph	[a]	-	-	-
52h	*m*-Cl-Ph	85	4.74	3.83	3.62
52i	*p*-Cl-Ph	90	4.75	3.83	3.61
52j	*o*-Br-Ph	80[b]	4.77	3.59	3.77
52k	*m*-Br-Ph	90	4.74	3.83	3.62
52l	*o*-I-Ph	[a]	-	-	-
52m	*m*-I-Ph	90	4.73	3.82	3.61
52n	*p*-I-Ph	85	4.73	3.82	3.61
52o	*o*-CF_3-Ph	82[b]	4.49	3.82	3.61
52p	*m*-CF_3-Ph	95	4.79	3.86	3.64
52q	*p*-CF_3-Ph	89	4.79	3.85	3.64
52r	*o*-NO_2-Ph	[a]	-	-	-
52s	*m*-NO_2-Ph	92	5.51	3.80	3.64
52t	*p*-NO_2-Ph	88	4.78	3.85	3.66
52u	*o*-CH_3-Ph	78	4.69	3.79	3.56
52v	*m*-CH_3-Ph	35	4.81	3.83	3.61
52w	*p*-CH_3-Ph	60	4.80	3.84	3.60
52x	2-Furyl-	60[b,c]	4.63	3.81	3.62

[a] Product not recovered when the reaction was run in parallel.
[b] Yields refer to the same reaction re run in normal glassware.
[c] Conversion judged by ^{1}H NMR spectroscopy.

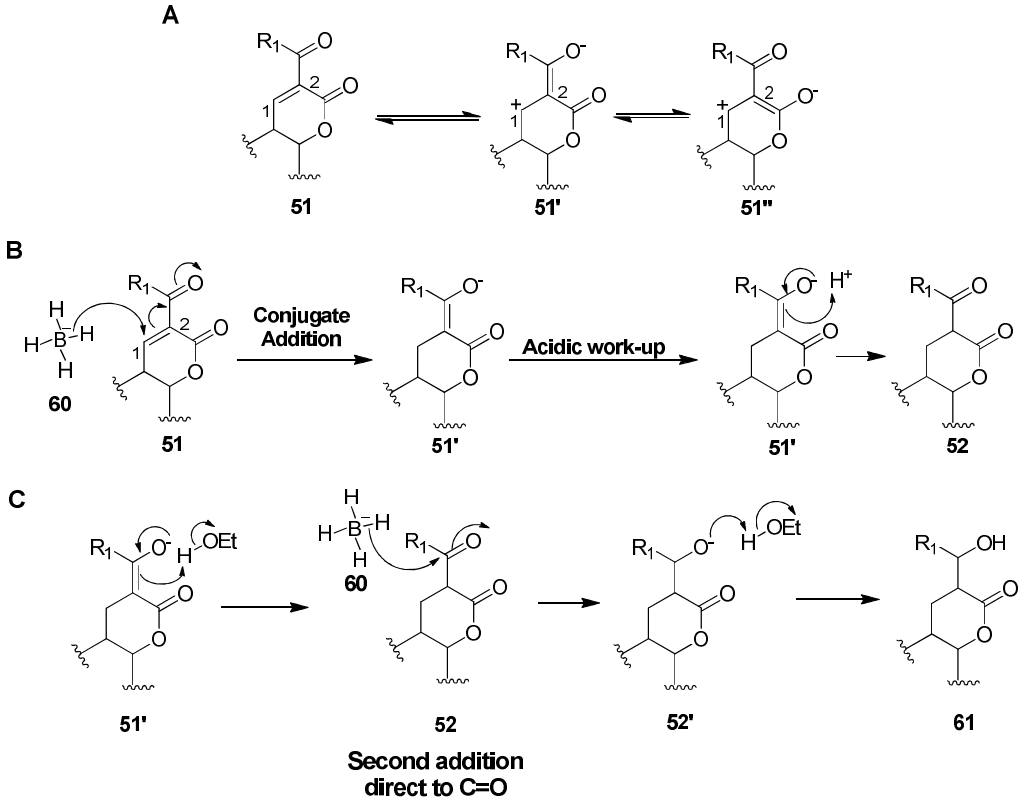

Scheme 2.2.2.2 A, B - A rationalisation of the selectivity observed in the second step of the parallel synthesis is provided. **C**, an explanation of the absence of over-reduction at the ketone carbonyl functionality is shown.

2.2.3 Second Step: Conjugated Reduction of the *ortho*-Substituted Ketocoumarins 51j, o and x.

In the second step of the parallel synthesis, reduction of the double bond in the *ortho*-substituted ketocoumarins was successful only for the starting materials **51d** and **51u**. In all other cases no product precipitate was observed after the acidic work-up. In the ^{1}H NMR spectra of the crude reaction mixtures the three main expected diagnostic signals for compounds **52g, j, l, o, r** and **x** could not be observed (**Table 2.2.2**). At first, these observations suggested that the reaction had not given the desired products.

The lack of a rational explanation for this failure prompted us to investigate these reactions further. It was decided to repeat the attempted synthesis in normal glassware. Three ketocoumarins (**51j, o, x**) were randomly selected and treated with $NaBH_4$ in pyridine at room temperature for 2 hours (METHOD C). After work up, a yellow solid was obtained for each.[106]

For ketocoumarin **51x**, it was discovered that the expected reduced product **52x** had formed with 60% conversion of **51x** to **52x**, as judged by analysis of the ^{1}H NMR spectrum of the crude reaction mixture. In fact, attempts to purify **52x** from traces of starting material by column chromatography were not successful. At this time it is difficult to rationalise the failure of this reaction during the parallel synthesis experiments.

^{1}H NMR analysis of the crude reaction mixtures obtained from reduction of ketocoumarins **51j** and **51o** indicated that the desired products **52j** and **52o** had formed in very low yields (**Figure 2.2.3.1**). Their formation was detected through the presence in the ^{1}H NMR spectrum of the three main diagnostic signals (double of doublets) arising from the C-1 and C-2 protons. Finally, ^{1}H NMR spectra also indicated the presence of a major product. This was characterised by the presence of 10 aromatic protons. Two aliphatic protons were present, as suggested by a broad singlet at 3.70 ppm integrating to 2 protons.

Assignment of the structure of both new products was carried out by means of [^{1}H-^{1}H] COSY, [^{1}H-^{13}C] HSQC and HMBC spectroscopy. Structures **52j'** and **52o'** (**Figure 2.2.3.1**) were assigned to the major species detected in the ^{1}H NMR spectra, whereas structures **52j**, **j''** and **52o**, **o''** were assigned to the other minor components present in the mixture.

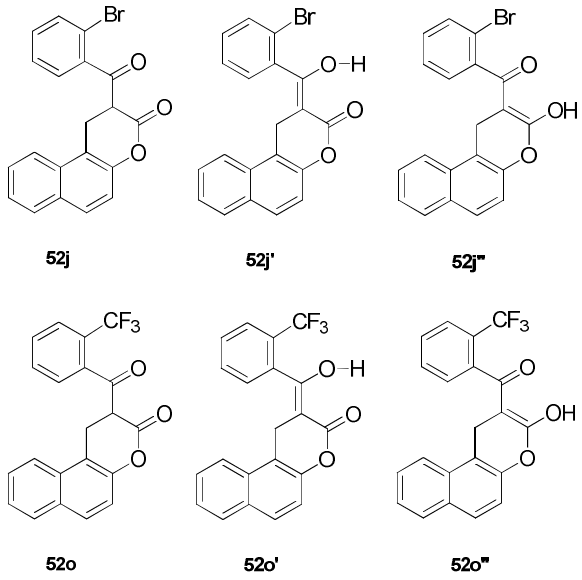

Figure 2.2.3.1 - Structures of products obtained from the reduction of ketocoumarins **51j** and **51o** with $NaBH_4$ in pyridine. Compounds **52j'** and **52o'** were the major products, whereas compounds **52j-j''** and **52o-o''** were present in small amounts.

Thus, **52j** and **o** appeared in the ^{1}H NMR spectrum mainly as the enol tautomers **52j'** and **52o'**. For this reason, successful formation of the desired reduced products could not be determined easily from analysis of the crude ^{1}H NMR spectra obtained during the parallel synthesis. To probe the successful formation of compound **52j'**, further X-ray crystal structure determination was carried out (**Figure 2.2.3.2**). Furthermore, it was decided to condense **52j'** with thiourea in order to form the corresponding cambinol analogue. The result of this experiment will be described in **Section 2.2.5**.

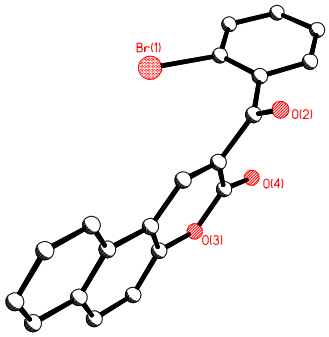

Figure 2.2.3.2 - Crystal structure of **52j'** determined by X-ray crystallography. Crystallisation was carried out by slow evaporation from ethanol.

Another interesting aspect is represented by the fact that when the *ortho* substituents were either fluorine (**51d**) or methyl (**51u**), the parallel synthesis reduction afforded the expected products and they appeared in their keto forms in the ^{1}H NMR experiments. The difference between the ^{1}H NMR spectra of **52d** and **52u** compared with the ^{1}H NMR spectra of **52j'** and **52o'** can be explained by the size of the substituents at the *ortho* position of the phenyl ring. For small substituents (eg. fluoro or methyl), in the ^{1}H NMR experiments the equilibrium between the keto form and the two possible enol forms lies towards the keto form, with no traces of the two enol forms detectable. For larger substituents, (eg. bromine or trifluoromethyl), the equilibrium lies towards one of the enol forms. For **52j'** or **52o'** it could be possible that the enol form is favoured in solution because it allows minimisation of the electrostatic repulsion existing between the large o*rtho* substituents (bromine or trifluoromethyl) and the ketone functionality.

2.2.4 Last step: Condensation of Ketocoumarins 52 with Thiourea 53

Starting materials of general structure **52** and thiourea **53** were poured into different vessels of the parallel synthesis apparatus and 2M NaOEt, previously prepared as a stock solution, was

added using a glass syringe (**Scheme 2.2.4.1**). After 24 hours heating at reflux, the solvent was evaporated in parallel and the residue of each reaction re-dissolved in water. Acidification of this aqueous solution afforded a series of precipitates which were analysed by ^{1}H NMR spectroscopy (METHOD D). These spectra clearly suggested that the formation of the desired products had occurred in most of the condensations.

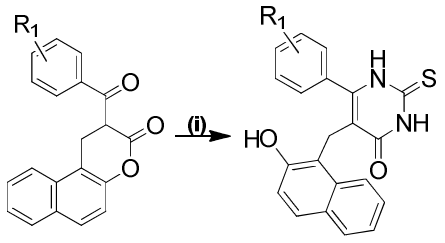

52 **62-76**

Scheme 2.2.4.1 - Step 3 of the parallel synthesis of new cambinol analogues. *Reagents and conditions*: (i) Na, EtOH, thiourea (**53**), 18 h, reflux.[106]

All the diagnostic signals of the expected products **62-76** were clearly detectable in the ^{1}H NMR spectrum of the crude precipitates (**Table 2.2.4**). Synthesis of analogue **46** was repeated as a control. Purification of all crude reaction mixtures by column chromatography was carried out. This method of purification afforded 13 desired products from the 16 reactions (**Table 2.2.4**). The yields observed after column chromatography were significantly lower than those observed when the synthesis of cambinol **39** was carried out in normal glassware (**Table 2.1.3**). Furthermore, for some of the compounds the purification was not optimal, as products **64, 68** and **72** co-eluted with different impurities. Thus, for these compounds determination of the yields and full spectroscopic characterisation was not possible.

Interestingly, purification by column chromatography helped to clarify the possible reasons for the low yields by enabling the identification of side-products in these reactions. Two main side-products were always eluted and separated. ^{1}H NMR, ^{13}C NMR and mass spectrometric analysis showed that the less polar compound was the reported compound commonly named as splitomicin **21**,[91] whereas the more polar was the corresponding substituted benzoic acid **78**.[108] Thus, this observation supported a competing degradation of the starting material **52** into these two products. It is possible that nucleophilic attack at the carbonyl ketone group of **52** by OH^{-} leads to a retro-Claisen reaction (**79**, **Scheme 2.2.4.2**). Acidic work-up (**80**) led to generation of splitomicin **21**. Due to time constraints, an accurate quantification of the amount of the two degradation products **21** and **78** in the different reactions was not carried out.

Table 2.2.4. Yields observed in the last step of the parallel synthesis.[106]

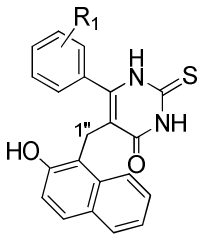

46, 62-76

Compound	R_1	Yield (%)	Diagnostic Signals (H-1'')
46	*p*-Br	30	3.91
62	*o*-F	10	3.90
63	*m*-F	10	3.92
64	*p*-F	-	-
65	*m*-Cl	32	3.92
66	*p*-Cl	18	3.91
67	*m*-Br	26	3.91
68	*m*-I	-	-
69	*p*-I	22	4.08
70	*m*-CF_3	12[a]	3.93
71	*p*-CF_3	25	3.95
72	*m*-NO_2	-	-
73	*p*-NO_2	18[a]	4.13
74	*o*-CH_3	57	3.88
75	*m*-CH_3	51	3.91
76	*p*-CH_3	50	3.89

[a] Percentage of conversion determined by analisis of the crude ^{1}H NMR integration value. Purification for these compounds was not succesfull and no *in vitro* biological experiment was run.

It is possible that the hydroxide responsible for this degradation reaction derives mainly from the formation of the expected products. Alternatively, the sodium hydroxide may come from reaction of sodium with the moisture in air. Despite all the efforts to guarantee dry conditions (dry solvents, glassware dried overnight, inert gas atmosphere), no significant improvement in the yields was achieved.

Secondly, it may also be possible that the presence of an electron-withdrawing group on the phenyl ring of the starting materials **52** enhances the electrophilic nature of the ketone functionalities, thus promoting the degradation reaction proposed. Consistent with this, higher

yields of the products were observed when this reaction was performed on ketocoumarins bearing electron-donating substituents on the phenyl ring (**52u-w, Table 2.2.2 and 2.2.4**).

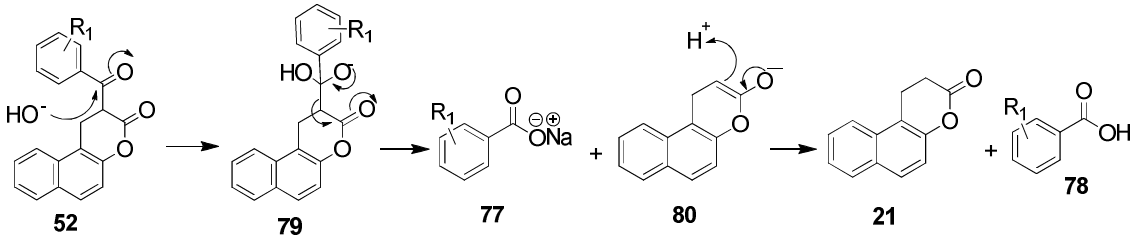

Scheme 2.2.4.2 - Possible mechanism for the degradation of the 1,2-didroketocoumarins **52** into splitomicin **21** and benzoic acid analogues **78** under the basic conditions used for the final step of the parallel synthesis.

2.2.5. Synthesis of the *ortho*-bromo Cambinol Analogue 81

To provide further evidence to support the successful synthesis of compound **52j'**, it was decided to react **52j'** with thiourea **53** in normal glassware, following the methodology reported in the previous synthetic studies. The new cambinol analogue substituted at the *ortho* position of the phenyl ring **81** was formed in 41% yield (METHOD E, **Scheme 2.2.5**). Its structure was confirmed by ^{1}H NMR and ^{13}C NMR spectroscopy and 2-dimensional NMR experiments.[106]

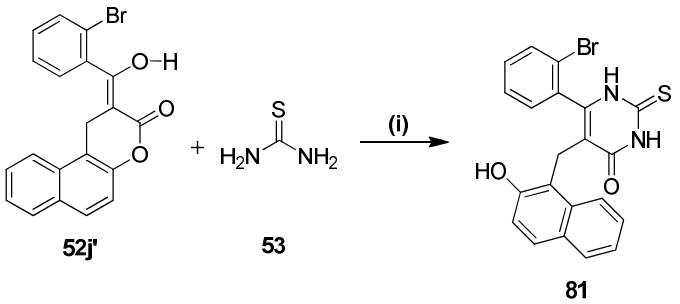

Scheme 2.2.5 - Synthesis of **81** from reduced ketocoumarin **52j'**. *Reagents and conditions:* (i) Na, EtOH, thiourea, 18 h, reflux.[106]

2.2.6 Synthesis of the *N*-1 Substituted Cambinol Analogues

The high level of potency and selectivity shown by compound **47** against SIRT2 (**Table 1.4.2.2, Introduction**) led to an attempt to prepare a series of cambinol analogues characterised by different substituents at the *N*-1 of cambinol. The target compounds were designed depending

on the commercial availability of the corresponding *N*-1 substituted thioureas (**Table 2.2.6**). Therefore, attempts were made to incorporate different aliphatic chains, both saturated (Et, *n*-propyl, *i*-propyl, *n*-butyl and *i*-butyl) and unsaturated (allyl), along with different aromatic substituents (benzyl and phenyl) at the *N*-1 position of the thiouracil core of **39** (**Table 2.2.6)**.[106]

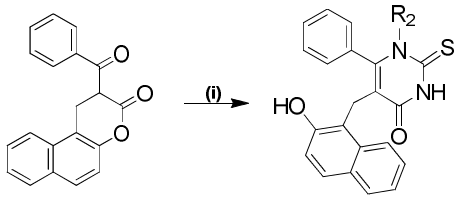

52a **82-89**

Scheme 2.2.6 - Synthesis of *N*-1 substituted cambinol analogues. *Reagents and conditions*: (i) NaOEt (2M), ethanol, *N*-substituted thiourea **55a-h**, 18 h, reflux.[106]

An initial attempt to prepare analogues **82-89** was made using a parallel synthesis approach. Compound **52a** was reacted with a range of commercially available *N*-substituted thioureas (**55a-h, Table 2.2.6**). These reactions proved to be unsuccessful on the small scale adopted for the parallel system. ^{1}H NMR analysis of the crude reaction mixtures suggested that some of the expected compounds had formed in the case of **82**, **83**, **85** and **87**. Column chromatography enabled the isolation of the previously described degradation products splitomicin **21** and benzoic acid **78**. Isolation of the products proved difficult due to the complexity of the crude reaction mixtures.

It was therefore decided to repeat each of these reactions in normal glassware on a larger scale, using 500 mg of **52a** instead of the 100 mg usually employed in the parallel synthesis work. The new analogues bearing at the *N*-1 Et (**82**), *n*-allyl (**87**), *n*-propyl (**83**) and *n*-butyl (**85**) were obtained in low yields (7-20%, METHOD F, **Table 2.2.6**).

Unfortunately, the synthesis of the other target compounds **84, 86, 88** and **89** was unsuccessful. No precipitate was observed after acidification of the crude reaction mixture. Careful analysis of the organic (DCM) phase derived from extraction of the acidic aqueous layers did not show the presence of the diagnostic peaks for these compounds. Again, the main constituents of these mixtures were splitomicin **21**, benzoic acid **78** and the excess of substituted thioureas **55**.

The failure of these reactions may be due to the steric hindrance exerted by the bulky substituents of the *N*-substituted thiourea precursors (R_2 = *iso*-prop, *iso*-butyl, phenyl and

benzyl, **Table 2.2.6**). The size of these substituents may represent an obstacle for the first nucleophilic attack to occur at the ketone functionality of **52a**. This raises the interesting question of why, if the *N*-substituted nitrogen of thioureas **55a-h** cannot react at the ketone of **52a**, does the reaction apparently not occur *via* the primary NH_2 of the *N*-substituted thiourea to form the regioisomer **82'-89'**(**Figure 2.2.6**). Careful analysis of the ^1H NMR of the crude reaction mixtures derived from the failed reactions suggested that these regioisomers had not formed during the reaction and **82'-89'** were not isolated following column chromatography.

Table 2.2.6. - *N*-1 substituted thioureas used and yield observed for the synthesis of the corresponding cambinol analogues substituted at *N*-1.[106]

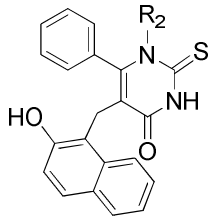

82-89

***N*-substituted thiourea**	**R_2**	**Analogue**	**Yield (%)**
55a	Et	**82**	20
55b	*n*-Pr	**83**	10
55c	*iso*-Pr	**84**	-
55d	*n*-Bu	**85**	7
55e	*iso*-Bu	**86**	-
55f	Allyl	**87**	15
55g	Phenyl	**88**	-
55h	Benzyl	**89**	-

- Synthesis failed.

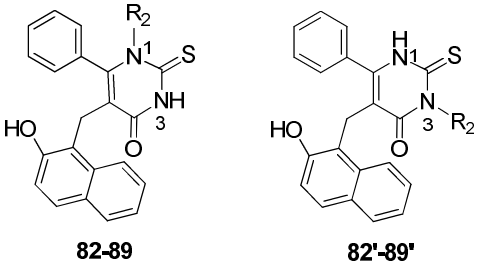

82-89 **82'-89'**

Figure 2.2.6 - Two possible regioisomers **82-89** and **82'-89'** which could potentially be formed when the *N*-monosubstituted thiourea is condensed with the reduced ketocoumarin **52a**.

2.2.7. Assignment of the Structure of Final Compounds 82, 83, 85 and 87

Due to the lack of an X-ray crystal structure, a series of spectroscopic studies was carried out in order to establish the regiochemistry of the new formed cambinol analogues **82, 83, 85** and **87**. The main aim was to ascertain that the new aliphatic substituents were, as required, at the *N*-1 position of the thiouracil core. During the previous MSc studies, this analysis was carried out by means of [^{1}H-^{13}C] HMBC experiments on analogue **47**.[103]

In the ^{1}H NMR spectra of compounds **82**, **83**, **85** and **87** the resonance corresponding to the CH_2 of the new aliphatic chain next to the *N*-1 always appeared as a broad signal integrating for two protons (4.00-3.80 ppm). Furthermore, this feature represented a problem in establishing the regiochemistry of this reaction. In fact, in the [^{1}H-^{13}C] HMBC spectra of these molecules no cross-peaks between these protons (C-1''') and the neighbouring carbons could be observed.[106]

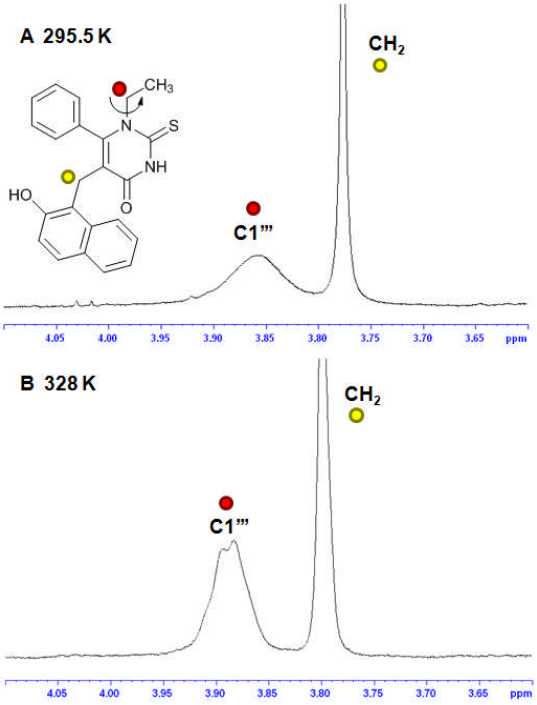

Figure 2.2.7.1 - Expansion of the region 4.10-3.60 ppm of the ^{1}H NMR spectrum of compound **82** at different temperatures (**A**, 295.5 K; **B**, 328 K) showing the broad signal derived from the protons at C-1''' (red) of the ethyl chain of **82**. **A**) At room temperature, the expected quartet appeared as a broad signal. **B**) In an analogous experiment run at 328 K, the expected multiplicity could be better appreciated. It was not possible to improve the quality of the shape of this signal further.[106]

The unexpected lack of multiplicity for the peak corresponding to the methylene group (C-1''') of the alkyl chain at *N*-1 could be rationalised by the restricted rotation about the CH_2-*N*-1 bond,

due to its proximity to the phenyl ring. High temperature ^{1}H NMR experiments at 328 K were run on **82** by Dr Tomas Lebl at the Univeristy of St Andrews with the goal of causing the signal corresponding to the C-1''' protons to sharpen, allowing better observation of the expected multiplicity (quartet, **Figure 2.2.7.1**). By this approach, correlations between the H-1''' proton and the carbons C-5 and C-2 could be detected in the corresponding [^{1}H-^{13}C] HMBC spectrum.

As shown in **Figure 2.2.7.2**, this was in fact the case and when the [^{1}H-^{13}C] HMBC experiment for **82** was repeated at high temperature (328 K), with cross peaks being observed for the C-1''' methylene protons of the ethyl chain, thus proving that compound **82** had the expected regiochemistry. In more detail, the pseudo-quartet corresponding to the two protons of carbon C-1''' in the ethyl chain exhibited only two cross peaks as expected. The first cross peak derived from the interaction with the carbon of the thiocarbonyl functionality in the thiouracil ring (175 ppm). The second arose from the interaction with a quaternary carbon at 152 ppm. The assignment of the signal at 152 ppm as corresponding to C-6 was also supported by an observed cross peak resulting from coupling to the two protons at the C-2' and C-6' of the phenyl ring (7.00 ppm) to the corresponding carbon atom at 152 ppm. A signal in this region at 153 ppm complicated the analysis but has been assigned to the quaternary carbon bearing the hydroxy functionality of the naphthol ring (C-2").[106] The same correlations were exhibited by the allyl methylene protons of **87** in the [^{1}H-^{13}C] HMBC experiment run at higher temperature (328 K), thus proving the same regiochemistry observed for **82** (**see supplementary**).

For analogues **83** and **85**, these correlations could not be observed in the [^{1}H-^{13}C] HMBC experiments run at high temperature. The fact that the methylene protons next to the *N*-1 appeared in the ^{1}H NMR spectra as broad singlets was used as a diagnostic element to confirm the proposed regiochemistry. [106] Further proof will come from the full characterisation of the *N*-3 substituted cambinol analogues (**Chapter 4**).

This regiochemistry was rationalised with the attack of the most nucleophilic secondary nitrogen of the *N*-substituted thioureas (**55a, b, d and f**) to the most electrophilic ketone carbonyl functionality of **52a**.

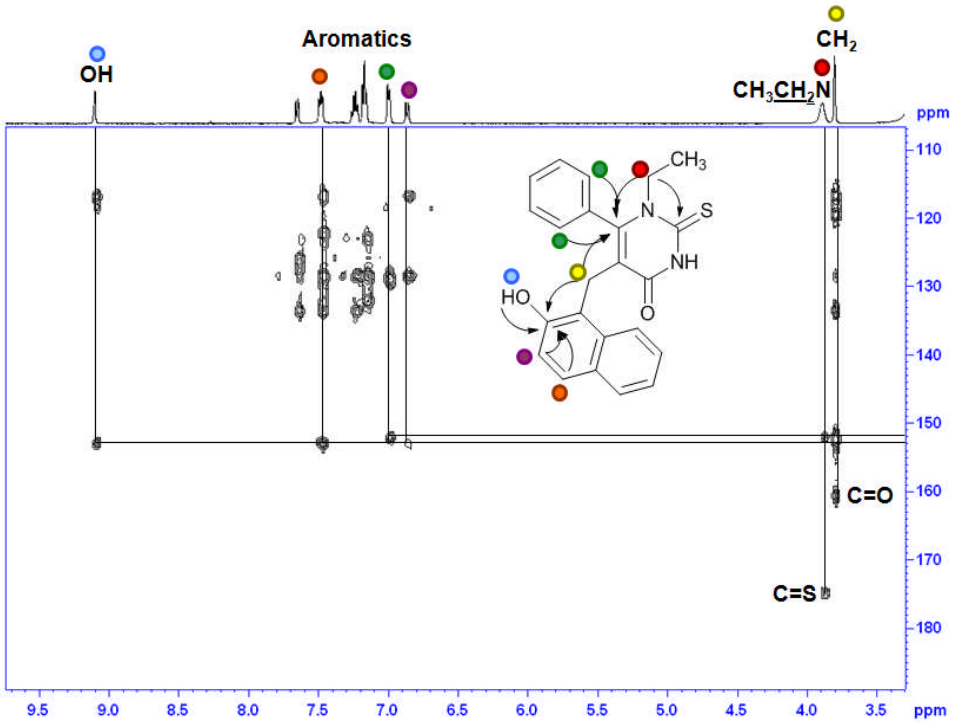

Figure 2.2.7.2 - Expansion of the [^{1}H-^{13}C] HMBC spectrum of compound **82**. Correlations between the protons of the C-1''' of the ethyl group (brs, 3.90 ppm, red) with the thiocarbonyl functionality (175 ppm) and the quaternary carbon at 152 ppm are shown.[106]

2.3. *In vitro* Biological Evaluation

The initial aim of this study was to explore the chemical space around the core structure of cambinol **39** and further improve the SAR data associated with this type of molecule. After the successful synthesis of sixteen new cambinol analogues (**62-63, 65-67, 69-71, 73-76** and **81-83, 85** and **87**) the following stage was to test these compounds for their *in vitro* inhibitory activity against SIRT1 and SIRT2. Initially, compounds were screened at a concentration of 60 μM against both enzymes and IC_{50} values were determined for compounds that exhibited higher than 60% inhibition at 60 μM.[106]

For the most active compounds (IC_{50} < 20µM) it was planned to investigate their activity in cells through the detection of the levels of important sirtuin target protein, such as acetylated-p53 (SIRT1) and acetylated-tubulin (SIRT2). These experiments were also important to assess other properties, such as cell permeability and cytotoxicity.

2.3.1 Inhibition of SIRT1 and SIRT2 by the Cambinol Analogues 62-63, 65-67, 69-71, 73-76

Only the new cambinol analogues synthesised in the parallel synthesis, which exhibited a good level of purity (**62-63, 65-67, 69, 71, 74-76** and **81**) were screened against SIRT1 and SIRT2. IC_{50} values were calculated for compounds with greater than 60% inhibition at 60μM (**Table 2.3.1**). These studies were run in collaboration with Dr Anna McCarthy and Dr Sonia Lain at the Medical School of the University of Dundee.

SIRT1 and SIRT2 inhibition assays were carried out using BIOMOL SIRT1 and SIRT2 *Fluor de lys*™ fluorimetric activity assays kits.[105] This assay is commercially available and well established in the sirtuin inhibitor area. In brief, the level of deacetylase activity is determined for recombinant human SIRT1 and SIRT2. The substrate for the deacetylation is part of the human p53 peptide (5aa, 317-320 for SIRT1, 379-382 for SIRT2). The assay's fluorescence signal is generated in proportion to the amount of deacetylated substrate produced by the activity of the two enzymes. After incubation with a potential inhibitor, the greater the signal registered, the greater the quantity of deacetylated peptide present and the lower the inhibitory effect of the compound on the enzyme.

Cambinol **39** and our previously tested new sirtuin inhibitors **46** and **47** were used as controls in these experiments. The percentage of inhibition detected for **39** was similar to that reported in the literature, as well as the IC_{50} values against the two enzymes (41 *vs* 56 μM for SIRT1 and 48 *vs* 59 μM for SIRT2).[18] The selective SIRT1 inhibitor **46** exhibited an IC_{50} of 12.5 ± 2 μM against the same enzyme, whereas **47** showed an IC_{50} of 20.1 ± 5 μM against SIRT2.

In this series of compounds, replacement of the *p*-bromo-substituent in **46** with chlorine, iodine or trifluoromethyl (**66, 69** and **71**, respectively) led to a significant decrease in activity against both enzymes. The position of the bromine atom in **46** appeared to be critical for activity against SIRT1, as this was lost when the bromine was placed at either the *o*- or *m*-position of the phenyl ring (analogues **81** and **67**). None of these compounds showed significant activity against SIRT2.

Similarly, incorporation of a *m*-chloro-substituent in analogue **65** resulted in reduced activity against SIRT1 and SIRT2. Interestingly, the use of a fluorine substituent led to analogues **62** and **63** which have comparable activity to **39** against SIRT1. The presence of fluorine at the

different positions of the aromatic ring was thought to reduce electron density without increasing steric bulk. Comparison of the data for compounds **62** and **63** with those of the good and selective SIRT1 inhibitor **46** suggested that the improved activity of the *p*-bromo-analogue **46** results from an increase in additional hydrophobic interactions rather than through a reduction in electron density associated with the aromatic ring. Again, none of these compounds showed inhibition of SIRT2.

Compounds characterised by a methyl substituent in different positions of the phenyl ring of cambinol **(74**, **75** and **76)** were good inhibitors of SIRT1. The IC_{50} recorded were similar to that of cambinol **39**. No activity against SIRT2 was detected for **74**, **75** and **76**.

Table 2.3.2 - Inhibitory activities of compounds of **62-63, 65-67, 69-71, 73-76**. Data are reported as percentage of inhibition at a concentration of 60 μM.[106]

Table 2.3.1

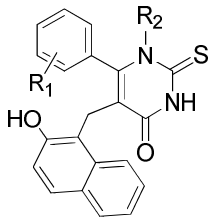

Compound	R_1	R_2	SIRT1[a]	IC_{50}[b](μM)	SIRT2[a]	IC_{50}[b](μM)
39[c]	H	H	59.5 ± 1.1	40.7 ± 11.1	51.9 ± 1.4	47.9 ± 11.7
46[c]	*p*-Br	H	82.3 ± 1.0	12.7 ± 1.9	9.4 ± 0.7	> 90
47[c]	H	Me	29.4 ± 1.3	> 90	80.4 ± 1.1	20.1 ± 5.0
66	*p*-Cl	H	13.7 ± 0.9	-	20.1 ± 1.3	-
69	*p*-I	H	7.7 ± 1.1	-	7.7 ± 1.1	-
71	*p*-CF_3	H	15.1 ± 0.7	-	6.7 ± 0.7	-
81	*o*-Br	H	19.7 ± 0.8	-	-	-
67	*m*-Br	H	4.8 ± 0.8	-	6.6 ± 3.2	-
65	*m*-Cl	H	11.3 ± 0.7	-	7.6 ± 5.8	-
62	*o*-F	H	89.0 ± 1.4	50.0 ± 1.3	19.5 ± 1.1	-
63	*m*-F	H	87.8 ± 1.1	38.3 ± 1.0	52.1 ± 1.3	-
74	*o*-CH_3	H	79.6 ± 1.3	43.0 ± 2.1	29.1 ± 1.7	-
75	*m*-CH_3	H	83.2 ± 4.2	44.2 ± 2.2	12.7 ± 1.8	-
76	*p*-CH_3	H	79.0 ± 1.9	44.5 ± 1.1	13.4 ± 3.2	-

[a] SE, standard error (n = 2).
[b] IC_{50} values were determined for compounds that had over 60% inhibition at 60 μM for SIRT1 and SIRT2 (repeated at least twice).
[c] Controls. - Not determined.

These data suggest that both the position and the size of the substituent in the phenyl ring of cambinol is important for potent and selective inhibition of SIRT1. Thus, a substituent of the same size of bromine at the *para*-position of the phenyl ring may be crucial in increasing the inhibitory potency against SIRT1. Furthermore, substitution of the phenyl ring is not tolerated for SIRT2 inhibition, thus suggesting that the area of the active site where the phenyl ring is accommodated may be smaller in SIRT1 than in SIRT2.

2.3.2 Inhibition of SIRT1 and SIRT2 by the Cambinol Analogues 82, 83, 85 and 87

In our previous studies, compound **47,** containing a methyl substituent at the *N*-1 of the thiouracil ring, showed good *in vitro* inhibitory activity towards SIRT2 (88.2%). The IC_{50} value observed for **47** was 20.1 ± 5 μM. The inhibitory activity of **47** against SIRT1 was poor, with an IC_{50} > 90 μM (see **Table 1.4.2.2, Introduction**). These results encouraged us to test the other analogues bearing different aliphatic chains at the same nitrogen of the thiouracil core (**Table 2.3.3**). Again, cambinol **39** and compounds **46** and **47** were used as controls.

In line with the previous observations for **47**, this series of compounds show a selective and relatively potent inhibition of SIRT2 over SIRT1. Interestingly, a progressive improvement in potency against SIRT2 was observed as the *N*-1 chain length increased, culminating in the *N*-1-*n*-butyl analogue **85** being the most potent and selective inhibitor of SIRT2, with an IC_{50} = 1.0 ± 1 μM for SIRT2. This represented a 50-fold improvement in the activity against SIRT2 in comparison with the modest and unselective cambinol **39**. A poor inhibitory activity was observed against SIRT1 for all the four new cambinol analogues **82**, **83**, **85** and **87**.

Thus, the presence of an aliphatic chain on the *N*-1 of the thiouracil of cambinol seems to be crucial for directing the selectivity of these molecules against SIRT2 and increasing their potency against the same enzyme. The length of this aliphatic chain partially correlates with the level of inhibition observed.

Table 2.3.3 - Inhibitory activities of compounds of general structure **82, 83, 85** and **87**. Data are reported as percentage of inhibition at a concentration of 60 μM. [106]

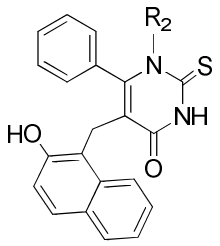

82-87

Compound	R_1	R_2	SIRT1[a]	IC_{50}[b](μM)	SIRT2[a]	IC_{50}[b](μM)
39[c]	H	H	59.5 ± 1.1	40.7 ± 11.1	51.9 ± 1.4	47.9 ± 11.7
46[c]	*p*-Br	H	82.3 ± 1.0	12.7 ± 1.9	9.4 ± 0.7	> 90
47[c]	H	Me	29.4 ± 1.3	> 90	80.4 ± 1.0	20.1 ± 5.0
82	H	Et	31.9 ± 1.4	-	86.8 ± 0.9	10.5 ± 3.1
87	H	Allyl	37.5 ± 0.7	-	88.3 ± 0.9	22.2 ± 0.8
83	H	*n*-Pr	25.0 ± 2.2	-	94.7 ± 0.7	4.8 ± 2.2
85	H	*n*-Bu	16.9 ± 0.9	-	97.6 ± 1.3	1.0 ± 1.1

[a] SE, standard error (n = 2).
[b] IC_{50} were determined for compounds that had over 60% inhibition at 60 μM for SIRT1 and SIRT2 (repeated at least twice).
[c] Controls. - Not determined.

It was surprising to observe that, despite the similar percentages of inhibition observed for **87** and **85** at 60 μM, the IC_{50} calculated for **87** (22 ± 1μM) was higher (4-fold) than that observed for analogue **85 (**4.8 ± 2 μM, **Table 2.3.3**). Due to the same number of carbon atoms in the aliphatic chains of these two compounds, this difference can be rationalised only with the different saturation level of the two chains. Thus, unsaturation of the aliphatic chain of compound **87** reduces its activity, possibly due to increased electron-density in this region and reduced flexibility of the chain.

These data also suggest that a longer aliphatic chain at the *N*-1 position may lead to higher levels of inhibition. Unfortunately, due to the limitation of the previously described synthetic approach, it was not possible to test this hypothesis. Furthermore, longer chains would be expected to be detrimental in terms of solubility.

At this point of the research, it was difficult to rationalise the inhibitory profile of the *N*-1 substituted cambinol analogues **82**, **83**, **85** and **87**. The presence of a hydrophobic channel or a pocket in the active site of SIRT2, which is able to accommodate this chain, was hypothesised.

In an attempt to rationalise the observed selectivity, a series of molecular docking studies of these compounds into the active site of SIRT2 was initiated. These results will be discussed in **Chapter 3**.

2.4 In cell Biological Evaluation

Encouraged by the good results obtained *in vitro*, it was decided to run a series of in cell experiments in order to better assess the activity of the new potent SIRT2 inhibitors **83** and **85**. Furthermore, compound **46**, our previously reported selective SIRT1 inhibitor, was tested for its capacity to regulate the expression of p53 and acetylated p53. All experiments reported in this section were run by Miss Jo Campbell and Mrs Maureen Higgins in the laboratory of Dr Sonia Lain, at the Medical School of the University of Dundee.[106]

2.4.1 Cambinol Analogue 85 Enhances the Levels of Acetylated α-tubulin in H1299 Cells

As SIRT2 inhibition is known to result in hyperacetylation at K49 of α-tubulin, western blot analysis was run to study the acetylation state of this protein in H1299 cells treated with our most active SIRT2 inhibitor **85 (Fig. 2.4.1)**.[18] When H1299 cells were treated with increasing concentration of **85**, only a slight increase in the levels of acetylated α-tubulin was observed across a concentration range of 10-50 μM (**Figure 2.4.1**). Unfortunately, this experiment could not be carried out at higher concentrations, possibly due to toxicity associated with **85**. Despite a slight improvement in the ability of **85** to increase the levels of acetylated α-tubulin in cells compared to **39**, the effect was much less than that expected, considering the 50-fold difference in the IC_{50} between **85** and **39** against SIRT2. Issues related to cell permeability, compartmentalisation and metabolism of this compound probably explain this difference in cells.

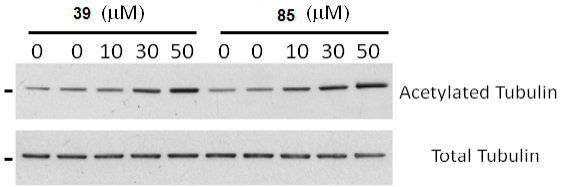

Figure 2.4.1 - Western blot analysis of the levels of acetylated α-tubulin in H1299 cells treated with increasing concentrations of cambinol **39** and analogue **85**. Trichostatin A, a known inhibitor of class I and II HDACs, was added in order to reduce the background effect of these deacetylases. [18,106]

2.4.2 SIRT2 Inhibitor 83 Induced Higher Levels of Acetylated α-tubulin than 46 in H1299 Cells.

A second experiment was performed using the SIRT1 selective inhibitor **46** and the new SIRT2 inhibitor **83** (**Fig. 2.4.2**). As inhibition of SIRT1 does not increase the levels of acetylated α-tubulin, the aim of this experiment was to confirm the selectivity of two of the most active compounds towards SIRT1 and SIRT2 in cells. H1299 cells were treated in parallel with different concentrations of the active inhibitors **46** and **83**. Tubulin was used as a loading control, whereas cambinol **39** represented the positive control (**Figure 2.4.2**).

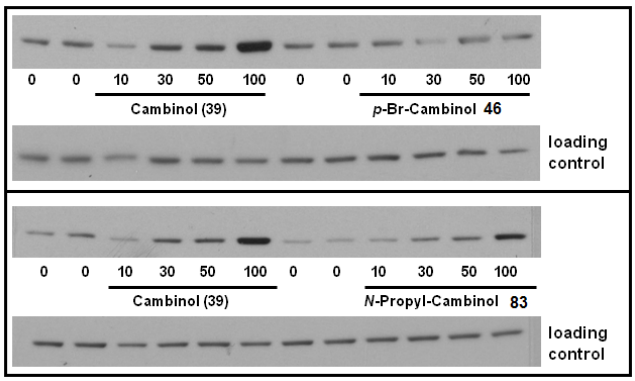

Figure 2.4.2. - Detection of the levels of acetylated α-tubulin into H1299 cells treated with different concentrations of the new SIRT1 (**46**) and SIRT2 (**83**) inhibitors. Levels of acetylated α-tubulin were increased by the SIRT2 inhibitor **83**. Tubulin was used as a loading control, whereas cambinol **39** was used a positive control. [106]

As expected, levels of acetylated α-tubulin did not increase when HT299 cells were treated with increasing concentrations of the selective SIRT1 inhibitor **46** whereas cambinol **39,** an unselective SIRT1 and SIRT2 inhibitor, induced a modest α-tubulin acetylation as expected. Excitingly, **83** induced a dose dependent increase in the levels of acetylated tubulin, with the highest levels detected at a concentration of 100 μM. These results suggest that our new SIRT2 selective inhibitor **83**, despite being less potent than **85** (IC_{50} 4.8 *vs* 1.0 μM, respectively) may be more cell permeable or less cytotoxic than **85**, thus leading to detectable levels of acetylated tubulin at 100 μM. Once again, for **83** the effect in cells was much less than that expected, considering the 50-fold difference in the IC_{50} between **83** and **39** against SIRT2. Furthermore, at 30, 50 and 100 μM concentration **39** induced higher levels of acetylated α-tubulin.

2.4.3 Compound 46 Increased the Levels of p53 and Acetylated p53

Inhibition of SIRT1 is known to cause an increase in the levels of p53 and acetylated p53.[18] As compound **46** was a relatively potent and selective inhibitor of SIRT1 (see **Table 1.4.2.2**, **Introduction**), it was decided to detect the levels of this target in cells incubated with **46**. MCF-7 breast adenocarcinoma cells were treated with different concentrations of **46** and etoposide and the levels of p53 and acetylated p53 were detected through immunoblotting analysis (**Figure 2.4.3**). Again, the known SIRT1 inhibitor cambinol **39** was used as a control (**Figure 2.4.3.A**). As cambinol was reported to increase the levels of both p53 and acetylated p53 in the presence of the genotoxic agent etoposide, the expression of p53 and acetylated p53 was detected in cells treated with **39** and **46** both in the presence and in the absence of the genotoxic agent etoposide.[18]

In line with what was observed for cambinol **39**, in the presence of etoposide, compound **46** increased the levels of p53 (**Figure 2.4.3.B**). At 50 μM **46** was better than **39** at increasing the levels of p53. In the case of **46**, the levels of p53 decreased at 100 μM, probably as a result of a cytotoxic activity of **46** at this concentration.

For **46,** the highest levels of acetylated p53 were observed at 100 μM. Surprisingly, at this concentration, treatment with cambinol **39** did not lead to detectable levels of acetylated p53. At higher concentrations (200 μM) no acetylated p53 was detected, probably as a result of a cytotoxic effect of **46**. Similar behaviour was observed for **39** at the same concentration.

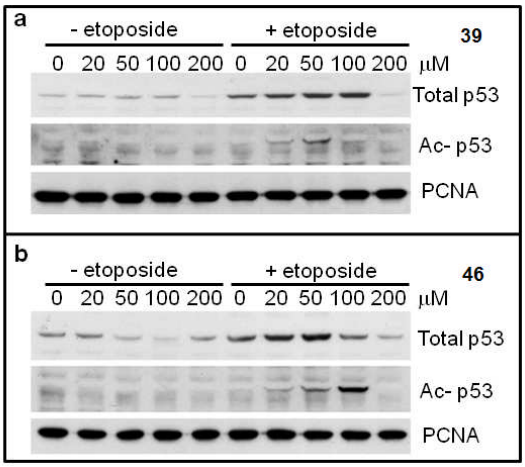

Figure 2.4.3 - Expression of p53 and acetylated p53 in MCF-7 breast adenocarcinoma cells treated with different concentrations of cambinol **39** and its SIRT1 selective inhibitor analogue **46**. Cells were also treated with the same compounds in the presence of the genotoxic agent etoposide. [106]

These observations are consistent with the good *in vitro* inhibitory activity observed for **46** against SIRT1. Despite the fact that **46** is 5 times more potent at inhibiting SIRT1 than cambinol **39**, this level of difference was not detectable in our in cell experiments. This may result from differences in cell absorption, metabolism and cytotoxicity between the two compounds tested**.** Furthermore, as observed for cambinol **39**, **46** was not able to induce expression of p53 and acetylated p53 in the absence of the etoposide-induced genotoxic stress.

2.5 Conclusions

In this chapter, the successful synthesis of sixteen new cambinol analogues was achieved by means of both parallel synthesis and normal glassware techniques. Despite the last step being characterised by low yields, our study showed that a parallel synthesis of a small collection of cambinol analogues was possible. Due to the potential biological and therapeutic uses of this type of molecule, application of this procedure to the preparation of larger collections or libraries of this type of molecules will be possible in the future.

The *in vitro* biological evaluation of the new compounds showed that the moderate and unselective sirtuin inhibitor cambinol **39** can be converted into a potent and selective SIRT2 inhibitor, with the most potent compound **85** exhibiting an IC_{50} of 1 ± 1 μM. The presence of a new aliphatic alkyl chain at the *N*-1 of cambinol proved to be crucial for the observed selectivity against this isoform. Furthermore, the increasing *in vitro* activity observed for **82**, **83**, **85** and **87** against SIRT2 clearly correlated with the increasing length of the previously mentioned chain. Thus, this new structural feature can be the starting point for further optimisation and improvement of the inhibitory activity against SIRT2.

In cell experiments aimed at detecting the expression levels of acetylated α-tubulin, a cytoplasmic target of SIRT2, in cell lines treated with the most potent SIRT2 inhibitors **83** and **85** further supported our previous *in vitro* data and support the concept that **83** and **85** target SIRT2 in cells.

Unfortunately no significant improvement has been achieved regarding the potent and selective inhibition of SIRT1. Despite this, the new cambinol analogues derived from the parallel synthesis work provided important SAR data about this type of molecule.

The logical continuation of these studies was a series of molecular modelling studies aimed to provide a possible rationalisation for the SAR data observed. In view of a possible optimisation and improvement of the inhibitory activity against SIRT1 and SIRT2 that could result, the second aim of these docking studies was to develop an improved understanding of the mode of binding of cambinol-like molecules in the active site of the sirtuins. These *in silico* studies are described in the next chapter.

3. COMPUTATIONAL STUDIES

This chapter describes a series of molecular modelling studies aimed at rationalising the SAR data reported in **Chapter 2**. Compounds **46** and **85**, relatively selective inhibitors of SIRT1 and SIRT2 respectively, are discussed in this chapter. In particular, the main aim was to understand the role played by the new alkyl chain at *N*-1 of cambinol **39** in increasing the selectivity and potency of these molecules against SIRT2. Furthermore, we aimed to improve our understanding of the binding mode of cambinol **39** in the sirtuin active site, possibly generating new ideas for the rational design of selective sirtuin inhibitors.

3.1. First Generation Computational Studies on the New Cambinol Analogues: A Potential Rationalisation of the Observed Activity

3.1.1 Preliminary Molecular Docking Studies on Cambinol 39

The initial molecular modelling studies were run in collaboration with Dr Rupert Russell at the University of St Andrews. Initially, the potential mode of binding of cambinol **39** was investigated by means of the automated molecular docking software GOLD.[109] The minimised energy conformation of the ligand was generated using the PRO-DRG server.[110] To date, within the sirtuin family of proteins, only the crystal structures of SIRT2, SIRT3 and SIRT5 have been reported.[36-39] Due to the high homology existing in the amino acid sequence of the sirtuins, we choose the X-ray structure of human SIRT2 for this study[36] This choice was also motivated by the fact that our best *in vitro* biological data were against SIRT2. Unfortunately, to date no ligand bound structures of human SIRT2 have been solved. Despite this, the structures of different SIRT2 homologs from yeast and *Archaeoglobus fulgidus* have been extensively studied with regard to the mode of substrate and cofactor binding.[31,34,41,45]

All sirtuin crystal structures so far reported are characterised by a highly-conserved catalytic domain of 270 amino acids. The structure is commonly divided into two main parts, a large classical Rossman-fold domain and a small zinc-binding subdomain. The active site is situated at the interface between the two domains and is commonly divided into A, B and C subpockets. This division is based on where the different parts of the NAD^+ cofactor were found to bind in the active site of the enzymes (A, adenine; B, ribose; C, nicotinamide) (**Figure 3.1.1.1**).[31]

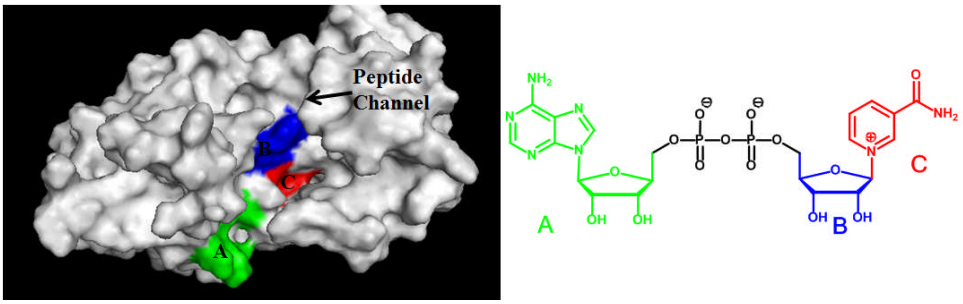

Figure 3.1.1.1 - General overview of the human SIRT2 crystal structure used in the computational studies reported in this chapter. The protein was crystallised in its APO form.[36] The active site is divided into three areas: **A** (green), **B** (blue) and C (red).[31]

The structure of cambinol **39** is characterised by a polar moiety, represented by the carbonyl and the thiocarbonyl groups of the thiouracil core and by two highly hydrophobic components, the naphthol and the phenyl rings. The naphthol moiety is considered to be the pharmacophore of the molecule.[18]

The exact mode of binding of cambinol **39** to sirtuins is still unknown. When these *in silico* studies were started, two studies had already been carried out. In SIRT2, Bedalov and co-workers showed (using Lineweaver-Burke experiments with NAD^+ and H4-peptide substrates) that cambinol **39** is competitive with the peptide and non-competitive with the NAD^+ cofactor.[18] In a second study based on GOLD docking simulations, Neugebauer reported cambinol **39** to interact with the nicotinamide subpocket (C) of the catalytic domain (**Figure 3.1.1.2**).[94]

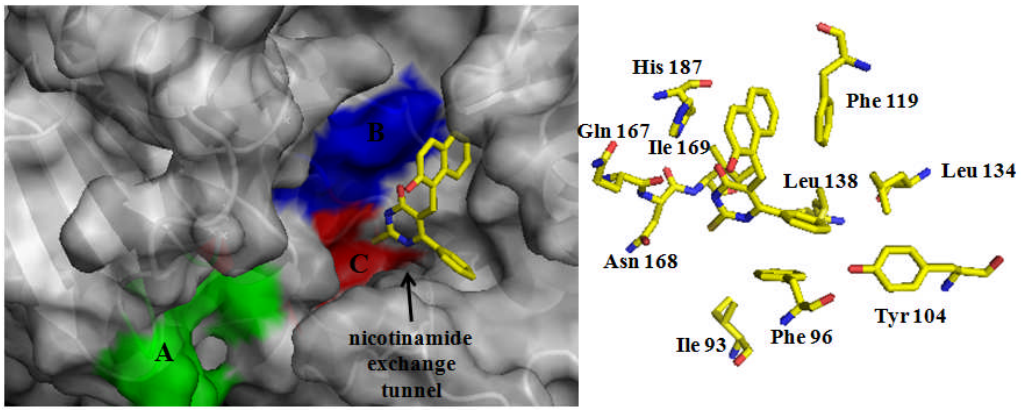

Figure 3.1.1.2 - Proposed binding mode of cambinol **39** in the active site of SIRT2.[94] Cambinol **39** binds in the C sub-pocket (red), with the naphthol moiety occupying the substrate binding tunnel (blue). Interestingly, the *N*-1 hydrogen points towards the nicotinamide exchange tunnel. The key residues involved in the binding of the ligand are labelled on the right.

In Neugebauer's model, the polar moiety of cambinol **39** was found to interact with the polar residues of Gln167, Asn168 and a proposed water molecule in the C subpocket. The naphthol substituent inserted into a hydrophobic channel sandwiched between the two aromatic residues Phe119 and His187, with potential π-stacking interactions probably contributing to the calculated stability of this binding mode. This channel represents the binding site for the acetylated peptide substrate. The phenyl group was found to be accommodated in a hydrophobic pocket created by the side chains of Phe96, Tyr104, Leu134 and Leu138. Interestingly, the *N*-1 hydrogen was proposed to point towards the so-called nicotinamide-exchange tunnel. This mode of binding is consistent with the kinetic data reported by Bedalov and co-workers.[18] In fact, due to the close proximity between the C sub-pocket and the substrate binding site, the binding of the polar moiety of cambinol **39** into the C pocket may lead to competition with the substrate, due to insertion of the naphthol substituent into the substrate binding channel.

When run in our lab, attempts to identify a binding mode for **39** using GOLD led to an analogous result to that previously reported by Neugebauer.[94] Cambinol **39** gives the lowest energy solutions when bound in the C-pocket, with the orientation of the different parts of the ligand (phenyl and naphthol) in close agreement with those already proposed.[106]

The docking simulations were repeated using the small molecule X-ray structure of **39** (see **Section 2.1.3**). Analogous final docking poses to those described previously were observed for **39** when this alternaltive starting conformation was used. Interestingly, the conformation observed in the crystal structure of **39** was characterised by an intramolecular hydrogen bond between the phenolic OH and the carbonyl functionality of the thiouracil. The similar results obtained suggested that loss of this hydrogen bond is not detrimental for binding to the protein. Formation of a hydrogen bonding interaction between the naphthol OH and an amino acid residue in the substrate binding tunnel cannot be ruled out as the OH group points into this area of the active site. However, no amino acid residue appeared to interact with the OH at this level of calculation.[106]

When applied to the new analogues of **39**, visual analysis of the highest scoring docking poses suggested a similar binding mode to the one previously reported by Neugebauer and repeated by us for cambinol **39** itself.[94,106] It was found that the *β*-naphthol ring of the molecules was always sandwiched in the hydrophobic channel between Phe119 and His187. Modest differences in the orientation of the *β*-naphthol moiety were observed across the different ligands. The thiouracil

core was always situated in the C-subpocket, whereas the differently substituted phenyl rings were always found to occupy a pocket bordered by Phe96, Leu138 and Phe190.

3.1.2. Molecular Modelling Studies on the New SIRT2 Selective Inhibitors: Rationalisation of the Improved Potency

In search of a potential explanation for the increased *in vitro* potency and selectivity towards the SIRT2 isoform, the mode of binding of analogues **47**, **82**, **83** and **85** were studied. Again, automated ligand docking studies were carried out using the GOLD software and the reported structure of human SIRT2 was used.[36] Visualisation of the highest-scoring docking poses obtained for these ligands in the active site of SIRT2 clearly suggested an analogous binding mode to the one previously found for **39** itself (**Figure 3.1.2**).[106]

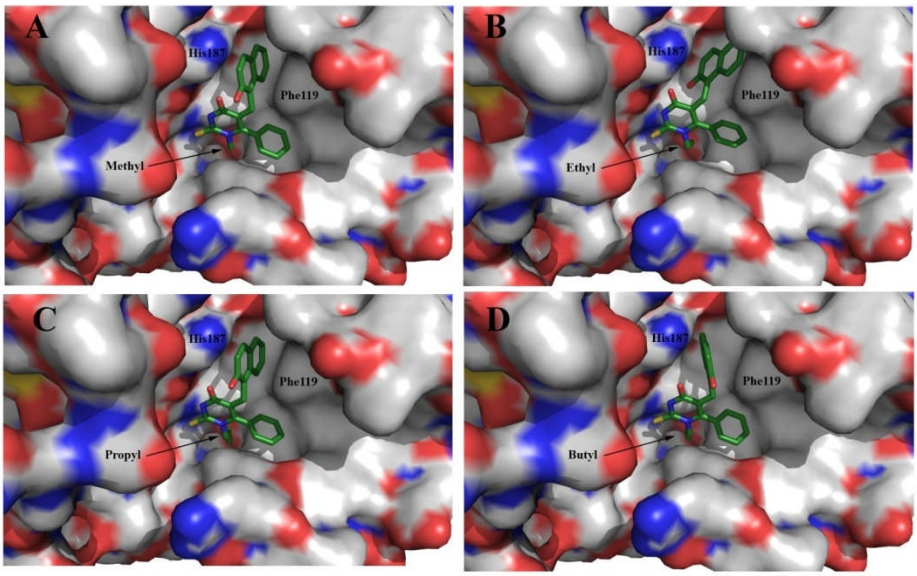

Figure 3.1.2. - Docking solutions obtained for the new potent SIRT2 inhibitors **47** (**A**), **82** (**B**), **83** (**C**) and **85** (**D**) (Green). The new aliphatic carbon chain of each inhibitor inserts into a narrow hydrophobic channel enclosed by Phe96, Leu 138 and Ile169. The molecular surface of the binding site is coloured according to the electrostatic potential (Blue, positive potential; red, negative potential; white-grey, neutral potential).

However, a key difference observed in this pose was the insertion of the new liphophilic carbon chains on the *N*-1 of the thiouracil core into a previously unoccupied narrow lipophilic channel adjacent to the C-subpocket. This channel was delimited by Phe96, Leu138 and Ile169. The proposed mode of binding was consistently observed for all four SIRT2 selective inhibitors. Interestingly, this channel was also reported in the crystal structures of the yeast and

Archaeoglubos fulgidus enzymes and it is commonly referred to as the nicotinamide-exchange tunnel. In particular, it reaches the opposite side of the protein and it is capable of changing its size and conformation after release of nicotinamide, which is the first product of the sirtuin-catalysed reaction.[42]

As the inhibitory activity and selectivity observed for analogues **47, 82, 83** and **85** against SIRT2 increased with the length of the linear substituents at *N*-1, it is possible that formation of additional hydrophobic interactions between these substituents and the above mentioned lipophilic tunnel led to increased stabilisation of the binding of these molecules to the active site, thus increasing the inhibition of SIRT2. Consistent with the potential insertion of the new *N*-1 aliphatic substituent into the tunnel, a structure of the *Archaeoglubos fulgidus* enzyme has been solved in which the same channel is occupied by a pentaethylene glycol molecule.[42]

At this time it remains difficult to explain why the *N*-1-allyl analogue **87** has reduced activity compared to the other *N*-1 substituted analogues.

Visual inspection of the reported human SIRT2 X-ray crystal showed that the above mentioned liphophilic channel is potentially capable of accommodating longer chains at *N*-1. Thus, it might be that increasing the number of carbon atoms in these chains may lead to higher levels of inhibition of the enzyme. Furthermore, due to the narrow nature of the channel, we initially speculated that there is not sufficient space to accommodate larger substituents, such as phenyl or benzyl, at the *N*-1 position. The fact that in a crystal structure of the yeast enzyme a nicotinamide molecule has been found in this hydrophobic channel, clearly suggests a certain level of flexibility.[111] Unfortunately, due to the limitations of our synthetic approach (**Chapter 2**), at this stage of the research it was not possible to address these interesting questions.

Although a potential explanation was found for the improved potency of the new cambinol analogues **47, 82, 83, 85** and **87** against SIRT2, further studies were required to explore the role played by this channel in the modulation of the selectivity of these ligands against SIRT2. These new studies will be discussed in **Chapter 5**.

3.1.3 Molecular Modelling Studies on the SIRT2 Selective Inhibitors: Rationalisation of the Improved Selectivity

The next question to address was why, given the presence of the lipohophilic channel in both SIRT1 and SIRT2, the *N*-1 alkyl substituent resulted in high selectivity for SIRT2 over SIRT1. We postulated that structural differences in the active site between the human SIRT2 and SIRT1 should explain the observed selectivity.

The absence of a crystal structure for SIRT1 represented a limitation in this study. This problem was partially overcome *via* generation of a homology model of human SIRT1 using the PHYRE server. Furthermore, an alignment of the amino acid sequence of the two isoforms of the enzyme was carried out in order to detect relevant variations (**Figure 3.1.3**).

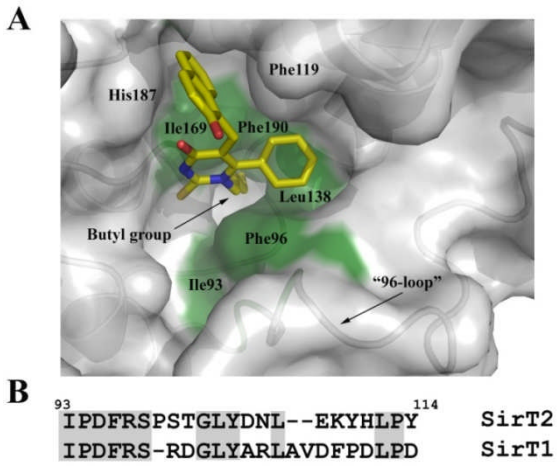

Figure 3.1.3 – A. Highest score pose obtained for *N*-1-butyl-substituted cambinol analog **85**. The 96-loop is labelled, along with the amino acids potentially involved in the binding. **B**. A comparison of the amino acid sequence for the 96-loop in human SIRT1 and SIRT2, underlying the differences between the two.[106]

As reported in the literature, the majority of the active site residues are highly conserved between the different sirtuins.[40] Careful analysis of the amino acid sequences of SIRT1 and SIRT2 suggested the presence of significant conformational differences in the area around the *N*-1 alkyl binding liphophilic tunnel (**Figure 3.1.3, A** and **B**). This area, named as the 96-loop, is characterised by a Phe96 which lines the above mentioned lipophilic channel. The main structural difference between the 96-loop of the two enzymes is due to an amino acid insertion and a two amino acid deletion following the Phe96 residue in SIRT2 compared to SIRT1 (**Figure 3.1.3.B**). Consistent with this observation, the human SIRT2 enzyme and its yeast homologue, despite possessing almost identical sequences in this loop, show conformational

differences. Thus, it can be concluded that despite the liphophilic channel being present in SIRT1, conformational changes at the base of the active site (96-loop) may render this channel less accessible in SIRT1 compared to SIRT2. This issue is revisited further in chapter 5.

3.1.4. Rationalisation of the Observed Selectivity for Analogues Incorporating a Substituent in the Phenyl Ring

The structural differences in the 96-loop of the two sirtuins studied may provide a potential explanation for the observed potency and selectivity of compound **46** (*para*-bromo substituent at the phenyl ring). In an attempt to rationalise this SIRT1 selectivity, **46** was docked into the active site of SIRT2. Furthermore, the homology model previously generated for SIRT1 was overlapped with the structure of human SIRT2 used in this docking study (**Figure 3.1.4.1**). Visual analysis of the docking poses of **46** along with the overlapped structures of the two proteins clearly suggested that SIRT2 does not possess sufficient space to accommodate a phenyl ring bearing a large *para*-substituent, such as the bromine, since it is not sufficiently flexible.[106]

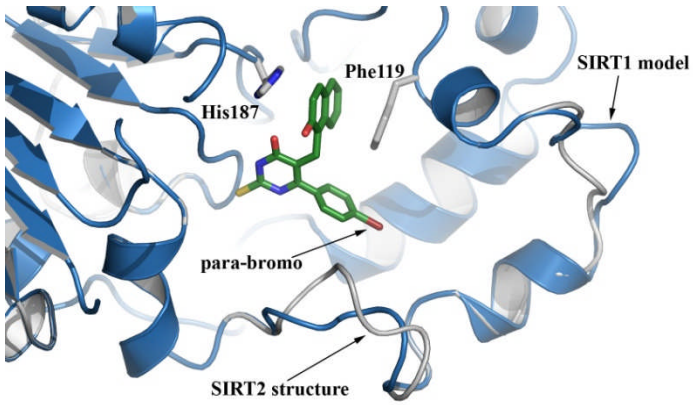

Figure 3.1.4.1 - Docking analysis of ligand **46** (green) in the overlapped active sites of SIRT1 (blue) and SIRT2 (grey). Due to the differences in the 96-loop of the active site, the *para*-substituted phenyl substituent of **46** does not find sufficient space in the active site of SIRT2, thus explaining the selectivity of this compound towards SIRT1. The structure of SIRT1 was generated as a homology model.[106]

Again, the conformation of the 96-loop could account for the observed selectivity. In particular, in this loop in SIRT2 the side chain of Tyr104 and Phe 96 are proposed to point into the pocket which accommodates the phenyl ring of **46** (**Figure 3.1.4.2**). Due to the proposed structural difference of the 96-loop between SIRT2 and SIRT1, this pocket is probably larger in SIRT1 compared to SIRT2 and consequently able to accommodate the *p*-bromo-substituent. This

result was consistent with the observed poor activity against SIRT2 of the *p*-iodo (**69**), *p*-methyl (**76**), *p*-chloro (**66**) and *p*-trifluoromethyl (**71**) analogues.[106]

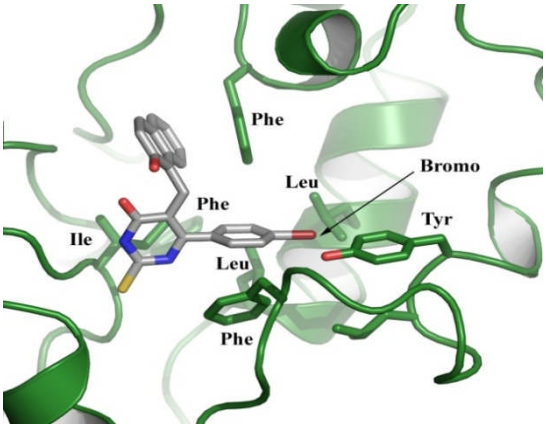

Figure 3.1.4.2 - Compound **46** is docked into the active site of SIRT2. A tyrosine residue is proposed to point into the pocket where the *para*-substituted phenyl ring of **46** is accommodated. This would render this area potentially too small for accommodating large substituents on the phenyl ring.[106]

3.2. Second Generation Computational Studies: Design of New Cambinol Analogues

After having identified a potential explanation for the SAR data reported in **Chapter 2**, we decided to assess further the hypothesis that insertion of a lipophilic moiety into the nicotinamide exchange channel is crucial for the observed potency and selectivity against SIRT2. Before starting new synthetic studies aimed at expanding the range of substituents at the *N*-1 position of cambinol, we carried out a series of automated molecular modelling GOLD simulations. The target of these second generation *in silico* studies was the identification of new substituents at the *N*-1 of **39** capable of being accommodated in the previously identified tunnel. Furthermore, the possible insertion of an aliphatic substituent at *N*-3 was investigated.

3.2.1 *N*-3 Substituted Cambinol Analogues

Two new analogues substituted at the *N*-3 position of the thiouracil core were docked into the active site of SIRT2. A new common binding mode characterised the highest score docking poses for **90** (R_2 = methyl) and **91** (R_2 = allyl) (**Figure 3.2.1**). The orientation of the thiouracil moiety of the two molecules was different to that previously observed in this chapter for **39** and

its analogues. In the absence of an alkyl substituent in **90** and **91**, the *N*-1 does not point towards the entrance of the nicotinamide-exchange tunnel. The C-6 phenyl group is now accommodated in the lipophilic area at the entrance of the nicotinamide-exchange tunnel. The area above the 96-loop, where the same phenyl substituent was previously found to be accommodated is now occupied by the new *N*-3 alkyl substituents. A certain level of flexibility was observed for these substituents across the highest scoring binding modes. Furthermore, the methyl (**90**) or the allyl (**91**) substituents were found to be potentially exposed to the solvent. In line with the previous observations, the naphthol moiety was accommodated in the acetyl-lysine substrate binding tunnel. This new binding mode can be rationalised due to the fact that there is insufficient space around *N*-3 to accommodate a substituent on *N*-3. Furthermore, due to the polar nature of the residues which define the C-subpocket (Gln167, Asn168), it may be possible that aliphatic substituents at *N*-3 are not tolerated.

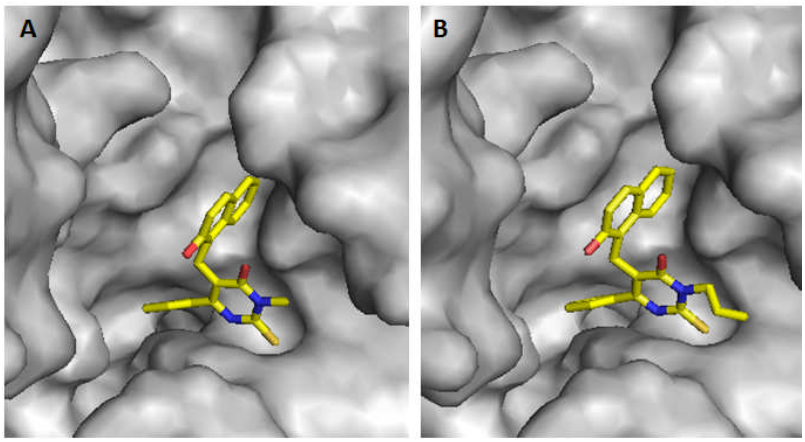

Figure 3.2.1 New binding mode observed for analogues **90** (A, R_2 = Me) and **91** (B, R_2 = Allyl into the active site of SIRT2.

This new binding mode led to the hypothesis that removal of the *N*-1 substituent and insertion of an alkyl group at the *N*-3 postition could be potentially dentrimental for the inhibitory activity against SIRT2. In order to test this hypothesis and validate further the proposed binding mode of cambinol **39** and analogues **82, 83, 85** and **87**, the synthesis of **90** and **91**, along with their *in vitro* biological evaluation was planned. These results will be discussed in **Chapter 4**.

3.2.2 New Substituents at *N*-1 of Cambinol

A preliminary visual inspection of the nicotinamide-exit tunnel in the active site of SIRT2 showed that the entrance to this tunnel was preceded by a largely lipophilic pocket. It was assumed that a benzyl-type substituent at the *N*-1 position of cambinol could be accommodated into this area of the enzyme. Furthermore, a *para* substituent on the same benzyl group would have the possibility to fit into the previously identified nicotinamide-exit tunnel. These assumptions led us to design and dock compound **92** in the active site of SIRT2 (**Figure 3.2.2.1**). The highest scoring pose of **92** showed the expected and previously described orientation**,** with the new *p*-methoxybenzyl substituent at the *N*-1 position not altering the previously reported pose. Interestingly, the methoxy substituent at the *para* position of the benzyl ring was predicted to be accommodated into the nicotinamide-exchange tunnel.

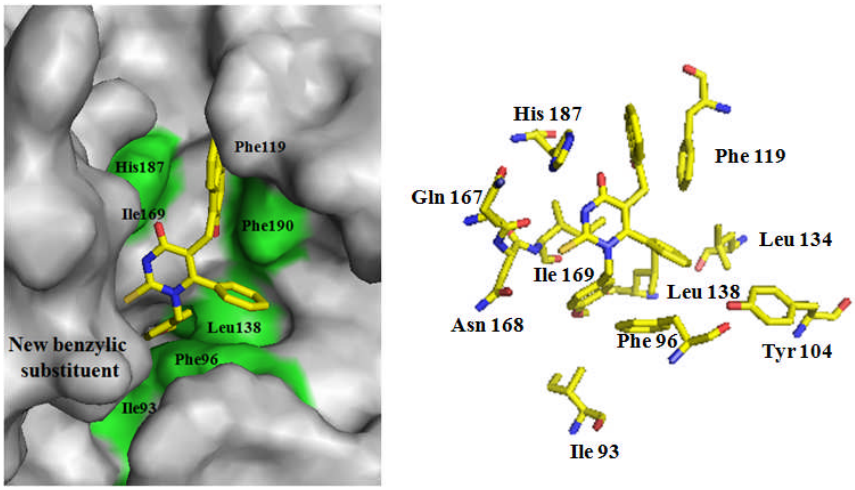

Figure 3.2.2.1 - Mode of binding of cambinol analogue **92** (yellow) into the active site of SIRT2. The active site is highlighted in green. The key residues involved in the binding of the ligand are labelled on the right.

In an analogous way, we docked analogues **93-96** and analysed the corresponding highest scoring docking poses (**Figure 3.2.2.2**).

The following considerations are based on a visual inspection of the highest scoring docking poses and require careful interpretation. In fact, it is reported that Gold score values cannot discriminate between less- and more-active compounds.[112] Furthermore, in many cases low correlations have often been observed between docking scores and inhibitory activities.[112]

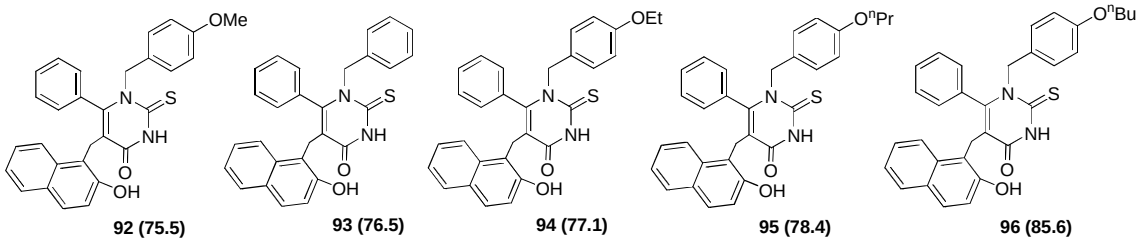

Figure 3.2.2.2 Structures of the new cambinol analogues of general structures **92-96** docked into the active site of SIRT2. The highest docking score is reported in blackets.

All analogues adopted similar docking poses to that reported in **Figure 3.2.2.1**. The presence of the benzyl ring at the *N*-1 position did not alter the expected relative orientation of the molecule in the active site. The new aromatic ring was found to be consistently accommodated in the liphophilic area at the entrance of the tunnel. In the absence of a *para*-alkoxy substituent (**93**), the benzyl group showed a certain level of flexibility, with a different orientation in the liphophilic pocket at the tunnel entrance. The highest scoring poses of analogues **94-96** were characterised by the *para*-alkoxy substituent always being inserted into the liphophilic nicotinamide-exchange tunnel. This may result in further stabilisation of the ligand-protein interaction. This interaction is not possible for analogue **93**. Thus, better *in vitro* inhibitory activity could be expected from **92** and **94-96** compared to **93**. Evaluation of the optimal length for the *para*-alkoxy substituent remained difficult. Despite the nicotinamide-exchange tunnel being expected to be particularly long, it was envisaged that excessive elongation of the *para*-alkoxy substituent would be detrimental for the aqueous solubility and cell permeability of the corresponding molecules. As a consequence, molecules having a *para*-alkoxy substituent longer than four atoms were not taken into account in this study.

The logical consequence of these new docking experiments was the synthesis and *in vitro* biological evaluation of cambinol analogues containing a *para*-substituted benzylic substituent at *N*-1 position. The synthesis and biological evaluatuion of these analogues will be described in **Chapter 5**.

3.3. Conclusions

In **Chapter 3**, the selectivity and increased potency of the new cambinol analogues, particularly **46** and **85**, towards SIRT1 and SIRT2 respectively, was rationalised by means of molecular docking studies.

The relatively potent inhibitory activity of analogues **47**, **82**, **83** and **85** towards SIRT2 was explained with the insertion on the new aliphatic alkyl chain at the *N*-1 position into a narrow hydrophobic tunnel adjacent to the C-subpocket of the active site. This tunnel was previously reported as the nicotinamide exchange-tunnel.[42] Furthermore, the selectivity observed across these SIRT2-selective inhibitors and the SIRT1-selective inhibitor **46** was put down to structural differences existing between the two enzymes in the conformation of both the nicotinamide-exchange tunnel and the 96-loop flexibility.

In the second generation of studies, a visual inspection of the active site of SIRT2 and the docking poses observed for compounds **92-96** suggested that a benzylic-type substituent at the *N*-1 of cambinol could be accommodated into a hydrophobic pocket positioned at the beginning of the nicotinamide-exchange tunnel. Analysis of the docking scores obtained for the same cambinol analogues suggested that inhibition of SIRT2 was possible.

Removal of the *N*-1 substiutent and insertion of an aliphatic substituent at the *N*-3 of **39**, an area of cambinol not previously explored, resulted in a new potential binding mode with predicted loss of inhibitory activity against the two isoforms of the enzyme

These *in silico* observations inspired a "second and third generation" synthetic study aimed at:

1. Synthesising and testing new cambinol analogues bearing an aliphatic substituent at *N*-3;

2. Due to the limitations of the synthetic route described in Chapter 2, the design of a new synthesis for *N*-1 benzyl-substituted analogues thus allowing their biological evaluation as SIRT2 inhibitors.

These aspects will be discussed, respectively, in **Chapters 4** and **5**.

4. *N*-3 SUBSTITUTED CAMBINOL ANALOGUES

In this chapter, two synthetic approaches to the functionalisation of the *N*-3 atom of cambinol **39** are described. As *N*-3 regioisomers were not isolated during the synthesis of analogues **82-89**, it was believed that their synthesis and *in vitro* biological evaluation would expand the SAR data associated with cambinol **39**. Furthermore, as previous molecular modelling studies suggested a lack of activity for **90** and **91** against SIRT2, it was envisaged that the synthesis of **90** and **91** would provide a way to probe the validity of the proposed binding mode of cambinol **39**. All analytical data associated with the compounds described in this chapter is reported in **Chapter 6, Part II**.

4.1. Synthesis of *N*-3 Substituted Analogues 90 and 91 *via* Protection at Sulfur

The work reported in this section was run in collaboration with a Postdoctoral Research Fellow, Dr Severine Poupart and an undergraduate project student, Mr David Bradshaw. As the sulfur atom was expected to be the most nucleophilic site in **39**, selective alkylation at *N*-3 in **39** was excluded. It was envisaged that treatment of cambinol **39** with different alkylating agents, such as benzyl bromide or allyl iodide under basic conditions would furnish the sulfur protected compounds **98** (R_1 = Bn) and **97** (R_1 = allyl).

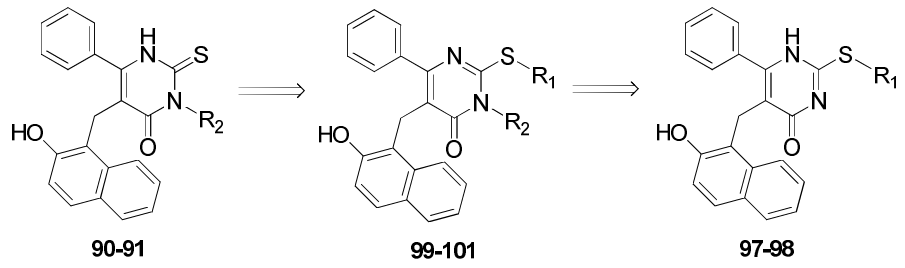

Scheme 4.1 - Retrosynthetic analysis of the preparation of new cambinol analogues **90** and **91** substituted at *N*-3.

After selective alkylation at the *N*-3 nitrogen to give **99-101**, subsequent deprotection of the sulfur atom would be expected to regenerate the thiocarbonyl functionality, thus providing new *N*-3 methyl functionalised cambinol analogues (**90, Scheme 4.1**). In addition, analogue **91** (R_2 = Allyl) could be obtained by means of a Pd-catalysed Claisen rearrangement of the allyl group of **97** to the *N*-3 position.

.

4.1.1. Alkylation of the Sulfur Atom in 39

Treatment of cambinol **39** with allyl bromide (1.3 eq) under basic conditions (KOH) at room temperature resulted in a mixture of two products (**Scheme 4.1.1.1**). Separation by silica-gel column chromatography revealed that the main product, as expected, was the *S*-substituted cambinol analogue **97**. A second product isolated from the reaction mixture was **99** resulting from double alkylation at both sulfur and at *N*-3 (**Table 4.1.1**). Determination of the regiochemistry of **97** and **99** was carried out by means of ^{13}C NMR, [^{1}H-^{1}H] COSY, [^{1}H-^{13}C] HSQC and HMBC spectroscopy. In the [^{1}H-^{13}C] HMBC spectrum of **97**, the signal corresponding to the protons of the allylic methylene group exhibited a cross peak with the carbon signal at 156.9 ppm, which was assigned to the quaternary C-2 of the thiouracil ring (**Scheme 4.1.1.1**).

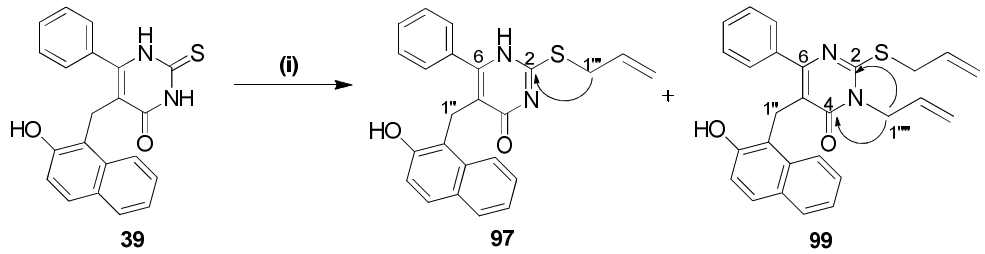

Scheme 4.1.1.1 - Alkylation of the sulphur atom in cambinol **39**. *Reagents and Conditions*: Allyl iodide (1.3 eq), KOH (3.3 eq.), MeOH, 24h (**97**, 85%, **99**, 12%). The diagnostic couplings observed in the [^{1}H-^{13}C] HMBC spectrum between the methylene allylic protons and the adjacent carbons are shown by curly arrows.

The ^{1}H NMR spectrum of compound **99** was characterised by two distinct sets of allyl signals. Analysis of the [^{1}H-^{13}C] HMBC spectrum of the same compound indicated that one allyl was on the sulfur atom (established as described for **97**), whereas the second allyl substituent was present on *N*-3. The signal corresponding to the methylene protons of the second allyl chain exhibited two cross peaks, the first with the C-2 carbon of the thiouracil ring and the second with the C-4 carbonyl carbon (**Scheme 4.1.1.1**). Furthermore, for both products, in the [^{1}H-^{13}C] HMBC spectra, no cross peaks between the signals of the allylic methylene protons and the peak of the quaternary carbon atom C-6 were observed, thus excluding the possibility that any substitution at *N*-1 had occurred.

Table 4.1.1 - Yields observed for compounds **97-99**. Chemical shift values for the diagnostic proton signals are listed. Yields refer to the amount of product isolated after silica-gel column chromatography purification.

Compound	Yield (%)	Diagnostic signals (ppm)
97	85	4.38 (H-1''), 3.88 (H-1''')
98	75	4.34 (H-1''), 4.41 (H-1''')
99	12	4.38 (H-1''), 3.83(H-1'''), 4.67 (H-1'''')

Similar results were observed when **39** was treated with benzyl bromide (1.3 equivalents) under basic conditions (NaOMe) (**Scheme 4.1.1.2**). The only product isolated from this reaction was analogue **98** (75%), containing a benzyl substituent at the sulfur. No side product with substitution at the sulfur and *N*-3 of the thiouracil was isolated. Again, the regiochemistry was deduced by means of [^{1}H-^{13}C] HMBC analysis. The lack of reaction at the *N*-3 position of the thiouracil ring can be justified by steric hindrance exerted by the new benzylic group at the sulfur on the *N*-3 position. It may be possible that adding more equivalents of base and alkylating agent, along with longer reaction time and higher temperatures, substitution would occur at the *N*-3 of **98** also.

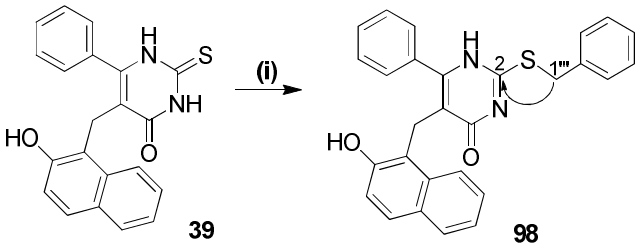

Scheme 4.1.1.2 - Synthesis of cambinol analogue **98**. *Reagents and Conditions*: (i) BnBr, (1.3 eq.), NaOMe (1.1 eq.), MeOH, 12 h, rt, 75%. The diagnostic couplings observed in the [^{1}H-^{13}C] HMBC spectrum between the benzylic protons C-1''' and the quaternary carbon C-2 is shown by a curly arrow.

Despite not being the target compounds, it was decided to test the new cambinol analogues **97-99** as sirtuin inhibitors. These results are reported in **Section 4.3.**

4.1.2. Methylation of the New Sulfur-Protected Cambinol Analogues 97 and 98

With analogues **97** and **98** in hand, a further alkylation at *N*-3 was attempted. Based on literature precedents, treatment of **97** and **98** with a methylating agent under basic conditions would be expected to furnish the *N*-3 methylated analogues.[113] This was indeed the case, and

when **97** and **98** were treated with Me_2SO_4 in the presence of base (NaOH), *N*-3 methylated analogues **100** and **101** were recovered in moderate and good yields respectively (**100-101**, **Table 4.1.2**).

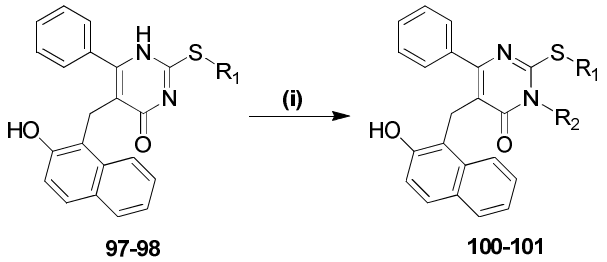

Scheme 4.1.2 - Synthesis of cambinol analogues **100** (R_1, Allyl, R_2, Methyl) and **101** (R_1, benzyl, R_2, Methyl). *Reagents and Conditions*: (i) Me_2SO_4 (4 eq.), NaOH (30%), 48h, rt (**100**, 48%; **101**, 78%).

Table 4.1.2 - New cambinol analogues **100** and **101** were obtained upon treatment of **97** and **98** under basic conditions. *Reagents and conditions*: Me_2SO_4, NaOH (10%), 4 h, rt.

Compound	R_1	R_2	Yield (%)	Diagnostic signal (*N*-3-CH_3) (ppm)
100	Allyl	CH_3	48	3.48
101	Benzyl	CH_3	78	3.49

In support of the successful formation of **100** and **101**, the ^{1}H NMR spectra showed the presence of a new singlet in the high-field region, integrating to three protons, which was assigned to the *N*-3 methyl group. Furthermore, the [^{1}H-^{13}C] HMBC spectra confirmed the predicted regiochemistry (**100**, **Figure 4.1.2**).

The *N*-3 methyl group correlated with the carbon atoms corresponding to the signals at ~158 ppm, derived from the C-2 quaternary carbon atom, and at ~166 ppm, corresponding to the C-4 carbonyl carbon.

Despite **100** and **101** not being the target compounds, it was decided to test them for their inhibitory activity against SIRT1 and SIRT2. These results are discussed in **Section 4.3**.

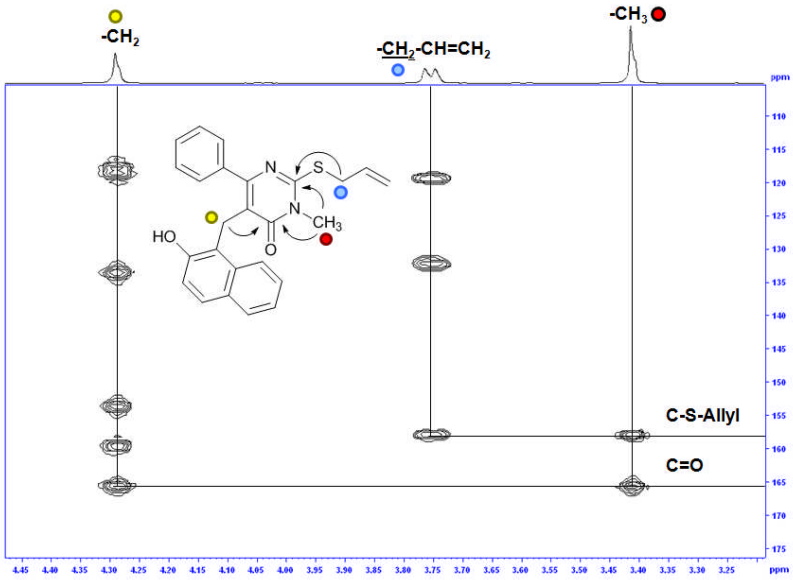

Figure 4.1.2 - Selected area of the [^{1}H-^{13}C] HMBC spectrum of compound **100**. The diagnostic interactions between the protons of the new *N*-3 methyl (red) and the quaternary carbon atoms at 158 ppm and 166 ppm are shown. The methylene protons of the *S*-allyl group (blue) exhibited a clear cross peak with the same quaternary carbon at 158 ppm.

4.1.3 Deprotection at Sulfur: Synthesis of Analogue 90

Removal of the allyl chain from a sulfur atom has been reported in the literature, including examples involving thiouracil moieties. It was decided to employ a Pd-catalysed protocol (**Table 4.1.3**).[114-117] Removal of the allyl group from the sulfur atom in **100** was not achieved in the presence of Pd^{II} [$Pd(OAc)_2$] (**Entry 1**). Similar results were observed when Pd^{0} was employed (**Entry 2-3**). In both cases, ^{1}H NMR analysis of the crude reaction mixtures confirmed the presence of unreacted starting material **100**.

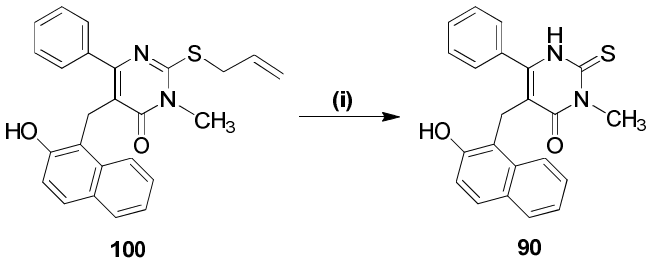

100 **90**

Scheme 4.1.3 - Removal of the allyl protecting group from the sulfur atom of **100**. *Reagents and Conditions*: (i) $Ph(PPh_3)_4$ (0.05 eq.), morpholine (5 eq.), THF, 24 h, reflux (88%).

When the same reaction was repeated with $Pd(PPh_3)_4$ in the presence of morpholine as additive, according to a reported procedure, total consumption of the starting material was observed by TLC (METHOD G, **Scheme 4.1.3**).[117] Product **90** was isolated by silica-gel column chromatography in 88% yield (**Entry 4**, **Table 4.1.3**).

Table 4.1.3 - Results for the treatment of analogue **100** with different Pd catalysts. S = starting material.

Ent	S	Pd Complex	Additive	Conditions	Yield (Product)
1	**100**	$Pd(OAc)_2$	-	THF, 24h, reflux	-
2	**100**	$PdCl_2(PhCN)_2$	-	THF, 24h, reflux	-
3	**100**	$Pd(PPh_3)_4$	-	THF, 24h, reflux	-
4	**100**	$Pd(PPh_3)_4$	Morpholine	THF, 24h, reflux	88% (**90**)

^{1}H NMR analysis of the isolated product confirmed the absence of the set of signals associated with the allylic substituent. Furthermore, in the ^{13}C NMR spectrum of **90**, the down-field quaternary carbon signal derived from the re-formed thiocarbonyl group was again detectable at 174.9 ppm.

Due to the good results obtained in the deprotection of the sulfur atom of **100**, removal of the benzyl group in compound **101** was not attempted.

4.1.4. Claisen Rearrangement of 97: Synthesis of Analogue 91

As Pd was reported to catalyse the Claisen rearrangement of the *S*-allyl group to the *N*-3 nitrogen in thiouracil systems, this isomerisation was attempted on analogue **97**.[114-117] The results are summarised in **Table 4.1.4**.

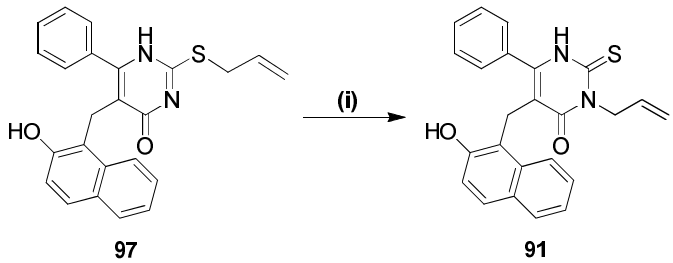

97 **91**

Scheme 4.1.4 – Claisen rearrangement of the allyl group of **97** to the *N*-3 nitrogen (**91**). *Reagents and Conditions*: (i) $PdCl_2(PhCN)_2$ (0.05 eq.), THF, 24 h, reflux (80%).

Table 4.1.4 - Results for the treatment of analogue **97** with different Pd catalysts. S = starting material.

Ent	S	Pd Complex	Additive	Conditions	Yield (Product)
1	**97**	$Pd(OAc)_2$	-	THF, 24h, reflux	-
2	**97**	$PdCl_2(PhCN)_2$	-	THF, 24h, reflux	80% (**91**)
3	**97**	$Pd(PPh_3)_4$	-	THF, 24h, reflux	-
4	**97**	$Pd(PPh_3)_4$	Morpholine	THF, 24h, reflux	50% (**39**)

Claisen rearrangement of the allyl group to the *N*-3 position was not achieved in the presence of Pd^{II} [$Pd(OAc)_2$, **Entry 1**]. Upon changing to a Pd^{II} complex **[**$PdCl_2(PhCN)_2$, **Entry 2**], Claisen rearrangement of the allyl group was observed (METHOD H). The new cambinol analogue **91**, selectively allylated at *N*-3, was recovered after column chromatography in 80% yield. The regiochemistry of **91** was unambiguously established by means of [^{1}H-^{13}C] HMBC analysis (**Figure 4.1.4**). In particular, the methylene protons of the allyl group now exhibited two cross peaks, the first with the C-2 quaternary thiocarbonyl carbon at 175 ppm, and the second with the C-4 quaternary carbonyl carbon at 164 ppm.

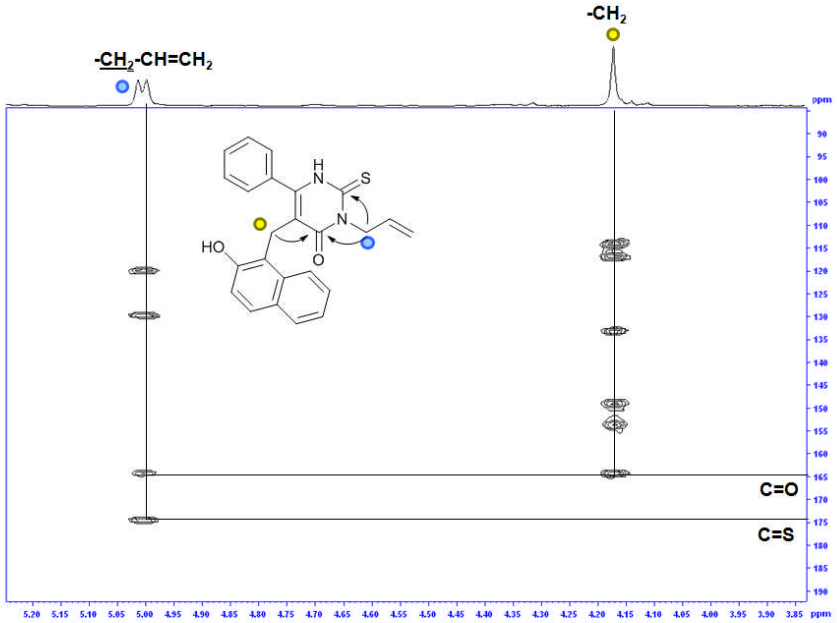

Figure 4.1.4 - Selected area of the [^{1}H-^{13}C] HMBC spectrum of compound **91**. The Claisen rearrangement of the allyl group form sulfur to *N*-3 was estabilished by analysis of the cross peaks between the allyl methylene protons (blue) and the two quaternary carbon atoms at 175 ppm and 164 ppm.

Interestingly, the protons of the methylene group of the allyl chain appeared in the ^{1}H NMR spectrum as a well defined doublet at 5.00 ppm. Furthermore, in the [^{1}H-^{13}C] HMBC spectrum, the cross peaks with the neighbouring carbons were easily detected at room temperature (**Figure 4.1.4**). This behaviour was quite different from that exhibited from the same protons when the allyl chain was on the *N*-1 (**87**, **Section 2.2.7**). In that case, they appeared in the ^{1}H NMR as a broad singlet and in the [^{1}H-^{13}C] HMBC their cross peaks were detectable only at high temperatures. The behaviour observed for analogue **91** suggests that the allyl chain does not experience restricted rotation when placed on the *N*-3 of the thiouracil ring. This aspect can be envisaged as a further diagnostic element in establishing the regiochemistry of **87**.

4.2. Synthesis of *N*-3 Substituted Cambinol Analogues 90-91 and 108 *via* Amides 102-104

4.2.1 Synthesis of Amides 102-104

The development of a second synthetic approach towards the synthesis of *N*-3 substituted cambinol analogues was carried out. More specifically, we planned to convert ketocoumarin **52a** into amides **102-104** (METHOD I, R_2, Me, allyl and *n*-hexyl, respectively). Further reaction of the new amides with TMSNCS would lead to ring closure and formation of the desired *N*-1 substituted cambinol analogues (**Scheme 4.2.1.1**). To the best of our knowledge, this approach to the thiouracil system has not been studied previously.

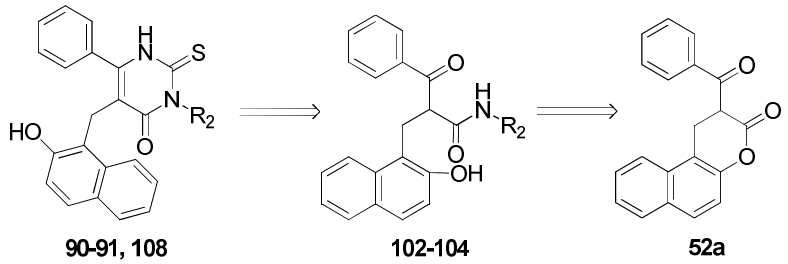

Scheme 4.2.1.1 - Retrosynthetic analysis for the alternative synthesis of *N*-3 functionalised cambinol analogues **90**, **91** and **108** *via* amides **102-104**.

When ketocoumarin **52a** was treated with methylamine (33% sol. in ethanol), allyl amine and *n*-hexylamine under acidic conditions (*p*-TosH, 0.5 eq.), consumption of the starting material **52a** was complete after 5 hours (**Scheme 4.2.1.2**).

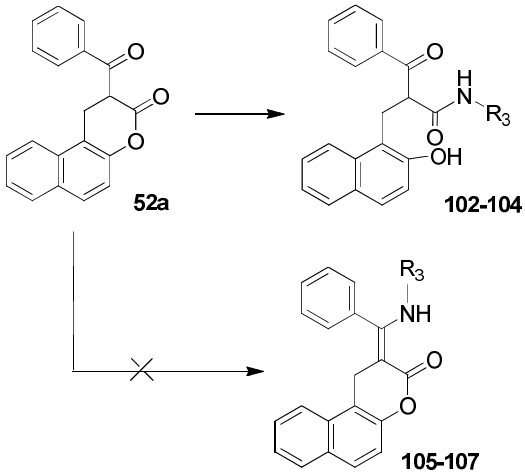

Scheme 4.2.1.2 - Synthesis of Amides **102-104**. Enamines **105-107** were not isolated from the reaction mixture. *Reagents and Conditions*: R_3NH_2 (1.1 eq.), *p*-TsOH (0.5 eq.), EtOH, 5 h, reflux. R_3 = Methyl (**102,** 55%), allyl (**103,** 78%), *n*-hexyl (**104**, not determined).

Analysis of the ^{1}H NMR spectra of the crude samples revealed the formation of a mixture of products. For **102** and **103** separation was achieved by silica-gel column chromatography. In both cases, a major product was isolated from the reaction mixture (**Table 4.2.1**).

Table 4.2.1 - Data for the formation of amides **102-104**. – not characterised

Compound	R_3	Yield (%)	Diagnostic Signals (ppm)
102	Methyl	55	9.67 (OH), 7.95-7.84 (NH), 2.30 (C$\underline{H_3}$N)
103	Allyl	78	9.63 (OH), 8.14 (NH), 3.61 (-C$\underline{H_2}$N)
104	*n*-hexyl	-	-

The high resolution mass spectrometric analysis showed the expected molecular ion peak for amides of general structure **102** and **103**. ^{1}H NMR, ^{13}C NMR and bidimensional [^{1}H-^{1}H] COSY, [^{1}H-^{13}C] HSQC, [^{1}H-^{13}C] HMBC data were consistent with formation of the above mentioned amides.

Enamines **105-107** were not recovered after column chromatography. Despite competing nucleophilic attack of the amine to the more electrophilic ketone functional group of **52a** was expected, this attack is reversible. Furthermore, if formed, enamines **105-107** would not survive purification by silica-gel column chromatography.

The HMBC spectrum was important in the structure determination of **102** and **103**. For simplicity, only a part of the HMBC of **102** will be described (**Figure 4.2.1**).

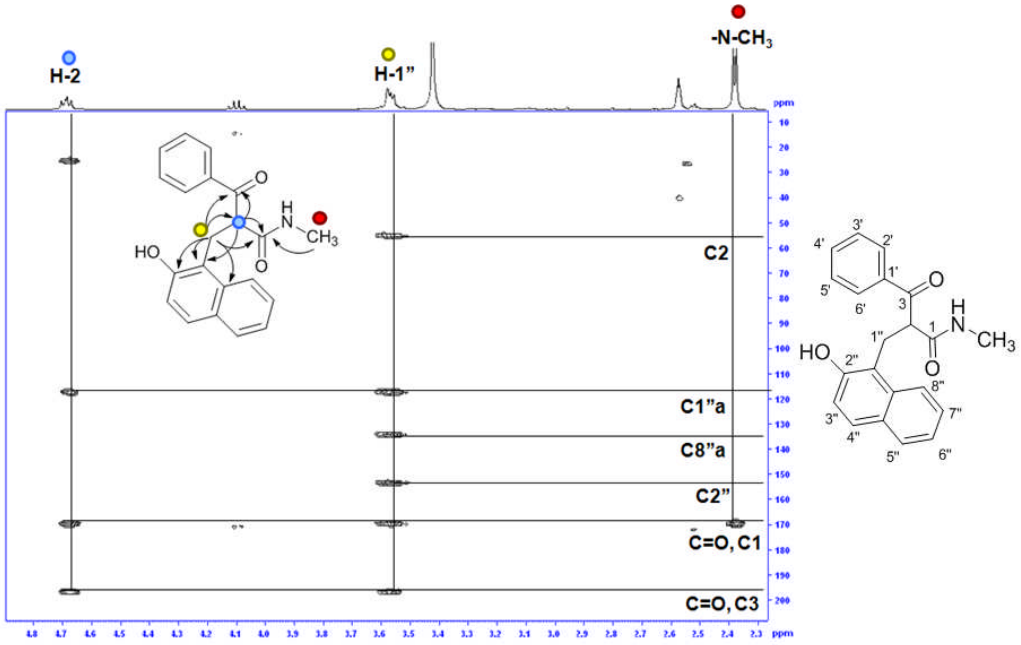

Figure 4.2.1 - Selected area of the [^{1}H-^{13}C] HMBC spectrum of amide **102**. The key interactions used for the determination of the structure are highlighted by arrows and cross-peak lines. For clarity, the numbering system adopted is shown on the structure on the left.

The doublet originating from the protons of the amide methyl group showed only one cross peak to the carbonyl group of the C-1 amide (169 ppm). Consistent with the proposed structure, the protons at C-1" also interacted with the carbonyl at C-3 and with the C-2 carbon. The other cross peaks exhibited by C-1" were with the carbons of the naphthol ring (C-2", C-8"a and C-1"a). The multiplet originating from the proton at C-2 showed cross peaks with the two carbonyl carbons C-1 and C-3, with C-1" and with the quaternary carbon C-1"a of the naphthol ring.

4.2.2 Synthesis of Cambinol Analogues 90, 91 and 108

Treatment of enamino esters with neat TMSNCS to obtain thiourea-type compounds has been described in the literature.[118] Preparation of thouracil rings with TMSNCS starting from keto amides instead of enamino esters has not, to the best of our knowledge, been reported in the literature. It was decided to apply this methodology to the cyclisation of amides **102-104** in order to obtain cambinol analogues **90**, **91** and **108**. Treatment of amides **102-104** with neat TMSNCS at reflux afforded **90**, **91** and **108** in modest yields (36% and 40% **90** and **91**, respectively; 12% over two steps for **108**).

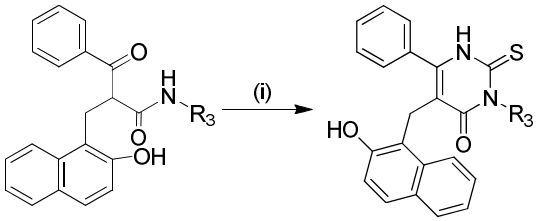

102-104 **90-91, 108**

Scheme 4.2.2 - Synthesis of cambinol analogues **90**-**91** and **108** from amides **102-104**. *Reagents and Conditions*: TMSNCS, 3 h, reflux. R_3 = Methyl (**90** from **101**, 36%), allyl (**91** from **102**, 40%). The yield of **108** from amide **104** was 12% over two steps.

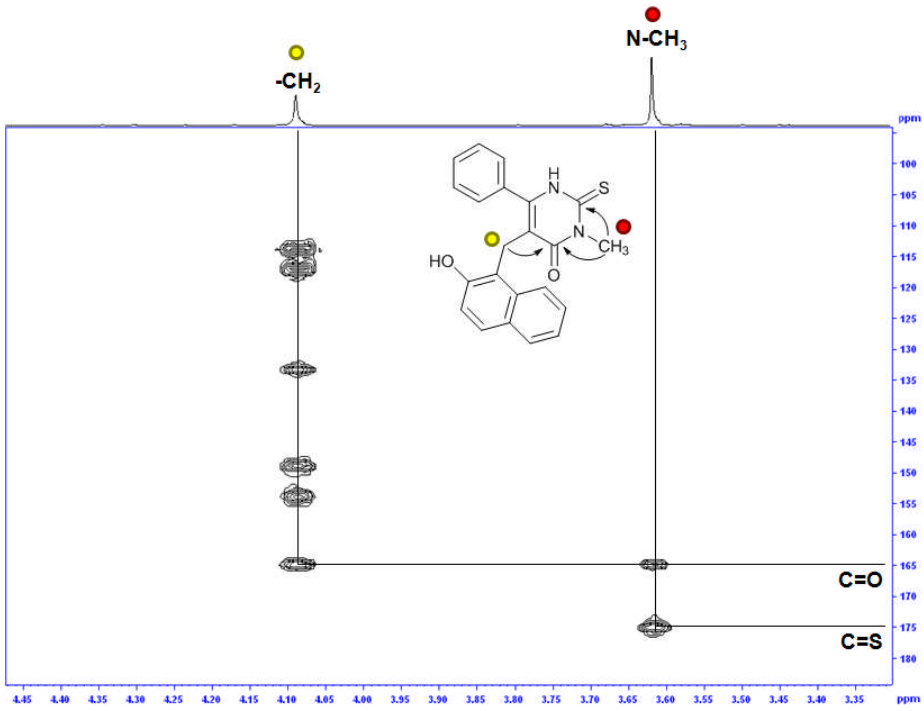

Figure 4.2.2. Selected area of the [^{1}H-^{13}C] HMBC spectrum of **90**. The key interactions used for the determination of the structure are highlighted by arrows and cross-peak lines. The new methyl protons (red) exhibited two cross peaks, the first with the carbonyl (C=O), the second with the thiocarbonyl carbon (C=S).

Once again, compounds **90**, **91** and **108** were fully characterised and the spectroscopic data were in agreement with those already observed for the same compounds (**90** and **91**, **Sections 4.1.3** and **4.1.4**). For all of these compounds the presence of the new aliphatic substituents at *N*-3 was unambiguously proved by means of [^{1}H, ^{13}C] HMBC experiments (**90, Figure 4.2.2**).

Regarding novel analogue **108**, of note for the structural assignment was the behaviour of the protons of the methyline group next to the *N*-3. As expected, they appeared in the ^{1}H NMR spectrum as a well-defined triplet. This behaviour was different from that exhibited from the

same protons when similar aliphatic substituents were at *N*-1 (**82**, **83** and **85**, **Section 2.2.7**). In this case, these protons (-C*H*$_2$-*N*-1) appeared as a broad singlet due to restricted rotation. Furthermore, the corresponding cross peaks were not visible in the [^{1}H, ^{13}C] HMBC experiments run at different temperatures (**83** and **85**). Thus, the above mentioned restricted rotation does not occur when the alkyl substituent is on the *N*-3 of the thiouracil ring. This aspect can be envisaged as further proof that analogues **81**, **83** and **85** (**Section 2.2.7**) had the described regiochemistry.

4.3 *In vitro* Inhibitory Activity of the New Analogues 90-91, 108, 100-101 and 97-98

The target *N*-3 substituted cambinol analogues **90**, **91** and **108**, along with **100-101** and **97-99**, were tested for their inhibitory activity against SIRT1 and SIRT2. The results are reported in **Table 4.3**.

In this series of analogues, the role of different liphophilic substituents at *N*-3 and at the sulfur atom of the thiouracil was investigated. The following observations can be withdrawn:

1. Insertion of a methyl (**90**), allyl (**91**) and *n*-hexyl (**108**) substituent at *N*-3 resulted in poor inhibitory activity against SIRT2, with 22 ± 4, 17 ± 3 and 12.3 ± 2 % inhibition respectively.

2. A partial recovery of the inhibitory activity was observed when a benzyl (**98,** 36.5 ± 5%) or an allyl (**97,** 42.3 ± 1%) group were placed on the sulfur.

3. Analogues **99-101** showed poor percentages of inhibition against SIRT2 (9 ± 2%, 17 ± 2% and 22 ± 5%, respectively).

4. Surprisingly, the presence of benzyl substituent on the sulphur (**98** and **101**) led to modest inhibition of SIRT1 (41 ± 4 and 57 ± 2% respectively). All the other compounds exhibited poor inhibitory activity against SIRT1.

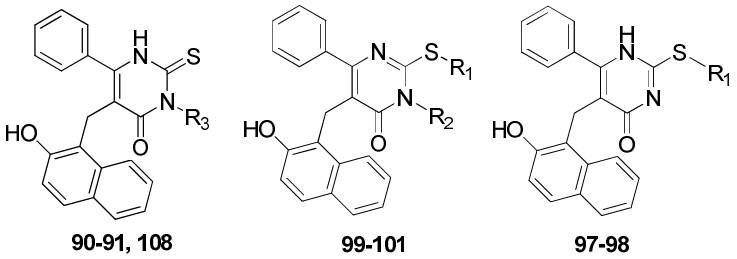

Table 4.3 Inhibitory activities of compounds **90-91**, **108**, **97-98** and **99-101**. Data are reported as percent of inhibition at a final concentration of 60 μM. The inhibition assays by Lisa Pirrie were performed at least in duplicate for each compound. IC_{50} values were calculated for compounds exhibiting a percentage of inhibition greater than 70%.

Compound	R_1	R_2	R_3	SIRT1 [a, b]	IC_{50}[b](μM)	SIRT2 [a, b]	IC_{50}[b](μM)
39[c]	-	-	-	59.5 ± 1.1	40.7 ± 11.1	51.9 ± 1.4	47.9 ± 11.7
46[c]	-	-	-	82.3 ± 1.0	12.7 ± 1.9	9.4 ± 0.7	> 90
47*c*	-	-	-	29.4 ± 1.3	> 90	80.4 ± 1.1	20.1 ± 5.0
90	-	-	Me	19.9 ± 8.3	-	22.1 ± 3.8	-
91	-	-	Allyl	30.8 ± 1.9	-	17.2 ± 2.9	-
108	-	-	Hexyl	40.5 ± 4.3	-	12.3 ± 1.8	-
97	Allyl	-	-	11.1 ± 1.1	-	36.5 ± 4.8	-
98	Benzyl	-	-	41.4 ± 3.8	-	42.3 ± 0.8	-
99	Allyl	Allyl	-	13.2 ± 2.9	-	9.2 ± 1.9	-
100	Allyl	Me	-	5.17 ± 1.1	-	17.0 ± 1.8	-
101	Benzyl	Me	-	57.5 ± 2.2	-	22.9 ± 4.7	-

[a] SE, standard error (n = 2).
[b] IC_{50} were determined for compounds that had over 60% inhibition at 60 μM for SIRT1 and SIRT2 (repeated at least twice).
- Not determined.
[c] Control.

4.4. Conclusions

In this chapter, two synthetic methods for the synthesis of *N*-3 substituted cambinol analogues have been described. The first was based on protection of the most nucleophilic sulphur atom in **39** to afford **97**. Compound **97** was converted in good yield into the *N*-3 allyl analogue **90** by means of Pd-catalysed Claisen rearrangement. After selective methylation of **97** on the *N*-3 to give **100**, the allyl group at the sulphur was removed using a Pd^0 catalyst in the presence of morpholine as additive to give **91**. In the second method, the amides **102-104** were treated with TMSNCS to afford the new analogues **90-91** and **108**. As far as we are aware, this cyclisation has not been reported before in the literature.

In vitro evaluation of the target compounds **90** and **91** showed poor levels of activity against SIRT2 and SIRT1. These results were expected based on the findings from the molecular docking studies run on the same compounds (**Chapter 3**). Thus, substitution at the *N*-3 was not tolerated, probably due to lack of space around the *N*-3 into the active site. Furthermore, it may be possible that the lipophilic nature of the two *N*-3 substituents (Methyl, **90**; Allyl, **91; 108**, n-hexyl) is not tolerated for the correct binding of the molecule, due to the polar residues present around the same nitrogen in the active site.

All other analogues synthesised in this work were also tested against the two isoforms of the enzyme. Poor levels of inhibition were observed for most compounds. Only analogues **97** and **98** showed a modest inhibitory activity against SIRT2. The improved activity suggests that the new liphophilic substituent at the sulphur atom may be accommodated into the liphophilic pocket at the entrance to the nicotinamide-exchange tunnel. At the moment this consideration needs careful interpretation. As expected, none of the new compounds showed significant inhibitory activity against SIRT1, except when a benzyl substituent was placed on the sulfur atom (**98** and **101**). The level of inhibition observed for **98** and **101** was modest (41 and 57%, respectively).

Despite the negative biological results, these data are consistent with the proposed binding mode. The expected crucial role played by an aliphatic substituent at the *N*-1 for potent and selective SIRT2 inhibition was further confirmed. In the future, it will be interesting to synthesise and test analogues characterised by polar substituents at the *N*-3 in order to test the hypothesis that this type of group would be better accommodated in the polar area proposed to host the *N*-3 position.

5. *N*-1 BENZYL CAMBINOL ANALOGUES

This chapter describes the synthesis and *in vitro* biological evaluation of a third series of cambinol analogues. The main difference with the previous collections of analogues is the presence of a benzylic substituent at the *N*-1 position. The design of these new compounds was based on the results of the computational studies reported in **Chapter 3**. As the final step of the synthetic route reported in **Chapter 2** proved to be unsatisfactory in terms of yields and reproducibility, a new 6-step synthetic approach was developed and is described. All analytical data associated with the compounds described in this chapter is reported in **Chapter 6, Part III**.

5.1. Synthesis of *N*-1 Benzyl Substituted Cambinol Analogues

5.1.1. Retrosynthetic Analysis

As the synthetic methodology reported in **Chapter 2** did not allow for the insertion of bulky aromatic substituents, such as benzyl or phenyl, at the *N*-1 position of cambinol **39**, a new synthesis of this type of molecule was designed. This new approach was based on the modification of the route adopted in **Chapter 2** (**Scheme 5.1.1**). There were three main differences as outlined below:

1. Formation of the lactone ring in intermediate **51** (**Chapter 2**) was avoided through protection of the phenol in naphthaldehyde **49** with an acid-stable protecting group (P, **109-110**);

2. Synthesis of the key-enamine intermediate **119-135**, followed by cyclisation and formation of the thiouracil moiety of **144-160**;

3. Final deprotection of the phenolic OH and formation of the desired cambinol analogues of general structure **92-95**.

Scheme 5.1.1 outlines the retrosynthetic approach. After protection of the naphthol group in **49**, Knoevenagel condensation of **109-110** with ethyl benzoylacetates **50a-i-v**, followed by reduction of the resulting conjugated double bond was expected to lead to ketoester **115-118.** Enamine formation would then occur by reaction at the ketone group in **115-118**. The thiouracil

core in **144-160** would then be formed by treatment of **119-135** with neat TMSNCS, according to a reported procedure.[118] Finally, deprotection of the naphthol OH would lead to the new cambinol analogues **92-95**.

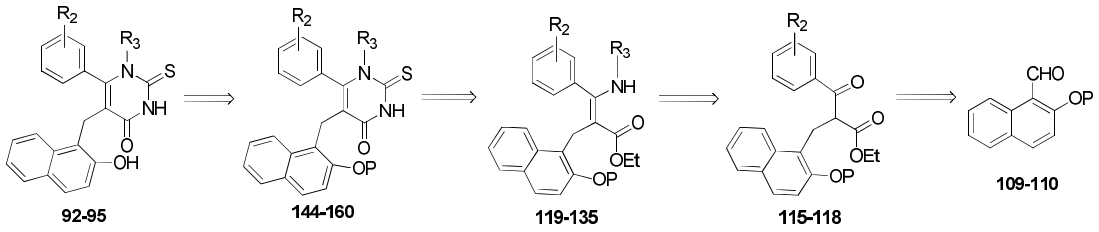

Scheme 5.1.1 - Retrosynthetic analysis for the synthesis of *N*-1 benzyl substituted cambinol **39** analogues. R_2 = varies; R_3 = benzyl; P = protecting group.

5.1.2 Step 1: Protection of 2-hydroxy-1-naphthaldehyde 49

Treatment of 2-hydroxy-1-naphthaldehyde **49** with benzyl bromide or methyl iodide (1.1 eq.) under basic conditions (K_2CO_3) afforded the known compounds **109** and **110** in good yields (83% and 81%, respectively, **Scheme 5.1.2, Table 5.1.2**).[119,120] The choice of these two acid-resistant protecting groups was due to the acidic conditions that were expected to be necessary for the formation of the enamine intermediates **119-135**. It was decided to carry out the new synthesis using two different protecting groups in order to allow flexibility during the deprotection to give the naphthol OH at a later stage in the synthesis.

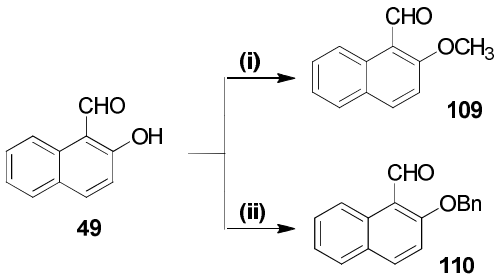

Scheme 5.1.2 - Protection of 2-hydroxy-1-naphthaldehyde **49**. *Reagents and Conditions*: (i) K_2CO_3 (2 eq.), MeI (1.1 eq.), DMF, rt, 18 h, (**109**, 83%); [119] (ii) K_2CO_3 (1.5 eq.), BnBr (1.1 eq.), acetone, reflux, 18 h, (**110**, 81%).[120]

After basic work-up, analysis of the crude ^{1}H NMR spectrum suggested successful formation of the desired products. Spectroscopic data were in an agreement with those reported in the

literature.[119,120] As the products were obtained with a high level of purity, as observed by ^{1}H NMR analysis, it was therefore decided to avoid further purification.

Table 5.1.2 - Yields observed for products **109-110** after the first step. Chemical shift values of the new diagnostic proton signals are reported. Yields refer to the amount of product isolated after basic work-up.

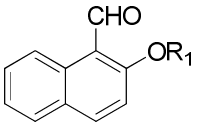

109-110

Compound	Yield (%)	Diagnostic Signals (^{1}H NMR, ppm)
109	83	4.02 (C*H*$_3$O)
110	81	5.33 (C*H*$_2$Ph)

5.1.3 Step 2: Knoevenagel Condensation of 109-110 with Ethyl Benzoylacetates 50a-i-v

As reported for the synthesis of intermediate **51** (**Chapter 2**), analogous treatment of **109-110** with ethyl benzoylacetate **50a**, **50i** and **50v** under basic conditions (piperidine) at reflux led to formation of acrylates **111-114** (**Scheme 5.1.3, Table 5.1.3**).

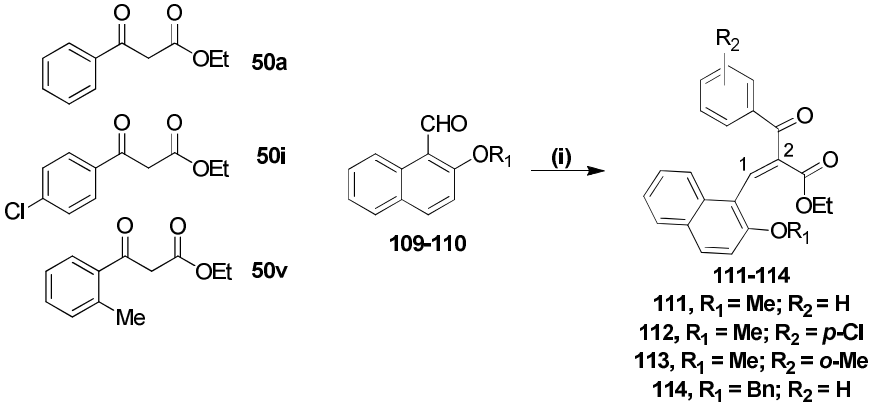

Scheme 5.1.3 - Formation of acrylates **111-114**. *Reagents and Conditions:* (i) ethyl benzoylacetate **50**, **50i** and **50v** (2 eq.), piperidine (cat.), EtOH, 18 h, reflux (**111**, 32% ; **112**, 46%; **113**, 43%; **114**, 42%).

Initially, the reaction was attempted on substrate **110** in order to obtain compound **114** (R_1 = Bn; R_2 = H). With the use of one equivalent of ethyl benzoylacetate **50a** (R_2 = H), completion of the reaction could not be achieved after 24 hours heating at reflux. Addition of a further equivalent

of **50a** and longer reaction time (48 hours) still did not lead to total consumption of **110**. Therefore, the reaction was stopped and analysed.

Several problems were encountered during the purification of **114**. Analysis of the ^{1}H NMR spectrum of the crude material suggested the presence of **110**, along with the expected product **114**. Analysis of the crude reaction mixture by TLC indicated similar R_f values for **114** and **110**, suggesting that purification by column chromatography was not optimal. In fact, when attempted this was found to be the case, with the compounds all co-eluting. Thus an alternative purification method was required. In the previous synthetic approach (**Chapter 2**) ketolactones **51 a-x**, characterised by a similar structure to **114**, exhibited low solubility in ethanol. This observation inspired attempts to precipitate **114** directly from the reaction. After repetition of the reaction, the ethanolic solution was cooled to 0 °C in an ice-water bath. After a few minutes, a yellow precipitate started to form. After isolation by filtration, ^{1}H NMR analysis of this solid revealed that the expected product had been successfully isolated in pure form as a microcrystalline yellow powder in a modest 42% yield.

The conditions described above were applied to the synthesis of the other three acrylates **111-113** (METHOD J). All the expected products were obtained as pure microcrystalline powders. The ^{1}H NMR spectrum of **111-114** showed a diagnostic singlet at around 8.40 ppm, which was assigned to the C-1 proton.

Table 5.1.3 - Yields observed in the synthesis of **111-114**. Chemical shift values of the diagnostic singlet derived from the H-1 proton are listed. Yields refer to the amount of product isolated by direct precipitation from the reaction mixture after cooling to 0 °C.

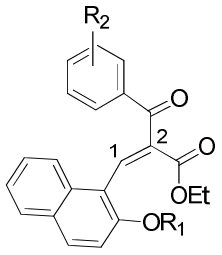

111-114

Compound	R_1	R_2	Yield (%)	Diagnostic Signals (H-1) (ppm)
111	CH_3	H	32	8.44
112	CH_3	*p*-Cl	46	8.45
113	CH_3	*o*-CH_3	43	8.31
114	Bn	H	42	8.33

Full characterisation of **111-114** was carried out by means of ^{13}C NMR, [^{1}H-^{1}H] COSY, [^{1}H-^{13}C] HSQC and HMBC experiments. Unfortunately, due to overlap of signals in the aromatic region, a complete assignment was not always possible. This was particularly true for compound **114**.

The modest yield observed for compounds **111-114** was partially rationalised by the incomplete consumption of **109-110**. Furthermore, the precipitation procedure adopted for the isolation of **111-114** may have not been optimal. In fact, it may be possible that the different products exhibit different solubility in ethanol, thus explaining the different yields observed. Consistent with this, after precipitation, ^{1}H NMR analysis of the supernatant revealed the presence of residual amounts of product.

5.1.4 Step 3: Reduction of the Conjugated 1,2 Double Bond

Reduction of the conjugated double bond present in acrylates **111-114** was carried out according to the same procedure described in **Chapter 2** for the synthesis of intermediates **52**. Again, this reaction was initially applied to compound **114** only. Treatment of **114** with $NaBH_4$ (1.1 eq.) in pyridine resulted in consumption of **114** after 2 hours at room temperature (METHOD K, **Scheme 5.1.4**). Acidic work-up, followed by purification by silica-gel column chromatography, afforded the expected reduced intermediate **118** in 71% yield as a colourless oil. ^{1}H NMR analysis of **118** showed the absence of the singlet at around 8.33 ppm corresponding to H-1 in **114**. The same spectrum was characterised by ten aromatic protons and by three new doublets of doublets assigned as shown in **Table 5.1.4**. This procedure was applied to the synthesis of all the propionates **115-117**. The results are listed in **Table 5.1.4**.

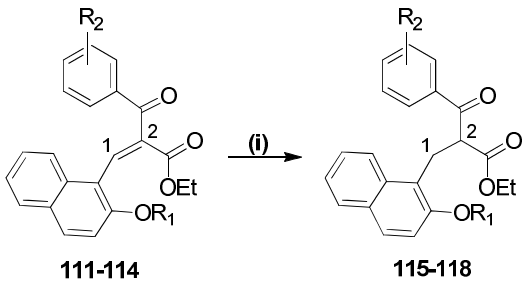

111-114 **115-118**

Scheme 5.1.4 - Formation of propionates **115-118**. *Reagents and Conditions*: (i) $NaBH_4$ (1.1 eq.), pyridine, 2 h, rt (**115**, 75%; **116**, 76%; **117**, 75%; **118**, 71%).

Table 5.1.4 - Yields observed for products **115-118** after the third step. Chemical shift values of the diagnostic doublets of doublets derived from the H-2 proton are listed. Yields refer to the amount of product isolated after silica-gel column chromatography purification.

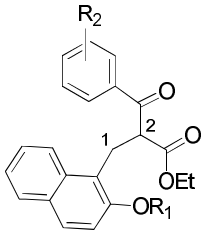

115-118

Compound	R_1	R_2	Yield (%)	Diagnostic Signal (H-2) (ppm)
115	CH_3	H	75	4.75
116	CH_3	*p*-Cl	76	4.68
117	CH_3	*m*-CH_3	75	4.70
118	Bn	H	71	4.85

5.1.5 Step 4: Formation of Enamines 119-135

Initially, formation of enamines **119-135** from **115-118** was attempted using a literature protocol (**Scheme 5.1.5.1**).[121] **118** was treated with excess benzylamine (5 eq.) in the presence of acetic acid (5 eq., **Table 5.1.5.1, Entry 1**). After 20 hours heating at reflux, no consumption of **118** was observed. The addition of 5 further equivalents of benzylamine was used and the reaction was stopped after 48 hours. Disappointingly, analysis of the ^{1}H NMR spectrum of the crude product after acidic work up (2M HCl) revealed the presence of only starting material **118**.

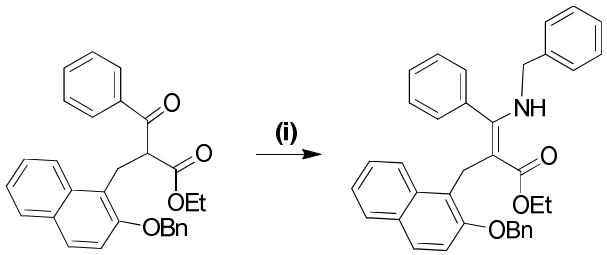

118 **127**

Scheme 5.1.5.1 - Synthesis of enamine **127**. *Reagents and conditions*: (i) $BnNH_2$ (10 eq.), AcOH (10 eq.), EtOH, 48 h, reflux.

When repeated using the same conditions previously described above, the progression of the reaction was studied by means of ^{1}H NMR spectroscopy on small aliquots of the reaction mixture (**Table 5.1.5.1, Entry 2**). Interestingly, the presence of a broad triplet at 9.54 ppm in

the ^{1}H NMR spectrum, assignable to the enamine NH proton of the product, was observed after a few hours. The intensity of this broad triplet did not increase with the time. When the reaction aliquots were worked-up (2M HCl), this signal was no longer observed in the ^{1}H NMR spectrum. Only unreacted starting material was detectable. When purification of the reaction mixture was attempted by silica-gel column chromatography, only starting material was recovered. These observations were consistent with the instability of the product during an acidic aqueous work-up or silica-gel chromatography.

An alternative work-up procedure was then employed (**Table 5.1.5.1, Entry 3**). The solvent was removed under reduced pressure and the residue purified by column chromatography using basic alumina. It was gratifying to find that the expected enamine **127** could be successfully isolated.

However, the presence of unreacted **118** still represented a problem. In fact, due to the similar R_f values of **118** and **127**, the purification on basic-alumina did not allow for complete separation. Thus, an exact yield for this reaction cannot be reported. ^{1}H NMR analysis of the crude reaction mixture suggested a 69% conversion of **118** to **127** (**Table 5.1.5.1, Entry 3**).

Table 5.1.5.1 - Summary of the initial optimisation conducted on the synthesis of **127** from **118**. *Reagents and conditions:* $BnNH_2$ (10 eq.), AcOH (10 eq.), EtOH, 48 h, reflux. [a] Percentage of conversion calculated by ^{1}H NMR integration of the relevant proton signals observed in the reaction crude spectrum. [b] Percentage of conversion calculated by ^{1}H NMR integration of the relevant proton signals observed in the spectrum obtained after the reported purification.

Entry	Work-up	Purification (column)	Conversion (%)
1	2M HCl, DCM	-	0 [a]
2	Solvent removal	Silica	0 [b]
3	Solvent removal	Alumina	69 [b]

In an attempt to optimise this reaction, it was decided to perform a series of model reactions on simple substrates and to try to determine the most successful conditions for this transformation (**Scheme 5.1.5.2**). When substrates **50a** and **136** were reacted with benzylamine (5 eq.) in the presence of acetic acid (5 eq.), all reactions were found to have gone to completion within 24 hours at reflux, as indicated by TLC analysis. No addition of further equivalents of benzylamine or acid was required. Furthermore, products **135** and **131** were stable to acidic work-up and the ^{1}H NMR spectra of the crude materials were characterised by a high level of

purity (METHOD L). Thus, further purification by column chromatography was not attempted. It was interesting to note that slow decomposition of **131** was observed upon storing at room temperature in air. Enamine **135** was stable under the same conditions for a longer period of time.

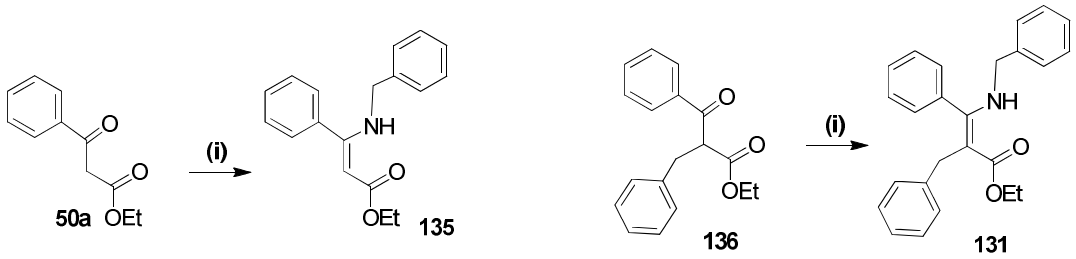

Schme 5.1.5.2 - Model reactions run on substrates **50a** and **135**. Total (**135**) conversion of starting material was observed within 24 h at reflux. *Reagents and conditions*: (i) $BnNH_2$ (5 eq.), AcOH (5 eq.), EtOH, 24 h, reflux (**135**, 100%; **131**, 95%).

The successful formation of enamines **131** and **135**, accompanied by total consumption of the starting materials, suggested that the 69% conversion observed for **127** (**Entry 3, Table 5.1.5.1**) could be due to the sterically bulky *O*-protected naphthol group in the starting material **127**. Further optimisation of the synthesis of **127** was attempted. Extending the reaction time to 7 days, along with addition of several equivalents of benzylamine and acetic acid did not lead to total consumption of the starting material **127**. The previous 69% conversion observed was considered acceptable for the continuation of the synthesis and therefore these optimisation studies were abandoned.

Once it had been established that this methodology was applicable to sterically hindered propionates of general structure **115-118**, it was decided to apply it to the synthesis of the corresponding enamines **119-135** (METHOD M). Propionates **115-118** were reacted with a range of *para*-alkoxy substituted benzylamines and aliphatic amines. Unfortunately, only benzylamine **137**, *p*-methoxybenzylamine **138**, methylamine **139** and butylamine **140** were commercially available. Thus, three *para*-substituted benzylamines **141-143** were synthesised in our laboratory according to previously reported procedures.[122]

In brief, *para*-hydroxybenzaldehyde **144** was treated under basic conditions with a series of alkylbromides or iodides. The freshly synthesised *para*-alkoxybenzaldehydes **145-147** were converted into the corresponding *para*-alkoxybenzaldoximes **148-150** after treatment with hydroxylamine hydrochloride. Finally, the required amines were obtained after reduction of

141-143 with nickel-aluminium alloy under basic conditions. These reactions are outlined in **Scheme 5.1.5.3** and the results summarised in **Table 5.1.5.2**.

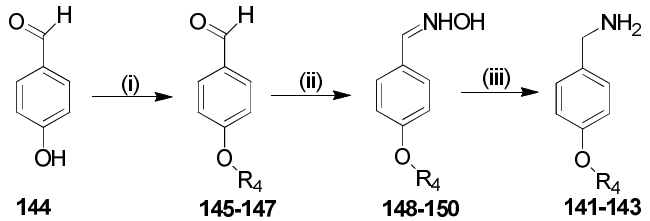

Scheme 5.1.5.3 - Outline of the three step syntheses of benzyl amines **141-143**. *Reagents and Conditions*: (i) Alkyl bromide (1.2 eq.), K_2CO_3 (2 eq.), H_2O-MeOH (1:1), 18 h, reflux; (ii) NH_2OH HCl (1.2 eq.), K_2CO_3 (2 eq.), H_2O-EtOH (1:1), 4 h, rt; (iii) Nickel-aluminium alloy, NaOH (10%, aq.), 4 h, rt.

Table 5.1.5.2 - Summary of the three step syntheses of benzyl amines **141-143**.

Amine	R_4	Yield (%) Step i	Yield (%) Step ii	Yield (%) Step iii
141	Et	76 (**145**)	62 (**148**)	62
142	*n*Pr	Quant. (**146**)	81 (**149**)	69
143	*n*Bu	Quant. (**147**)	78 (**150**)	65

With the required amines in hand, the synthesis of enamines **119-135** could be attempted. The results of the formation of the new enamines, along with those previously described in this section (**127, 131** and **135**) are summarised in **Table 5.1.5.3**. Due to the incomplete consumption of starting material and the challenge in purifying **119-135**, the yield for the formation of the products could not be calculated. Thus, the results are reported as percentage conversions. A further proof for the successful synthesis of enamines **119-135** comes from their subsequent chemistry (**Section 5.1.6**).

Table 5.1.5.3 - Conversion of propionates **115-118** into enamines **119-135**. Chemical shift values for the diagnostic enamine proton are listed. Conversion was calculated by ^{1}H NMR integration of the relevant proton signals in the analysis of the ^{1}H NMR reaction crude. *Reagents and conditions*: Amine (5 or 10 eq.), AcOH (equimolar with amine), EtOH, 48 h, reflux.

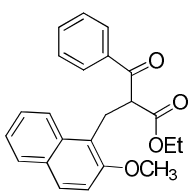

115

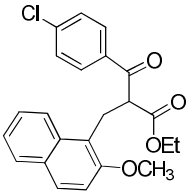

116

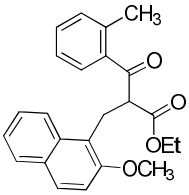

117

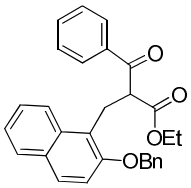

118

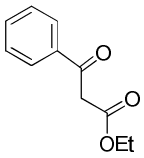

50a

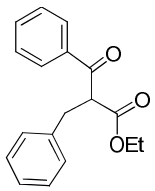

136

139

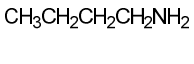

140

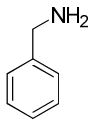

137

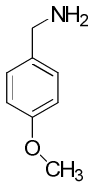

138

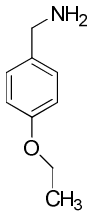

141

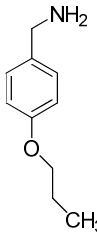

142

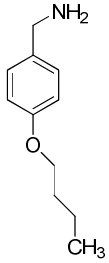

143

Starting Material	Amine (eq.)	Product	% conversion	Diagnostic Signals (NH) (ppm)
115	**137 (10)**	**119**	70	9.54
115	**138 (10)**	**120**	55	9.52
115	**141 (10)**	**121**	59	9.46
115	**142 (10)**	**122**	81	9.46
115	**143 (10)**	**123**	61	9.46
115	**139 (5)**	**124**	31	9.09
116	**140 (5)**	**125**	87	9.14
117	**140 (5)**	**126**	69	9.30
118	**137 (10)**	**127**	55	9.57
118	**138 (10)**	**128**	64	9.63
118	**141 (10)**	**129**	30	9.51
118	**142 (10)**	**130**	62	9.52
136	**137 (10)**	**131**	95	9.64
136	**138 (10)**	**132**	73	9.56
136	**141 (10)**	**133**	77	9.55
136	**143 (10)**	**134**	74	9.57
50a	**137 (5)**	**135**	100	9.50

In summary, no reaction was found to reach completion after two days at reflux, except for the less sterically hindered product **135**. Formation of the different enamines from **136** led to an

average conversion of 80% (n = 4). When the more sterically hindered **115** was used, the average conversion decreased to 59% (n = 6). Consistent with this, the presence of an extra benzyl group in **118** led to a lower average conversion (52%, n = 4). Thus, the steric hindrance of the starting propionates **115-118** seems to affect the conversions observed in these reactions. Enamines **119-135** were not fully characterised and they were directly reacted in the next step.

5.1.6 Step 5: Formation of the Thiouracil Ring, Preliminary Studies

Therkelsen and co-workers reported the reaction of enamino-esters of structure **161** with neat TMSNCS at reflux to afford the corresponding cyclised thiouracil products **162** in good yields after purification by column chromatography (**Scheme 5.1.6.1**).[118]

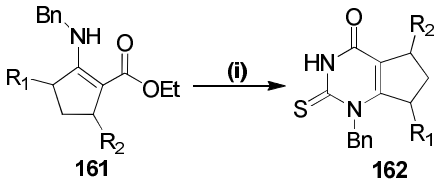

Scheme 5.1.6.1 - Ring closing reaction of enamino-esters **161** with neat TMSNCS to form thiouracil compounds **161** (R_1 = Ph or H; R_2 = CH_3 or H). *Reagents and Conditions*: (i) TMSNCS, 2 h, reflux (**162**, R_1 = Ph; R_2 = Me, 92%). The stereochemistry of **161** and **162** is not indicated in the reference paper. [118]

It was decided to apply this methodology to our system. Initially, only three enamines (**127, 131** and **135**, **Scheme 5.1.6.2**) were reacted with neat TMSNCS. Small aliquots were taken every hour, worked up and analysed by TLC and ^{1}H NMR spectroscopy. After 2 hours, complete consumption of **127, 131** and **135** was observed by TLC.

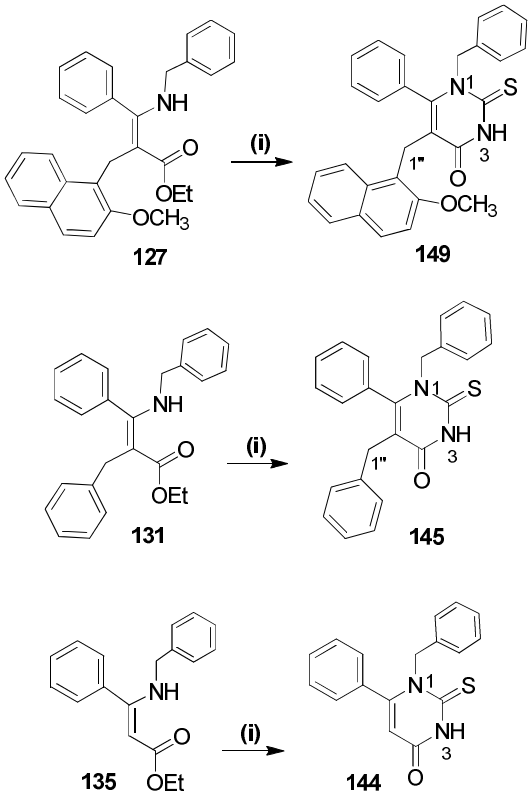

Sheme 5.1.6.2 - Cyclisation of crude enamines **127**, **131** and **135** with TMSNCS. Analogues **144**, **145** and **149** were obtained. *Reagents and Conditions*: (i) TMSNCS (neat), 2 h, reflux.

Furthermore, in the ^{1}H NMR spectrum of the crude reaction mixture, the absence of the signals corresponding to the down-field broad triplet assigned to the enamine NH proton was observed. The reactions were therefore quenched with aqueous $NaHCO_3$ and worked-up. The products (**Table 5.1.6**) were easily purified by silica-gel column chromatography and the structure determined in the usual way (METHOD N).

Table 5.1.6 - Yields observed for cyclisation products **144, 145** and **147**. Chemical shift values for the diagnostic protons signals are listed. Yields refer to the amount of product isolated after silica-gel column chromatography purification.

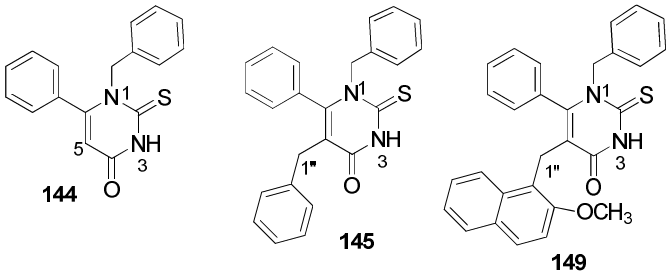

Starting material	Product	Yield (%)	Diagnostic Signals (ppm)	
135	**144**	80	10.77 (NH)	5.90 (H-5)
131	**145**	76	9.66 (NH)	3.41 (H-1")
127	**149**	23	9.77 (NH)	4.07 (H-1")

5.1.7 Structural Determination of Cambinol Analogues 144, 145 and 149

The successful formation of cambinol analogues **144**, **145** and **149** was confirmed using ^{1}H NMR, ^{13}C NMR, [^{1}H-^{1}H] COSY, [^{1}H-^{13}C] HSQC and HMBC spectroscopy. Further support for the confirmed structures came from HRMS and IR analysis. Interestingly, in the ^{1}H NMR spectra, the *N*-3 amino proton was always observed in the low field region around 10.70-9.70 ppm (**Figure 5.1.7.1, Table 5.1.6**). In the ^{1}H NMR spectrum of **144**, the signal associated with the protons of the benzylic methylene group at C-1''' appeared as a broad singlet at 5.52 ppm (**Figure 5.1.7.2.A**). This particular shape suggested restricted rotation of the new benzylic substituent at *N*-1 which is likely to be due to a steric clash with the adjacent phenyl and thiocarbonyl moieties.

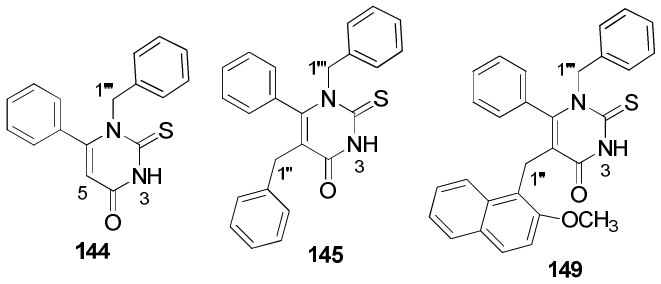

Figure 5.1.7.1 - Structures of the new cyclised products **144, 145** and **149**.

The structural determination of **145** and **149** was found to be more problematic. For compound **145**, in the ^{1}H NMR spectrum, the peak assigned to the benzylic protons at C1''' again appeared as a broad singlet, now integrating to less then 2 protons (**Figure 5.1.7.2.B**). Regarding compound **149**, the same signal could not be observed in the ^{1}H NMR experiment (**Figure 5.1.7.2.C**). In the ^{13}C NMR spectra of both molecules, the C-1''' peaks were absent. The benzylic carbon C-1''' could also not be observed in the 2-dimensional [^{1}H-^{13}C] HSQC and HMBC spectra. This result appeared even more contradictory because in both the ^{1}H and ^{13}C NMR spectra of the two molecules, the correct number of aromatic proton signals and aromatic carbon signals were observed. Furthermore, the molecular weights of the compounds as determined by high resolution mass spectrometry were in agreement with those calculated for the two compounds.

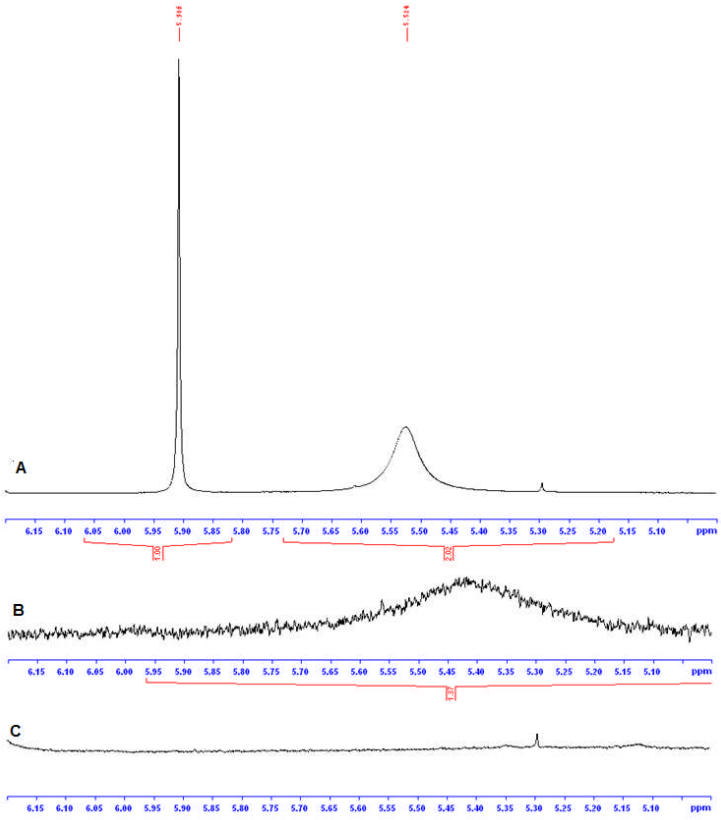

Figure 5.1.7.2 – Section of the ^{1}H NMR spectra of compounds **144, 145** and **149** between 6.10-5.00 ppm. While the spectrum of **144** (**A**) shows the expected broad singlet for the new benzylic protons at C-1''', the signals expected from the same protons were not detected in the spectrum of compounds **145** and **149** (**B** and **C**, respectively). The other singlet present in the spectrum of **144** derives from the proton at C-5.

Fortunately, this problem was solved by means of X-ray crystallography, as compound **149** afforded small crystals that were suitable for X-ray structure determination on slow evaporation

from ethanol. Analysis of this crystal structure confirmed that the expected new analogue **149** had been successfully synthesised. The particular behaviour of the benzylic methylene proton and carbon atoms in the NMR spectrum can be explained by the restricted rotation of the new benzylic *N*-1 substituent. A closer inspection of the crystal structure of **149** (**Figure 5.1.7.3**) showed the phenyl ring at C-6 and the naphthol substituent parallel to each other, probably interacting by means of π-stacking interactions. The *N*-1 benzyl group was found to be perpendicular to both the thiouracil ring and the C-5 phenyl ring. As the crystal structure of the smaller analogues **144** and **145** was not determined, it is possible that in progressing from having no substituent at C-5 (**144**), to a benzyl substituent (**145**) and finally to a naphthol group (**149**), the mentioned restricted rotation effect increases, thus gradually broadening the proton and carbon signals associated with the benzylic methylene functionalities.

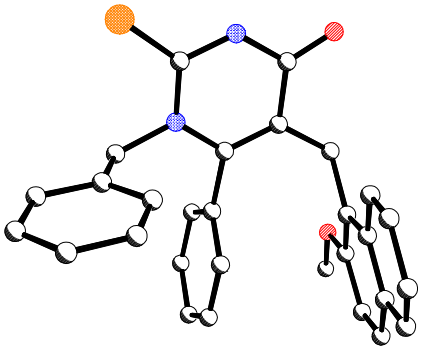

Figure 5.1.7.3 - Crystal structure determination of **149**. Crystals were obtained by slow evaporation from ethanol

Having established the correct structure for **144** and **149**, the cyclisation step was extended to the other enamines. At this point some uncertainties were still present regarding the structure of **145**. In the absence of a crystal structure, it was decided to compare the ^{1}H NMR spectra of the closely related analogues **146-148** (**Section 5.1.8**) in order to obtain further evidence for the successful synthesis of **145**.

5.1.8 Step 5: Formation of the Thiouracil Ring

All the enamines synthesised in **Section 5.1.5** were reacted with neat TMSNCS according to the previously described experimental procedure giving fourteen new cambinol analogues. Three of these contained a benzyl group in place of the naphthol group (**146-148**, **Table 5.1.8.1**). The

other eleven that contained a naphthol substituent at the C-5 position, are reported in **Table 5.1.8.2**.

Table 5.1.8.1 - Yields observed for cyclisation products **146-148**. Chemical shift values for the diagnostic peaks in the ^{1}H NMR spectrum are listed. Yields refer to the amount of product isolated after silica-gel column chromatography purification. The yield was calculated after one step from the enamines starting materials.

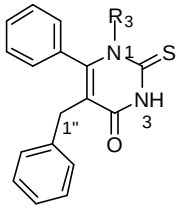

146-148

Starting material	Product	R_3	Yield (%)	Diagnostic Signals (H-1'') (ppm)
132	**146**	*p*-MeOBn	60	3.76
133	**147**	*p*-EtOBn	68	3.97
134	**148**	*p*-*n*BuOBn	57	3.90

Table 5.1.8.2 - Yields observed for cyclisation products **150-160**. Chemical shifts values for the diagnostic proton peaks are listed. Yields refer to the amount of product isolated after silica-gel column chromatography purification and was calculated after two steps from **115-118**.

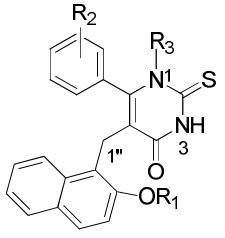

150-160

Compound[a]	R_1	R_2	R_3	Yield (%)	Diagnostic Signals (H-1'', ppm)
150 (120)	Me	H	*p*-MeOBn	33	4.06
151 (121)	Me	H	*p*-EtOBn	26	3.97
152 (122)	Me	H	*p*-PrOBn	39	4.05
153 (123)	Me	H	*p*-BuOBn	20	4.06
154 (124)	Me	H	Me	24	3.92
155 (125)	Me	*p*-Cl	*n*-Bu	33	4.10
156 (126)	Me	*o*-Me	*n*-Bu	31	4.28-4.02*
157 (127)	Bn	H	Bn	31	4.73
158 (128)	Bn	H	*p*-MeOBn	25	4.12
159 (129)	Bn	H	*p*-EtOBn	39	4.11
160 (130)	Bn	H	*p*-PrOBn	21	4.12

[a] The corresponding crude enamine starting material in indicated in brackets. * Singlet overlapped with other signals.

Despite the lack of the signal derived from the benzylic methylene C-1''' hydrogen and carbon atoms, particularly for analogues **146-148**, **150-153** and **157-160** the presence of the signal derived from the *para*-alkoxy chains of the *N*-1 benzyl group in both the ^{1}H and ^{13}C NMR spectra further supported the successful synthesis of these new analogues.

Regarding the mechanism of the cyclisation, it is probable that the reaction starts with the attack of the most nucleophilic amine of the enamine at the central carbon of the thiocyanate group in TMSNCS (**Scheme 5.1.8**). After proton transfer (**163**), reaction of *N*-silyl-substituted nitrogen on the ester functionality would give **144-160** after loss of the TMS protecting group. It cannot be ruled out that the loss of the TMS group occurs prior to cyclisation.[123]

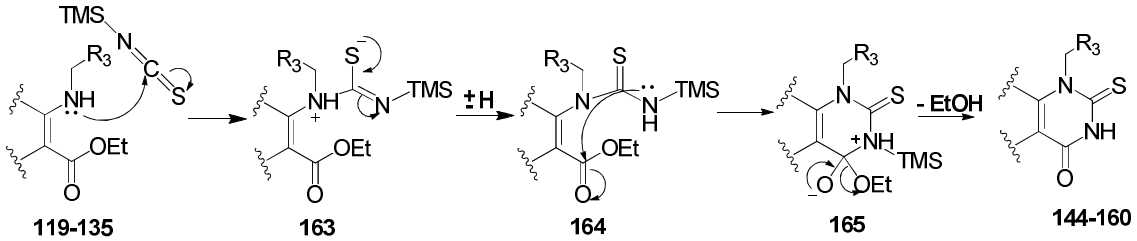

Scheme 5.1.8 - Proposed mechanism for the formation of the thiouracil ring with TMSNCS.[123]

5.1.9 Step 6: Deprotection of the Phenol Group

The final step of this synthetic approach was the preparation of the cambinol analogues without a substituent on the naphthol OH group. With compounds **150-153** in hand, initial attempts focused on the deprotection of the analogues bearing a methyl protecting group. The first reagent attempted was BBr_3 (1.0 M sol. in DCM) as the majority of literature reports listed it as the first choice reagent for the selective cleavage of alkyl ethers.[124] Two possible problems were anticipated with the reagent:

1. The necessity to add several equivalents of BBr_3 in order to drive the reaction to completion due to the large number of heteroatoms in **150-153**;

2. The possibility of competing deprotection due to the presence in **150-153** not only of the naphthol methoxy group but also of the alkoxy ether at the *para*-position of the *N*-1 benzylic substituent. This problem would possibly be more serious in cases where addition of several equivalents of BBr_3 was required.

When substrate **153** was reacted with one equivalent of BBr_3 (**Scheme 5.1.9.1**), the expected problems were experienced.

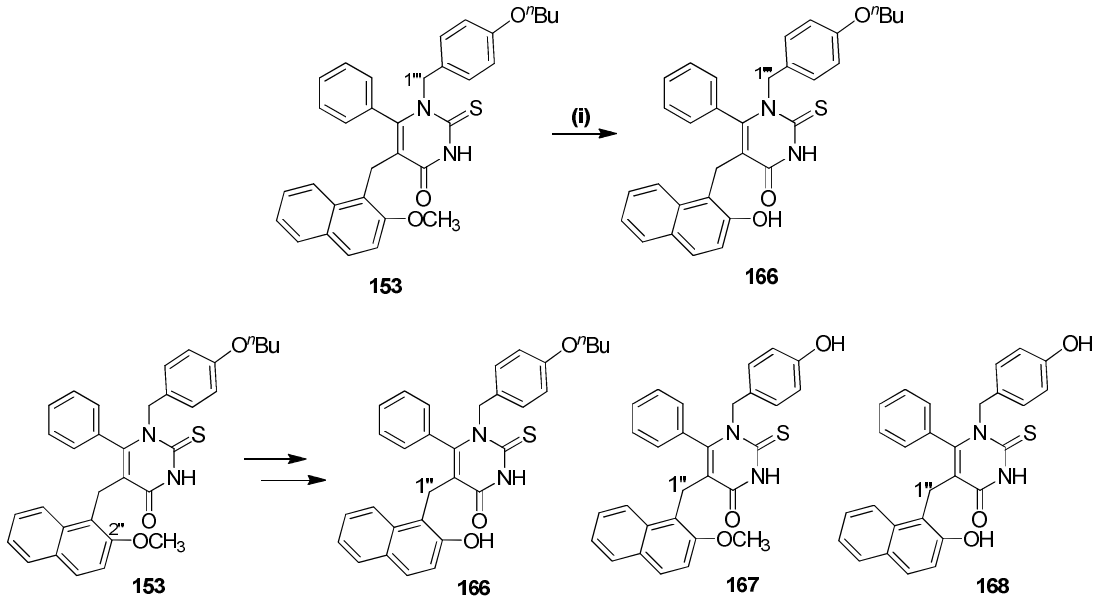

Scheme 5.1.9.1 - Attempted selective deprotection of the naphtholic OH of **153** over the phenolic OH. *Reagents and Conditions*: (i) BBr_3 (1.0 M in DCM, 11 eq.), DCM, rt, 48 h. The products which potentially formed in the reaction are shown (interpretation based on the crude reaction ^{1}H NMR spectrum).

A series of new spots began to form on analysis by TLC. After adding a total of 11 equivalents of BBr_3 and having extended the reaction time to several days, **153** was still present in the reaction mixture. Analysis of the crude reaction mixture by ^{1}H NMR spectroscopy suggested the presence of three products, along with **153**. A series of broad singlets assignable to different aromatic OH groups were observed in the low-field region of the spectrum. Furthermore, three new singlets around 4.00 ppm, assignable to different sets of H-1" protons, were observed. Despite the increased polarity expected for the new products due to the deprotected OH, column chromatography purification proved unsuccessful, with observed co-elution. At this point, the structure of the products can be only tentatively assigned to structures **166, 167** and **168** (**Scheme 5.1.9.1**). Thus, this approach was abandoned.

A group at Pfizer has reported the selective deprotection of a benzyl phenolic protecting group in the presence of a methoxy group in **169** to give **170 (Scheme 5.1.9.2**). This methodology was based on the use of boron trichloride in the presence of tetra-*n*-butylammonium iodide. The reported yield was 64%.[125]

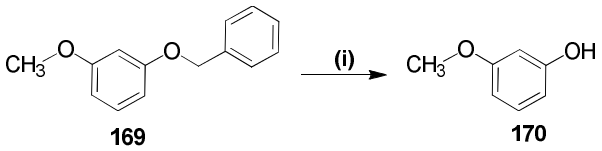

169 **170**

Scheme 5.1.9.2 - Reported selective deprotection of a benzylic phenol protecting group in the presence of a methoxy group (**169** to **170**). *Reagents and Conditions*: (i) BCl_3 (1.5 eq.), *n*-Bu_4NI (1.1 eq.), -78-0 °C, 2 h (64%).[125]

It was therefore decided to apply this experimental procedure on cambinol analogues **157-160** (**Scheme 5.1.9.3**).

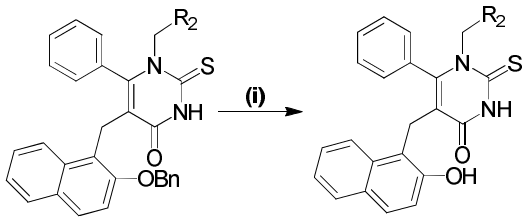

157-160 **92-95**

Scheme 5.1.9.3 - Final step in the preparation of new cambinol analogues **92-95**. *Reagents and Conditions*: (i) BCl_3 (1.5 eq), *n*-Bu_4NI (1.1 eq), -78 to 0°C, 2 h. (**92**, 46%; **93**, 53%; **94**, 22%; **95**, 25%).

When applied to substrates **157** and **158**, formation of a new single spot was detected by TLC within 2 hours at 0 °C. Longer reaction times did not lead to further consumption of the starting material. Addition of further equivalents of BCl_3 and *n*-Bu_4NI and longer reaction times for substrate **157** did not lead to completion of the reaction. These changes were avoided on substrate **158** in order to prevent eventual concurrent deprotection at the *para*-methoxy group. After work-up, column chromatography led to isolation of the new products, which were found to be the new expected cambinol analogues **92** and **93**. ^1H NMR analysis revealed the loss of the benzyl protecting group. Only fifteen (**92**) and sixteen (**93**) aromatic protons were now detected in the down-field region of the spectra. Importantly, a new broad singlet was observed at ~8.70 ppm which integrated as one proton and was assigned to the naphthol OH. Furthermore, in the case of **92**, the singlet assigned to the methyl of the *para*-methoxy

substituent at the *N*-1 position was still observed at 3.75 ppm, confirming that the deprotection had occured only at the naphthol OH group.

The same methodology was applied to substrates **159** and **160**. The products, yields and diagnostic ^{1}H NMR peaks of the products are summarised in **Table 5.1.9.**

Table 5.1.9 - Yields observed for the final deprotection of **157-160**. Chemical shift values for the diagnostic proton signals are listed. Yields refer to the amount of product isolated after silica-gel column chromatography purification. The starting materials are indicated in brackets.

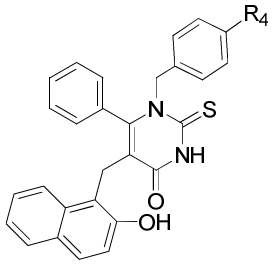

92-96

Compound	R_4	Yield (%)	Diagnostic Signals (^{1}H NMR) (ppm)
93 (157)	H	53	8.69 (OH)
92 (158)	MeO	46	8.70 (OH); 3.75 (MeO, R_4)
94 (159)	EtO	22	8.72 (OH); 3.97, 1.39 (EtO, R_4)
95 (160)	*n*-PrO	25	8.72 (OH); 3.85, 1.84-1.71, 1.02 (*n*-PrO, R_4)

The low yields observed, particularly for compounds **94** and **95**, can be explained by the presence of large amounts of unreacted starting material when the reaction was stopped. These reactions always appeared difficult to drive to completion. A possible explanation could be the partial inactivation of the BCl_3 through chelation to the other heteroatoms present in the starting materials. In order to avoid unselective deprotection at the *para*-alkoxy groups, it was decided not to increase the number of equivalents of BCl_3 and nBu$_4$NI used. For the same reason, higher temperatures or longer reaction times were not used. It may also possible that the quality of the nBu$_4$NI salt had decreased over time. This salt has been reported to be highly hygroscopic and requires frequent recrystallisations from hot toluene in order to eliminate the excess of water.[125] Unfortunately, due to time constrains, it was not possible to test this hypothesis on our substrates.

Regarding the mechanism, it is proposed that the iodide acts as a stabilising ligand on boron (**Scheme 5.1.9.4**).[125] Formation of BCl_2I may be followed by coordination with the naphthol

oxygen. After formation of **171**, one chlorine atom is lost, generating **172**. At this point the iodine or chlorine in solution may displace the benzyl protecting group to give **173**.

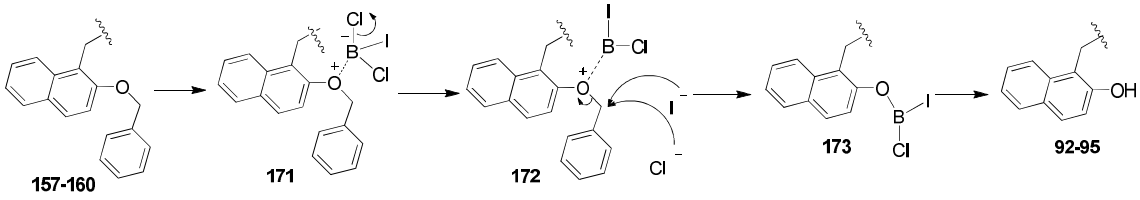

Scheme 5.1.9.4 - Proposed mechanism of the final debenzylation reaction.

Whilst coordination of BCl_2I may occur also at the oxygen of the *para*-alkoxy substituent of the *N*-1 benzyl ring, the deprotection selectively occurs at the naphthol OH. This may be explained by a better stabilisation of a "partial" positive charge development at the benzylic methylene carbon with the final nucleophilic substitution having partial S_N1 character.

5.2. *In vitro* Biological Evaluation

5.2.1 *In vitro* Inhibitory Activity of the New Analogues Against SIRT1 and SIRT2

Cambinol analogues **144-160** and **92-95** synthesised in this chapter were screened for *in vitro* inhibitory activity against SIRT1 and SIRT2 using the commercially available fluorescent assay used for screening the previous analogues (**Chapters 2** and **4**). Initially, all the compounds were tested at 60 μM concentration. The IC_{50} values were determined only for compounds that had over 70% inhibition at 60 μM. Cambinol (**39**) and previously described inhibitors **46** and **47** were used as controls in these studies.[18,106] The experiments were carried out by Miss Lisa Pirrie at the University of St Andrews.

5.2.2 *In vitro* Inhibitory Activity of the New Analogues 149-160

Intermediates **149-160** exhibited a wide range of inhibitory activities at 60 μM (**Table 5.2.2**).

The most important observation was regarding the role of the naphthol OH. Protection of the naphthol OH group of **47** with a methyl group (**154**), resulted in significant loss of inhibitory activity against SIRT2, with **154** showing a poor 37.7 ± 2% inhibition. This value represents

approximately one half of the inhibitory activity showed by the selective SIRT2 inhibitor **47** (80.4 ± 1%) and suggests that the naphthol OH is critical for high levels of inhibition against SIRT2. Compound **154** was a poor inhibitor of SIRT1 (36.2 ± 5%).

Analogues **157-160**, characterised by a benzyl protecting group at the naphthol OH, exhibited a wide range of activity against SIRT2 (48-67%, **Figure 5.2.2.1**). Interestingly, the activity improved with the length of substituent at the *para*-position of the *N*-1 benzyl ring. In the presence of an unsubstituted benzyl group, **157** showed a moderate inhibition of SIRT2 (48 ± 3%). Insertion of a methoxy (**158**) or ethoxy (**159**) chain at the *para*-position resulted in better activity against SIRT2 (57 ± 1 and 67 ± 4%, respectively). Longer chains (*n*-propoxy, **160**) led to a slight decrease in activity against the same enzyme. Analogues **157-160** all exhibited poor activity against SIRT1 (23-37%).

Table 5.2.2. - Inhibitory activities of **149-159**. Data are reported as percentage of inhibition at a concentration of 60 μM. [a]SE, standard error (n = 2); [b]IC_{50} were determined for compounds that had over 70% inhibition at 60 μM for SIRT2 (repeated at least twice); (-) Not determined; [c]Used as control.

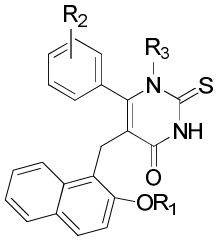

149-159

Compound	R_1	R_2	R_3	SIRT1[a]	IC_{50}[b](μM)	SIRT2[a]	IC_{50}[b](μM)
39[c]	H	H	H	59.5 ± 1.1	40.7 ± 11.1	51.9 ± 1.4	47.9 ± 11.7
46[c]	H	*p*-Br	H	82.3 ± 1.0	12.7 ± 1.9	9.4 ± 0.7	> 90
47[c]	H	H	Me	29.4 ± 1.3	> 90	80.4 ± 1.1	20.1 ± 5.0
154	Me	H	Me	36.2 ± 4.9	-	37.7 ± 1.9	-
157	Bn	H	Bn	25.4 ± 1.8	-	48.4 ± 2.7	-
158	Bn	H	*p*-MeOBn	29.8 ± 2.2	-	56.9 ± 1.1	-
159	Bn	H	*p*-EtOBn	36.6 ± 0.6	-	67.2 ± 3.8	-
160	Bn	H	*p*-*n*PrOBn	22.8 ± 3.3	-	65.1 ± 5.2	-
149	Me	H	Bn	48.6 ± 0.9	-	37.7 ± 11.4	-
150	Me	H	*p*-MeOBn	8.8 ± 0.9	-	66.1 ± 3.7	-
151	Me	H	*p*-EtOBn	19.3 ± 0.9	-	72.2 ± 2.2	16 ± 4.1
152	Me	H	*p*-*n*PrOBn	38.0 ± 1.1	-	71.8 ± 0.8	11 ± 2.4
153	Me	H	*p*-*n*BuOBn	32.7 ± 2.2	-	66.1 ± 0.9	-
155	Me	*p*-Cl	*n*Bu	18.4 ± 6.8	-	49.4 ± 5.0	-
156	Me	*o*-Me	*n*Bu	11.5 ± 0.8	-	37.3 ± 2.2	-

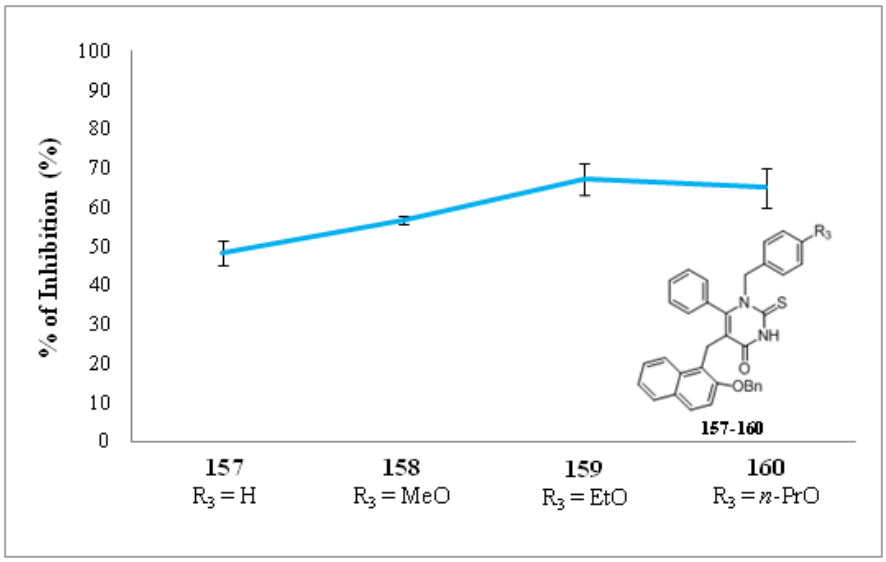

Figure 5.2.2.1 – Graphical representation of the inhibitory activity of analogues **157-160** against SIRT2.

Similarly to that observed for **157-160**, the presence of a methyl protecting group on the naphthol OH of **149-153** resulted in moderate to good inhibition of SIRT2 (37-72%, **Figure 5.2.2.2**). Once again, the *para*-methoxy moiety on the *N*-1 benzyl group (**150**) led to a consistent improvement in the *in vitro* activity in comparison to that observed for **149** (66 ± 4 *vs* 37 ± 11%, respectively). An improved inhibitory activity was observed when the length of the new alkoxy substituent at the *para*-position of the *N*-1 benzyl group was extended by two carbons (**151**, 72 ± 1%). The ethoxy group resulted in the optimal substituent at the *para*-position. In fact, elongation of the chain (**152**, **153**) led to a small decrease of the potency against SIRT2 (71% ± 1 and 66 ± 1% respectively). The inhibitory activity of **149-153** against SIRT1 was modest, with values ranging from 8 ± 1% (**150**) to 48 ± 1% (**149**).

These data suggest that the presence of *para*-alkoxy substituent on the *N*-1 benzyl ring is important for increasing the potency of the new compounds against SIRT2. This behaviour was previously predicted in **Chapter 3.2.1**. In fact, during the docking studies, the presence of the new *para*-substituent on the *N*-1 benzyl ring resulted in higher docking scores, with the same substituent consistently inserted into the nicotinamide-exchange channel. This insertion is proposed to stabilise the interaction between these ligands and the protein

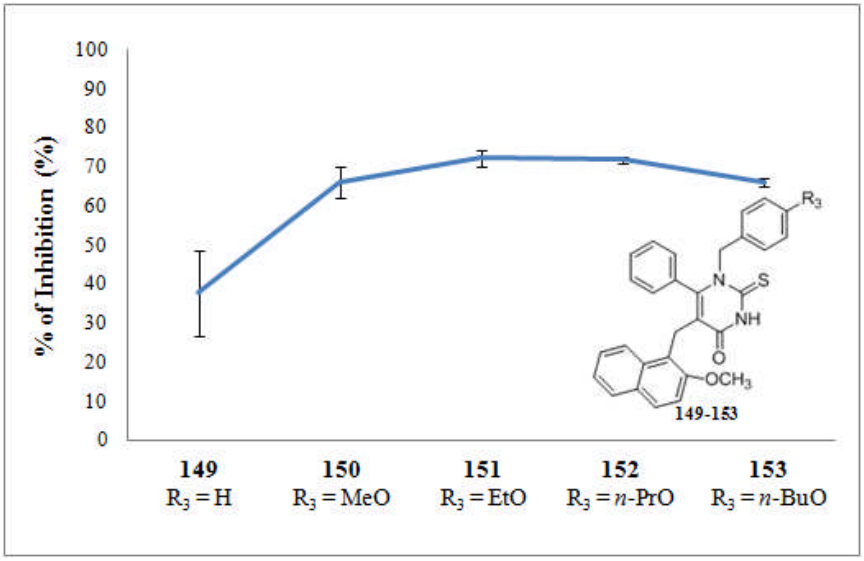

Figure 5.2.2.2 – Graphical representation of the inhibitory activity of analogues **149-153** against SIRT2.

The presence of a *n*-butyl chain at the *N*-1 position, along with a bulky substituent at the C-6 phenyl ring (**155**, *p*-Cl; **156**, *o*-Me), did not lead to potent inhibition of SIRT2. The inhibitory activity of these two new analogues was modest (49 ± 5% and 37 ± 2, respectively). These data suggested that *N*-1 butyl substitution does not guarantee high levels of potency in the presence of a bulky substituent at the C-6 phenyl ring. It has already been proposed that the area where the phenyl ring is accommodated is smaller in SIRT2 than in SIRT1, due to projection of Tyr96 into the active site (**Chapter 3**). Both **155** and **156** were poor inhibitors of SIRT1, with percentages of inhibition below 20%.

5.2.3 *In vitro* Inhibitory Activity of Analogues 92-95

The presence of the naphthol OH in **92-95** led to significant improvement in the activity against SIRT2 (**Table 5.2.3, Figure 5.2.3**).

Table 5.2.3 - Inhibitory activities of compounds of general structure **92-95**. Data are reported as percentage of inhibition at a concentration of 60 μM. [a] SE, standard error (n = 2); [b] IC_{50} were determined for compounds that had over 70% inhibition at 60 μM for SIRT2 (repeated at least twice); [c] Used as control. (-) Not determined.

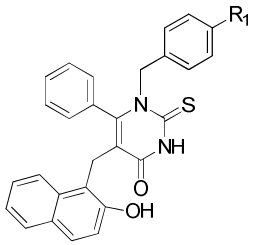

92-95

Compoud	R_1	SIRT1[a]	IC_{50}[b](µM)	SIRT2[a]	IC_{50}[b](µM)
39[c]	H	59.5 ± 1.1	40.7 ± 11.1	51.9 ± 1.4	47.9 ± 11.7
46[c]	H	82.3 ± 1.0	12.7 ± 1.9	9.4 ± 0.7	> 90
47[c]	H	29.4 ± 1.3	> 90	80.4 ± 1.1	20.1 ± 5.0
93	H	10.8 ± 3.9	-	62.0 ± 1.2	-
92	*p*-MeO	43.5 ± 2.1	-	73.4 ± 2.1	13 ± 1.1
94	*p*-EtO	13.4 ± 8.3	-	88.9 ± 0.9	4 ± 1.4
95	*p*-PrO	15.6 ± 5.6	-	85.4 ± 1.8	6 ± 2.7

Analogue **93** was more potent that its methoxy- and benzyl-protected versions **149** and **157** (**Table 5.2.2**) exhibiting a good inhibition of 62 ± 1 % at 60 μM. Once again, when an alkoxy substituent was inserted at the *para*-position of the *N*-1-benzyl ring (**92-94-95**), a significant improvement of the inhibitory activity against SIRT2 was observed, with analogue **94**, containing an ethoxy substituent, being the most potent compound (88.9 ± 1%, IC_{50} 4 ± 1 µM). For longer alkoxy substituents such as *n*-propyloxy (**95**), a slight decrease in inhibitory activity was observed (85.4 ± 2%, IC_{50} 6 ± 3µM). No significant inhibion of SIRT1 was observed for **92-95**.

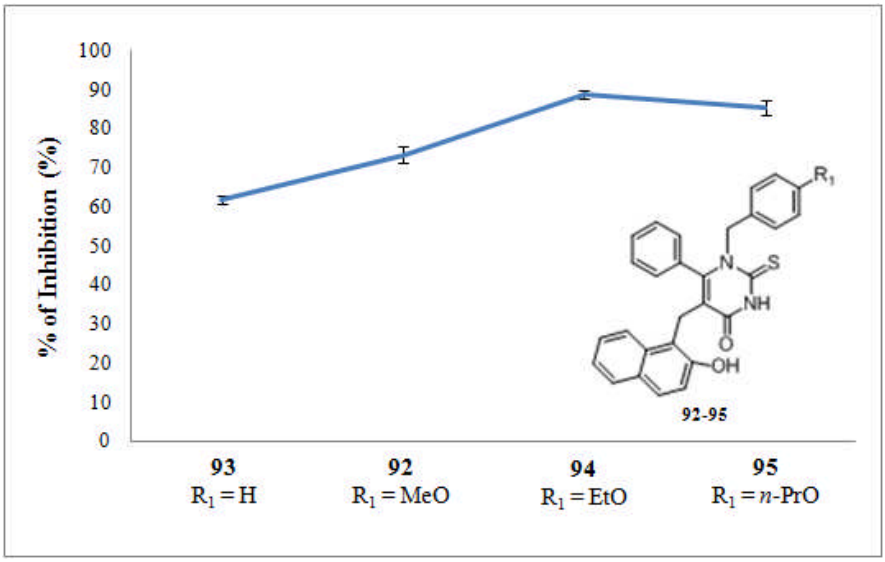

Figure 5.2.3 – Graphical representation of the inhibitory activity of analogues **92-95** against SIRT2.

These data were consistent with those previously reported (**Section 5.2.2**) and with the conclusions of **Chapter 3**. More specifically:

1. As previously observed for **47** and **154** (**Table 5.2.2**), the presence of the free naphthol OH moiety leads to better *in vitro* inhibition of SIRT2. Thus, a potential hydrogen-bond interaction of the OH with an amino acid, possibly Glu116, may be the determining factor for this improved activity.

2. The presence of the *para*-alkoxy substiuent on the *N*-1 benzyl ring leads to better *in vitro* inhibition of the enzyme. The ethoxy chain was consistently the optimal substituent. The improved stabilisation of the ligand-protein binding can be rationalised by insertion of the new alkoxy chain into the liphophilic nicotinamide-exchange tunnel. This behaviour was predicted by our second generation docking studies in **Chapter 3.**

5.2.4 *In vitro* Inhibitory Activity of Analogues 144-148.

As with analogues **149-160** and **92-95**, compounds **144-148** were screened against SIRT2. Results are reported in **Table 5.2.4** and **Figure 5.2.4**.

Table 5.2.4 - Inhibitory activities of compounds of general structure **144-148**. Data are reported as percentage of inhibition at a concentration of 60 μM.[a]SE, standard error (n = 2); [b]IC_{50} were determined for compounds that had over 70% inhibition at 60 μM for SIRT2 (repeated at least twice); (-) Not determined;[c] Used as control. IC_{50} of the control compounds **39**, **46** and **47** are reported.

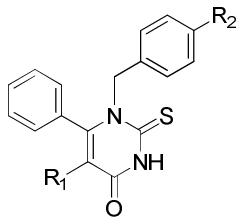

144-148

Compoud	R_1	R2	SIRT1	IC_{50}[b](μM)	SIRT2	IC_{50}[b](μM)
39[c]	-	-	59.5 ± 1.1	40.7 ± 11.1	51.9 ± 1.4	47.9 ± 11.7
46[c]	-	-	82.3 ± 1.0	12.7 ± 1.9	9.4 ± 0.7	> 90
47[c]	-	-	29.4 ± 1.3	> 90	80.4 ± 1.1	20.1 ± 5.0
144	H	H	1.8 ± 1.9	-	27.0 ± 9.1	-
145	Bn	H	23.0 ± 4.1	-	45.1 ± 0.	-
146	Bn	*p*-MeO	32.2 ± 4.1	-	67.0 ± 2.1	-
147	Bn	*p*-EtO	35.0 ± 4.4	-	73.3 ± 1.1	10 ± 6.2
148	Bn	*p*-BuO	8.5 ± 0.6	-	63.3 ± 0.9	-

No significant loss in the activity against SIRT2 was detected after replacement of the naphthol moiety in compounds **149-160** with a benzyl group (**145-148**). Once again, analogues characterised by a *para*-alkoxy substituent in the *N*-1 benzyl ring (**146-148**) exhibited better inhibitory activity (67 ± 2%, 73 ± 1% and 63 ± 1%, respectively) than analogue **145** (45 ± 1%). In line with the data in **Tables 5.2.2**, **5.2.3** and the *para*-ethoxy chain led to the highest level of activity against SIRT2 (**147**, 73 ± 1%, IC_{50} 10 ± 6 μM). A decrease in the activity was observed for longer chains (**148**, 63 ± 1%). Interestingly, when the benzyl moiety at C-5 was not present (**144**), poor inhibitory activity was observed against SIRT2 (27 ± 9%). All compounds **144-148** showed poor inhibitory activity against SIRT1.

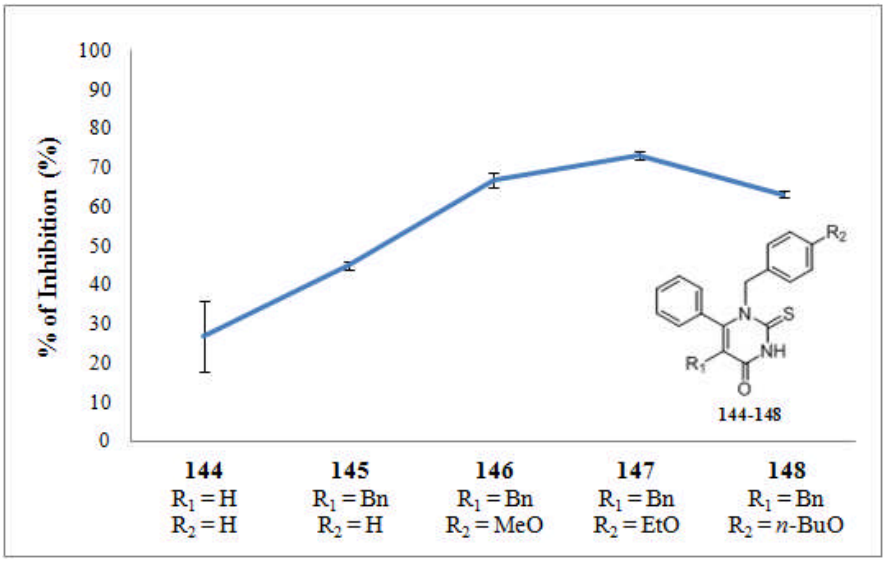

Figure 5.2.4 – Graphical representation of the inhibitory activity of analogues **144-148** against SIRT2.

This data reinforced the role played by an aromatic substituent at C-5, previously proposed to be sandwiched between the aromatic residues Phe119 and His187 in the active site of SIRT2 and SIRT1. While no difference in the activity was observed between analogues **144-148** and **149-160** (benzyl *vs* naphthol), the poor inhibition observed for **144** is consistent with the results of our previous *in silico* studies**.**

5.3. An Improved Understanding of the Binding Mode of Cambinol Analogues

In order to improve the quality of our previous *in silico* studies (**Chapter 3**) and to better understand the key interactions which stabilise the binding of cambinol **39** and its analogues into the active site of SIRT1 and SIRT2, modelling studies were continued by means of molecular dynamics analysis (MD) of the ligand-target interactions. These studies were run in collaboration with Dr Chandra Verma and Dr Thomas Joseph at the Bioinformatics Institute in Singapore. The AMBER 9 software was used in these simulations.[126]

5.3.1 Molecular Dynamics Studies on Analogue 85

While GOLD is a docking tool, MD can support the docking poses previously generated with GOLD by analysing the energy and stability of the ligand within the binding pocket and thus rationalising the energetics of the various poses. In MD, the protein and the ligand structures

are allowed flexibility, something GOLD is not capable of doing. Thus, an improved understanding of the protein-ligand interaction is often possible. Furthermore, the structures of the protein with and without the ligand can be compared, allowing a better analysis of how the neighbouring residues of the active site interact with the different parts of the ligand.

MD studies further confirmed the conclusions previously achieved with GOLD and by comparison of the amino acid sequence of the SIRT1 and SIRT2 active sites (**Chapter 3**). When the best docking poses of compound **85** were re-analysed with MD, the *N*-1 butyl chain was always found to be inserted into the nicotinamide-exchange tunnel of SIRT2 during the time course experiment (**Figure 5.3.1.1, A-D**). In particular, the glutamic acid 116 residue comes in close proximity with the naphthol OH of **85** within 3 ns (**Figure 5.3.1.1, C**) and a hydrogen bond is proposed to form between the same OH and the side chain carbonyl of Glu116. Interaction of the naphthol OH with the carboxylate oxygen (COO^-) of the same glutamic acid cannot be ruled out (**Figure 5.3.1.1, A-D**). Furthermore, many sirtuin inhibitors so far reported, including sirtinol, contain a naphthol OH.[74-77] In an *in silico* study, Poso and co-workers have already described Glu116 as a key residue for the binding of other SIRT2 inhibitors to the active site of the protein.[127]

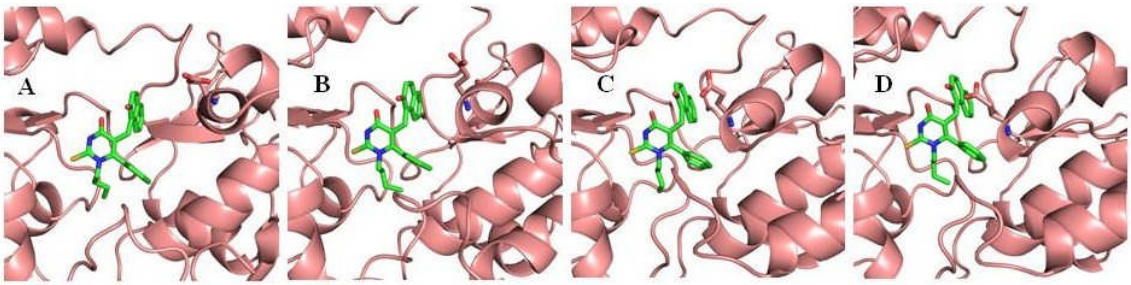

Figure 5.3.1.1 - A-D. Time-course MD simulations for the selective SIRT2 inhibitor **85** in the active site of SIRT2. Each image (A-D) shows the conformational changes of the ligand and the SIRT2 active site from 1 ns (**A**) to 4 ns (**D**). While the *N*1-butyl chain always fits in the nicotinamide-exchange tunnel, at 3 ns (**C**) the naphthol OH and the carbonyl backbone of Glu116 are in close enough proximity to form a hydrogen bond. The structure of the protein is depicted as a cartoon and Glu116 is shown as sticks.

The potential hydrogen bond existing between the naphthol OH of **85** and the amino acid residue Glu116 provides a rational explanation for the difference in activity observed between analogues **92-96** (OH free) and **148-159** (OH protected).

A comparison between the amino acid sequences of SIRT1 and SIRT2 showed that in SIRT1 Glu116 is replaced by a glutamine residue at the equivalent 296 position. This residue should

also be capable of forming a hydrogen bond with the naphthol OH of **85**. However, when the MD simulations experiments were carried out, the naphthol OH did not appear to be a selectivity discriminating element for either of the two isoforms of the enzyme (**Figure 5.3.1.2, B**).

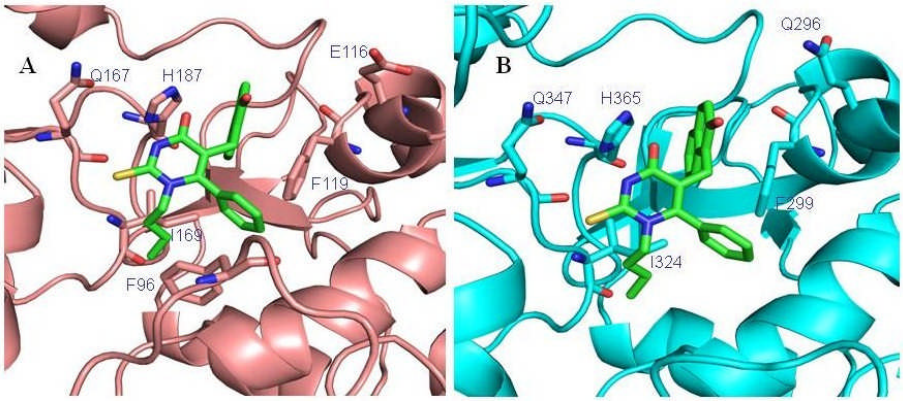

Figure 5.3.1.2 - A-B. A direct comparison of the active sites of SIRT2 (**A**) and SIRT1 (**B**) with the potent SIRT2 inhibitor **85** docked into the active site. The residues which contribute to the binding of the ligand are labelled and shown as sticks.

MD simulations further confirmed the structural differences observed previously in the so-called 96-loop (**Figure 5.3.1.2;** see also movies in **supplementary material**). When **85** was docked into the active site of SIRT1 and SIRT2, further analysis with MD showed how the 96-loop is very flexible in SIRT1, making the base of the active site less able to form a robust interaction with **85**. In particular, in SIRT1 the *N*-1 butyl chain appears free to move without forming significant interactions. Only at the end of time course experiment does the *N*-1 *n*-butyl chain seem to enter into the nicotinamide-exchange tunnel of SIRT1.

In contrast, in SIRT2 the 96-loop is less flexible and contributes to a better defined active site around **85**. For this protein, the *N*-1 *n*-butyl substituent was consistently accommodated into the nicotinamide-exchange tunnel throughout the experiment. This observation highlights the role played by the 96-loop in creating structural differences between SIRT1 and SIRT2, particularly in the conformation of the nicotinamide-exchange tunnel and in the shape of the base of the active site.

Consistent with these considerations, SIRT1 has been reported to exhibit no substrate specificity *in vitro*.[128] In an attempt to identify deacetylase sequence specificity through the screening of peptide libraries containing acetylated lysine, Blander and co-workers suggested that substrate

recognition by SIRT1 is not dependent on the amino acid sequence next to the acetyl lysine.[128] This study was not able to clarify which factors guarantee substrate specificity *in vivo* for SIRT1. In an independent report, Gurard-Levin and co-workers prepared a series of isoform selective peptides to measure the deacetylase activity of different HDACs, including SIRT1.[129] Amongst the enzymes studied in this work, SIRT1 displayed low substrate specificity *in vitro*.

5.4 Conclusions

This chapter described the successful synthesis and *in vitro* evaluation of twenty-one new cambinol analogues as SIRT2 selective inhibitors. A new flexible synthetic approach to this type of analogue has been developed. Despite containing a greater number of steps, this new synthetic route allowed us to overcome the majority of limitations of the synthetic procedure reported in **Chapter 2**.

The *in vitro* biological evaluation carried out on this second collection of molecules was aimed at confirming the observations of the computational studies reported in **Chapter 2**. Two main conclusions can be drawn:

1. The presence of the *N*-1 benzyl substituent leads to good inhibition of SIRT2. Insertion of a *para*-alkoxy substituent on the same group consistently resulted in increased levels of activity against SIRT2. Amongst the different alkoxy substituents inserted, the ethoxy group always gave the best results. This behaviour had partially been predicted by the computational studies presented in **Chapter 3**.

2. For the *N*-1 benzyl substituted analogues, the presence of a free naphthol OH was important for increasing the potency against SIRT2, thus re-enforcing the view that this group is involved in a strong interaction with a residue in the active site, possibly Glu116.

These interesting results led us to study further the binding mode of cambinol **39** within the sirtuin active site. In line with the observed SARs, MD simulations run on **85** suggested that the naphthol OH is involved in an important hydrogen bond in the active site of SIRT2. In the same study, the 96-loop appeared to be more flexible in SIRT1 than in SIRT2. This structural

difference between SIRT1 and SIRT2 may provide an explanation for the selectivity observed by the analogues described in **Chapters 2**, **4** and **5**.

PART I: CONCLUSIONS

The studies reported in **Part I** of the thesis focused on the exploration of the chemical space around cambinol **39**. The main aim was to improve the potency and selectivity of new analogues towards SIRT1 and SIRT2, two enzymes involved in the modulation of the activity of p53. These investigations were motivated by the fact that:

1. Besides the tenovins, cambinol **39** is the only sirtuin inhibitor reported in the literature with an *in vivo* activity in a mouse xenograft model of cancer;
2. Cambinol **39** is a modest and unselective inhibitor of SIRT1 and SIRT2;
3. Only one inactive analogue of **39**, ADS012 **40**, had been described at the point at which this research began (**Figure I.1**).

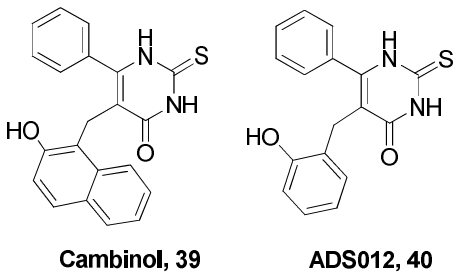

Figure I.1 – Structure of Cambinol **39** and the only reported analogue **40**.

Therefore, new analogues of cambinol with improved selectivity towards and potency against SIRT1 and SIRT2 were required. To the best of our knowledge, this work represents the first robust exploration of the SAR of the core structure of **39**, the details of which are outlined below:

1. Three series of novel cambinol analogues were synthesised by means of four different synthetic approaches. All routes presented were characterised by high flexibility and allowed the introduction of a significant range of diversity at various parts of the core structure of **39** (**Figure I.2**).

2. Amongst the modifications introduced, aliphatic substituents at the *N*-1 position of the thiouracil core of **39** led to potent and selective inhibitors of SIRT2 (**83**, **85**, **94** and **95**)

3. Substitutions at the phenyl ring of **39** with fluorine (**62** and **63**), bromine (**46**) or a methyl group (**74-76**) resulted in an improved selectivity towards SIRT1 over SIRT2 in comparison to cambinol **39**. The introduction of an aliphatic substituent at the sulfur atom of cambinol **39** (giving compound **98**) also showed a greater inhibition of SIRT1 over SIRT2.

4. The activity of the most selective SIRT1 and SIRT2 inhibitors was further proven with a series of in-cell experiments aimed at detecting the expression of known cellular targets of the two enzymes, such as p53 and α-tubulin.

5. The SAR associated with the most selective inhibitors was rationalised by means of computational studies. This work culminated in the proposal of a potential binding mode for the most potent SIRT2 inhibitors. In particular, the aliphatic substituent at the *N*-1 position of **39** was proposed to be involved in lipophilic interactions with the nicotinamide-exchange tunnel in SIRT2. This observation was used for the rational design of the second and third generation analogues, which showed the expected potency and selectivity.

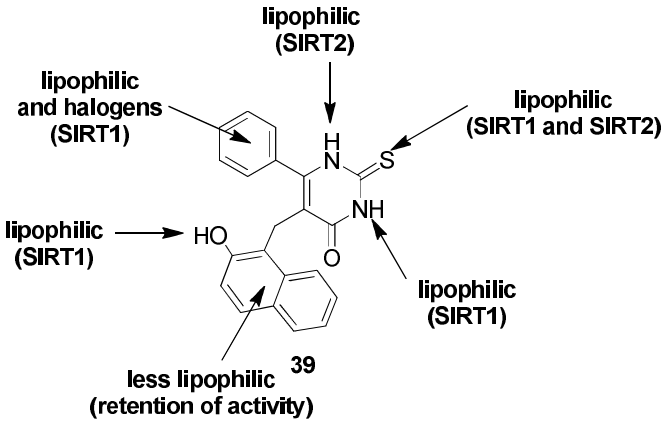

Figure I.2 – An overview of the diversity introduced on the core structure of cambinol **39** during this study. The nature of the substituents introduced is described, along with the selectivity observed for each of them.

To date, the identification of highly potent and selective inhibitors of SIRT1 and SIRT2 remains an unsolved problem. Only the mechanism-based thiopeptide inhibitors have provided inhibitory activity in the nanomolar range.[77] The activity of the most potent SIRT1 inhibitor **19** (**Figure I.3**) remains controversial as different values have been reported in different independent studies.[86,87] Furthermore, many potent inhibitors show low selectivity between the

two isoforms. These aspects can be partially explained by the fact that these enzymes were only discovered recently and that they are still poorly characterised in terms of structure and biochemistry.

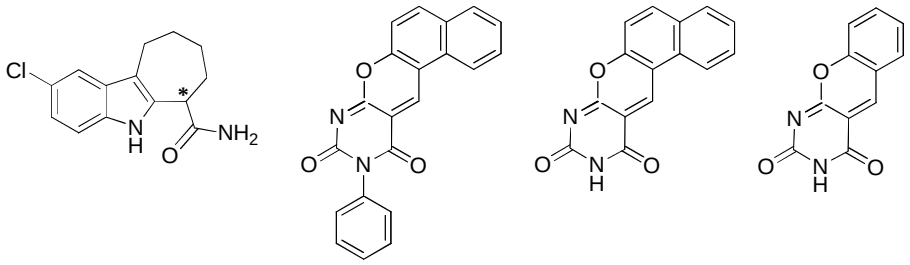

19 **41** **42** **43**

Figure I.3 - The most potent SIRT1 inhibitor reported to date (**19**) and the new cambinol analogues **41-43** reported by Mai and co-workers. [102]

It is still unclear as to why cambinol **39** is difficult to be converted into a potent and selective inhibitor of SIRT1. The inhibitory activities displayed by the new analogues presented in this thesis (**Chapters 2, 4** and **5**) suggest that the achievement of potent *in vitro* inhibition of SIRT1 by this type of molecule is not trivial. This conclusion is also supported by the lack of *in vitro* selectivity observed for SIRT1 in other inhibitor series. Recently May and co-workers reported cambinol analogues **41-43** which are equipotent with our inhibitor **46**.[102] The increased activity of **41-43** compared to cambinol **39** was rationalised by the increased stability of the inhibitor associated with the formation of the ring connecting the naphthol and the ketone functionalities. However, no biochemical studies and docking simulations have been reported for **41-43**. The most active SIRT1 inhibitor so far reported, **19** (**Figure 5.5.2**) has been proposed to bind into the C-subpocket.[86] In an independent *in silico* study, Poso and co-workers further validated the binding of **19** into the C-subpocket.[88] A crystal structure of **19** co-crystallised with cambinol **39** in the active site of SIRT1 would significantly aid the clarification of such aspects.

Our work reports one of the most potent and selective non-peptide SIRT2 inhibitors (**85**, IC_{50} 1 ± 1 μM) developed so far. Other analogues prepared here, such as **83**, **94** and **95**, displayed a comparable level of activity against SIRT2. As SIRT2 inhibition has been reported as a potential therapeutic approach for the treatment of cancer and neurodegenerative diseases, our work represents the starting point for further development of potent inhibitors of this isoform.
In this context, the most active compounds developed in this study can be used as "molecular tools" for studying the biochemistry of this class of enzymes.

On the other hand, the insertion of halogens, such as bromine or fluorine, or methyl substituents at the C-6 phenyl ring of **39** represents a suitable starting point for the development of compounds displaying higher potency and selectivity against SIRT1. The presence of a benzyl substituent at the sulphur atom also results in greater selectivity and potency towards SIRT1. We have therefore identified structural features within the same core structure which can be tuned accordingly to result in selectivity towards either SIRT1 or SIRT2 as desired.

A robust rationalisation of the observed SAR was proposed. To the best of our knowledge, this study has identified, for the first time, three structural differences between the active sites of SIRT1 and SIRT2 which can be used to further improve the potency and selectivity of potential inhibitors or indeed the inhibitors developed thus far. These structural differences between the active sites are outlined as follows:

1. The nicotinamide-exchange tunnel, present in both SIRT1 and SIRT2, appears to be better defined in SIRT2, therefore providing an important handle for the selective inhibition of SIRT2.

2. The 96-loop introduces significant differences in the shape and stability of the active sites of the two isoforms. In particular, the active site of SIRT2 appears to be well defined and less flexible due to the lower flexibility of the 96-loop in comparison to that of SIRT1.

3. The hydrogen bond between Glu116 of SIRT2 and the phenolic hydroxyl group of **39** adds stabilisation to the binding, which is not observed in the case of SIRT1.

Indeed, the differences in the accessibility and shape of the nicotinamide-exchange tunnel, as previously described, appears to be influenced by differences that exist between SIRT1 and SIRT2 in the 96-loop. Although studies relating to the selectivity of SIRT2 for different peptides *in vitro* have not been reported to date, our studies suggest that the lipophilic nicotinamide-exchange tunnel plays a critical role for the selective and potent inhibition of SIRT2.

PART I: FUTURE WORK

Due to the reported therapeutic relevance of SIRT2 inhibition, the preparation of new potent and selective inhibitors is of high priority. As a result of the flexibility of the synthetic approaches reported in this thesis, we believe that these routes can be applied to the development of larger collections of analogues. Therefore, we propose that the chemical space around cambinol **39** can be further explored as follows:

1. As the thiouracil moiety could potentially be accommodated in a hydrophilic area of the enzyme, insertion of polar substituents at the sulphur atom and *N*-3 position is suggested. This may result in novel interactions with improvement of the potency against both SIRT1 and SIRT2.

2. Further exploration of different substituents at the *N*-1 position is required. Having established the role played by lipophilic substituents (both linear and aromatic) in directing the selectivity and potency of the inhibitors, the insertion of polar moieties should be carried out for comparison. The effects of polar moieties on the selectivity and potency is potentially implied by the molecule of PEG found co-crystallised inside the nicotinamide-exchange tunnel.

3. Based on the SAR data reported in Chapter 5, we suggest the preparation of a novel series of analogues where the naphthol moiety is replaced by a phenol group. Retention of activity is expected for these analogues, which would subsequently exhibit reduced molecular weight and lipophilicity. Both of these factors are beneficial for the effectiveness of an orally-active drug.

4. We recommend the synthesis of an analogue comprised of a combination of all structural features which resulted in improved potency and selectivity against SIRT1. These include: a) the introduction of a halogen (bromine or fluorine) or methyl groups on the C-6 phenyl ring of **39**; and b) the introduction of a benzyl ring at the sulphur atom of **39**. These modifications may result in a significant improvement in the IC_{50} value observed for **46** against SIRT1 (13 μM).

We believe that due to the flexibility of our synthetic routes, these proposed studies may lead, in a short period of time, to not only a range of novel, more potent and selective inhibitors of the

two isoforms, but also to an improved understanding of the mode of binding of cambinol-based compounds into the active site of sirtuins.

6. EXPERIMENTAL

6.1 Instrumentation and General Techniques

All chemicals and solvents were purchased from Aldrich (UK) or Alfa-Aesar and used without further purification. All reactions were carried out under a positive pressure of nitrogen or argon in flame or oven-dried glassware. Ethanol was dried over Mg/I_2, and pyridine was dried over KOH pellets.

Thin layer chromatography (TLC) analysis was performed on silica pre-coated SIL G-25 UV_{254} sheets (layer: 0.25 mm silica gel with fluorescent indicator UV_{254}, Alugram, UK). Compounds were visualized by UV light (UV lamp, model UVGL-58, Mineralight LAMP, Multiband UV-254/365 nm) and stained with potassium permanganate. Flash column chromatography was carried out on silica gel (40-63 μm, Fluorochem, UK) or, where indicated, on basic alumina (Brockmann I, Sigma-Aldrich).

Melting points were measured with an Electrothermal 9100 capillary melting point apparatus and are uncorrected.

Fourier Transform infra-red spectra (FT-IR) were acquired on a Perkin Elmer paragon 1000 FT spectrometer. Absorption maxima are reported in wavenumbers (cm^{-1}).

Unless otherwise stated, ^1H NMR spectra were measured at room temperature (298 K) on a Bruker DPX 400 (^1H = 400 MHz) and Bruker Avance 300 (^1H = 300.1 MHz) instruments. Deuterated solvents were used and ^1H NMR chemical shifts were internally referenced to $CHCl_3$ (7.26 ppm) in chloroform-d_1 solution, to $CD_2HSO_2CHD_2$ (2.50 ppm) in dimethylsulfoxide-d_6 solution and to CD_3COCHD_2 (2.09 ppm) in acetone-d_6. Chemical shifts are expressed as δ in unit of ppm.

^{13}C NMR spectra were recorded in the same conditions and in the same solvents using the PENDANT sequence mode on a Bruker DPX 400 (^{13}C = 100 MHz). Data processing was carried out using TOPSPIN 2 NMR version (Bruker UK, Ltd). In ^1H NMR assignment the multiplicity used is indicated by the following abbreviations: s = singlet, d = doublet, dd = doublet of doublets, t = triplet, q = quartet, m = multiplet, brs = broad singlet. Signals of

protons and carbons were assigned, as far as possible, by using the following two-dimensional NMR spectroscopy techniques: [^{1}H-^{1}H] COSY, [^{1}H-^{13}C] COSY (HSQC: Heteronuclear Single Quantum Coherence) and long range [^{1}H-^{13}C] COSY (HMBC: Heteronuclear Multiple Bond Connectivity).

Mass spectrometry (electrospray mode, ES; chemical ionization mode, CI) were recorded on a high performance orthogonal acceleration reflecting TOF mass spectrometer operating in positive and negative mode, coupled to a Waters 2975 HPLC.

6.2 PART I: General Experimental Procedures

6.2.1 Synthesis of 2-benzoyl-benzo[*f*]coumarins 51a and 51c-x (METHOD A)

A range of phenyl-substituted ethyl benzoylacetates **50a and 50c-x** (1 eq.) and 2-hydroxy-1-naphthaldehyde **49** (430 mg, 1 eq.) were combined in separate vessels of the parallel synthesis apparatus and ethanol (4 mL) added. The reaction was warmed to 50 °C and piperidine (5 drops) added to each vessel. The reaction was heated at reflux for 2 h and the solid products collected by parallel filtration and washed with ethanol to yield the desired compounds **51a** and **51c-x.**

2-Benzoyl-3*H*-benzo[*f*]chromen-3-one (51a)

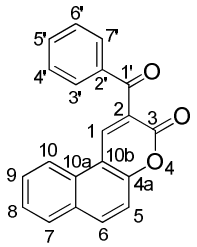

From Method A, synthesised in parallel (×4). **49** (430 mg) yielded **51a** as a yellow powder (568-599 mg, 1.90-1.99 mmol, 75-80%). Mp 208-210 °C (*lit.*[130,131] 209 °C); δ_H (300 MHz, $CDCl_3$) 8.93 (s, 1H, H-1), 8.27 (d, 1H, *J* = 8.2 Hz, H-10), 8.12 (d, 1H, *J* = 9.0 Hz, H-6), 7.98-7.90 (m, 3H, H-7 + 2×ArH), 7.77-7.70 (m, 1H, H-9), 7.67-7.59 (m, 2H, H-8 + 1×ArH) and 7.56-7.47 (m, 3H, H-5, ArH); *m/z* (ES^+) 323.06 [$(M+Na)^+$, 100%].

2-(5'-Bromobenzoyl)-3*H*-benzo[*f*]chromen-3-one (51c)

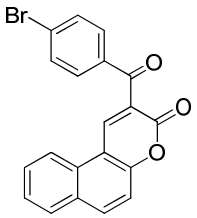

From Method A, **49** (430 mg) yielded **51c** as a yellow powder (600 mg, 1.58 mmol, 93%). Mp 245-248 °C (*lit.*[130] 246-247 °C); δ_H (400 MHz, $CDCl_3$) 8.98 (s, 1H, H-1), 8.29 (d, 1H, *J* = 8.3 Hz, H-10), 8.13 (d, 1H, *J* = 9.0 Hz, H-6), 7.96 (d, 1H, *J* = 8.2 Hz, H-7), 7.81-7.73 (m, 3H, H-9, H-3', H-7'), 7.64 (m, 3H, H-8, H-4', H-6') and 7.51 (d, 1H, *J* = 9.0 Hz, H-5); *m/z* (ES^+) 401.07 [$(M+Na)^+$, 100%].

2-(3'-Fluorobenzoyl)-3*H*-benzo[*f*]chromen-3-one (51d)

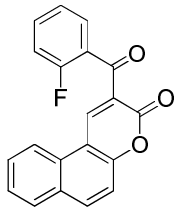

From Method A, **49** (430 mg) yielded **51d** as a yellow powder (685 mg, 2.15 mmol, 86%). Mp 190-192 °C; δ_H (300 MHz, $CDCl_3$) 9.08 (s, 1H, H-1), 8.35 (d, 1H, *J* = 8.4 Hz, H-10), 8.11 (d, 1H, *J* = 8.9 Hz, H-6), 7.89-7.75 (m, 2H, H-9, H-7), 7.67-7.61 (m, 1H, H-8), 7.59-7.54 (m, 2H, ArH), 7.51 (d, 1H, *J* = 8.9 Hz, H-5), 7.34-7.30 (m, 1H, ArH) and 7.13-7.09 (m, 1H, ArH); *m/z* (ES^+) 341.05 [$(M+Na)^+$, 100%].

2-(4'-Fluorobenzoyl)-3*H*-benzo[*f*]chromen-3-one (51e)

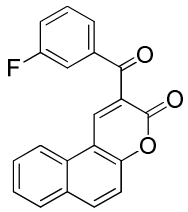

From Method A, **49** (430 mg) yielded **51e** as a yellow powder (630 mg, 1.98 mmol, 79%). Mp 226-228 °C; δ_H (300 MHz, $CDCl_3$) 8.98 (s, 1H, H-1), 8.29 (d, 1H, *J* = 8.3 Hz, H-10), 8.14 (d, 1H, *J* = 9.0 Hz, H-6), 7.99-7.92 (m, 1H, H-7), 7.77-7.71 (m, 1H, H-9), 7.70-7.62 (m, 1H, H-8), 7.66-7.59 (m, 2H, ArH), 7.53 (d, 1H, *J* = 9.0 Hz, H-5), 7.47-7.41 (m, 1H, ArH) and 7.38-7.30 (m, 1H, ArH); *m/z* (ES^+) 341.07 [$(M+Na)^+$, 100%].

2-(5'-Fluorobenzoyl)-3*H*-benzo[*f*]chromen-3-one (51f)

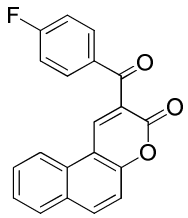

From Method A, **49** (430 mg) yielded **51f** as a yellow powder (664 mg, 2.08 mmol, 84%). Mp 214-215 °C; ν_{max} cm^{-1} (KBr): 1755, 1455 (C=O), 1285, 1222 (C-O), 1140, 743 (C-F); δ_H (300 MHz, $CDCl_3$) 8.95 (s, 1H, H-1), 8.29 (d, 1H, *J* = 8.4 Hz, H-10), 8.13 (d, 1H, *J* = 9.0 Hz, H-6), 8.00-7.93 (m, 3H, H-7, H-3', H-7'), 7.78-7.70 (m, 1H, H-9), 7.66-7.60 (m, 1H, H-8), 7.52 (d, 1H, *J* = 9.0 Hz, H-5) and 7.16 (d, 2H, AA'BB', *J* = 8.8 Hz, H-4', H-6'); δ_C (100 MHz, $CDCl_3$) 190.9 (C1'), 164.5 (C5'), 158.2 (C3), 155.6 (C4a), 141.7 (C1), 135.0 (C6), 131.8 (C3', C7'), 130.4 (C6a), 130.6 (C7), 129.7 (C2'), 129.5 (C10a), 128.5 (C9), 126.7 (C8), 125.2 (C2), 121.6 (C10), 116.9 (C5), 113.3 (C4', C6') and 112.1 (C10b); *m/z* (ES^+) 341.07 [$(M+Na)^+$, 100%].

2-(3'-Chlorobenzoyl)-3*H*-benzo[*f*]chromen-3-one (51g)

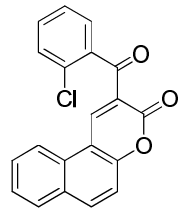

From Method A, **49** (430 mg) yielded **51g** as a yellow powder (690 mg, 2.06 mmol, 83%). Mp 225-227 °C; δ_H (300 MHz, $CDCl_3$) 9.23 (s, 1H, H-1), 8.36 (d, 1H, *J* = 8.1 Hz, H-10), 8.12 (d, 1H, *J* = 8.8 Hz, H-6), 7.95 (d, 1H, *J* = 8.1 Hz, H-7), 7.80-7.72 (m, 1H, H-9), 7.65-7.57 (m, 2H, H-8 + 1 × ArH) and 7.52-7.39 (m, 4H, H-5 + 3 × ArH); *m/z* (ES^+) 356.99 [$(M+Na)^+$, 100%].

2-(4'-Chlorobenzoyl)-3*H*-benzo[*f*]chromen-3-one (51h)

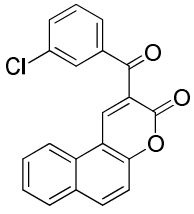

From Method A, **49** (430 mg) yielded **51h** as a yellow powder (722 mg, 2.16 mmol, 87%). Mp 228-230 °C; δ_H (400 MHz, $CDCl_3$) 8.98 (s, 1H, H-1), 8.29 (d, 1H, *J* = 8.3 Hz, H-10), 8.14 (d, 1H, *J* = 9.0 Hz, H-6), 7.96 (d, 1H, *J* = 7.9 Hz, H-7), 7.90-7.86 (m, 1H, ArH), 7.78-7.72 (m, 2H, H-9 + 1 × ArH), 7.67-7.60 (m, 1H, H-8), 7.62-7.58 (m, 1H, ArH), 7.53 (d, 1H, *J* = 9.0 Hz, H-5)

and 7.46-7.42 (m, 1H, ArH); HRMS (Cl^+) [Found: $(M+H)^+$, 335.0467, $C_{20}H_{12}O_3Cl$ requires 335.0475] (-2.4 ppm).

2-(5'-Chlorobenzoyl)-3*H*-benzo[*f*]chromen-3-one (51i)

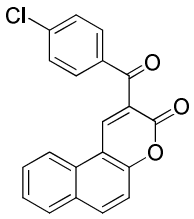

From Method A, **49** (430 mg) yielded **51i** as a yellow powder (614 mg, 1.83 mmol, 74%). Mp 230-233 °C (*lit.*[130] 232-233 °C); δ_H (400 MHz, $CDCl_3$) 8.97 (s, 1H, H-1), 8.28 (d, 1H, *J* = 8.3 Hz, H-10), 8.12 (d, 1H, *J* = 9.0 Hz, H-6), 7.96 (d, 1H, *J* = 7.8 Hz, H-7), 7.86 (d, 2H, AA'BB', *J* = 8.9 Hz, H-3', H-7'), 7.78-7.70 (m, 1H, H-9), 7.66-7.60 (m, 1H, H-8), 7.52 (d, 1H, *J* = 9.0 Hz, H-5) and 7.47 (d, 2H, AA'BB', *J* = 8.9 Hz, H-4', H-6'); *m/z* (ES^+) 357.03 [$(M+Na)^+$, 100%].

2-(3'-Bromobenzoyl)-3*H*-benzo[*f*]chromen-3-one (51j)

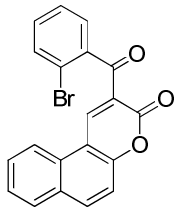

From Method A, **49** (430 mg) yielded **51j** as a yellow powder (761 mg, 2.01 mmol, 76%). Mp 238-240 °C; δ_H (400 MHz, $CDCl_3$) 9.27 (s, 1H, H-1), 8.36 (d, 1H, *J* = 8.3 Hz, H-10), 8.13 (d, 1H, *J* = 8.8 Hz, H-6), 7.95 (d, 1H, *J* = 7.8 Hz, H-7), 7.80-7.71 (m, 1H, H-9), 7.63 (m, 2H, H-8 + 1×ArH), 7.55-7.43 (m, 3H, H-5 + 2 × ArH) and 7.41-7.36 (m, 1H, ArH); *m/z* (ES^+) 401.05 [$(M+Na)^+$, 100%].

2-(4'-Bromobenzoyl)-3*H*-benzo[*f*]chromen-3-one (51k)

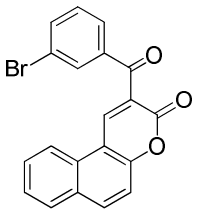

From Method A, **49** (430 mg) yielded **51k** as a yellow powder (785 mg, 2.07 mmol, 83%). Mp 213-215 °C; ν_{max} cm^{-1} (KBr): 1708 (CO), 1275, 1210 (C-O), 750, 666 (C-Br); δ_H (400 MHz, $CDCl_3$) 8.98 (s, 1H, H-1). 8.29 (d, 1H, *J* = 8.3 Hz, H-10), 8.13 (d, 1H, *J* = 9.0 Hz, H-6), 8.04 (t,

1H, *J* = 1.8 Hz, H-3'), 7.96 (d, 1H, *J* = 8.1 Hz, H-7), 7.84-7.79 (m, 1H, ArH), 7.78-7.72 (m, 2H, H-9 + 1×ArH), 7.66-7.50 (m, 1H, H-8), 7.53 (d, 1H, *J* = 9.0 Hz, H-5) and 7.37 (t, 1H, *J* = 7.8 Hz, ArH); δ_C (100 MHz, $CDCl_3$) 192.3 (C1'), 158.3 (C3), 156.5 (C4a), 143.7 (C1), 140.8 (C4'), 136.5 (C6), 133.1 (Ar), 132.1 (Ar), 130.4 (C6a), 129.7 (Ar), 129.4 (C9), 129.3 (C7) , 129.2 (C10a), 127.8 (Ar), 126.8 (C8), 123.7 (C2), 122.8 (C10), 119.6 (C2'), 116.9 (C5) and 113.2 (C10b); HRMS (ES^+) [Found: $(M+Na)^+$, 400.9786, $C_{20}H_{11}O_3Na^{79}Br$ requires 400.9789] (-0.8 ppm); [Found: $(M+Na)^+$, 402.9785, $C_{20}H_{11}O_3Na^{81}Br$ requires 402.9769] (-1.9 ppm)

2-(3'-Iodobenzoyl)-3*H*-benzo[*f*]chromen-3-one (51l)

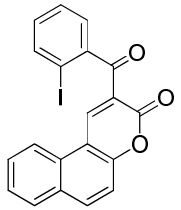

From Method A, **49** (430 mg) yielded **51l** as a yellow powder (853 mg, 2.00 mmol, 80%). Mp 239-240 °C; δ_H (400 MHz, $CDCl_3$) 9.29 (s, 1H, H-1), 8.35 (d, 1H, *J* = 8.4 Hz, H-10), 8.14 (d, 1H, *J* = 8.9 Hz, H-6), 7.98-7.90 (m, 2H, H-7, + 1×ArH), 7.80-7.74 (m, 1H, H-9), 7.67-7.61 (m, 1H, H-8), 7.53-7.42 (m, 3H, H-5, + 2×ArH) and 7.18-7.24 (m, 1H, ArH); HRMS (ES^+) [Found: $(M+Na)^+$, 448.9652, $C_{20}H_{11}O_3NaI$ requires 448.9651] (+0.1 ppm).

2-(4'-Iodobenzoyl)-3*H*-benzo[*f*]chromen-3-one (51m)

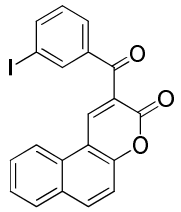

From Method A, **49** (430 mg) yielded **51m** as a yellow powder (861 mg, 2.02 mmol, 80%). Mp 237-239 °C; δ_H (400 MHz, $CDCl_3$) 8.97 (s, 1H, H-1), 8.29 (d, 1H, *J* = 8.4 Hz, H-10), 8.23 (t, 1H, *J* = 1.7 Hz, H-3'), 8.14 (d, 1H, *J* = 9.0 Hz, H-6), 7.99-7.92 (m, 2H, H-7 + 1×ArH), 7.87-7.81 (m, 1H, ArH), 7.79-7.71 (m, 1H, H-9), 7.67-7.61 (m, 1H, H-8), 7.53 (d, 1H, *J* = 9.0 Hz, H-5) and 7.24 (d, 1H, *J* = 7.8 Hz, ArH); *m/z* (ES^+) 449.02 [$(M+Na)^+$, 100%].

2-(5'-Iodobenzoyl)-3*H*-benzo[*f*]chromen-3-one (51n)

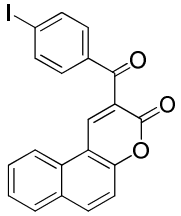

From Method A, **49** (430 mg) yielded **51n** as a yellow powder (874 mg, 2.05 mmol, 98%). Mp 249-252 °C; δ_H (400 MHz, $CDCl_3$) 8.97 (s, 1H, H-1), 8.28 (d, 1H, *J* = 8.3 Hz, H-10), 8.13 (d, 1H, *J* = 9.0 Hz, H-6), 7.96 (d, 1H, *J* = 8.0 Hz, H-7), 7.86 (d, 2H, AA'BB', *J* = 8.5 Hz, H-3', H-7'), 7.78-7.70 (m, 1H, H-9), 7.67-7.61 (m, 3H, H-8, H-4', H-6') and 7.52 (d, 1H, *J* = 9.0 Hz, H-5); *m/z* (ES^+) 449.04 [$(M+Na)^+$, 100%].

2-(3'-Trifluoromethyl-benzoyl)-3*H*-benzo[*f*]chromen-3-one (51o)

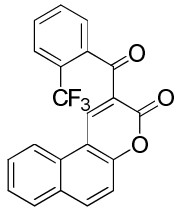

From Method A, **49** (430 mg) yielded **51o** as a yellow powder (637 mg, 1.73 mmol, 70%). Mp 187-189 °C; δ_H (400 MHz, $CDCl_3$) 9.34 (s, 1H, H-1), 8.33 (d, 1H, *J* = 8.3 Hz, H-10), 8.12 (d, 1H, *J* = 9.0 Hz, H-6), 7.94 (d, 1H, *J* = 8.0 Hz, H-7), 7.80-7.73 (m, 2H, H-9 + 1×ArH), 7.68-7.58 (m, 3H, H-8 + 2×ArH) and 7.49-7.44 (m, 2H, H-5 + 1×ArH); HRMS (ES^+) [Found: $(M+Na)^+$, 391.0563, $C_{21}H_{11}O_3NaF_3$ requires 391.0558] (+1.4 ppm).

2-(4'-Trifluoromethyl-benzoyl)-3*H*-benzo[*f*]chromen-3-one (51p)

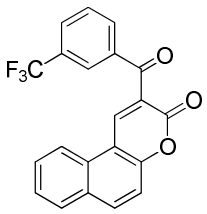

From Method A, **49** (430 mg) yielded **51p** as a yellow powder (761 mg, 2.06 mmol, 83%). Mp 247-250 °C; δ_H (400 MHz, $CDCl_3$) 9.06 (s, 1H, H-1), 8.31 (d, 1H, *J* = 8.2 Hz, H-10), 8.19-8.12 (m, 2H , H-3', H-6), 8.06 (d, 1H, *J* = 7.8 Hz, ArH), 7.97 (d, 1H, *J* = 8.1 Hz, H-7), 7.87 (d, 1H, *J* = 7.8 Hz, ArH), 7.80-7.72 (m, 1H, H-9), 7.64 (m, 2H, H-8 + 1×ArH) and 7.54 (d, 1H, *J* = 9.0 Hz, H-5); *m/z* (ES^+) 391.08 [$(M+Na)^+$, 100%].

2-(5'-Trifluoromethylbenzoyl)-3*H*-benzo[*f*]chromen-3-one (51q)

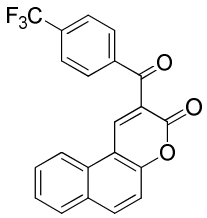

From Method A, **49** (430 mg) yielded **51q** as a yellow powder (707 mg, 1.92 mmol, 77%). Mp 192-195 °C; δ_H (400 MHz, $CDCl_3$) 9.00 (s, 1H, H-1), 8.30 (d, 1H, *J* = 8.3 Hz, H-10), 8.14 (d, 1H, *J* = 9.0 Hz, H-6), 7.99 (d, 2H, AA'BB', *J* = 8.0 Hz, H-3', H-7'), 7.96 (d, 1H, *J* = 8.7 Hz, H-7), 7.79-7.72 (m, 3H, H-9, H-4', H-6'), 7.68-7.64 (m, 1H, H-8) and 7.53 (d, 1H, *J* = 9.0 Hz, H-5); *m/z* (ES^+) 391.09 [$(M+Na)^+$, 100%].

2-(3'-Nitro-benzoyl)-3*H*-benzo[*f*]chromen-3-one (51r)

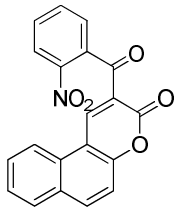

From Method A, **49** (430 mg) yielded **51r** as a yellow powder (847 mg, 2.45 mmol, 98%). Mp 218-221 °C; δ_H (400 MHz, $CDCl_3$) 9.64 (s, 1H, H-1), 8.46 (dd, 1H, ^2J = 8.2 Hz, ^3J = 0.9 Hz, H-10), 8.28 (d, 1H, *J* = 8.2 Hz, ArH), 8.13 (d, 1H, *J* = 9.0 Hz, H-6), 7.95 (d, 1H, *J* = 8.1 Hz, H-7), 7.84-7.76 (m, 2H, H-9 + 1 × ArH), 7.70-7.62 (m, 2H, H-8 + 1 × ArH) and 7.48-7.42 (m, 2H, H-5 + 1 × ArH); *m/z* (ES^+) 368.11 [$(M+Na)^+$, 100%].

2-(4'-Nitrobenzoyl)-3*H*-benzo[*f*]chromen-3-one (51s)

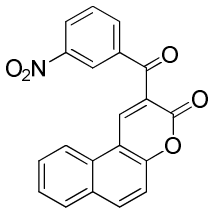

From Method A, **49** (430 mg) yielded **51s** as a yellow powder (694 mg, 2.00 mmol, 80%). Mp 243-246 °C; δ_H (400 MHz, $CDCl_3$) 9.15 (s, 1H, H-1), 8.69 (t, 1H, *J* = 1.8 Hz, H-3'), 8.47 (m, 1H, H-10), 8.35 (d, 1H, *J* = 8.3 Hz, ArH), 8.23-8.15 (m, 2H, H-6 + 1×ArH), 7.99 (d, 1H, *J* = 7.9 Hz, H-7), 7.81-7.76 (m, 1H, H-9), 7.73-7.63 (m, 2H, H-8 + 1×ArH) and 7.55 (d, 1H, *J* = 9.0 Hz, H-5); *m/z* (ES^+) 368.14 [$(M+Na)^+$, 100%].

(5'-Nitro-benzoyl)-3*H*-benzo[*f*]chromen-3-one (51t)

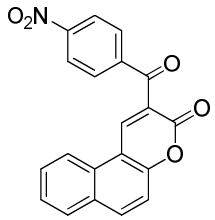

From Method A, **49** (430 mg) yielded **51t** as a yellow powder (694 mg, 2.00 mmol, 80%). Mp 270-273 °C; ν_{max} cm^{-1} (NaCl): 1710 (CO), 1251, 1070 (C-O); δ_H (400 MHz, $CDCl_3$) 9.15 (s, 1H, H-1), 8.38-8.30 (m, 3H, H-10, H-3', H-7'), 8.17 (d, 1H, *J* = 9.0 Hz, H-6), 8.00 (d, 2H, AA'BB', *J* = 9.0 Hz, H-4', H-6'), 7.98 (d, 1H, *J* = 8.1 Hz, H-7), 7.82-7.76 (m, 1H, H-9), 7.70-7.64 (m, 1H, H-8) and 7.55 (d, 1H, *J* = 9.0 Hz, H-5); δ_C (100 MHz, $CDCl_3$) 191.1 (C1'), 158.3 (C3), 151.1 (C4a), 150.4 (C2'), 144.2 (C1), 141.9 (C5'), 136.7 (C6), 130.5 (C4', C6'), 130.2 (C6a), 129.7 (C10a), 129.6 (C7), 129.5 (C3', C5'), 129.3 (C9), 127.0 (C8), 123.8 (C2), 121.6 (C10), 116.8 (C5) and 112.9 (C10b); HRMS (ES^+) [Found: $(M+Na)^+$, 368.0528, $C_{20}H_{11}NO_5Na$ requires 368.0535] (-2.0 ppm).

2-(3'-Methylbenzoyl)-3*H*-benzo[*f*]chromen-3-one (51u)

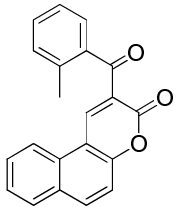

From Method A, **49** (430 mg) yielded **51u** as a yellow powder (624 mg, 1.98 mmol, 79%). Mp 208-210 °C; δ_H (300 MHz, $CDCl_3$) 9.02 (s, 1H, H-1), 8.27 (d, 1H, *J* = 8.2 Hz, H-10), 8.12 (d, 1H, *J* = 9.0 Hz, H-6), 7.95 (d, 1H, *J* = 7.6 Hz, H-7), 7.77-7.71 (m, 1H, H-9), 7.66-7.60 (m, 1H, H-8), 7.54-7.46 (m, 2H, H-5 + 1×ArH), 7.47-7.40 (m, 1H, ArH), 7.36-7.31 (m, 1H, ArH), 7.28-7.24 (m, 1H, ArH) and 2.55 (s, 3H, CH_3); *m/z* (ES^+) 337.11 [$(M+Na)^+$, 100%].

2-(4'-Methylbenzoyl)-3*H*-benzo[*f*]chromen-3-one (51v)

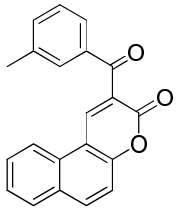

From Method A, **49** (430 mg) yielded **51v** as a yellow powder (280 mg, 0.89 mmol, 66%). Mp 194-196 °C; δ_H (300 MHz, $CDCl_3$) 8.91 (s, 1H, H-1), 8.27 (d, 1H, *J* = 8.4 Hz, H-10), 8.11 (d, 1H, *J* = 9.1 Hz, H-6), 7.96 (d, 1H, *J* = 7.6 Hz, H-7), 7.78-7.66 (m, 3H, H-9 + 2×ArH), 7.66-7.62

(m, 1H, H-8), 7.53 (d, 1H, *J* = 9.1 Hz, H-5), 7.47-7.34 (m, 2H, ArH) and 2.42 (s, 3H, CH_3); *m/z* (ES^+) 337.11 [$(M+Na)^+$, 100%].

2-(5'-Methylbenzoyl)-3*H*-benzo[*f*]chromen-3-one (51w)

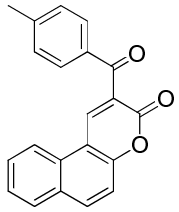

From Method A, **49** (430 mg) yielded **51w** as a yellow powder (490 mg, 1.56 mmol, 62%). Mp 190-192 °C (*lit.*[130] 190-191 °C); ν_{max} cm^{-1} (KBr): 1745 (C=O), 1224, 1147, 1139 (C-O), 1678 (C-CH_3); δ_H (300 MHz, $CDCl_3$) 8.89 (s, 1H, H-1), 8.26 (d, 1H, *J* = 8.2 Hz, H-10), 8.10 (d, 1H, *J* = 9.0 Hz, H-6), 7.95 (d, 1H, *J* = 8.1 Hz, H-7), 7.83 (d, 2H, AA'BB', *J* = 8.0 Hz, H-3', H-7'), 7.76-7.71 (m, 1H, H-9), 7.66-7.60 (m, 1H, H-8), 7.52 (d, 1H, *J* = 9.0 Hz, H-5), 7.30 (d, 2H, AA'BB', *J* = 8.0 Hz, H-4', H-6'), and 2.44 (s, 3H, CH_3); δ_C (100 MHz, $CDCl_3$) 191.7 (C1'), 158.7 (C3), 155.3 (C4a), 144.8 (C5'), 141.5 (C1), 135.3 (C6), 133.8 (C2'), 130.3 (C6a), 129.9 (C3', C7'), 129.4 (C2', C6'), 129.3 (C10a), 129.1 (C7), 128.7 (C9), 126.6 (C2), 126.4 (C8), 121.5 (C10), 116.6 (C5) and 112.9 (C10b), 21.9 (CH_3); HRMS (ES^+) [Found: $(M+Na)^+$, 337.0928, $C_{21}H_{14}ONa$ requires 337.0935] (-2.0 ppm).

2-(Furan-2'-carbonyl)-3*H*-benzo[*f*]chromen-3-one (51x)

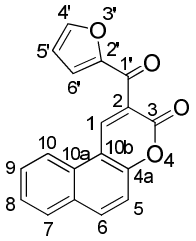

From Method A, **49** (430 mg) yielded **51x** as a yellow powder (327 mg, 1.12 mmol, 45%). Mp 227-230 °C; ν_{max} cm^{-1} (KBr): 1710, 1459 (CO), 1215 (C-O); δ_H (400 MHz, $CDCl_3$) 8.95 (s, 1H, H-1), 8.28 (d, 1H, *J* = 8.3 Hz, H-10), 8.10 (d, 1H, *J* = 9.0 Hz, H-6), 7.94 (d, 1H, *J* = 8.0 Hz, H-7), 7.78-7.73 (m, 1H, H-9), 7.70-7.68 (m, 1H, H-4'), 7.65-7.60 (m, 1H, H-8), 7.51 (d, 1H, *J* = 9.0 Hz, H-5), 7.43 (m, 1H, H-6') and 6.63 (dd, 1H, ^3J = 3.6 Hz, $^{3'}J$ = 1.6 Hz, H-5'); δ_C (100 MHz, $CDCl_3$) 178.3 (C1'), 158.3 (C3), 155.4 (C4a), 151.8 (C2'), 147.7 (C4'), 141.9 (C1), 135.6 (C6), 130.3 (C6a), 129.9 (C7), 129.4 (C10a), 129.2 (C9), 126.6 (C8), 124.6 (C2), 121.5 (C10), 120.8 (C6'), 116.7 (C5), 113.1 (C10b) and 112.6 (C5'); HRMS (ES^+) [Found: $(M+Na)^+$, 313.0482, $C_{18}H_{10}O_4Na$ requires 313.0477] (+1.8 ppm).

6.2.2 Synthesis of 3-benzoyl-1,2-dihydrocoumarins 52 (METHOD B)

To a stirring solution of the desired 3-benzoyl-5,6-benzocoumarin (**51**) (400 mg, 1 eq.) in dry pyridine (4 mL) was added $NaBH_4$ (1.1 eq.) and the resulting mixture stirred at room temperature for 2 h. The reaction mixture was then poured into cold 2M HCl. A white precipitate formed, which was collected by parallel filtration, was washed with 2M HCl and recrystallised in parallel from ethanol.

2-Benzoyl-1,2-dihydro-benzo[*f*]chromen-3-one (52a)

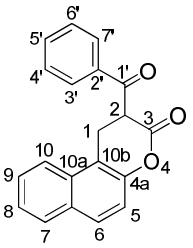

From Method B, synthesised in parallel (×4), **51a** (500 mg) yielded **52a** as a white powder (275-311 mg, 0.91-1.02 mmol, 55-61%). Mp 158-160 °C (*lit.*[132] 158-160 °C); δ_H (300 MHz, $CDCl_3$) 8.03-7.98 (m, 2H, ArH), 7.90-7.85 (m, 2H, H-10, H-7), 7.81 (d, 1H, *J* = 9.0 Hz, H-6), 7.67-7.61 (m, 1H, H-9), 7.59-7.52 (m, 1H, H-8), 7.54-7.45 (m, 3H, ArH), 7.29 (d, 1H, *J* = 9.0 Hz, H-5), 4.82 (dd, 1H, ^3J = 10.2 Hz, $^{3'}J$ = 6.8 Hz, H-2), 3.85 (dd, 1H, ^2J = 16.7 Hz, ^3J = 10.4 Hz, H-1) and 3.62 (dd, 1H, ^2J = 16.7 Hz, ^3J = 6.8 Hz, H-1); *m/z* (ES^+) 325.10 [$(M+Na)^+$, 100%].

2-(5'-Bromobenzoyl)-1,2-dihydro-benzo[*f*]chromen-3-one (52c)

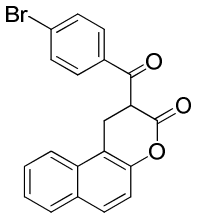

From Method B, **51c** (400 mg) yielded **52c** as a white powder (280 mg, 0.73 mmol, 93%). Mp 221-223 °C; δ_H (400 MHz, $CDCl_3$) 7.91-7.84 (m, 4H, H-7, H-10, H-4', H-6'), 7.82 (d, 1H, *J* = 8.8 Hz, H-6), 7.65 (d, 2H, AA'BB', *J* = 8.6 Hz, H-3', H-7'), 7.62-7.54 (m, 1H, H-9), 7.52-7.45 (m, 1H, H-8), 7.28 (d, 1H, *J* = 8.8 Hz, H-5), 4.74 (dd, 1H, ^3J = 10.5 Hz, $^{3'}J$ = 6.7 Hz, H-2), 3.83 (dd, 1H, ^2J = 16.6 Hz, ^3J = 10.5 Hz, H-1) and 3.62 (dd, 1H, ^3J = 16.6 Hz, ^2J = 6.7 Hz, H-1); *m/z* (ES^-) 379.09 [$(M-H)^-$, 100%].

2-(3'-Fluoro-benzoyl)-1,2-dihydro-benzo[*f*]chromen-3-one (52d)

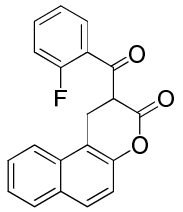

From Method B, **51d** (400 mg) yielded **52d** as a white powder (50 mg, 0.15 mmol, 40%). Mp 122-124 °C; δ_H (300 MHz, $CDCl_3$) 8.02-7.81 (m, 4H, H-10, H-7, H-6 + 1×ArH), 7.65-7.44 (m, 3H, H-9, H-8 + 1×ArH), 7.29 (d, 2H, *J* = 8.6 Hz, H-5 + 1×ArH), 7.22-7.15 (m, 1H, ArH), 4.74 (dd, 1H, ^{3}J = 10.5 Hz, $^{3'}J$ = 7.4 Hz, H-2) and 3.76-3.64 (m, 2H, H-1); *m/z* (ES^+) 343.09 [$(M+Na)^+$, 100%].

2-(4'-Fluoro-benzoyl)-1,2-dihydro-benzo[*f*]chromen-3-one (52e)

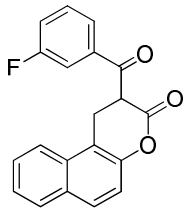

From Method B, **51e** (400 mg) yielded **52e** as a white powder (77 mg, 0.24 mmol, 62%). Mp 143-145 °C; δ_H (300 MHz, $CDCl_3$) 7.92-7.76 (m, 4H, H-10, H-7, H-6 + 1×ArH), 7.72-7.66 (m, 1H, ArH), 7.61-7.55 (m, 1H, H-9), 7.53-7.46 (m, 2H, H-8 + 1×ArH), 7.37-7.23 (m, 2H, H-5 + 1×ArH), 4.75 (dd, 1H, ^{3}J = 10.5 Hz, $^{3'}J$ = 6.7 Hz, H-2), 3.84 (dd, 1H, ^{2}J = 16.6 Hz, ^{3}J = 10.5 Hz, H-1) and 3.62 (dd, 1H, ^{2}J = 16.6 Hz, ^{3}J = 6.7 Hz, H-1); *m/z* (ES^+) 343.11 [$(M+Na)^+$, 100%]; (ES^-) 319.10 [$(M-H)^-$, 100%]; HRMS (ES^+) [Found: $(M+Na)^+$, 343.0750, $C_{20}H_{13}O_3NaF$ requires 343.0746] (+1.0 ppm).

2-(5'-Fluoro-benzoyl)-1,2-dihydro-benzo[*f*]chromen-3-one (52f)

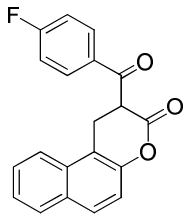

From Method B, **51f** (400 mg) yielded **52f** as a white powder (100 mg, 0.31 mmol, 71%). Mp 139-141 °C; δ_H (300 MHz, $CDCl_3$) 7.87-7.79 (m, 2H, H-7, H-10), 7.76 (d, 2H, AA'BB', *J* = 8.7 Hz, H-3', H-7'), 7.56 (d, 1H, *J* = 9.0 Hz, H-6), 7.56-7.48 (m, 1H, H-9), 7.48-7.40 (m, 1H, H-8), 7.32 (d, 1H, *J* = 9.0 Hz, H-5), 7.22 (d, 2H, AA'BB', *J* = 8.7 Hz, H-4', H-6'), 4.80 (dd, 1H,

^{3}J = 10.2 Hz, $^{3'}J$ = 6.8 Hz, H-2), 3.78 (dd, 1H, ^{2}J = 16.6 Hz, ^{3}J = 10.2 Hz, H-1) and 3.59 (dd, 1H, ^{2}J = 16.6 Hz, ^{3}J = 6.8 Hz, H-1); *m/z* (ES^{+}) 343.08 [$(M+Na)^{+}$, 100%].

2-(4'-Chloro-benzoyl)-1,2-dihydro-benzo[*f*]chromen-3-one (52h)

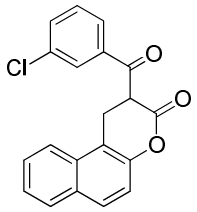

From Method B, **51h** (400 mg) yielded **52h** as a white powder (340 mg, 1.01 mmol, 85%). Mp 172-174 °C; δ_H (300 MHz, $CDCl_3$) 7.97 (t, 1H, *J* = 1.8 Hz, H-3'), 7.92-7.85 (m, 3H, H-10, H-7 + 1×ArH), 7.82 (d, 1H, *J* = 9.0 Hz, H-6), 7.63-7.54 (m, 2H, H-9 + 1×ArH), 7.52-7.42 (m, 2H, H-8 + 1×ArH), 7.29 (d, 1H, *J* = 9.0 Hz, H-5), 4.74 (dd, 1H, ^{3}J = 10.7 Hz, $^{3'}J$ = 6.8 Hz, H-2), 3.83 (dd, 1H, ^{2}J = 16.6 Hz, ^{3}J = 10.8 Hz, H-1) and 3.62 (dd, 1H, ^{2}J = 16.6 Hz, ^{3}J = 6.8 Hz, H-1); *m/z* (ES^{+}) 337.06 [$(M+H)^{+}$, 100%].

2-(5'-Chlorobenzoyl)-1,2-dihydro-benzochromen-3-one (52i)

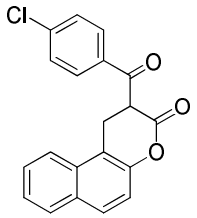

From Method B, **51i** (400 mg) yielded **52i** as a white powder (360 mg, 1.07 mmol, 90%). Mp 206-208 °C; ν_{max} cm^{-1} (NaCl): 1755 (C=O), 1223, 1148 (C-O), 1678 (C-Cl); δ_H (400 MHz, $CDCl_3$) 7.95 (d, 2H, AA'BB', *J* = 8.8 Hz, H-3', H-7'), 7.85-7.91 (m, 2H, H-7, H-10), 7.82 (d, 1H, *J* = 8.8 Hz, H-6), 7.61-7.53 (m, 1H, H-9), 7.42-7.54 (m, 3H, H-8, H-4', H-6'), 7.28 (d, 1H, *J* = 8.8 Hz, H-5), 4.75 (dd, 1H, ^{3}J = 10.5 Hz, $^{3'}J$ = 6.8 Hz, H-2), 3.83 (dd, 1H, ^{2}J = 16.6 Hz, ^{3}J = 10.5 Hz, H-1) and 3.61 (dd, 1H, ^{2}J = 16.6 Hz, ^{3}J = 6.8 Hz, H-1); δ_C (75.5 MHz, $CDCl_3$) 192.9 (C1'), 165.9 (C3), 148.0 (C4a), 139.6 (C5'), 134.4 (C2'), 131.9 (C6a) , 131.3 (C10a), 130.6 (C-3', C-7'), 129.6 (C6), 129.6 (C-4', C-6'), 129.5 (C7), 127.7 (C8), 125.7 (C9), 123.1 (C10), 117.3 (C5), 114.8 (C10b), 46.8 (C2) and 23.3 (C1); HRMS (ES^{+}) [Found: $(M+Na)^{+}$, 337.0630, $C_{20}H_{14}O_3Cl$ requires 337.0631] (-0.3 ppm).

2-(4'-Bromobenzoyl)-1,2-dihydro-benzo[*f*]chromen-3-one (52k)

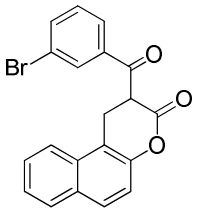

From Method B, **51k** (400 mg) yielded **52k** as a white powder (340 mg, 0.89 mmol, 90%). Mp 219-221 °C; ν_{max} cm^{-1} (NaCl): 1745 (CO), 1283, 1222, 1150 and 1071 (C-O), 743 (C-Br); δ_H (300 MHz, $CDCl_3$) 7.97 (t, 1H, *J* = 1.9 Hz, H-3'), 7.91-7.71 (m, 5H, H-10, H-7, H-6 + 2×ArH), 7.63-7.54 (m, 1H, H-9), 7.53-7.43 (m, 1H, H-8), 7.38 (t, 1H, *J* = 7.9 Hz, ArH), 7.29 (d, 1H, *J* = 8.9 Hz, H-5), 4.74 (dd, 1H, ^3J = 10.7 Hz, $^{3'}J$ = 6.8 Hz, H-2), 3.83 (dd, 1H, ^2J = 16.6 Hz, ^3J = 10.8 Hz, H-1) and 3.62 (dd, 1H, ^2J = 16.6 Hz, ^3J = 6.8 Hz, H-1); δ_C (75.5 MHz, $CDCl_3$) 192.8 (C1'), 164.5 (C3), 149.0 (C4a), 137.6 (C2'), 136.9 (C6'), 131.9 (Ar), 131.3 (C6a) 131.1 (C10a), 130.6 (Ar), 129.5 (C6), 129.0 (C7), 127.5 (C8), 127.4 (Ar), 125.6 (C9), 123.4 (C4'), 122.9 (C10), 117.0 (C5), 114.5 (C10b), 46.6 (C1) and 23.1 (C2); *m/z* (ES^-) 379.09 [$(M-H)^-$, 100%].

2-(4'-Iodobenzoyl)-1,2-dihydro-benzo[*f*]chromen-3-one (52m)

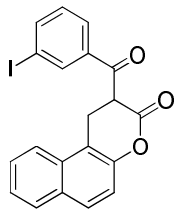

From Method B, **51m** (400 mg) yielded **52m** as a white powder (360 mg, 0.84 mmol, 90%). Mp 199-202 °C; ν_{max} cm^{-1} (NaCl): 1705 (C=O), 1262, 1217, 1066 and 1057 (C-O), 750 (C-I); δ_H (400 MHz, $CDCl_3$) 8.31 (t, 1H, *J* = 1.7 Hz, H-3'), 7.98-7.72 (m, 5H, H-10, H-7, H-6 + 2×ArH), 7.62-7.53 (m, 1H, H-9), 7.53-7.44 (m, 1H, H-8), 7.31-7.20 (m, 2H, 2 × ArH), 4.73 (dd, 1H, ^3J = 10.8 Hz, $^{3'}J$ = 6.8 Hz, H-2), 3.82 (dd, 1H, ^2J = 16.6 Hz, ^3J = 10.8 Hz, H-1) and 3.61 (dd, 1H, ^3J = 16.6 Hz, ^2J = 6.8 Hz, H-1); δ_C (100 MHz, $CDCl_3$) 192.8 (C1'), 165.7 (C3), 149.1 (C4a), 142.9 (C6'), 136.9 (C3'), 136.4 (C2'), 131.1 (C6a), 131.0 (C10a), 130.6 (Ar), 129.5 (Ar), 129.0 (C6), 128.2 (C7), 127.6 (C8), 125.6 (C9), 122.9 (C10), 117.2 (C5), 114.6 (C10b), 93.6 (C4'), 46.5 (C2) and 23.1 (C1); HRMS (CI^+) [Found: $(M+H)^+$, 428.9985, $C_{20}H_{14}O_3I$ requires 428.9988] (-0.6 ppm).

2-(5'-Iodobenzoyl)-1,2-dihydro-benzo[*f*]chromen-3-one (52n)

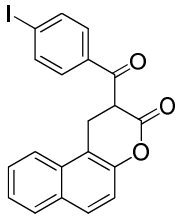

From Method B, **52n** (400 mg) yielded **51n** as a white powder (340 mg, 0.79 mmol, 85%). Mp 229-233 °C; δ_H (300 MHz, $CDCl_3$) 7.92-7.85 (m, 4H, H-7, H-10,H-3', H-7'), 7.81 (d, 1H, *J* = 8.8 Hz, H-6), 7.70 (d, 2H, AA'BB', *J* = 8.7 Hz, H-4', H-6'), 7.61-7.53 (m, 1H, H-9), 7.53-7.45 (m, 1H, H-8), 7.28 (d, 1H, *J* = 8.8 Hz, H-5), 4.73 (dd, 1H, ^3J = 10.5 Hz, $^{3'}J$ = 6.8 Hz, H-2), 3.82 (dd, 1H, ^2J = 16.6 Hz, ^3J = 10.6 Hz, H-1) and 3.61 (dd, 1H, ^2J = 16.6 Hz, ^3J = 6.8 Hz, H-1); *m/z* (CI^+) 428.99 [$(M+H)^+$, 100%].

2-(4'-Trifluoromethylbenzoyl)-1,2-dihydro-benzo[*f*]chromen-3-one (52p)

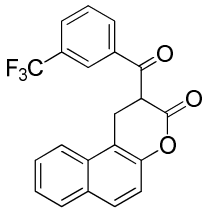

From Method B, **51p** (400 mg) yielded **52p** as a white powder (270 mg, 0.73 mmol, 95%). Mp 205-208 °C; δ_H (300 MHz, $CDCl_3$) 8.26 (s, 1H, H-3'), 8.20 (d, 1H, *J* = 8.0 Hz, ArH), 7.94-7.83 (m, 3H, H-10, H-7 + 1×ArH), 7.82 (d, 1H, *J* = 8.9 Hz, H-6), 7.71-7.46 (m, 3H, H-9, H-8 + 1×ArH), 7.29 (d, 1H, *J* = 8.9 Hz, H-5), 4.79 (dd, 1H, ^3J = 10.9 Hz, $^{3'}J$ = 6.8 Hz, H-2), 3.86 (dd, 1H, ^2J = 17.0 Hz, ^3J = 10.8 Hz, H-1) and 3.64 (dd, 1H, ^2J = 17.0 Hz, ^3J = 6.8 Hz, 1-H); HRMS (ES^-) [Found: $(M-H)^-$, 369.0746, $C_{21}H_{12}O_3F_3$ requires 369.0739] (+1.9 ppm).

2-(5'-Trifluoromethylbenzoyl)-1,2-dihydro-benzo[*f*]chromen-3-one (52q)

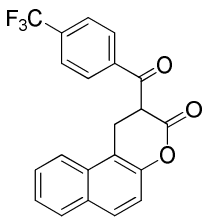

From Method B, **51q** (400 mg) yielded **52q** as a white powder (360 mg, 0.97 mmol, 89%). Mp 192-193 °C; ν_{max} cm^{-1} (NaCl): 1710 (C=O), 1251 (C-O), 747, 691 (C-F); δ_H (400 MHz, $CDCl_3$) 8.12 (d, 2H, AA'BB', *J* = 8.2 Hz, H-3', H-7'), 7.93-7.86 (m, 2H, H-7, H-10), 7.83 (d, 1H, *J* = 8.8 Hz, 6-H), 7.78 (d, 2H, AA'BB', *J* = 8.2 Hz, H-4', H-6'), 7.62-7.54 (m, 1H, H-9), 7.54-7.45 (m, 1H, H-8), 7.28 (d, 1H, *J* = 8.8 Hz, H-5), 4.79 (dd, 1H, ^3J = 10.7 Hz, $^{3'}J$ = 6.7 Hz, H-2),

3.85 (dd, 1H, ^{2}J = 16.6 Hz, ^{3}J = 10.8 Hz, H-1) and 3.64 (dd, 1H, ^{2}J = 16.6 Hz, ^{3}J = 6.7 Hz, H-1); δ_C (75.5 MHz, $CDCl_3$) 193.0 (C1'), 164.4 (C3), 147.9 (C4a), 137.4 (C2'), 134.9 (C5'), 131.7 (C10a), 131.1 (C6a), 129.5 (C3', C7'), 129.1 (C7), 128.7 (C6), 127.6 (C8), 126.1 (C4', C6'), 125.6 (C9), 122.9 (C10), 121.9 (CF_3), 117.0 (C5), 114.5 (C10b), 45.7 (C2) and 21.8 (C1); HRMS (ES^-) [Found: $(M-H)^-$, 369.0737, $C_{21}H_{12}O_3F_3$ requires 369.0739] (-0.5 ppm).

2-(4'-Nitrobenzoyl)-1,2-dihydro-benzo[*f*]chromen-3-one (52s)

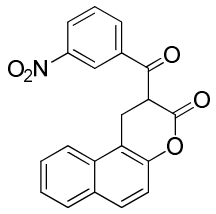

From Method B, **51s** (400 mg) yielded **52s** as a white powder (279 mg, 0.80 mmol, 92%). Mp 203-206 °C; δ_H (300 MHz, DMSO-d_6) 8.86 (t, 1H, *J* = 1.8 Hz, H-3'), 8.59-8.48 (m, 2H, H-10, H-7), 8.06-7.93 (m, 3H, H-6 + 2×ArH), 7.86 (t, 1H, *J* = 8.0 Hz, ArH), 7.65-7.57 (m, 1H, H-9), 7.56-7.48 (m, 1H, H-8), 7.38 (d, 1H, *J* = 8.8 Hz, H-5), 5.51 (dd, 1H, ^{3}J = 11.8 Hz, $^{3'}J$ = 6.8 Hz, H-2), 3.80 (dd, 1H, ^{2}J = 16.5 Hz, ^{3}J = 6.8 Hz, H-1) and 3.64 (dd, 1H, ^{2}J = 16.5 Hz, ^{3}J = 11.8 Hz, H-1); HRMS (ES^-) [Found: $(M-H)^-$, 346.0711, $C_{20}H_{12}NO_5$ requires 346.0715] (-1.3 ppm).

2-(5'-Nitrobenzoyl)-1,2-dihydro-benzo[*f*]chromen-3-one (52t)

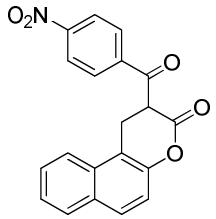

From Method B, **51t** (400 mg) yielded **52t** as a white powder (293 mg, 0.84 mmol, 88%). Mp 209-211 °C; δ_H (300 MHz, $CDCl_3$) 8.36 (d, 2H, AA'BB', *J* = 9.0 Hz, H-6', H-4'), 8.17 (d, 2H, AA'BB', *J* = 9.0 Hz, H-3', H-7'), 7.93-7.81 (m, 2H, H-7, H-10), 7.80 (d, 1H, *J* = 8.8 Hz, H-6), 7.63-7.43 (m, 2H, H-9, H-8), 7.29 (d, 1H, *J* = 8.8 Hz, H-5), 4.78 (dd, 1H, ^{3}J = 11.0 Hz, $^{3'}J$ = 6.7 Hz, H-2), 3.85 (dd, 1H, ^{2}J = 16.7 Hz, ^{3}J = 11.0 Hz, H-1) and 3.66 (dd, 1H, ^{2}J = 16.7 Hz, ^{3}J = 6.7 Hz, H-1); *m/z* (ES^-) 346.10 [$(M-H)^-$, 100%].

2-(3'-Methyl-benzoyl)-1,2-dihydro-benzo[*f*]chromen-3-one (52u)

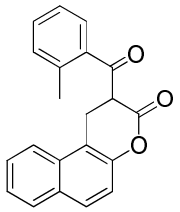

From Method B, **51u** (400 mg) yielded **52u** as a white powder (310 mg, 0.98 mmol, 78%). Mp 123-126 °C; δ_H (300 MHz, $CDCl_3$) 7.92-7.76 (m, 3H, H-7, H-10 + 1 × ArH), 7.63 (d, 1H, *J* = 7.8 Hz, H-6), 7.59-7.37 (m, 3H, H-9, H-8 + 1×ArH), 7.34-7.19 (m, 3H, H-5 + 2×ArH), 4.69 (dd, 1H, *J*, ^3J = 8.7 Hz, $^{3'}J$ = 6.6 Hz, H-2), 3.79 (dd, 1H, ^2J = 16.5 Hz, ^3J = 8.8 Hz, H-1), 3.56 (dd, 1H, ^2J = 16.5 Hz, ^3J = 6.6 Hz, H-1) and 2.24 (s, 3H, CH_3); *m/z* (ES^+) 337.11 [$(M+Na)^+$, 100%]. .

2-(4'-Methyl-benzoyl)-1,2-dihydro-benzo[*f*]chromen-3-one (52v)

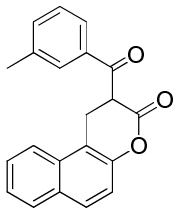

From Method B, **51v** (400 mg) yielded **52v** as a white powder (65 mg, 0.20 mmol, 35%). Mp 180-183 °C; δ_H (300 MHz, $CDCl_3$) 7.91-7.76 (m, 5H, H-10, H-7, H-6 + 2×ArH), 7.60-7.52 (m, 1H, H-9), 7.52-7.46 (m, 1H, H-8), 7.45-7.36 (m, 2H, ArH), 7.29 (d, 1H, *J* = 9.0 Hz, H-5), 4.81 (dd, 1H, ^3J = 10.3 Hz, $^{3'}J$ = 6.9 Hz, H-2), 3.83 (dd, 1H, ^2J = 16.7 Hz, ^3J = 10.4 Hz, H-1), 3.61 (dd, 1H, ^2J = 16.7 Hz, ^3J = 6.9 Hz, H-1) and 2.42 (s, 3H, CH_3); *m/z* (ES^+) 337.11 [$(M+Na)^+$, 100%].

2-(5'-Methyl-benzoyl)-1,2-dihydro-benzo[*f*]chromen-3-one (52w)

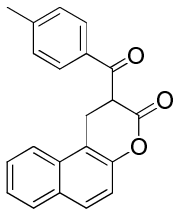

From Method B, **51w** (400 mg) yielded **52w** as a white powder (230 mg, 0.72 mmol, 60%). Mp 173-175 °C; δ_H (300 MHz, $CDCl_3$) 7.93-7.78 (m, 5H, H-10, H-7, H-6, H-7', H-3'), 7.60-7.52 (m, 1H, H-9), 7.51-7.44 (m, 1H, H-8), 7.34-7.24 (m, 3H, , H-5, H-4', H-6'), 4.80 (dd, 1H, ^3J = 10.1 Hz, $^{3'}J$ = 6.9 Hz, H-2), 3.84 (dd, 1H, ^2J = 16.6 Hz, ^3J = 10.2 Hz, H-1), 3.60 (dd, 1H, ^2J = 16.6 Hz, ^3J = 6.9 Hz, H-1) and 2.43 (s, 3H, CH_3); *m/z* (ES^+) 337.14 [$(M+Na)^+$, 100%].

6.2.3 Synthesis of 3-benzoyl-1,2-dihydrocoumarins 52j, o and x (METHOD C)

To a stirring solution of **51j**, **o** and **x** (1 eq.) in dry pyridine (4 mL) was added $NaBH_4$ (1.1 eq.) and the resulting mixture stirred at room temperature for 2 h. The reaction mixture was then poured into cold 2M HCl. A yellow precipitate formed, which was collected by filtration, washed with 2M HCl and purified by column chromatography (Hexane/EtOAc, 80:20).

2-(3'-Bromobenzoyl)-1*H*-benzo[*f*]chromen-3(2*H*)-one (52j)

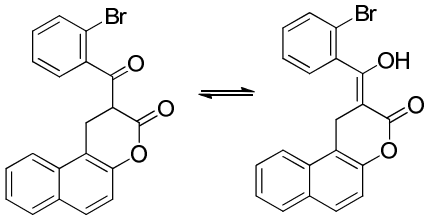

52j **52j'**

From Method C, **51j** (50 mg) yielded **52j'** as a yellow powder (41 mg, 0.1 mmol, 80%). An equilibrium with the enol form **52j'** was observed (ratio 1:14, **52j**:**52j'**). The signal derived from the proton at the C2 of the keto form **52j** was observed at 4.77 ppm (dd, ^{3}J = 10.2 Hz, $^{3'}J$ = 7.0 Hz). Data for **52j'**: δ_H (400 MHz, $CDCl_3$) 7.88-7.71 (m, 3H, H-10, H-7, H-6), 7.54-7.36 (m, 6H, H-9, H-8 + 4 × ArH), 7.28-7.21 (m, 1H, H-5) and 3.71 (brs, 2H, H-1); δ_C (75.5 MHz, $CDCl_3$) 169.2 (C3), 164.2 (C1'), 147.5 (C4a), 135.3 (C2'), 133.6 (C4'), 131.6 (C6), 131.1 (C6a), 131.0 (C10a), 129.2 (CH, Ar), 129.1 (CH, Ar), 128.8 (C7), 128.2 (CH, Ar), 127.2 (C8), 125.4 (C9), 122.6 (C10), 120.9 (C3'), 117.4 (C5), 112.8 (C10b), 93.4 (C2) and 23.7 (C1); HRMS (CI^+) [Found: $(M+Na)^+$, 402.9762, $C_{20}H_{11}O_3Na^{79}Br$ requires 402.9769] (-1.9 ppm).

2-(3'-(Trifluoromethyl)benzoyl)-1*H*-benzo[*f*]chromen-3(2*H*)-one (52o)

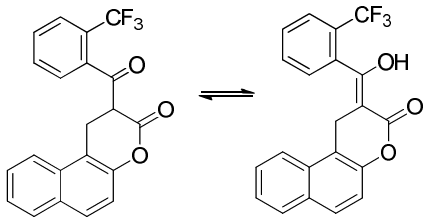

52o **52o'**

From Method C, **51o** (50 mg) yielded **52o'** as a yellow powder (40 mg, 82%). An equilibrium with the enol form **52o'** was observed (ratio 1:13, **52o**:**52o'**). The signal derived from the protons at H-1 and H-2 of **52o** were observed at 4.49 ppm (dd, ^{3}J = 6.6 Hz, $^{3'}J$ = 8.9 Hz, H-2), 3.82 ppm (dd, ^{2}J = 16.6 Hz, ^{3}J = 9.8 Hz, H-1) and 3.61 ppm (dd, ^{2}J = 16.6 Hz, ^{3}J = 6.6 Hz, H-1 Data for **52o'**: δ_H (400 MHz, $CDCl_3$) 7.88 (d, 1H, J = 7.9 Hz, ArH), 7.84-7.67 (m, 4H, ArH),

7.52-7.48 (m, 1H, ArH), 7.47-7.41 (m, 3H, ArH), 7.24 (d, 1H, *J* = 8.9 Hz, H-5) and 3.71 (brs, 2H, H-1); δ_C (75.5 MHz, $CDCl_3$) 173.9 (C3), 169.1 (C1'), 147.3 (C, Ar), 132.7 (CH, Ar), 132.0 (C, Ar × 2), 131.9 (CH, Ar), 131.1 (C, Ar), 130.9 (C, Ar), 130.5 (CH, Ar), 129.2 (CH, Ar), 129.2 (CH, Ar), 128.8 (CH, Ar), 127.2 (CH, Ar), 125.4 (CH, Ar), 122.4 (CH, Ar), 116.8 (CH, Ar), 112.6 (C, Ar) and 93.0 (C); *m/z* (ES^+) 392.95 [$(M+Na)^+$, 100%].

2-(Furan-1'-carbonyl)-1*H*-benzo[*f*]chromen-3(2*H*)-one (52x)

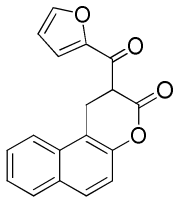

From Method C, **51x** (50 mg) yielded **52x** as a yellow powder (60%, conversion). δ_H (400 MHz, $CDCl_3$) 7.93-7.77 (m, 3H, H-10, H-7, H-6), 7.66-7.45 (m, 3H, H-9, H-8 + 1×ArH), 7.38 (dd, 1H, ^3J = 3.6 Hz, ^4J = 0.7 Hz, ArH), 7.28 (d, 1H, *J* = 9.0 Hz, H-5), 6.62 (dd, 1H, ^3J = 3.6 Hz, ^4J = 1.7 Hz, ArH), 4.63 (dd, 1H, ^3J = 6.9 Hz, $^{3'}J$ = 11.5 Hz, H-2), 3.81 (dd, 1H , ^2J = 16.5 Hz, ^3J = 11.5 Hz, H-1) and 3.62 (dd, 1H, ^2J = 16.5 Hz, ^3J = 6.9 Hz, H-1); *m/z* (ES^+) 314.92 [$(M+Na)^+$, 100%].

6.2.4 Parallel synthesis of Cambinol 39 and Analogues 46, 62-63, 65-67, 69, 71, 74-76 (METHOD D)

2M NaOEt stock solution (5 mL), previously prepared by dissolving Na metal in dry ethanol, was added to parallel synthesis reaction vessels containing both thiourea (**53**, 15.6 eq.) and the desired intermediate (**52**) (100 mg, 1 eq.). Each reaction mixture was then heated at reflux for 18 h, after which time the solvents were removed at reduced pressure. The crude residues were dissolved in the minimum amount of distilled water and 2M HCl added till a white precipitate had formed. The resulting precipitates were collected by filtration, purified by column chromatography (Hexane/EtOAc) and recrystallised from chloroform.

5-[2''-Hydroxynaphthyl-(1'')-methyl]-6-phenyl 2-thioxo-2,3-dihydro-1*H*-pyrimidin-4-one (39, Cambinol)

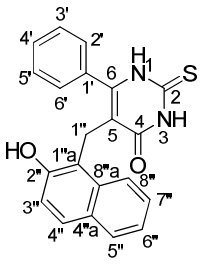

From Method D and synthesised in parallel (x 4), **51a** (100 mg) yielded **39** as a white powder after recrystallisation from ethanol (38-50 mg, 0.10-0.13 mmol, 32-46%). Mp 253-255 °C (*lit.*[104] 253 °C); ν_{max} cm^{-1} (NaCl): 3111 (OH), 2804 (CH_2), 1628 (C=O), 1556 (NH), 1494 (C-N), 1212 (C=S, CSNH), 877 and 766 (C-HAr); δ_H (400 MHz, DMSO-d_6) 12.55 (brs, 1H, NH), 12.30 (brs, 1H, NH), 9.44 (s, 1H, OH), 7.64 (d, 1H, *J* = 7.7 Hz, H-5''), 7.48 (d, 1H, *J* = 8.8 Hz, H-4''), 7.44-7.11 (m, 8H, H-6'', H-7'', H-8'' + 5×ArH), 6.90 (d, 1H, *J* = 8.8 Hz, H-3'') and 3.90 (s, 2H, CH_2); δ_C (100 MHz, DMSO-d_6) 173.8 (C=S), 162.2 (C=O), 152.7 (C2''), 150.1 (C6), 133.1 (C8''a), 131.6 (C1'), 129.4 (C4'), 128.5 (C5', C3'), 128.0 (C5''), 128.0 (C4''a), 127.8 (C2', C6'), 127.5 (C4''), 125.5 (C7''), 122.8 (C6''), 121.9 (C8''), 118.3 (C3''), 116.4 (C1''a), 115.2 (C5) and 21.5 (CH_2); *m/z* (ES^+) 382.97 [$(M+Na)^+$, 100%]; *m/z* (ES^-) 358.78 [$(M-H)^-$, 100%]; HRMS (ES^-) [Found: $(M-H)^-$, 359.0858, $C_{21}H_{15}N_2O_2S$ requires 359.0854] (-0.9 ppm). A sample of **39** was further recrystallised from ethanol to give crystals of sufficient size for small molecule X-ray crystallographic analysis. Crystallographic data for cambinol was deposited at the Cambridge Crystallographic Data Centre and allocated the deposit number CCDC 704011.

5-[2''-Hydroxynaphthyl-(1'')-methyl]-6-(2'-fluorophenyl)-2-thioxo-2,3-dihydro-1*H*-pyrimidin-4-one (62)

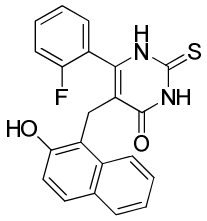

From Method D, **52d** (100 mg) yielded **62** as a white powder after column chromatography (Hexane/EtOAc, 2:1) and recrystallisation from chloroform (12 mg, 0.03 mmol, 10%). Mp 197 °C (decomposes); ν_{max} cm^{-1} (KBr): 3316 and 2935 (OH), 2885 (CH_2), 1630 (C=O), 1558 (NH), 1439 (C-N), 1269 and 1216 (C-F), 1131 (C-O, C=S) 816 and 751 (C-HAr); δ_H (400 MHz, DMSO-d_6) 12.61 (brs, 1H, NH), 12.35 (brs, 1H, NH), 9.27 (s, 1H, OH), 7.63 (d, 1H, *J* = 7.3 Hz, H-5''), 7.53-7.43 (m, 2H, H-4'', H-8''), 7.30-7.22 (m, 2H, H-7'' + 1×ArH), 7.17-7.12 (m, 1H, H-

6"), 7.13-7.05 (m, 1H, ArH), 7.00-6.92 (m, 2H, ArH), 6.82 (d, 1H, *J* = 8.8 Hz, H-3") and 3.90 (s, 2H, CH_2); δ_C (100 MHz, DMSO-d_6) 173.3 (C=S), 161.9 (C=O), 159.9 (C2'), 157.4 (C6), 152.7 (C2"), 132.9 (C8"a), 131.5 (d, *J* = 8.0 Hz, C-F), 130.3 (C4'), 128.0 (C5"), 127.8 (C4"a), 127.4 (C4"), 125.4 (C7"), 123.7 (C5'), 122.6 (C8"), 121.8 (C6"), 121.7 (C1'), 117.7 (C3"), 117.2 (C5) , 115.8 (C3'), 115.1 (C1"a) and 20.5 (C1"); *m/z* (ES^+) 401.10 [$(M+Na)^+$, 100%]; *m/z* (ES^-) 377.14 [$(M-H)^-$, 100%]; HRMS (CI^+) [Found: $(M+H)^+$, 379.0911, $C_{21}H_{16}N_2O_2SF$ requires 379.0919] (-1.5 ppm).

5-[2''-Hydroxynaphthyl-(1'')-methyl]-6-(3'-fluorophenyl)-2-thioxo-2,3-dihydro-1*H*-pyrimidin-4-one (63)

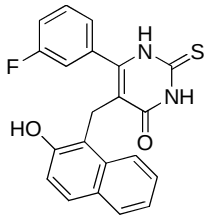

From Method D, **52e** (100 mg) yielded **63** as a white powder after column chromatography (Hexane/EtOAc, 2:1) and recrystallisation from chloroform (12 mg, 0.03 mmol, 10%). Mp 150 °C (decomposes); ν_{max} cm^{-1} (KBr): 3378, 3126, 3059 (OH), 2941 (CH_2), 1630 (C=O), 1554 (NH), 1439 (C-N), 1268 (C-F), 1199 (C=S, CSNH), 1158 and 1119 (C-O, C=S), 821, 792 and 746 (C-HAr); δ_H (400 MHz, DMSO-d_6) 12.58 (brs, 1H, NH), 12.24 (brs, 1H, NH), 9.41 (s, 1H, OH), 7.64 (d, 1H, *J* = 7.5 Hz, H-5"), 7.48-7.45 (m, 2H, H-4", H-8"), 7.30-6.99 (m, 4H, H-7", H-6" + 2 × ArH), 6.93-6.68 (m, 3H, H-3" + 2 × ArH) and 3.92 (s, 2H, CH_2); δ_C (100 MHz, DMSO-d_6) 173.8 (C=S), 162.6 (C3'), 162.1 (C=O), 159.5 (C6), 152.7 (C2"), 134.1 (C1'), 133.0 (C8"a), 129.7 (d, *J* = 8.4 Hz, C-F), 128.1 (C5"), 128.0 (C4"a), 127.5 (C4"), 125.6 (C7"), 124.4 (C6'), 122.8 (C8"), 121.9 (C6"), 117.9 (C3"), 116.3 (C1"a), 116.0 (CH, Ar), 115.7 (C5), 115.4 (CH, Ar) and 20.8 (C1"); HRMS (ES^+) [Found: $(M+Na)^+$, 401.0735, $C_{21}H_{15}N_2O_2SFNa$ requires 401.0736] (-0.2 ppm).

5-[2''-Hydroxynaphthyl-(1'')-methyl]- 6-(3'-chlorophenyl)-2-thioxo-2,3-dihydro-1*H*-pyrimidin-4-one (65)

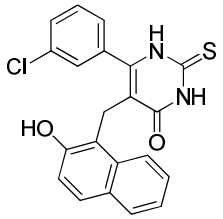

From Method D, **52h** (100 mg) yielded **65** as a white powder after column chromatography (Hexane/EtOAc, 2:1) and recrystallisation from chloroform (37 mg, 0.09 mmol, 32%). Mp 229-232 °C; ν_{max} cm^{-1} (KBr): 3086 (OH), 2941 (CH_2), 2363, 1635 (C=O), 1556 (NH) 1439 (C-N), 1257 and 1213 (C=S, CSNH), 1129 (C-O), 1041 and 1027 (C-O), 819, 750 (C-HAr). δ_H (400 MHz, acetone-d_6) 11.59 (brs, 1H, NH), 11.22 (brs, 1H, NH), 9.25 (s, 1H, OH), 7.68 (d, 1H, *J* = 7.6 Hz, H-5"), 7.57 (d, 1H, *J* = 8.8 Hz, H-4"), 7.53-7.40 (m, 4H, H-8" + 3×ArH), 7.23-7.08 (m, 3H, H-7", H-6" + 1×ArH), 7.00 (d, 1H, *J* = 8.8 Hz, H-3") and 3.92 (s, 2H, H-1"); δ_C (100 MHz, acetone-d_6) 175.0 (C=S), 164.7 (C=O), 154.3 (C2"), 150.6 (C6), 134.7 (C3'), 134.5 (C1'), 133.5 (C8"a), 131.1 (CH, Ar), 131.0 (CH, Ar), 130.0 (C4"a), 129.9 (CH, Ar), 129.3 (C4"), 129.2 (C5"), 128.3 (CH, Ar), 126.6 (C7"), 123.8 (C8"), 123.3 (C6"), 120.1 (C3"), 117.8 (C1"), 116.0 (C5) and 22.1 (C1"); *m/z* (ES^+) 417.10 [$(M+Na)^+$, 100%]; *m/z* (ES^-) 393.12 [$(M-H)^-$, 100%]; HRMS (ES^-) [Found: $(M-H)^-$, 393.0461, $C_{21}H_{14}N_2O_2SCl$ requires 393.0465] (-0.9 ppm).

5-[2''-Hydroxynaphthyl-(1'')-methyl]-6-(4'-chlorophenyl)-2-thioxo-2,3-dihydro-1*H*-pyrimidin-4-one (66)

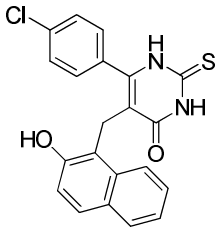

From Method D, **52i** (100 mg) yielded **66** as a white powder after column chromatography (Hexane/EtOAc, 2:1) and recrystallisation from chloroform (21 mg, 0.05 mmol, 18%). Mp 287-289 °C; ν_{max} cm^{-1} (KBr): 3277 and 3030 (OH), 2941 (CH_2), 1702 and 1633 (C=O), 1545 (NH), 1448 (C-N), 1219 and 1204 (C=S, CSNH), 1114, 1127 and 1090 (C=S), 1090 and 1014 (C-O), 837 and 820 (C-HAr); δ_H (400 MHz, DMSO-d_6) 12.57 (brs, 1H, NH), 12.23 (brs, 1H, NH), 9.38 (s, 1H, OH), 7.64 (d, 1H, *J* = 7.5 Hz, H-5"), 7.49-7.41 (m, 2H, H-4", H-8"), 7.30-7.22 (m, 1H, H-7"), 7.21-7.14 (m, 3H, H-6", H-3", H-5"), 7.04 (d, 2H, *J* = 8.3 Hz, AA'BB', H-2', H-6'), 6.85 (d, 1H, *J* = 8.7 Hz, H-3") and 3.91 (s, 2H, H-1"); δ_C (100 MHz, DMSO-d_6) 174.2 (C=S), 160.6 (C=O), 152.7 (C2"), 151.6 (C6), 133.8 (C4'), 133.0 (C8"a), 132.9 (C1'), 130.4 (C3', C5'), 128.4 (C5"), 127.9 (C2', C6'), 127.9 (C4"a), 127.8 (C4"), 125.9 (C7"), 123.1 (C8"), 122.3 (C6"), 118.4 (C3"), 116.8 (C1"a), 115.9 (C5) and 20.9 (C1"); *m/z* (ES^+) 416.97 $[M+Na]^+$ (100%); HRMS (ES^+) [Found: $(M+Na)^+$, 417.0443, $C_{21}H_{15}N_2O_2NaSCl$ requires 417.0440] (+3.1 ppm).

5-[2''-Hydroxynaphthyl-(1'')-methyl]- 6-(3'-bromophenyl)-2-thioxo-2,3-dihydro-1*H*-pyrimidin-4-one (67)

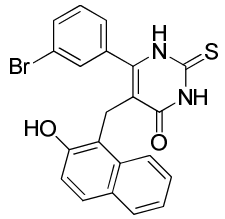

From Method D, **52k** (100 mg) yielded **67** as a white powder after column chromatography (Hexane/EtOAc, 2:1) and recrystallisation from chloroform (29 mg, 0.06 mmol, 26%). Mp 237-239 °C; ν_{max} cm^{-1} (KBr): 3114 and 3081 (OH), 2935 (CH_2), 1713 and 1629 (C=O), 1561 (NH), 1462 and 1439 (C-N), 1199 (C=S, CSNH), 1119 (C-O, C=S), 820, 806 and 746 (C-HAr), 697 (C-Br); δ_H (400 MHz, DMSO-d_6) 12.58 (brs, 1H, NH), 12.21 (brs, 1H, NH), 9.36 (s, 1H, OH), 7.63 (d, 1H, *J* = 7.7 Hz, H-5''), 7.51-7.47 (m, 2H, H-4'', H-8''), 7.40-7.35 (m, 1H, ArH), 7.31-7.25 (m, 1H, H-7''), 7.20-7.15 (m, 1H, H-6''), 7.12-6.99 (m, 3H, ArH), 6.85 (d, 1H, *J* = 8.8 Hz, H-3'') and 3.91 (s, 2H, H-1''); δ_C (100 MHz, acetone-d_6) 175.3 (C=S), 164.7 (C=O), 154.3 (C2''), 150.5 (C6), 134.8 (C1'), 134.3 (C8''a), 134.0 (CH, Ar), 132.7 (CH, Ar), 131.2 (CH, Ar), 130.0 (C4''a), 129.3 (CAr), 129.2 (C4''), 128.8 (C5''), 126.6 (C7''), 123.8 (C8''), 123.3 (C6''), 122.7 (C3'), 120.3 (C3''), 117.9 (C1''a), 116.0 (C5) and 22.2 (C1''); *m/z* (ES^-) 436.99 $[M-H]^-$ (100%), 439.00 $[M-H]^-$ (100%); HRMS (ES^-) [Found: $(M-H)^-$, 436.9966, $C_{21}H_{14}N_2O_2S^{79}Br$ requires 436.9959] (+1.5 ppm), [Found: $(M-H)^-$, 438.9948, $C_{21}H_{14}N_2O_2S^{81}Br$ requires 438.9939] (+2.1 ppm).

5-[2''-Hydroxynaphthyl-(1'')-methyl]-6-(4'-bromophenyl)-thioxo-2,3-dihydro-1*H* pyrimidin-4-one (46)

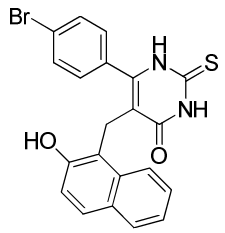

From Method D, **52c** (100 mg) yielded **46** as a white powder after column chromatography (Hexane/EtOAc, 2:1) and recrystallisation from ethanol (34 mg, 0.07 mmol, 30%). Mp 282-287 °C; ν_{max} cm^{-1} (NaCl): 3413 (OH), 1699 and 1634 (C=O), 1547 (NH), 1445 (C-N), 1189 (C=S, CSNH), 1158, 1124 and 1112 (C-O and C=S), 1070 (C-O), 971, 827 and 742 (C-HAr), 668 (C-Br); δ_H (400 MHz, DMSO-d_6) 12.56 (brs, 1H, NH), 12.22 (brs, 1H, NH), 9.42 (s, 1H, OH), 7.71 (d, 1H, *J* = 7.5 Hz, H-5''), 7.47 (d, 1H, *J* = 8.8 Hz, H-4''), 7.44 (d, 1H, *J* = 8.7 Hz, H-8''), 7.32 (d, 2H, AA'BB', *J* = 8.4 Hz, H-2', H-6'), 7.30-7.22 (m, 1H, H-7''), 7.20-7.14 (m, 1H, H-

6"), 6.98 (d, 2H, AA'BB', *J* = 8.4 Hz, H-3', H-5'), 6.87 (d, 1H, *J* = 8.7 Hz, H-3") and 3.91 (s, 2H, H-1"); δ_C (100 MHz, DMSO-d_6) 173.8 (C=S), 161.9 (C=O), 152.6 (C2"), 148.8 (C6), 132.9 (C1'), 130.6 (C8"a), 130.4 (C3', C5'), 130.1 (C2', C6), 128.0 (C5"), 127.9 (C4"a), 127.4 (C4"), 125.5 (C7"), 122.7 (C6"), 121.8 (C8"), 117.9 (C3"), 116.3 (C1"a), 115.7 (C5) and 20.9 (C1"); *m/z* (ES^+) 462.96 $[M+Na]^+$ (100%); *m/z* (ES^-) 436.93 $[M-H]^-$ (100%); HRMS (ES^-) [Found: $(M-H)^-$, 438.9946, $C_{21}H_{12}N_2O_2S^{79}Br$ requires 436.9945] (+0.1 ppm), [Found: $(M-H)^-$, 436.9970, $C_{21}H_{12}N_2O_2S^{81}Br$ requires 436.9960] (+0.2 ppm).

5-[2''-Hydroxynaphthyl-(1'')-methyl]-6-(4'-iodophenyl)-2-thioxo-2,3-dihydropyrimidin-1*H*-4-one (69)

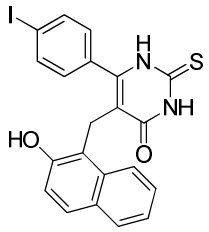

From Method D, **52n** (100 mg) yielded **69** as a white powder after column chromatography (Hexane/EtOAc, 2:1) and recrystallisation from chloroform (24 mg, 0.05 mmol, 22%). Mp > 250 °C (decomposes); ν_{max} cm^{-1} (KBr): 3090 (OH), 1628 (C=O), 1560 (NH), 1427 (C-N), 1208 (C=S, CSNH), 1154 and 1126 (C-O, C=S), 1008 (C-O), 850, 814 and 754 (C-HAr); δ_H (400 MHz, DMSO-d_6) 12.55 (brs, 1H, NH), 12.21 (brs, 1H, NH), 9.38 (s, 1H, OH), 7.64 (d, 1H, *J* = 8.4 Hz, H-5"), 7.52-7.39 (m, 4H, H-4", H-8", H-2', H-6'), 7.28-7.15 (m, 2H, H-7", H-6"), 6.86-6.83 (m, 3H, H-3", H-3', H-5'), 3.88 (s, 2H, H-1"); *m/z* (ES^+) 508.02 $[M+Na]^+$ (100%).

5-[2''-Hydroxynaphthyl-(1'')-methyl]- 6-(4'-trifluoromethylphenyl)-2-thioxo-2,3-dihydro-1*H*-pyrimidin-4-one (71)

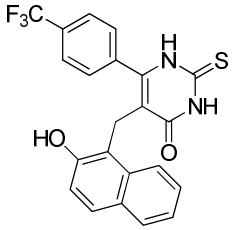

From Method D, **52q** (100 mg) yielded **71** as a white powder after column chromatography (Hexane/EtOAc, 2:1) and recrystallisation from chloroform (28 mg, 0.06 mmol, 25%). Mp > 250 °C (decomposes); ν_{max} cm^{-1} (KBr): 2970 (OH), 2912 (CH_2), 1691, 1549 and 1428 (C-N), 1635 (C=O), 1515 (CSNH), 1409 (OH), 1321, 1286 and 1167 (C-F), 1131 and 1112 (C=S), 1065 and 1017 (C-O), 860 and 702 (C-H), 821, 778 and 743 (C-HAr); δ_H (400 MHz, DMSO-d_6)

12.67 (brs, 1H, NH), 12.28 (brs, 1H, NH), 9.40 (brs, 1H, OH), 7.65 (d, 1H, *J* = 8.3 Hz, H-5''), 7.52-7.35 (m, 4H, H-4'', H-8'', H-2', H-6'), 7.17 (m, 1H, H-7''), 7.17-7.12 (m, 3H, H-6'', H-3', H-5'), 6.80 (d, 1H, *J* = 8.8 Hz, H-3'') and 3.95 (s, 2H, H-1''); δ_C (100 MHz, DMSO-d_6) 173.9 (C=S), 161.9 (C=O), 152.2 (C2''), 148.8 (C6), 135.3 (C1'), 132.9 (C8''a), 129.3 (C4'), 129.0 (q, *J* = 26.8 Hz, CF_3), 128.8 (C3', C5'), 128.0 (C4''), 127.9 (C5''), 127.8 (C4''a), 125.6 (C7''), 124.1 (C2', C6'), 122.6 (C6''), 121.9 (C8''), 117.6 (C3''), 116.2 (C1''a), 116.0 (C5) and 20.5 (C1''); *m/z* (ES^+) 451.05 $[M+Na]^+$ (100%).

5-[2''-Hydroxynaphthyl-(1'')-methyl]-6-(2'-methylphenyl)-2-thioxo-2,3-dihydro-1*H*-pyrimidin-4-one (74)

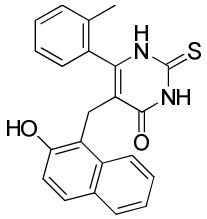

From Method D, **52u** (100 mg) yielded **74** as a white powder after column chromatography (Hexane/EtOAc, 2:1) and recrystallisation from chloroform (67 mg, 0.18 mmol, 57%). Mp 170-172 °C; ν_{max} cm^{-1} (KBr): 2988 (OH), 2902 (CH_3, CH_2), 1627 (C=O), 1554 (NH), 1453 (CSNH), 1394 and 1255 (OH), 1211 (C=S), 1075 and 1057 (C-O), 819, 808 and 744 (C-HAr), 729 (C-H); δ_H (400 MHz, DMSO-d_6) 12.60 (brs, 1H, NH), 12.17 (brs, 1H, NH), 9.21 (brs, 1H, OH), 7.63 (d, 1H, *J* = 8.1 Hz, H-5''), 7.43 (d, 1H, *J* = 8.8 Hz, H-4''), 7.39 (d, 1H, *J* = 7.4 Hz, H-8''), 7.26-7.08 (m, 3H, H-6'', H-7'' + 1×ArH), 7.03-6.99 (m, 2H, ArH), 6.90 (d, 1H, *J* = 7.1 Hz, ArH), 6.78 (d, 1H, *J* = 8.8 Hz, H-3''), 3.88 (s, 2H, H-1'') and 1.62 (s, 3H, CH_3); δ_C (100 MHz, DMSO-d_6) 173.3 (C=S), 162.4 (C=O), 152.6 (C2''), 150.0 (C6), 135.6 (C2'), 132.9 (C1'), 131.0 (C8''a), 129.2 (CH, Ar), 129.0 (CH, Ar), 128.4 (C5''), 128.0 (C4''), 127.8 (C4''a), 127.2 (CH, Ar), 125.4 (C7''), 125.1 (CH, Ar), 122.6 (C8''), 121.8 (C6''), 117.8 (C3''), 116.0 (C5), 115.9 (C1''a), 20.1 (C1'') and 18.36 (CH_3); *m/z* (ES^+) 397.12 $[M+Na]^+$ (100%); HRMS (ES^+) [Found: $(M+Na)^+$, 397.0987, $C_{20}H_{18}N_2O_2SNa$ requires 397.0987] (+0.1 ppm).

5-[2''-Hydroxynaphthyl-(1'')-methyl]-6-(3'-methylphenyl)-2-thioxo-2,3-dihydro-1*H*-pyrimidin-4-one (75)

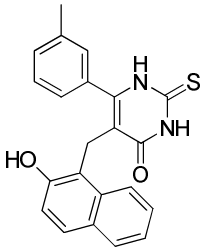

From Method D, **52v** (100 mg) yielded **75** as a white powder after column chromatography (Hexane/EtOAc, 2:1) and recrystallisation from chloroform (60 mg, 0.16 mmol, 51%). Mp 235-237 °C; ν_{max} cm^{-1} (KBr): 3767 and 2988 (OH), 2902 (CH_3, CH_2), 1646 (C=O), 1563 (NH), 1465 (CSNH), 1403, 1394 and 1233 (OH), 1211, 1198 and 1128 (C=S), 1066, 1044 and 1017 (C-O), 993 (C-H), 823 and 747 (C-HAr); δ_H (400 MHz, DMSO-d_6) 12.55 (brs, 1H, NH), 12.22 (brs, 1H, NH), 9.41 (brs, 1H, OH), 7.65 (d, 1H, *J* = 7.9 Hz, H-5''), 7.47 (d, 1H, *J* = 8.8 Hz, H-4''), 7.36 (d, 1H, *J* = 8.5 Hz, H-8''), 7.26-7.09 (m, 4H, H-7'', H-6'' + 2×ArH), 7.00-6.96 (m, 1H, ArH), 6.93-6.85 (m, 2H, H-3'' + 1×ArH), 3.91 (s, 2H, CH_2) and 2.18 (s, 3H, CH_3); δ_C (100 MHz, DMSO-d_6) 173.8 (C=S), 162.4 (C=O), 152.7 (C2''), 150.9 (C6), 136.9 (C3'), 133.0 (C8''a), 131.5 (C1'), 129.9 (C2'), 128.9 (CH, Ar), 128.3 (C4''a), 128.0 (C4''), 127.6 (C5''), 127.4 (CH, Ar), 126.2 (CH, Ar), 125.4 (C7''), 122.7 (C8''), 121.8 (C6''), 118.2 (C3''), 116.5 (C1''a), 115.0 (C5), 21.3 (C1'') and 20.2 (CH_3); *m/z* (ES^+) 397.10 $[M+Na]^+$ (100%); HRMS (ES^+) [Found: $(M+Na)^+$, 397.0988, $C_{20}H_{18}N_2O_2SNa$ requires 397.0987] (+0.1 ppm).

5-[2''-Hydroxynaphthyl-(1'')-methyl]-6-(4'-methylphenyl)-2-thioxo-2,3-dihydro-1*H*-pyrimidin-4-one (76)

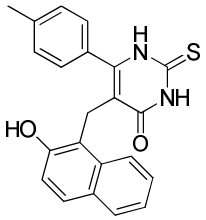

From Method D, **52w** (100 mg) yielded **76** as a white powder after column chromatography (Hexane/EtOAc, 2:1) and recrystallisation from chloroform (59 mg, 0.15 mmol, 50%). Mp 220-221 °C; ν_{max} cm^{-1} (KBr): 3663 and 2988 (OH), 2902 (CH_3, CH_2), 1630 (C=O), 1540 (NH), 1515 (CSNH), 1445 (C-N), 1405, 1349 and 1250 (OH), 1226 and 1208 (C=S), 1066 and 1028 (C-O), 818, 744 and 729 (C-HAr); δ_H (300 MHz, DMSO-d_6) 12.52 (brs, 1H, NH), 12.26 (brs, 1H, NH), 9.46 (brs, 1H, OH), 7.65 (d, 1H, *J* = 7.4 Hz, H-5''), 7.50 (d, 1H, *J* = 8.7 Hz, H-4''), 7.35 (d, 1H, ^3J = 7.7 Hz, H-8''), 7.22-7.08 (m, 6H, H-7'', H-6'', H-2', H-3', H-5', H-6'), 6.92 (d,

1H, *J* = 8.7 Hz, H-3"), 3.89 (s, 2H, H-1") and 2.29 (s, 3H, CH_3); δ_C (100 MHz, DMSO-d_6) 173.8 (C=S), 162.2 (C=O), 152.7 (C2"), 150.1 (C6), 139.1 (C4'), 133.0 (C8"a), 128.7 (C4"a), 128.5 (CH, Ar), 128.4 (CH, Ar), 128.0 (C5"), 127.4 (C4"), 125.7 (C7"), 122.8 (C8"), 121.8 (C6"), 118.4 (C3") 116.5 (C1"a), 115.1 (C5), 21.1 (C1") and 20.9 (CH_3); *m/z* (ES^+) 397.09 $[M+Na]^+$ (100%); HRMS (ES^+) [Found: $(M+Na)^+$, 397.0989, $C_{20}H_{18}N_2O_2SNa$ requires 397.0987] (+0.1 ppm).

6.2.5 Preparation of Analogue 81 (METHOD E)

To a stirring solution of thiourea **53** (15.6 eq.) in 2M NaOEt (10 mL) was added **52j'** (1 eq.) and the reaction was stirred at reflux for 18 h. After cooling the reaction mixture to room temperature, the solvent was removed at reduced pressure, the crude residue dissolved in water and the solution acidified with 2M HCl until a white solid had formed. The precipitate was collected by filtration and purified by flash column chromatography (Hexane/EtOAc, 2:1).

5-[2''-Hydroxynaphthyl-(1'')-methyl]-6-(2'-bromophenyl)-2-thioxo-2,3-dihydro-1*H*-pyrimidin-4-one (81)

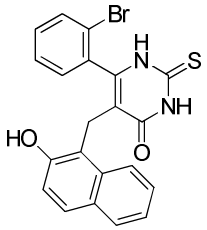

From Method E, **52j'** (150 mg) yielded **81** as a white powder after column chromatography (Hexane/EtOAc, 2:1) and recrystallisation from chloroform (34 mg, 0.07 mmol, 20%). Mp 224-226 °C; ν_{max} cm^{-1} (KBr): 3055 (OH), 2927 (CH_2), 1627 (C=O), 1548 (N-H), 1436 (C-N), 1196 (C=S, CSNH), 1132 and 1117 (C-O, C=S), 1027 (C-O), 813 and 740 (C-H_{Ar}), 678 (C-Br); δ_H (300 MHz, acetone-d_6) 11.61 (brs, 1H, NH), 11.23 (brs, 1H, NH), 8.93 (brs, 1H, OH), 7.74-7.60 (m, 1H, H-5'), 7.61-7.52 (m, 2H, H-4", H-8"), 7.38-7.11 (m, 6H, H-6", H-7" + 4 × ArH), 6.88 (d, 1H, *J* = 8.8 Hz, H-3"), 4.13 (d, 1H, AB, *J* = 15.6 Hz, H-1") and 3.98 (d, 1H, AB, *J* = 15.6 Hz, H-1"); δ_C (100 MHz, DMSO-d_6) 175.3 (C=S), 164.5 (C=O), 154.6 (C2"), 150.6 (C6), 134.4 (C1'), 133.4 (C8"a), 133.6 (CH, Ar), 131.9 (CH, Ar), 132.5, (CH, Ar), 129.9 (C4"a), 129.1 (C4"), 129.0 (CH, Ar), 128.3 (C5"), 126.7 (C7"), 123.6 (C8"), 123.3 (C2'), 123.1 (C6"), 119.7 (C3"), 117.0 (C1"a), 117.0 (C5) and 21.4 (C1"); *m/z* (ES^+) 460.92 $[M+Na]^+$ (100%); *m/z* (ES^-) 437.01 $[M-H]^-$ (100%); HRMS (ES^+) [Found: $(M+Na)^+$, 460.9941,

$C_{21}H_{15}N_2O_2SNa^{79}Br$ requires 460.9935] (+1.3 ppm), [Found: $(M+Na)^+$, 462.9903, $C_{21}H_{15}N_2O_2SNa^{81}Br$ requires 462.9915] (-2.6 ppm).

6.2.6 Synthesis of Analogues 82-83-85 and 87 (METHOD F)

To a stirring solution of the desired *N*-substituted thiourea (15.6 eq.) in 2M NaOEt (10 mL) was added **52a** (500 mg, 1 eq.) in one portion and the reaction mixture stirred at reflux for 18 h. After cooling to room temperature, the solvent was removed at reduced pressure. The resulting residue was dissolved in the minimum amount of distilled water and acidified with 2M HCl until pH 2. The aqueous layer was extracted with DCM (3 × 50 mL), the combined organic layers dried ($MgSO_4$) and the solvent removed at reduced pressure. The products were purified by flash column chromatography (Hexane/EtOAc) and recrystallised from ethanol.

1-Ethyl -5-[2''-hydroxynaphthyl-(1'')-methyl]-6-phenyl-2-thioxo-2,3-dihydro-1*H*-pyrimidin-4-one (82)

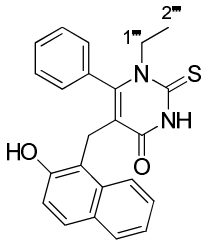

From Method F, **52a** (500 mg) yielded **82** as a white powder after column chromatography (Hexane/EtOAc, 80:20) and recrystallisation from ethanol (128 mg, 0.33 mmol, 20%). Mp 256-258 °C ν_{max} cm^{-1} (KBr): 3676, 2988 and 2972 (OH), 2902 (CH_2, CH_3), 1633 (C=O), 1437 (C-N), 1394 and 1241 (OH), 1217 and 1103 (C=S), 1076, 1057 and 1028 (C-O), 812, 767 and 741 (C-HAr); δ_H (400 MHz, DMSO-d_6) 12.75 (brs, 1H, NH), 9.20 (brs, 1H, OH), 7.65 (d, 1H, *J* = 7.1 Hz, H-5''), 7.51-7.45 (m, 2H, H-4'', H-8''), 7.27-7.17 (m, 5H, H-6'', H-7'', H-3', H-4', H-5'), 6.98 (d, 2H, *J* = 7.1 Hz, H-2', H-6'), 6.84 (d, 1H, *J* = 8.6 Hz, H-3''), 3.86 (brs, 2H, H-1'''), 3.77 (s, 2H, H-1'') and 0.92 (t, 3H, *J* = 7.0 Hz, H-2'''); δ_C (100 MHz, DMSO-d_6) 175.5 (C=S), 161.4 (C=O), 153.6 (C2''), 152.6 (C6), 132.7 (C8''a), 131.6 (C1'), 129.1 (C4'), 128.9 (C3', C5'), 128.9 (C4''a), 128.3 (C2', C6'), 127.9 (C5''), 127.2 (C4''), 126.5 (C7''), 123.6 (C8''), 122.8 (C6''), 118.9 (C3''), 117.2 (C1''a), 116.1 (C5), 46.9 (C1'''), 23.0 (C1'') and 13.7 (C2'''); *m/z* (ES^+) 411.33 $[M+Na]^+$ (100%); *m/z* (ES^-) 387.16 $[M-H]^-$ (100%); HRMS (ES^+) [Found: $(M+Na)^+$, 411.1149, $C_{23}H_{20}N_2O_2SNa$ requires 411.1143] (+1.3 ppm).

1-Allyl-5-[2''-hydroxynaphthyl-(1'')-methyl]-6-phenyl-2-thioxo-2,3-dihydro-1*H*-pyrimidin-4-one (87)

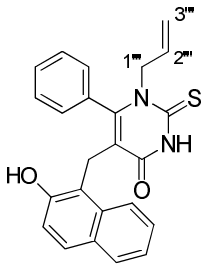

From Method F, **52a** (500 mg) yielded **87** as a white powder after column chromatography (Hexane/EtOAc, 80:20) and recrystallisation from ethanol (99 mg, 0.24 mmol, 15%). Mp 175-177 °C; ν_{max} cm^{-1} (KBr): 3676 and 2988 (OH), 2902 (CH_2), 1626 (C=O), 1479 (CSNH), 1406, 1394 and 1242 (OH), 1075, 1057 and 1028 (C-O), 892, 823 and 747 (C-HAr), 701 (C-H); δ_H (400 MHz, DMSO-d_6) 12.82 (brs, 1H, NH), 9.22 (brs, 1H, OH), 7.65 (d, 1H, *J* = 7.1 Hz, H-5''), 7.52-7.43 (m, 2H, H-4'', H-8''), 7.28-7.18 (m, 5H, H-6'', H-7'', H-3', H-4', H-5'), 6.93 (d, 2H, *J* = 7.0 Hz, H-2', H-6'), 6.85 (d, 1H, *J* = 8.8 Hz, H-3''), 5.61-5.50 (m, 1H, H-2'''), 4.98 (dd, 1H, ^3J = 10.5 Hz, ^4J = 1.2 Hz, H-3'''), 4.64 (dd, 1H, ^3J = 17.3 Hz, ^4J = 1.2 Hz, H-3'''), 4.50 (m, 2H, H-1''') and 3.78 (s, 2H, H-1''); δ_C (100 MHz, DMSO-d_6) 174.8 (C=S), 160.7 (C=O), 152.7 (C2''), 151.7 (C6), 133.0 (C8''a), 131.9 (C2'''), 131.4 (C1'), 128.9 (C3', C5'), 128.4 (C2', C6'), 128.1 (C5''), 128.0 (C4'), 127.8 (C4''a), 127.2 (C4''), 125.5 (C7''), 122.5 (C8''), 121.7 (C6''), 117.8 (C3''), 117.1 (C3'''), 116.5 (C1''a), 116.1 (C5), 52.5 (C1''') and 22.19 (C1''); *m/z* (ES^+) 423.12 $[M+Na]^+$ (100%); HRMS (ES^+) [Found: $(M+Na)^+$, 423.1142, $C_{24}H_{20}N_2O_2SNa$ requires 423.1143] (-0.3 ppm).

1-Propyl-5-[2''-hydroxynaphthyl-(1'')-methyl]-6-phenyl-2-thioxo-2,3-dihydro-1*H*-pyrimidin-4-one (83)

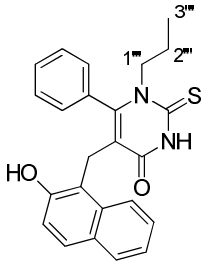

From Method F, **52a** (500 mg) yielded **83** as a white powder after column chromatography (Hexane/EtOAc, 80:20) and recrystallisation from ethanol (66 mg, 0.16 mmol, 10%). Mp 227-229 °C; ν_{max} cm^{-1} (KBr): 3676 and 2988 (OH), 2969 and 2902 (CH_3, CH_2), 1630 (C=O), 1482 (CSNH), 1432 (C-N), 1206, 1131 and 1108 (C=S), 1075, 1066 and 1057 (C-O), 880, 820 and 767 (C-HAr), 745, 701 and 666 (C-H); δ_H (400 MHz, DMSO-d_6) 12.77 (brs, 1H, NH), 9.21 (s,

1H, OH), 7.65 (d, 1H, *J* = 8.8 Hz, H-5''), 7.55-7.45 (m, 2H, H-4'', H-8''), 7.29-7.12 (m, 5H, H-6'', H-7'', H-3', H-4', H-5'), 6.97 (d, 2H, *J* = 7.0 Hz, H-2', H-6'), 6.84 (d, 1H, *J* = 8.8 Hz, H-3''), 3.78 (s, 2H, H-1''), 3.69 (br, 2H, H-1'''), 1.41 (m, 2H, H-2''') and 0.43 (t, 3H, *J* = 7.4 Hz, H-3'''); δ_C (100 MHz, DMSO-d_6) 174.8 (C=S), 160.4 (C=O), 152.7 (C2''), 151.7 (C6), 133.1 (C8''a), 131.7 (C1'), 129.3 (C4'), 128.9 (C5', C3'), 128.6 (C2', C6'), 128.1 (C5''), 128.0 (C4''), 127.8 (C4''a), 125.6 (C7''), 122.6 (C8''), 121.8 (C6''), 119.0 (C1''a), 117.9 (C3''), 116.2 (C5), 52.1 (C1'''), 22.1 (C1''), 20.3 (C2''') and 10.5 (C3'''); HRMS (ES^+) [Found: $(M+Na)^+$, 425.1307, $C_{24}H_{22}N_2O_2SNa$ requires 425.1307] (+0.2 ppm).

1-Butyl-5-[2''-hydroxynaphthyl-(1'')-methyl]-6-phenyl-2-thioxo-2,3-dihydro-1*H*-pyrimidin-4-one (85)

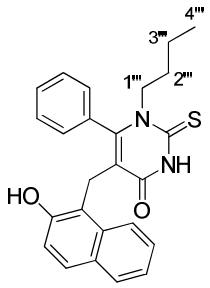

From Method F, **52a** (500 mg) yielded **85** as a white powder after column chromatography (Hexane/EtOAc, 90:10) and recrystallisation from ethanol (48 mg, 0.01 mmol, 7%). Mp 201-203 °C; ν_{max} cm^{-1} (KBr): 3667 and 3213 (OH), 2972 and 2902 (CH_3, CH_2), 1645 (C=O), 1487 (CSNH), 1428 (C-N), 1394 and 1233 (OH), 1204, 1179, 1129 and 1104 (C=S), 1067 and 1057 (C-O), 823 and 747, (C-HAr), 705 and 756 (C-H); δ_H (400 MHz, DMSO-d_6) 12.75 (s, 1H, NH), 9.20 (s, 1H, OH), 7.65 (d, 1H, *J* = 8.2 Hz, H-5''), 7.51-7.45 (m, 2H, H-8'', H-4''), 7.24-7.14 (m, 5H, H-7'', H-6'', H-3', H-4', H-5'), 6.98 (d, 2H , *J* = 7.0 Hz, H-2', H-6'), 6.84 (d, 1H , *J* = 8.7 Hz, H-3''), 3.79 (s, 4H, H-1'', H-1'''), 1.40 (brs, 2H, H-2'''), 0.90-0.80 (m, 2H, H-3''') and 0.50 (t, 3H, *J* = 7.3 Hz, H-4'''); δ_C (100 MHz, DMSO-d_6) 174.6 (C=S), 160.4 (C=O), 152.7 (C2''), 151.7 (C6), 133.1 (C8''a), 131.6 (C1'), 128.9 (C3', C5'), 128.1 (C2', C6'), 128.0 (C4'), 128.0 (C5''), 127.9 (C4''a), 127.6 (C4''), 125.6 (C7''), 122.6 (C8''), 121.8 (C6''), 119.1 (C3''), 117.9 (C1''a), 116.2 (C5), 50.3 (C1'''), 28.6 (C2'''), 22.0 (C1''), 18.9 (C3'''), 12.9 (C4'''); *m/z* (ES^+) 439.05 $[M+Na]^+$ (100%); *m/z* (ES^-) 415.16 $[M-H]^-$ (100%); HRMS (ES^+) [Found: $(M+Na)^+$, 439.1473, $C_{25}H_{24}N_2O_2SNa$ requires 439.1456] (+3.8 ppm).

6.3 Part II: Novel Cambinol Analogues Substituted at *N*-3 and Sulfur

6.3.1 Chemistry

2-(Allylthio)-5-[2''-hydroxynaphthyl-(1'')-methyl]-6-phenyl-pyrimidin-4-(1*H*)-one (97)

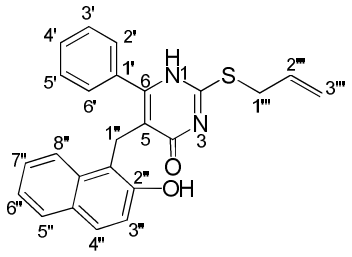

To a stirring solution of cambinol **39** (492 mg, 1.36 mmol, 1 eq.) and sodium methoxide (263 mg, 4.37 mmol, 3.3 eq.) in methanol (30 mL) was added allyl bromide (0.153 mL, 1.76 mmol, 1.3 eq.). The resulting suspension was stirred at room temperature for 24 h. After addition of water (30 mL) the product **97** was obtained as a white precipitate, which was filtered and dried (462 mg, 1.15 mmol, 85 %). Mp 153-155 °C; ν_{max} cm^{-1} (KBr): 3324 (CONH), 3079 (OH), 1628 (C=O); δ_H (300 MHz, $CDCl_3$) 12.49 (brs, 1H, NH), 9.75 (brs, 1H, OH), 7.79-7.75 (m, 2H, H-4", H-5"), 7.67-7.57 (m, 5H, H-2', H-6', H-3', H-5', H-4'), 7.20-7.16 (m, 2H, H-8", H-3"), 6.96 (dt, 1H, ^2J = 7.6 Hz, ^3J = 1.3 Hz, H-7"), 6.77 (d, 1H, J = 8.6 Hz, H-6"), 6.00-5.86 (m, 1H, H-2'"), 5.32 (dd, 1H, ^2J = 17.1 Hz, ^3J = 1.3 Hz, H-3'"), 5.17 (dd, 1H, ^2J = 10.1 Hz, ^3J = 1.3 Hz, H-3'"), 4.38 (s, 2H, H-1") and 3.88 (d, 2H, J = 7.0 Hz, 2H, H-1'"); δ_C (75.5 MHz, $CDCl_3$) 167.7 (C=O), 163.4 (C6), 157.1 (C2), 153.7 (C2"), 138.8 (C1'), 133.8 (C8"a), 132.7 (C2'"), 130.5 (C4'), 130.1 (C2', C6'), 129.8 (C4"a), 129.1 (C5"), 129.0 (C3', C5'), 128.8 (C4"), 126.0 (C7"), 123.7 (C6"), 123.0 (C8"), 121.6 (C3"), 119.5 (C3'"), 119.2 (C5), 118.8 (C1"a), 34.0 (C1'") and 23.6 (C1"); *m/z* (ES^+) 422.87 [$(M+Na)^+$, 100%]; HRMS (ES^+) [Found: $(M+Na)^+$, 423.1129, $C_{24}H_{20}N_2O_2SNa$ requires 423.1143] (-3.4 ppm).

2-(Allylthio)-3-allyl-5-[2''-hydroxynaphthyl-(1'')-methyl]-6-phenyl-pyrimidin-4-(3*H*)-one (99)

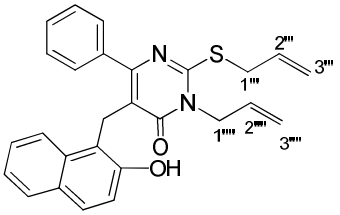

Obtained as a side product during the synthesis of **97** (71 mg, 0.16 mmol, 12%)Mp 135-138 °C; ν_{max} cm^{-1} (KBr): 3057 (OH), 1627 (C=O); δ_H (300 MHz, $CDCl_3$) 10.37 (br, 1H, OH), 7.78-7.74

(m, 2H, H-4'', H-5''), 7.66-7.58 (m, 5H, H-2', H-3', H-4', H-5', H-6'), 7.24 (m, 1H, H-3''), 7.14 (m, 1H, H-8''), 6.95 (m, 1H, H-7''), 6.77 (m, 1H, H-6''), 5.93-5.82 (m, 2H, H-2''', H-2''''), 5.38-5.28 (m, 3H, H-3''' + H-3''''×2), 5.15 (dd, 1H, ^2J = 10.0 Hz, ^3J = 1.3 Hz, H-3'''), 4.67 (dd, 2H, ^2J = 5.8, ^3J = 1.3 Hz, H-1''''), 4.38 (s, 2H, H-1''), 3.83 (dd, 2H, ^2J = 7.0 Hz, ^3J = 1.0 Hz, H-1''') ; δ_C (75.5 MHz, $CDCl_3$) 165.4 (C=O), 159.7 (C6), 157.5 (C2), 153.6 (C2''), 138.6 (C1'), 133.5 (C8''a), 132.1 (C2'''), 129.9 (C2''''), 129.7 (CH, Ar), 129.6 (CH, Ar), 129.3 (C4''a), 128.7 (CH, Ar), 128.6 (CH, Ar), 128.4 (C4''), 125.5 (C7''), 123.3 (C8''), 122.4 (C6''), 121.2 (C3''), 119.7 (C3''''), 119.3 (C3'''), 118.4 (C5), 118.4 (C1''a), 47.4 (C1''''), 35.0 (C1'''), 23.8 (C1''); HRMS (ES^+) [Found: $(M+Na)^+$, 463.1460, $C_{27}H_{24}N_2O_2SNa$ requires 463.1456] (+0.4 ppm).

2-(Allylthio)-5-[2''-hydroxynaphthyl-(1'')-methyl]-3-methyl-6-phenyl-pyrimidin-4-(3*H*)-one (100)

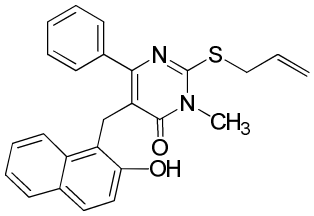

To a stirring solution of **97** (100 mg, 0.25 mmol, 1 eq.) in ethanol (3 mL) were added 30% aqueous NaOH (110 µL) and Me_2SO_4 (94 µL, 1.00 mmol, 4 eq.). The reaction mixture was stirred for 2 days at rt. After this time, water (3 mL) was added and the product isolated as a white microcrystalline powder after filtration (50 mg, 0.12 mmol, 48%). Mp 164-166 °C; ν_{max} cm^{-1} (KBr): 3419 (OH), 3056 (OH), 1626 (C=O), 1513 (NH), 1412 (CSNH), 1225 (C=S), 1081 (C=S); δ_H (300 MHz, $CDCl_3$) 10.35 (s, 1H, OH), 7.74-7.65 (m, 2H, H-4'', H-5''), 7.63-7.49 (m, 5H, H-2', H-3', H-4', H-5', H-6'), 7.17 (d, 1H, J = 8.9 Hz, H-8''), 7.12-7.03 (m, 1H, H-3''), 6.93-6.84 (m, 1H, H-7''), 6.72 (d, 1H, J = 8.6 Hz, H-6''), 5.92-5.73 (m, 1H, H-2'''), 5.22 (dd, 1H, ^2J = 17.0 Hz, ^3J = 1.0 Hz, H-3'''), 5.09 (d, 1H, J = 10.1 Hz, H-3'''), 4.32 (s, 2H, H-1''), 3.78 (d, 2H, J = 7.0 Hz, H-1''') and 3.48 (s, 3H, NCH_3); δ_C (75.5 MHz, $CDCl_3$) 165.7 (C=O), 159.7 (C2), 157.9 (C6), 153.7 (C2''), 138.7 (C1'), 133.5 (C8''a), 132.1 (CH, Ar), 131.1 (C2'''), 129.9 (CH, Ar), 129.7 (CH, Ar), 129.4 (C4''a), 128.7 (CH, Ar), 128.7 (CH, Ar), 128.5 (CH, Ar), 125.6 (C7''), 123.4 (C6''), 122.5 (C8''), 121.3 (C3''), 119.4 (C3'''), 118.5 (C1''a), 118.0 (C5), 34.9 (C1'''), 31.2 (CH_3), and 23.9 (C1''); *m/z* (ES^+) 436.79 [$(M+Na)^+$, 100%]; HRMS (ES^+) [Found: $(M+Na)^+$, 437.1304, $C_{25}H_{22}N_2O_2SNa$ requires 437.1300] (+0.9 ppm).

2-(Benzylthio)-5-[2''-hydroxynaphthyl-(1'')-methyl]-6-phenyl-pyrimidin-4-(1*H*)-one (98)

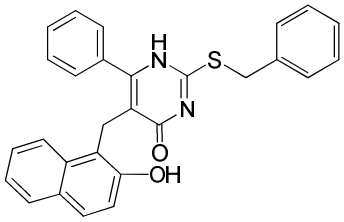

To a suspension of cambinol **39** (50 mg, 0.11 mmol, 1 eq.) and NaOMe (25 mg, 0.46 mmol, 1.1 eq.) in methanol (1.5 mL) was added benzyl bromide (21 µL, 0.18 mmol, 1.3 eq.) and the resulting mixture stirred for at rt for 12 h (a white precipitate formed after 1 h). After addition of water (2 mL) the product was isolated as a white solid after filtration (37 mg, 0.08 mmol, 75%). Mp 229-231 °C; ν_{max} cm^{-1} (KBr): 3053 (OH), 1617 (C=O), 1402, 1295 (C=S), 1231 (C=S); δ_H (400 MHz, DMSO-d_6) 10.31 (brs, 1H, NH), 9.90 (brs, 1H, OH), 7.78-7.69 (m, 2H, H-4", H-5"), 7.65-7.58 (m, 4H, ArH), 7.56 (d, 1H, J = 8.9 Hz, ArH), 7.37-7.22 (m, 5H, H-2"', H-3"', H-4"', H-5"', H-6"'), 7.17-7.09 (m, 2H, H-3", H-8"), 6.93 (t, 1H, J = 6.7 Hz, H-7"), 6.72 (d, 1H, J = 8.5 Hz, H-6"), 4.41 (s, 2H, H-1"') and 4.34 (s, 2H, H-1"); δ_C (100 MHz, DMSO-d_6) 165.0 (C=O), 156.9 (C2), 159.0 (C6), 153.3 (C2"), 138.5 (C1"'a), 137.0 (C1'), 133.1 (C8"a), 129.3 (C4"a), 129.0 (CH, Ar), 128.9 (CH, Ar), 128.3 (CH, Ar × 2), 128.1 (CH, Ar), 128.0 (CH, Ar), 127.7 (CH, Ar), 127.2 (CH, Ar), 125.4 (C7"), 122.8 (C6"), 122.0 (C8"), 119.7 (C3"), 119.3 (C1"a), 117.3 (C5), 33.6 (C1"'), 22.7 (C1"); *m/z* (ES^+) 472.72 [$(M+Na)^+$, 100%], *m/z* (ES^-) 448.84 [$(M-H)^-$, 100%]; HRMS (ES^-) [Found: $(M-H)^-$, 449.1322, $C_{28}H_{21}N_2O_2S$ requires 449.1324] (-0.5 ppm).

2-(Benzylthio)-5-[2''-hydroxynaphthyl-(1'')-methyl]-3-methyl-6-phenyl-pyrimidin-4-(3*H*)-one (101)

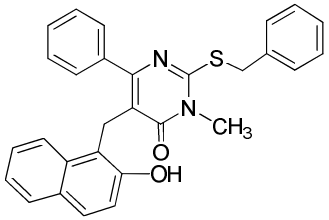

Aqueous NaOH (30%, 48 µL) was added to a suspension of **98** (50 mg, 0.11 mmol, 1 eq.) in ethanol (1.5 mL). Me_2SO_4 (42 µL, 0.44 mmol, 4 eq) was added and the reaction stirred for 3 h at rt. A white precipitate formed after 30 min. H_2O was added and the mixture filtered to afford the pure product as a microcrystalline powder (40 mg, 0.086 mmol, 78%). Mp 165-170 °C; ν_{max} cm^{-1} (KBr): 3449 (CONH) , 2925 (OH), 1740 (C=O), 1628 (C=O), 1513 (NH), 1412 (CSNH), 1261 (C=S), 1172 (C=S); δ_H (400 MHz, $CDCl_3$) 10.38 (brs, 1H, OH), 7.76-7.70 (m, 2H, H-4", H-5"), 7.67-7.56 (m, 5H, H-2', H-3', H-5', H-4', H-6'), 7.36-7.19 (m, 6H, H-3", H-2"', H-3"', H-

4''', H-5''', H-6'''), 7.14 (dt, 1H, ^2J = 7.8 Hz, ^3J = 0.9 Hz, H-8''), 6.93 (dt, 1H, ^2J = 8.3 Hz, ^3J = 0.9 Hz, H-7''), 6.77 (d, 1H, J = 8.5 Hz, H-6''), 4.40 (s, 2H, H-1'''), 4.36 (s, 2H, H-1''), 3.49 (s, 3H, N-CH_3); δ_C (100 MHz, $CDCl_3$) 165.8 (C=O), 159.8 (C6), 157.7 (C2), 153.9 (C2''), 138.8 (C1'), 135.9 (C1'''a), 133.6 (C8''a), 130.0 (CH, Ar), 129.8 (CH, Ar), 129.5 (CH, Ar), 129.4 (C4''a), 128.8 (CH, Ar), 128.7 (CH, Ar × 2), 128.5 (CH, Ar), 127.9 (CH, Ar), 125.6 (C7''), 123.4 (C8''), 122.6 (C6''), 121.3 (C3''), 118.6 (C1''a), 118.1 (C5), 36.7 (C1'''), 31.2 (N-CH_3), 23.9 (C1''); *m/z* (ES^+) 486.72 [$(M+Na)^+$, 100%]; HRMS (ES^+) [Found: $(M+Na)^+$, 487.1469, $C_{29}H_{24}N_2O_2SNa$ requires 487.1456] (+ 2.6 ppm).

3-Allyl-5-[2''-hydroxynaphthyl-(1'')-methyl]-6-phenyl-2-thioxo-2,3-dihydro-1*H*-pyrimidin-4-one (91)

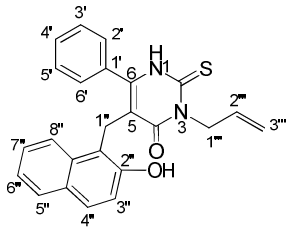

METHOD H: A solution of **97** (50 mg, 0.12 mmol, 1 eq.) and $PdCl_2(PhCN)_2$ (2.4 mg, 6.2 µmol, 0.05 eq.) in THF (2 mL) was prepared and stirred at reflux for 24 h. After consumption of the starting material, the reaction mixture was cooled to room temperature, the solvent removed at reduced pressure and the product purified by column chromatography (Hexane/EtOAc, 85:15). The desired product **91** was isolated as a white microcrystalline powder (40 mg, 0.096 mmol, 80%).

METHOD I: A solution of amide **103** (140 mg, 0.39 mmol, 1 eq) in TMSNCS (2 mL) was stirred at reflux for 2 h. The reaction was cooled to room temperature and saturated $NaHCO_3$ solution (10 mL) was added dropwise. The resulting mixture was extracted with DCM (3 × 10 mL), the organic layers dried ($MgSO_4$) and the solvent removed at reduced pressure. The pure product was obtained after purification by silica column chromatography (Hexane/EtOAc, 80:20) as a white powder (62 mg, 0.15 mmol, 40%).

Mp 188-190 °C; ν_{max} cm^{-1} (KBr): 3153 (NH), 3006 (OH), 1640 (C=O), 1222 (C=S); δ_H (400 MHz, $CDCl_3$) 9.50 (brs, 1H, NH), 9.35 (brs, 1H, OH), 7.72-7.65 (m, 4H, H-4', H-5', H-3', H-5''), 7.64-7.60 (m, 3H, H-6', H-2', H-4''), 7.23-7.13 (m, 2H, H-3'', H-6''), 6.93 (m, 1H, H-7''), 6.62 (m, 1H, H-8''), 5.99-5.88 (m, 1H, H-2'''), 5.38 (d, 1H, J = 17.2 Hz, H-3'''), 5.27 (d, 1H, J = 10.2 Hz, H-3'''), 4.99 (m, 2H, H-1''') and 4.15 (s, 2H, H-1''); δ_C (100 MHz, $CDCl_3$) 174.6

(C=S), 164.3 (C=O), 153.6 (C2"), 148.8 (C6), 133.1 (C8"a), 131.8 (C1'), 129.8 (C3', C5'), 129.7 (C4"), 129.4 (C4"a), 129.1 (C4', C2'"), 128.7 (C2', C6'), 128.7 (C5"), 125.6 (C7"), 122.6 (C8"), 122.6 (C6"), 120.9 (C3"), 119.9 (C3'"), 116.8 (C1"a), 114.0 (C5), 49.6 (C1'") and 22.7 (C1"); *m/z* (ES^+) 422.89 [$(M+Na)^+$, 100%]; HRMS (ES^+) [Found: $(M+Na)^+$, 423.1153, $C_{24}H_{20}N_2O_2SNa$ requires 423.1143] (+2.2 ppm).

3-Methyl-5-[2''-hydroxynaphthyl-(1'')-methyl]-6-phenyl-2-thioxo-2,3-dihydro-1*H*-pyrimidin-4-one (90)

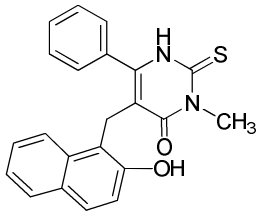

METHOD G: A solution of **100** (40 mg, 0.096 mmol, 1 eq.), $Pd(PPh_3)_4$ (3 mg, 3 µmol, 0.05 eq.) and morpholine (26 µL, 0.30 mmol, 5 eq.) in THF (2 mL) was prepared and the resulting mixture heated at reflux for 24 h. The reaction was cooled down to room temperature, the solvent removed at reduced pressure and the residue partitioned between H_2O-DCM (1:1, 5 mL). After extraction with DCM (3 × 5 mL), the organic layer was dried ($MgSO_4$) and the solvent removed under reduced pressure to afford the crude product which was purified by column chromatography (Hexane/EtOAc, 85:15), yielding 20 mg **90** (0.054 mmol, 88%) as a white solid.

METHOD I: Starting from amide **102** (200 mg, 0.63 mmol, 1 eq.) and TMSNCS (4 mL), yielded 84 mg (22.6 mmol, 36%).

ν_{max} cm^{-1} (KBr): 1635 (C=O), 1287 (C=S), 1152 (OH), 1025 (C=S); δ_H (400 MHz, $CDCl_3$) 9.52 (s, 1H, NH), 9. 38 (brs, 1H, OH), 7.70-7.61 (m, 7H, ArH), 7.22-7.14 (m, 2H, ArH), 6.93 (dt, 1H, ^2J = 7.8 Hz, ^3J = 1.3 Hz, ArH), 6.63 (d, 1H, J = 8.5Hz, ArH), 4.16 (s, 2H, H-1"), 3.69 (s, 3H, N-CH_3) ; δ_C (100 MHz, $CDCl_3$); 174.9 (C=S), 164.7 (C=O), 153.7 (C2"), 148.7 (C6), 133.2 (C8"a), 131.9 (CH, Ar), 129.9 (CH, Ar), 129.5 (C4"a), 129.2 (CH, Ar), 128.8 (CH, Ar), 128.8 (CH, Ar), 125.7 (C7"), 122.7 (C8"), 122.6 (C6"), 121.1 (C3"), 117.0 (C1"a), 113.7 (C5), 34.7 (N-CH_3), 22.9 (C1"); *m/z* (ES^+) 396.80 [$(M+Na)^+$, 100%]; HRMS (ES^+) [Found: $(M+Na)^+$, 397.0999, $C_{22}H_{18}N_2O_2NaS$ requires 397.0987] (+ 3.2 ppm).

2-[2''-Hydroxynaphthyl-(1'')-methyl]-*N*-methyl-3-oxo-3-phenylpropanamide (102)

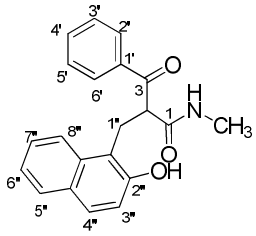

METHOD I: To a stirring solution of ketocoumarin **52a** (400 mg, 1.32 mmol, 1 eq.) in dry ethanol (5 mL), methylamine (33 % solution in ethanol, 200 µL, 1.45 mmol, 1.1 eq.) and *p*-TsOH (130 mg, 0.66 mmol, 0.5 eq.) were added and the reaction stirred at reflux for 5 h. After cooling to room temperature, the solvent was removed under reduced pressure, the residue partitioned between H_2O-DCM (1:1, 5 mL) and extracted (3 × 5 mL) with further portions of DCM. The organic layers were collected, dried ($MgSO_4$) and the solvent removed under reduced pressure to afford the crude product which was purified by column chromatography (Hexane/EtOAc, 80:20) to give the desired product as a white solid (241 mg, 0.72 mmol, 55%). ν_{max} cm^{-1} (KBr): 3500 (CONH), 1662 (C=O), 1152 (OH); δ_H (300 MHz, $CDCl_3$) 9.67 (brs, 1H, OH), 7.95-7.84 (m, 4H, H-2', H-6', H-8'', NH), 7.73 (d, 1H, *J* = 8.1 Hz, H-5''), 7.65-7.57 (m, 2H, H-4', H-4''), 7.46 (t, 2H, *J* = 7.7 Hz, H-3', H-5'), 7.38 (dt, 1H, ^2J = 7.1 Hz, ^3J = 1.0 Hz, H-7''), 7.23 (t, 1H, *J* = 7.3 Hz, H-6''), 7.15 (d, 1H, *J* = 8.7 Hz, H-3''), 4.62-4.59 (m, 1H, H-2), 3.50-3.48 (m, 2H, H-1'') and 2.30 (d, 3H, *J* = 4.5 Hz, N-CH_3); δ_C (100 MHz, $CDCl_3$) 196.0 (C=O), 169.0 (C=O), 152.8 (C2''), 136.2 (C1'), 133.5 (C8''a), 133.3 (C4'), 128.6 (C3', C5'), 128.2 (CH, Ar), 128.0 (C4''a), 127.8 (CH, Ar), 127.7 (CH, Ar), 125.8 (C7''), 122.9 (C8''), 122.1 (C6''), 117.8 (C3''), 116.8 (C1''a), 54.4 (C2), 25.9 (N-CH_3) and 24.6 (C1''); *m/z* (ES^+) 355.92 [$(M+Na)^+$, 100%]; *m/z* (ES^-) 331.98 [$(M-H)^-$, 100%]; HRMS (ES^+) [Found: $(M-H)^-$, 332.1275, $C_{21}H_{18}NO_3$ requires 332.1287] (-3.5 ppm).

***N*-Allyl-2-[2''-hydroxynaphthyl-(1'')-methyl]-3-oxo-3-phenylpropanamide (103)**

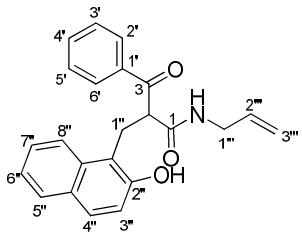

From **METHOD I**, yielded **103** (370 mg, 1.03 mmol, 78%) as a white microcrystalline powder from ketocoumarin **52a** (400 mg, 1.32 mmol). Mp 146-148 °C; ν_{max} cm^{-1} (KBr): 3061 (CONH), 1675 (C=O), 1046 (OH); δ_H (300 MHz, $CDCl_3$) 9.63 (brs, 1H, OH), 8.14 (t, 1H, *J* = 5.5 Hz, NH), 7.97 (dd, 2H, ^2J = 7.1 Hz, ^3J = 1.4 Hz, H-2', H-6'), 7.86 (d, 1H, *J* = 8.5 Hz, H-5''), 7.73 (d,

1H, *J* = 7.7 Hz, H-8"), 7.65-7.56 (m, 2H, H-4', H-4"), 7.47-7.34 (m, 3H, H-3', H-5', 7"), 7.23 (dt, 1H, ^{2}J = 7.6 Hz, ^{3}J = 0.8 Hz, H-6"), 7.15 (d, 1H, *J* = 8.8 Hz, H-3"), 5.40-5.20 (m, 1H, H-2'"), 4.78-4.59 (m, 3H, H-2, H-3'"), 3.59-3.36 (m, 4H, H-1'", H-1"). δ_C (100 MHz, $CDCl_3$) 195.9 (C=O), 168.3 (C=O), 152.8 (C2"), 136.1 (C1'), 134.5 (C2'"), 133.5 (C8"a), 133.2 (C4'), 128.5 (CH, Ar), 128.1 (CH, Ar), 128.0 (CH, Ar), 127.9 (C4"a), 127.7 (CH, Ar), 125.8 (C7"), 123.4 (C8"), 122.9 (C6"), 122.0 (C3"), 117.8 (C3'"), 116.7 (C1"a), 114.7 (C3'"), 54.4 (C2), 40.9 (C1'"), 24.5 (C1"); *m/z* (ES^+) 382.86 [$(M+Na)^+$, 100%]; HRMS (ES^+) [Found: $(M + Na)^+$, 382.1429 , $C_{23}H_{21}NO_3Na$ requires 382.1419] (2.5 ppm).

3-Hexyl-5-[2''-hydroxynaphthyl-(1'')-methyl]-6-phenyl-2-thioxo-2,3-dihydro-1*H*-pyrimidin-4-one (108)

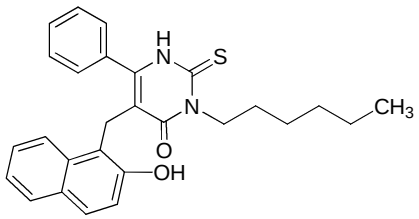

Prepared using **METHOD I** to yield **108** (70 mg, 0.16 mmol, 12%) from **52a** (400 mg, 1.32 mmol) over two steps. ν_{max} cm^{-1} (KBr): 3180 (NH), 2926 (OH), 1635 (C=O), 1522 (NH), 1444 (CSNH), 1200 (C=S); δ_H (400 MHz, DMSO-d_6) 12.46 (brs, 1H, NH), 9.72 (brs, 1H, OH), 7.68-7.60 (m, 1H, ArH), 7.49 (d, 1H, *J* = 8.4 Hz, ArH), 7.42-7.23 (m, 6H, ArH), 7.22-7.10 (m, 2H, ArH), 6.91 (d, 1H, *J* = 8.4 Hz, ArH), 4.28 (t, 2H, *J* = 7.4 Hz, N-C$\underline{H_2}$$CH_2CH_2CH_2CH_2CH_3$), 3.96 (s, 2H, H-1"), 1.73-1.51 (brs, 2H, N-$CH_2C\underline{H_2}CH_2CH_2CH_2CH_3$), 1.37-1.15 (brs, 6H, N-$CH_2CH_2C\underline{H_2}C\underline{H_2}C\underline{H_2}CH_3$), 0.84 (t, 3H, *J* = 6.8 Hz, N-$CH_2CH_2CH_2CH_2CH_2C\underline{H_3}$); δ_C (100 MHz, $CDCl_3$) 174.6 (C=S), 159.5 (C=O), 155 (C2"), 152.8 (C6), 133.1 (C8"a), 129.1 (CH, Ar), 129.0 (C4"a), 128.6 (CH, Ar × 2), 128.0 (CH, Ar), 127.7 (CH, Ar × 2), 125.4 (CH, Ar), 122.8 (CH, Ar), 121.8 (CH, Ar), 118.7 (C1"a), 116.4 (C5), 45.9, 30.8, 26.0, 25.7, 22.5 (N-$\underline{C}H_2\underline{C}H_2\underline{C}H_2\underline{C}H_2\underline{C}H_2CH_3$), 21.9 (C1"), 13.8 (N-$CH_2CH_2CH_2CH_2CH_2\underline{C}H_3$); *m/z* ($ES^-$) 443.12 [$(M-H)^-$, 100%]; HRMS ($ES^+$) [Found: $(M-H)^-$, 443.1790, $C_{22}H_{18}N_2O_2NaS$ requires 443.1793] (-0.6 ppm).

6.4 PART III: Novel *N*-1 Benzyl Cambinol Analogues

6.4.1 Chemistry

6.4.1.1 Synthesis of Known Intermediates 135, 109 and 110

Ethyl 2-benzyl-3-oxo-3-phenyloxopropanoate (135)[133]

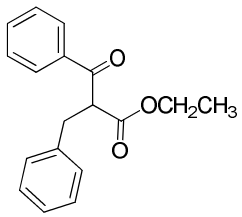

A solution of NaOEt was prepared by addition of Na metal (0.25 g, 10.8 mmol) to dry ethanol (10 mL). Ethyl benzoylacetate **50a** (4.6 mL, 40 mmol, 1 eq.) was added and the resulting solution stirred at room temperature for 10 min. Benzyl bromide (1.18 mL, 10 mmol, 0.25 eq.) was added and the reaction heated at reflux for 15 h. After removing the solvent at reduced pressure, the resulting residue was dissolved in ether (10 mL) and washed with water (3 × 10 mL). The organic layers were collected, dried ($MgSO_4$) and concentrated at reduced pressure. Purification by Kugelrohr distillation afforded the product as an orange oil (3 g, 10.6 mmol, 27%). δ_H (300 MHz, $CDCl_3$) 7.92-7.85 (m, 2H, ArH), 7.49 (dt, 1H, ^2J = 7.5 Hz, ^3J = 1.2 Hz, ArH), 7.37 (dt, 2H, ^2J = 8.0 Hz, ^3J = 1.4 Hz, ArH), 7.22-7.07 (m, 5H, ArH), 4.55 (t, 1H, J = 7.3 Hz, H-2), 4.02 (q, 2H, J = 7.1 Hz, O-C$\underline{H_2}$CH$_3$), 3.25 (dd, 2H, ^2J = 7.6 Hz, ^3J = 2.5 Hz, H-1') and 1.04 (t, 3H, J = 7.1 Hz, O-CH$_2$C$\underline{H_3}$); *m/z* (ES$^+$) 304.82 [(M+Na)$^+$, 100%].

2-Methoxy-naphthalene-1-carbaldehyde (109)[119]

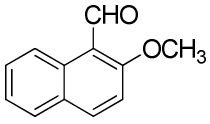

To a stirring solution of 2-hydroxy-1-naphthaldehyde **49** (1 g, 5.8 mmol, 1 eq.) in dry DMF (40 mL), K_2CO_3 (1.60 g, 11.6 mmol, 2 eq.) was added and the resulting suspension stirred at rt for 15 min. MeI (300 µl, 5.8 mmol, 1 eq.) was added and the reaction stirred at rt for 18 h. A solution of NaOH (aqueous, 5%, 20 mL) was added and the resulting mixture extracted with DCM (3 × 30 mL). The organic layers were collected and washed with water (3 × 50 mL), dried ($MgSO_4$) and concentrated at reduced pressure to afford the crude product as colourless crystals (900 mg, 4.8 mmol, 83%) which was used without further purification. Mp 84-86 °C (*lit.*[119] 84 °C); δ_H (300 MHz, $CDCl_3$) 10.86 (s, 1H, CHO), 9.24 (dd, 1H, J = 8.8 Hz, J = 1.0 Hz,

ArH), 8.03 (d, 1H, *J* = 9.1 Hz, ArH), 7.59 (dt, 1H, ^{2}J = 7.7 Hz, ^{3}J = 1.5 Hz, ArH), 7.38 (dt, 1H, ^{2}J = 7.5 Hz, ^{3}J = 1.1 Hz, ArH), 7.23 (d, 1H, *J* = 6.7 Hz, ArH) and 4.02 (s, 3H, O-CH_3); *m/z* (ES^+) 208.91 [$(M+Na)^+$, 100%].

2-Benzyloxy-naphthalene-1-carbaldehyde (110)[120]

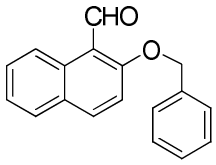

To a stirring solution of 2-hydroxy-1-naphthaldehyde **49** (2 g, 11.6 mmol, 1 eq.) in acetone (30 mL) was added K_2CO_3 (2.40 g, 17.4 mmol, 1.5 eq.) and the reaction mixture stirred at room temperature for 15 min. Benzyl bromide (2.57 mL, 12.7 mmol, 1.1 eq.) was added and the reaction stirred at reflux for 18 h. After filtering through a celite pad, the resulting acetone solution was concentrated at reduced pressure, the residue partitioned between EtOAc-H_2O (1:1, 100 mL), the organic layer washed with water (3 × 50 mL), brine (50 mL), dried ($MgSO_4$) and concentrated at reduced pressure. The product was obtained as brown solid (2.45 g, 81%) and used without further purification. Mp 119-121 °C (*lit* [120] 118-119 °C); δ_H (300 MHz, $CDCl_3$) 10.98 (s, 1H, CHO), 9.23 (d, 1H, *J* = 8.8 Hz, ArH), 8.03 (d, 1H, *J* = 8.9 Hz, ArH), 7.77 (d, 1H, *J* = 7.5 Hz, ArH), 7.66-7.54 (m, 1H, ArH), 7.50-7.33 (m, 7H, ArH) and 5.33 (s, 2H, C$\underline{H_2}$-Ph); *m/z* (ES^+) 284.86 [$(M+Na)^+$, 100%].

6.4.1.2 Synthesis of Acrylates 111-114

METHOD J: To a stirring solution of **109** or **110** (1 eq.) in dry ethanol (10 mL), were added ethyl benzoylacetate (2 eq.) and piperidine (10 drops) and the reaction stirred at reflux for 18 h. After cooling to 0 °C, each product was precipitated as a yellow microcrystalline powder which was isolated by filtration and washed with cold ethanol.

Ethyl 2-benzoyl-3-(2''-methoxynaphthalen-1''-yl)acrylate (111)

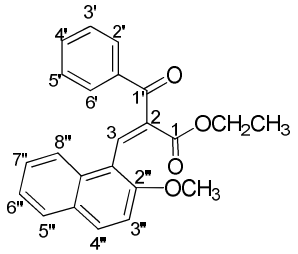

From **METHOD J** yielded **111** (250 mg, 0.69 mmol, 32%) from **109** (0.404 g, 2.1 mmol?) as a yellow microcrystalline powder. Mp 128-130 °C; ν_{max} cm^{-1} (KBr) 2940, 2836 (C-O-CH_2), 1720 (C=O), 1590, 1510 (C-HAr) ; δ_H (300 MHz, $CDCl_3$) 8.44 (s, 1H, H-3), 7.96 (dd, 1H, ^2J = 8.5 Hz, ^3J = 0.6 Hz, H-8''), 7.90-7.84 (m, 2H, ArH), 7.74 (t, 2H, J = 7.7 Hz, ArH), 7.57-7.28 (m, 5H, ArH), 7.02 (d, 1H, J = 9.0 Hz, H-3''), 4.25 (q, 2H, J = 7.0 Hz, O-C$\underline{H_2}$$CH_3$), 3.35 (s, 3H, CH_3O) and 1.16 (t, 3H, J = 7.0 Hz, O-CH_2C$\underline{H_3}$); δ_C (100 MHz, $CDCl_3$) 193.2 (C=O), 166.3 (C=O), 154.4 (C2''), 141.5 (C2), 139.0 (C3), 137.5 (C1'a), 133.0 (C8''a), 132.8 (C4'), 132.3 (CH, Ar), 129.0 (C7''), 128.8 (C4''a), 128.7 (C4''), 128.3 (C5''), 127.7 (CH, Ar), 124.3 (C6''), 123.9 (C8''), 116.0 (C1''), 112.6 (C3''), 61.8 (O-$\underline{C}H_2CH_3$), 54.9 (O-CH_3) and 14.4 (O-$CH_2\underline{C}H_3$); *m/z* (ES^+) 382.85 [$(M+Na)^+$, 100%]; HRMS (ES^+) [Found: $(M+Na)^+$, 383.1271, $C_{23}H_{20}O_4Na$ requires 383.1259] (+3.0 ppm).

Ethyl 2-(4'-chlorobenzoyl)-3-(2''-methoxynaphthalen-1''-yl)acrylate (112)

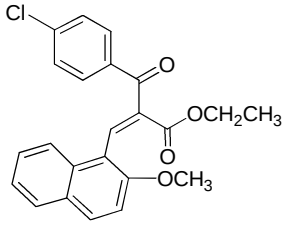

From **METHOD J** yielded **112** (706 mg, 1.79 mmol, 46%) from **109** (723 mg, 3.88 mmol?) as a yellow microcrystalline solid. Mp 126-128 °C; ν_{max} cm^{-1} (KBr): 2983 (C-O-CH_2), 1715 (C=O), 1679 (C=O), 1613 (C-HAr), 1508 (C-HAr); δ_H (300 MHz, $CDCl_3$) 8.45 (s, 1H, H-3), 7.94 (d, 1H, J = 8.5 Hz, H-8''), 7.86-7.79 (m, 4H, H-2', H-6', H-5'', H-7''), 7.57-7.49 (m, 1H, H-4''), 7.42-7.20 (m, 3H, H-3', H-5', H-6''), 7.04 (d, 1H, J = 9.4 Hz, H-3''), 4.26 (q, 2H, J = 7.1 Hz, O-C$\underline{H_2}$$CH_3$), 3.40 (s, 3H, O-$CH_3$) and 1.19 (t, 3H, J = 7.1 Hz, O-CH_2C$\underline{H_3}$); δ_C (100 MHz, $CDCl_3$) 192.0 (C=O), 165.7 (C=O), 154.2 (C2''), 139.1 (C3), 138.9 (C4'), 135.7 (C2), 133.8 (C1'a), 132.6 (C8''a), 132.3 (C3', C5'), 130.3 (C2', C6'), 128.7 (C4''a), 128.6 (C4''), 128.5 (C5''), 127.6 (C7''), 124.2 (C6''), 123.6 (C8''), 115.5 (C1''), 112.3 (C3''), 61.6 (O-C$\underline{H_2}$$CH_3$), 54.7 (O-$CH_3$) and 14.2 (O-$CH_2\underline{C}H_3$); *m/z* ($ES^+$) 416.81 [$(M+Na)^+$, 100%]; HRMS ($ES^+$) [Found: $(M+Na)^+$, 417.0874, $C_{23}H_{19}O_4NaCl$ requires 417.0870] (+1.0 ppm).

Ethyl 3-(2''-methoxynaphthalen-1''-yl)-2-(2'-methylbenzoyl)acrylate (113)

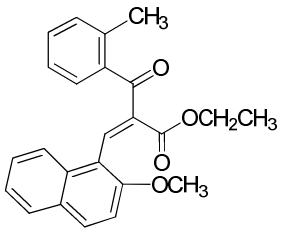

From **METHOD J** yielded **113** (386 mg, 1.03 mmol, 43%) from **109** (447 mg, 2.40 mmol?) as a yellow microcrystalline solid. Mp 146-148 °C; ν_{max} cm^{-1} (KBr): 2937, 2841 (C-O-CH_2), 1726, 1670 (C=O), 1621 (C-HAr), 1508 (C-HAr); δ_H (300 MHz, $CDCl_3$) 8.31 (s, 1H, H-3), 7.87 (d, 1H, J = 8.7 Hz, H-8''), 7.76-7.65 (m, 3H, ArH), 7.49 (dt, 1H, ^2J = 7.6 Hz, ^3J = 1.3 Hz, ArH), 7.34 (dt, 1H, ^2J = 7.5 Hz, ^3J = 1.0 Hz, ArH), 7.23-7.18 (m, 1H, ArH), 7.11-6.99 (m, 3H, H-3'' + 2 × ArH), 4.21 (q, 2H, J = 7.0 Hz, O-C$\underline{H_2}$$CH_3$), 3.55 (s, 3H, O-$CH_3$), 2.29 (s, 3H, CH_3) and 1.16 (t, 3H, J = 7.0 Hz, O-CH_2C$\underline{H_3}$); δ_C (100 MHz, $CDCl_3$) 195.2 (C=O), 165.8 (C=O), 153.9 (C2''), 139.4 (C3), 139.2 (C2'), 136.8 (C1'a), 136.3 (C2), 132.4 (C8''a), 131.5 (C4'), 131.3 (C3'), 130.6 (C6'), 128.6 (C4''), 128.4 (C5''), 127.4 (C7''), 124.9 (C5'), 124.0 (C6''), 123.9 (C8''), 116.2 (C1''), 112.3 (C3''), 61.3 (O-C$\underline{H_2}$$CH_3$), 55.2 (O-$CH_3$), 20.8 ($CH_3$) and 14.0 (O-$CH_2C\underline{H_3}$); *m/z* ($ES^+$) 396.86 [$(M+Na)^+$, 100%]; HRMS ($ES^+$) [Found: $(M+Na)^+$, 397.1414, $C_{24}H_{20}O_4Na$ requires 397.1416] (-0.3 ppm).

Ethyl 2-benzoyl-3-(2''-benzyloxynaphthalen-1''-yl)acrylate (114)

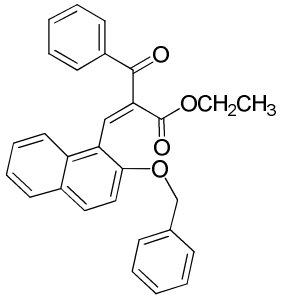

From **METHOD J** yielded **114** (358 mg, 0.82 mmol, 42%) from **109** (513 mg, 1.95 mmol) as a yellow microcrystalline solid. Mp 122-124 °C; ν_{max} cm^{-1} (KBr): 3065 (CO-CH), 2982 (C-O-C), 1706 (C=O), 1670 (C=O), 1591 (C-HAr), 1509 (C-HAr); δ_H (300 MHz, $CDCl_3$) 8.33 (s, 1H, H-3), 7.94 (dd, 1H, J = 8.6 Hz, J = 0.5 Hz, H-8''), 7.81 (dd, 2H, ^2J = 8.4 Hz, ^3J = 1.0 Hz, ArH), 7.66 (d, 1H, J = 8.1 Hz, ArH), 7.61 (d, 1H, J = 9.1 Hz, ArH), 7.50 (dt, 1H, ^2J = 7.7 Hz, ^3J = 1.5 Hz, ArH), 7.39-7.17 (m, 9H, ArH), 6.94 (d, 1H, J = 9.1 Hz, ArH), 4.82 (s, 2H, OC$\underline{H_2}$-Ph), 4.27 (q, 2H, J = 7.2 Hz, O-C$\underline{H_2}$$CH_3$) and 1.18 (t, 3H, J = 7.2 Hz, O-CH_2C$\underline{H_3}$); δ_C (75.5 MHz, $CDCl_3$) 193.2 (C=O), 165.7 (C=O), 153.3 (C2''), 139.2 (C3), 137.1 (C1'a), 137.0 (C2'''a), 135.0 (C2), 132.7 (C8''a), 132.5 (CH, Ar), 131.5 (CH, Ar), 128.8 (CH, Ar), 128.7

(C4"a), 128.6 (CH, Ar), 128.3 (CH, Ar), 128.0 (CH, Ar), 127.8 (CH, Ar), 127.4 (CH, Ar), 126.5 (CH, Ar), 124.2 (C8"), 124.0 (C6"), 116.6 (C1"), 114.0 (C3"), 70.0 (<u>C</u>H_2-Ph), 61.6 (O-<u>C</u>H_2CH_3) and 14.1 (O-CH_2<u>C</u>H_3); *m/z* (ES^+) 458.95 [$(M+Na)^+$, 100%]; HRMS (ES^+) [Found: $(M+Na)^+$, 459.1574, $C_{29}H_{24}O_4Na$ requires 459.1572] (+0.4 ppm).

6.4.1.3 Synthesis of Propionates 115-118

METHOD K: To a stirring solution of acrylates **111-114** (1 eq.) in pyridine (10 mL), was added $NaBH_4$ (1.1 eq.) and the reaction mixture stirred at rt for 2 h. After pouring into cold 2M HCl (40 mL) the mixture was extracted with DCM (3 × 50 mL), the organic layers dried ($MgSO_4$) and concentrated at reduced pressure. Purification by column chromatography (Hexane/EtOAc 95:5) afforded the pure products as colourless oils.

Ethyl 2-[2''-methoxynaphthyl-(1'')-methyl]-3-oxo-3-phenylpropanoate (115)

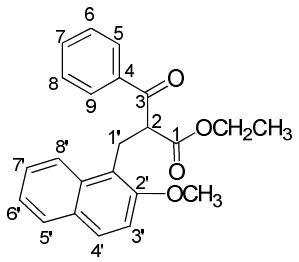

From **METHOD K** yielded **115** (706 mg, 1.94 mmol, 75%) from **111** (936 mg, 2.58 mmol) as a colourless oil after purification by column chromatography (Hexane/EtOAc, 95:5). ν_{max} cm^{-1} (KBr): 3065, 2982 (C-O-CH_2), 1706 (C=O), 1670 (C=O), 1591 (C-HAr), 1509 (C-HAr); δ_H (300 MHz, $CDCl_3$) 8.04 (dd, 1H, ^2J = 8.7 Hz, ^3J = 0.6 Hz, H-8'), 7.88-7.82 (m, 2H, ArH), 7.78-7.69 (m, 2H, H-4' + 1 × ArH), 7.54-7.42 (m, 2H, ArH), 7.40-7.26 (m, 3H, ArH), 7.18 (d, 1H, *J* = 9.0 Hz, H-3'), 4.75 (m, 1H, H-2), 4.04-3.80 (m, 6H, H-1', O-C<u>*H*</u>$_2CH_3$, O-C<u>*H*</u>$_3$), 3.72 (d, 1H, *J* = 6.5 Hz, H-1') and 0.99 (t, 3H, *J* = 7.2 Hz, O-CH_2C<u>*H*</u>$_3$); δ_C (75.5 MHz, $CDCl_3$) 195.9 (C=O), 170.4 (C=O), 155.2 (C2'), 136.7 (C4), 133.5 (C7), 133.3 (C8'a), 129.4 (C4'a), 128.9 (CH, Ar), 128.8 (CH, Ar), 128.7 (C5'), 128.6 (C4'), 126.8 (C7'), 123.5 (C6'), 123.4 (C8'), 119.7 (C1'a), 112.7 (C3'), 61.6 (O-CH_3), 56.3 (O-<u>C</u>H_2CH_3), 54.0 (C2), 25.0 (C1') and 14.0 (O-CH_2<u>C</u>H_3); *m/z* (ES^+) 484.87 [$(M+Na)^+$, 100%]; HRMS (ES^+) [Found: $(M+Na)^+$, 385.1428, $C_{23}H_{22}O_4Na$ requires 385.1416] (+3.1 ppm).

Ethyl 3-(4-chlorophenyl)-2-[2''-methoxynaphthyl-(1'')-methyl]-3-oxopropanoate (116)

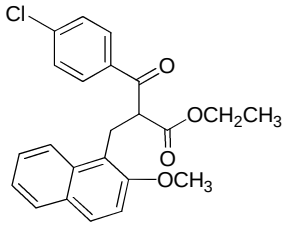

From **METHOD K** yielded **116** (400 mg, 1.00 mmol, 76%) from **112** (523 mg, 1.38 mmol) as a colourless oil after purification by column chromatography (Hexane/EtOAc, 95:5). ν_{max} cm^{-1} (KBr): 2800 (C-O-CH_2), 1750 (C=O), 1680 (C=O), 1550 (C-HAr), 1510 (C-HAr); δ_H (300 MHz, $CDCl_3$) 8.00 (d, 1H, *J* = 8.0 Hz, H-8'), 7.82-7.67 (m, 4H, H-5, H-9, H-4', H-5'), 7.53-7.45 (m, 1H, H-7'), 7.37-7.22 (m, 3H, H-6, H-8, H-6'), 7.17 (d, 1H, *J* = 9.0 Hz, H-3'), 4.68 (t, 1H, *J* = 7.1 Hz, H-2), 3.85 (q, 2H, *J* = 7.1 Hz, O-C$\underline{H_2}$$CH_3$), 3.90-3.80 (m, 4H, O-C$\underline{H_3}$, H-1'), 3.70 (m, 1H, H-1') and 1.01 (t, 3H, *J* = 7.1 Hz, O-CH_2C$\underline{H_3}$); δ_C (75.5 MHz, $CDCl_3$) 194.7 (C=O), 169.9 (C=O), 154.9 (C2'), 139.7 (C7), 134.8 (C4), 133.0 (C8'a), 129.9 (C5, C9), 129.2 (C4'a), 128.9 (C8, C6), 128.8 (C4'), 128.6 (C5'), 126.7 (C7'), 123.4 (C8'), 123.2 (C6'), 119.2 (C1'a), 112.5 (C3'), 61.5 (O-$\underline{C}$$H_2CH_3$), 56.1 (C2), 53.7 (O-$CH_3$), 24.8 (C1') and 13.8 (O-$CH_2\underline{C}H_3$); *m/z* (ES^+) 418.81 [$(M+Na)^+$, 100%]; HRMS (ES^+) [Found: $(M+Na)^+$, 419.1034, $C_{23}H_{21}O_4NaCl$ requires 419.1026] (+1.8 ppm).

Ethyl 2-[2''-methoxynaphtyl-(1'')-methyl]-3-oxo-3-(*o*-tolyl)-propanoate (117)

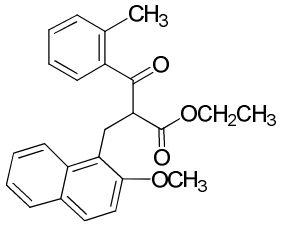

From **METHOD K** yielded **117** (338 mg, 0.89 mmol, 75%) from **113** (448 mg, 1.19 mmol) as a colourless oil after purification by column chromatography (Hexane/EtOAc, 95:5). ν_{max} cm^{-1} (KBr): 2900 (C-O-CH_2), 1739 (C=O), 1514 (C-HAr); δ_H (300 MHz, $CDCl_3$) 8.05 (d, 1H, *J* = 8.7 Hz, H-8'), 7.79-7.67 (m, 2H, H-4', H-5'), 7.51-7.40 (m, 2H, H-6', H-7'), 7.36-7.04 (m, 5H, H-3', H-6, H-7, H-8, H-9), 4.70 (t, 1H, *J* = 7.3 Hz, H-2), 4.06-3.84 (m, 6H, CH_3O, O-C$\underline{H_2}$$CH_3$, H-1'), 3.76 (d, 2H, *J* = 7.3 Hz, H-1'), 2.40 (s, 3H, O-CH_3) and 0.97 (t, 3H, *J* = 7.0 Hz, O-CH_2C$\underline{H_3}$); δ_C (75.5 MHz, $CDCl_3$) 199.1 (C=O), 170.1 (C=O), 155.0 (C2'), 138.8 (C5), 137.5 (C4), 133.1 (C8'a), 131.8 (CH, Ar), 131.4 (CH, Ar), 129.2 (C4'a), 128.7 (C4'), 128.5 (C5'), 126.6 (C7'), 125.4 (C8), 123.4 (C8'), 123.3 (C6'), 119.6 (C1'a), 112.6 (C3'), 61.2 (O-$\underline{C}$$H_2CH_3$), 56.1 (O-$CH_3$), 24.5 (C1'), 20.9 ($CH_3$) and 13.8 (O-$CH_2\underline{C}H_3$); *m/z* ($ES^+$) 398.85 [$(M+Na)^+$, 100%]; HRMS ($ES^+$) [Found: $(M+Na)^+$, 399.1567, $C_{24}H_{24}O_4Na$ requires 399.1572] (-1.4 ppm).

Ethyl 2-[2''-benzyloxynaphthyl-(1'')-methyl]-3-oxo-3-phenylpropanoate (118)

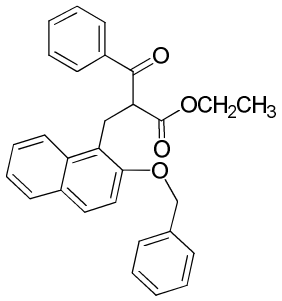

From **METHOD K** yielded **118** (378 mg, 0.86 mmol, 71%) from **114** (537 mg, 1.23 mmol) as a colourless oil after purification by column chromatography (Hexane/EtOAc, 95:5). ν_{max} cm^{-1} (KBr): 3065, 2982 (C-O-CH_2), 1706 (C=O), 1670 (C=O), 1591 (C-HAr), 1509 (C-HAr); δ_H (300 MHz, $CDCl_3$) 8.06 (d, 1H, *J* = 8.5 Hz, H-8'), 7.82-7.66 (m, 4H, ArH), 7.54-7.18 (m, 11H, ArH), 5.18 (s, 2H, OC$\underline{H_2}$-Ph), 4.85 (dd, 1H, *J* = 6.4 Hz, H-2), 4.00-3.80 (m, 3H, O-C$\underline{H_2}$$CH_3$, H-1'), 3.76 (d, 1H, *J* = 6.6 Hz, H-1') and 0.91 (t, 3H, *J* = 7.2 Hz, O-CH_2C$\underline{H_3}$); δ_C (100 MHz, $CDCl_3$) 195.7 (C=O), 170.0 (C=O), 154.3 (C2'), 137.2 (C2"a), 136.5 (C4), 133.3 (CH, Ar), 133.2 (C8'a), 129.4 (C4'a), 128.7 (CH, Ar), 128.6 (CH, Ar), 128.5 (CH, Ar), 128.5 (CH, Ar), 128.0 (CH, Ar), 127.3 (CH, Ar), 126.6 (CH, Ar), 126.4 (CH, Ar), 124.0 (C8'), 123.5 (C6'), 120.1 (C1'a), 113.9 (C3'), 70.9 ($\underline{C}H_2$-Ph), 61.3 (O-$\underline{C}H_2CH_3$), 53.9 (C2), 25.0 (C1') and 13.8 (O-$CH_2\underline{C}H_3$); *m/z* (ES^+) 460.90 [$(M+Na)^+$, 100%]; HRMS (ES^+) [Found: $(M+Na)^+$, 461.1728, $C_{29}H_{26}O_4Na$ requires 461.1729] (-0.2 ppm).

6.4.1.4 Preparation of Benzylamines 141-143

Prepared according to the 3 steps synthetic methods described by Coxon *et al*.[122]

STEP 1, SYNTHESIS OF 4-ALKYLOXIBENZALDEHYDES 145-147. To a stirring solution of 4-hydroxybenzylaldehyde **144** (9.05 g, 74 mmol, 1 eq.) in water/methanol (1:1, 200 mL) were added the required alkyl bromide (2 eq.), K_2CO_3 (1.2 eq) and the reaction mixture stirred at reflux for 18 h. After cooling to room temperature, the solvent was removed at reduced pressure. The resulting residue was dissolved in diethyl ether (100 mL) and washed with 10% aqueous NaOH (3 × 100 mL). The organic layers were combined, dried ($MgSO_4$) and concentrated at reduced pressure to afford the crude product as a colourless oil which was used without further purification.

STEP 2, SYNTHESIS OF 4-ALKYLOXYBENZALDOXYMES 148-150. To a stirring solution of 4-alkoxybenzaldehyde **145-147** (1 eq.) and K_2CO_3 (2 eq) in water/ethanol (1:1, 200 mL, 0.2 M) was added a solution of hydroxylammonium chloride (1.2 eq.) in water (20 mL). The reaction mixture was stirred at room temperature for 4 h. After removing the suspension of K_2CO_3 by filtration, the reaction was cooled to 0 °C and the aldoxime products obtained as colourless crystals which were filtered, dried and used without further purification.

STEP 3, SYNTHESIS OF 4-ALKYLOXYBENZAMINES 141-143. To a stirring solution of 4-alkoxybenzaldoxime **148-150** (1 eq.) in ethanol (200 mL, 0.12 M) and 10% aqueous NaOH (200 mL) was added *with caution* portionwise nickel aluminium alloy (240 mg per mmol of aldoxyme). The reaction mixture was stirred at room temperature for 4 h, filtered through a pad of celite and the solvent removed at reduced pressure. DCM (200 mL) was added to the residue and the resulting solution washed with brine (3 × 100 mL). The organic layers were dried ($MgSO_4$) and concentrated at reduced pressure to afford 4-alkoxybenzylamines **141-143** as pale yellow oils which were used without further purification.

4-Ethoxybenzaldehyde (145)[122]

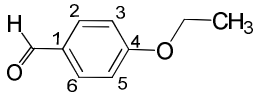

From 4-hydroxybenzaldehyde **144** (9.05 g, 74.1 mmol), yielded **145** (8.43 g, 0.56 mmol, 76%) as a yellow oil. δ_H (400 MHz, $CDCl_3$) 9.85 (s, 1H, CHO), 7.80 (d, 2H, *J* = 8.8 Hz, AA'BB', H-2, H-6), 6.96 (d, 2H, *J* = 8.8 Hz, AA'BB', H-3, H-5), 4.09 (q, 2H, *J* = 7.0 Hz, O-C$\underline{H_2}$$CH_3$) and 1.43 (t, 2H, *J* = 7.0 Hz, O-CH_2C$\underline{H_3}$). Data is in agreement with the literature.[122]

4-Propyloxybenzaldehyde (146)[134]

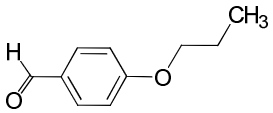

From 4-hydroxybenzaldehyde **144** (9.05 g, 74.1 mmol), yielded **146** (12.14 g, 74.9 mmol, quant.) as an orange oil. δ_H (400 MHz, $CDCl_3$) 9.87 (s, 1H, CHO), 7.81 (d, 2H, *J* = 8.8 Hz, AA'BB', H-2, H-6), 6.98 (d, 2H, *J* = 8.8 Hz, AA'BB', H-3, H-5), 3.99 (t, 2H, *J* = 6.5 Hz, O-C$\underline{H_2}$$CH_2CH_3$), 1.85-1.80 (m, 2H, O-$CH_2C\underline{H_2}$$CH_3$) and 1.05 (t, 3H, *J* = 7.4 Hz, O-CH_2CH_2C$\underline{H_3}$). Data is in agreement with the literature.[134]

4-Butoxybenzaldehyde (147)[134]

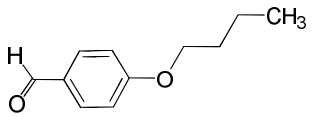

From 4-hydroxybenzaldehyde **144** (4.50 g, 74.1 mmol), yielded **147** (6.50 g, 36.4 mmol, quant.) as an orange oil. δ_H (400 MHz, $CDCl_3$) 9.86 (s, 1H, CHO), 7.81 (d, 2H, *J* = 9.0 Hz, AA'BB', H-2, H-6), 6.98 (d, 2H, *J* = 9.0 Hz, AA'BB', H-3, H-5), 4.03 (t, 2H, *J* = 6.5 Hz, O-C$\underline{H_2}$$CH_2CH_2CH_3$), 1.86-1.72 (m, 2H, O-$CH_2C\underline{H_2}$$CH_2CH_3$), 1.58-1.42 (m, 2H, O-$CH_2CH_2C\underline{H_2}$$CH_3$) and 0.95 (t, 3H, *J* = 6.5 Hz, O-$CH_2CH_2CH_2$C$\underline{H_3}$). Data is in agreement with the literature.[134]

4-Ethoxybenzaldoxime (148)[122]

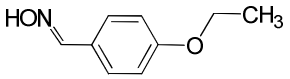

From 4-ethoxybenzaldehyde **145** (8.43 g, 56.1 mmol), yielded **148** (5.70 g, 34.5 mmol, 62%) as a white microcrystalline solid. Mp 83-85 °C (*lit.* 81-86 °C); δ_H (400 MHz, $CDCl_3$) 8.33 (brs, 1H, OH), 8.09 (s, 1H, C$\underline{H}$=NOH), 7.50 (d, 2H, *J* = 8.8 Hz, AA'BB', H-2, H-6), 6.89 (d, 2H, *J* = 8.8 Hz, AA'BB', H-3, H-5), 4.05 (q, 2H, *J* = 7.0 Hz, O-C$\underline{H_2}$$CH_3$) and 1.42 (t, 3H, *J* = 7.0 Hz, O-CH_2C$\underline{H_3}$). Data is in agreement with the literature.[122]

4-Propyloxybenzaldoxyme (149)[135]

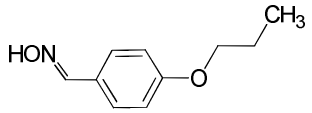

From 4-propyloxybenzaldehyde **146** (6.92 g, 42.1 mmol), yielded **149** (6.00 g, 33.5 mmol, 81%) as a white microcrystalline solid. Mp 80-83 °C (*lit.* 82-83 °C); δ_H (400 MHz, $CDCl_3$) 8.08 (s, 1H, C$\underline{H}$=NOH), 7.49 (d, 2H, *J* = 8.8 Hz, AA'BB', H-2, H-6), 6.89 (d, 2H, *J* = 8.8 Hz, AA'BB', H-3, H-5), 3.94 (t, 2H, *J* = 6.6 Hz, O-C$\underline{H_2}$$CH_2CH_3$), 1.85-1.75 (m, 2H, O-$CH_2C\underline{H_2}$$CH_3$) and 1.04 (t, 3H, *J* = 7.5 Hz, O-CH_2CH_2C$\underline{H_3}$). Data is in agreement with the literature.[135]

4-Butoxybenzaldoxyme (150)[136]

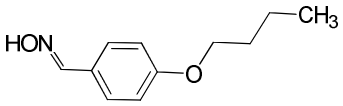

From 4-butoxybenzaldehyde **147** (6.90 g, 38.7 mmol), yielded **150** (5.80 g, 30.0 mmol, 78%) as a white microcrystalline solid. Mp 55-57 °C (*lit.* 54-56 °C); δ_H (400 MHz, $CDCl_3$) 8.08 (s, 1H, C$\underline{H}$=NOH), 7.53-7.46 (m, 3H, AA'BB', H-2, H-6, NO$\underline{H}$), 6.89 (d, 2H, *J* = 9.0 Hz, AA'BB', H-3,

H-5), 3.98 (t, 2H, *J* = 6.5 Hz, O-C<u>*H*</u>$_2$CH$_2$CH$_2$CH$_3$), 1.82-1.71 (m, 2H, O-CH$_2$C<u>*H*</u>$_2$CH$_2$CH$_3$) 1.56-1.43 (m, 2H, O-CH$_2$CH$_2$C<u>*H*</u>$_2$CH$_3$) and 0.97 (t, 3H, *J* = 7.4 Hz, O-CH$_2$CH$_2$CH$_2$C<u>*H*</u>$_3$). Data is in agreement with the literature.[136]

4-Ethoxybenzylamine (141)[122]

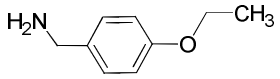

From 4-ethoxybenzaldoxime **148** (5.60 g, 33.9 mmol), yielded **141** (3.20 g, 21.1 mmol, 62%) as a white solid. Mp 224-228 °C (*lit* [18] 226-227 °C); δ_H (400 MHz, $CDCl_3$) 7.20 (d, 2H, *J* = 8.6 Hz, AA'BB', H-2, H-6), 6.85 (d, 2H, *J* = 8.6 Hz, AA'BB', H-3, H-5), 4.01 (q, 2H, *J* = 6.8 Hz, O-C<u>*H*</u>$_2$CH$_3$), 3.79 (s, 2H, CH$_2$), 1.49 (br, 2H, NH$_2$) and 1.40 (t, 3H, *J* = 6.8 Hz, O-CH$_2$C<u>*H*</u>$_3$). Data is in agreement with the literature.[122]

4-Propiloxybenzylamine (142)[137]

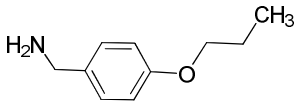

From 4-propyloxybenzaldoxime **149** (6.00 g, 33.5 mmol), yielded **142** (3.80 g, 23.0 mmol, 69%) as a colourless oil. δ_H (400 MHz, $CDCl_3$) 7.20 (d, 2H, *J* = 8.6 Hz, AA'BB', H-2, H-6), 6.86 (d, 2H, *J* = 8.6 Hz, AA'BB', H-3, H-5), 3.94 (t, 2H, *J* = 6.2 Hz, O-C<u>*H*</u>$_2$CH$_2$CH$_3$), 3.78 (s, 2H, CH$_2$), 1.79-1-71 (m, 2H, O-CH$_2$C<u>*H*</u>$_2$CH$_3$), 1.44-1.32 (m, 2H, NH$_2$) and 0.96 (t, 3H, *J* = 7.4 Hz, O-CH$_2$CH$_2$C<u>*H*</u>$_3$). Data is in agreement with the literature.[137]

4-Butoxybenzylamine (143)[138]

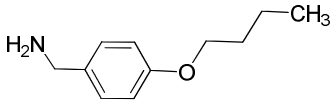

From 4-butoxybenzaldoxime **150** (5.80 g, 30.0 mmol), yielded **143** (3.50 g, 19.5 mmol, 65%) as a white solid. Mp 96-98 °C (*lit.* 95-100 °C); δ_H (400 MHz, $CDCl_3$) 7.20 (d, 2H, *J* = 8.8 Hz, AA'BB', H-2, H-6), 6.86 (d, 2H, *J* = 8.8 Hz, AA'BB', H-3, H-5), 3.94 (t, 2H, *J* = 6.6 Hz, O-C<u>*H*</u>$_2$CH$_2$CH$_2$CH$_3$), 3.78 (s, 2H, CH$_2$), 1.82-1-67 (m, 2H, O-CH$_2$C<u>*H*</u>$_2$CH$_2$CH$_3$), 1.60-1.41 (m, 4H, O-CH$_2$CH$_2$C<u>*H*</u>$_2$CH$_3$ + NH$_2$) and 0.96 (t, 3H, *J* = 7.4 Hz, O-CH$_2$CH$_2$CH$_2$C<u>*H*</u>$_3$). Data is in agreement with the literature.[138]

6.4.1.4 Synthesis of the Final Cambinol Analogues

STEP 1, ENAMINE FORMATION, GENERAL METHOD L (131-135): To a stirring solution of the ketoester **(**1 eq.) in dry ethanol (10 mL), were added the amine (5 eq.) and acetic acid (5 eq.) and the reaction mixture stirred at reflux for 24 h. After the reaction had gone to completion, the solvent was removed at reduced pressure, the residue dissolved in DCM and washed with 1M HCl (2 × 20 mL). The organic layers were dried ($MgSO_4$) and concentrated at reduced pressure to afford the crude enamine which was used in the next step without further purification.

STEP 1, ENAMINE FORMATION, GENERAL METHOD M (119-130): Analogous to **METHOD M**, using 10 equivalents of amine and acetic acid. After removal of the solvent at reduced pressure, purification by basic alumina column chromatography (Hexane/EtOAc, 97.5:2.5 to 95:5) afforded the crude products **119-130** which were used in the next step without further purification.

STEP 2, CYCLISATION, GENERAL METHOD N (144-160): Crude enamine was dissolved in TMSNCS (2-3 mL) and the reaction mixture stirred at reflux for 3 h. After cooling to room temperature, saturated $NaHCO_3$ solution (10 mL) was added dropwise. The resulting mixture was extracted with DCM (3 × 10 mL), the organic layers dried ($MgSO_4$) and the solvent removed at reduced pressure. The pure products were obtained after purification by silica column chromatography (Hexane/EtOAc).

1-Benzyl-6-phenyl-2-thioxo-2,3-dihydropyrimidin-4(1*H*)-one (144)

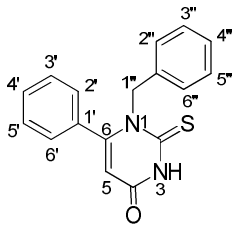

Yielded **144** (175 mg, 0.59 mmol, 80%) from enamine **135** (210 mg, 0. 74 mmol) as a white microcrystalline powder after column chromatography (Hexane/EtOAc, 80:20). Mp 184-186 °C; ν_{max} cm^{-1} (KBr): 3180 (CONH), 3060 (CONH), 2928 (CH_2), 1670 (C=O), 1594 (NH), 1489 (CSNH), 1411 (CSNH), 1246 (C=S); δ_H (300 MHz, $CDCl_3$) 10.77 (brs, 1H, NH), 7.48-7.37 (m, 1H, ArH), 7.36-7.14 (m, 5H, ArH), 7.11-7.00 (m, 2H, ArH), 6.92-6.81 (m, 2H, ArH), 5.90 (s, 1H, H-5) and 5.52 (brs, 2H, H-1"); δ_C (100 MHz, $CDCl_3$) 178.5 (C=S), 159.6 (C=O),

157.7 (C6), 135.5 (C1"a), 133.2 (C1'), 130.3 (CH, Ar), 128.7 (CH, Ar), 128.6 (CH, Ar), 127.9 (CH, Ar), 127.7 (CH, Ar), 126.5 (CH, C4'), 109.1 (C5) and 54.6 (C1"); *m/z* (ES^+) 316.89 [$(M+Na)^+$, 100%]; HRMS (ES^+) [Found: $(M+Na)^+$, 317.0722, $C_{17}H_{14}N_2ONaS$ requires 317.0725] (-0.9 ppm).

1,5-Dibenzyl-6-phenyl-2-thioxo-2,3-dihydro-1*H*-pyrimidin-4-one (145)

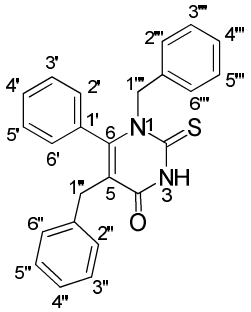

Yielded **145** (117 mg, 0.30 mmol, 76%) from enamine **131** (150 mg, 0.40 mmol) as a white microcrystalline powder after column chromatography (Hexane/EtOAc, 80:20). Mp 135-137 °C; ν_{max} cm^{-1} (KBr): 3060 (CONH), 2930 (CH_2), 1662 (C=O), 1494 (CSNH), 1259 (C=S); δ_H (300 MHz, $CDCl_3$) 9.66 (brs, 1H, NH), 7.39 (dt, 1H, ^2J = 5.5 Hz, ^3J = 1.2 Hz, ArH), 7.31-7.07 (m, 9H, ArH), 6.89-6.70 (m, 5H, ArH) and 3.41 (s, 2H, H-1"); δ_C (100 MHz, $CDCl_3$) 176.9 (C=S), 159.9 (C=O), 154.1 (C6), 138.8 (C1"a), 135.5 (C1'"a), 131.5 (C1'), 130.0 (CH, Ar), 128.7 (CH, Ar), 128.5 (CH, Ar), 128.6 (CH, Ar × 2), 128.5 (CH, Ar), 128.4 (CH, Ar), 127.6 (CH, Ar), 126.4 (CH, Ar), 119.6 (C5) and 32.1 (C1"); *m/z* (ES^+) 406.92 [$(M+Na)^+$, 100%]; HRMS (ES^+) [Found: $(M+Na)^+$, 407.1194, $C_{24}H_{20}N_2ONaS$ requires 407.1194] (-0.1 ppm).

1-(4'''-Methoxybenzyl)-5-benzyl-6-phenyl-2-thioxo-2,3-dihydro-1*H*-pyrimidin-4-one (146)

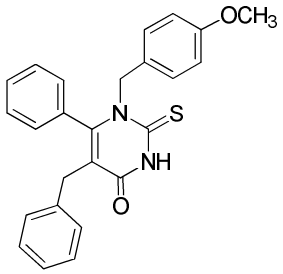

Yielded **146** (298 mg, 0.71 mmol, 60%) over 2 steps from ketoester **136** (510 mg, 1.27 mmol) as a white microcrystalline powder after column chromatography (Hexane/EtOAc, 90:10 to 80:20). Mp 192-195 °C; ν_{max} cm^{-1} (KBr): 3108 (CONH), 2953 (CH_2), 2832 (C-O-CH_2), 1697 (C=O), 1595 (NH), 1489 (CSNH), 1244 (C=S); δ_H (500 MHz, $CDCl_3$) 9.90 (brs, 1H, NH), 7.41 (dt, 1H, ^2J = 5.7 Hz, ^3J = 1.1 Hz, ArH), 7.32-7.23 (m, 2H, ArH), 7.15-7.10 (m, 3H, ArH), 6.89-6.67 (m, 8H, H-2'", H-3'", H-5'", H-6'" + 4 × ArH), 3.76 (s, 3H, O-CH_3) and 3.40 (s, 2H, H-1");

δ_C (100 MHz, $CDCl_3$) 176.8 (C=S), 160.0 (C=O), 159.1 (C4'''), 154.1 (C6), 138.8 (C1"a), 131.5 (C1'), 130.0 (CH, Ar), 128.7 (CH, Ar), 128.5 (CH, Ar), 128.4 (CH, Ar), 128.3 (CH, Ar), 127.9 (CH, Ar), 127.5 (C1'"a), 126.4 (CH, Ar), 119.5 (C5), 113.9 (CH, Ar), 55.4 (O-CH_3) and 32.1 (C1"); *m/z* (ES^+) 436.76 [$(M+Na)^+$, 100%]; HRMS (ES^+) [Found: $(M+Na)^+$, 437.1308, $C_{25}H_{22}N_2O_2NaS$ requires 437.1300] (+1.9 ppm).

1-(4'''-Ethoxybenzyl)-5-benzyl-6-phenyl-2-thioxo-2,3-dihydro-1*H*-pyrimidin-4-one (147)

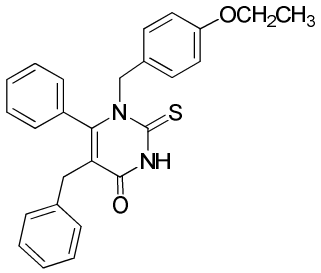

Yielded **147** (359 mg, 0.83 mmol, 68%) over 2 steps from ketoester **136** (512 mg, 1.23 mmol) as a white microcrystalline powder after column chromatography (Hexane/EtOAc, 90:10 to 80:20). Mp 203-206 °C; ν_{max} cm^{-1} (KBr): 3450 (NH), 3092 (CH_2), 2976 (C-O-CH_2), 1696 (C=O), 1594 (NH), 1491 (CSNH), 1247 (C=S); δ_H (400 MHz, $CDCl_3$) 9.70 (brs, 1H, NH), 7.40 (dt, 1H, ^2J = 7.5 Hz, ^3J = 1.2 Hz, ArH), 7.33-7.22 (m, 2H, ArH), 7.17-7.07 (m, 3H, ArH), 6.91-6.64 (m, 8H, H-2''', H-3''', H-5''', H-6''' + 4 × ArH), 3.97 (q, 2H, *J* = 7.0 Hz, O-C$\underline{H_2}$$CH_3$), 3.40 (s, 2H, H-1") and 1.39 (t, 3H, *J* = 7.0 Hz, O-CH_2C$\underline{H_3}$); δ_C (100 MHz, $CDCl_3$) 177.1 (C=S), 160.0 (C=O), 158.5 (C4'''), 154.1 (C6), 138.8 (C1"a), 131.6 (C1'), 130.0 (CH, Ar), 128.7 (CH, Ar), 128.6 (CH, Ar), 128.5 (CH, Ar), 128.3 (CH, Ar), 127.9 (CH, Ar), 127.4 (C1'"a), 126.4 (CH, Ar), 119.6 (C5), 114.5 (CH, Ar), 63.6 (O-$\underline{C}H_2CH_3$), 32.1 (C1") and 14.9 (O-$CH_2\underline{C}H_3$); *m/z* (ES^+) 450.80 [$(M+Na)^+$, 100%]; HRMS (ES^+) [Found: $(M+Na)^+$, 451.1440, $C_{26}H_{24}N_2O_2NaS$ requires 451.1452] (-0.1 ppm).

1-(4'''-Butoxybenzyl)-5-benzyl-6-phenyl-2-thioxo-2,3-dihydro-1*H*-pyrimidin-4-one (148)

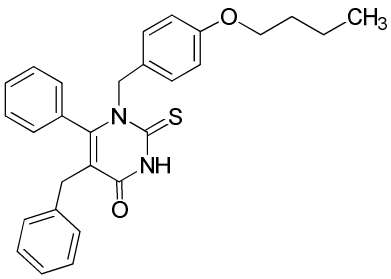

Yielded **148** (263 mg, 0.57 mmol, 57%) over 2 steps from ketoester **136** (450 mg, 1.0 mmol) as a white microcrystalline powder after column chromatography (Hexane/EtOAc, 90:10 to 80:20). Mp 140-142 °C; ν_{max} cm^{-1} (KBr): 2944 (CH_2), 1673 (C=O), 1508 (NH), 1228 (C=S); δ_H

(300 MHz, $CDCl_3$) 9.69 (brs, 1H, NH), 7.40 (t, 1H, J = 7.6 Hz, ArH), 7.35-7.20 (m, 2H, ArH), 7.18-7.06 (m, 3H, ArH), 6.91-6.64 (m, 8H, H-2''', H-3''', H-5''', H-6''' + 4 × ArH), 3.90 (t, 2H, J = 6.6 Hz, O-C$\underline{H_2}$$CH_2CH_2CH_3$), 3.40 (s, 2H, H-1''), 1.81-1.66 (m, 2H, O-CH_2C$\underline{H_2}$$CH_2CH_3$), 1.53-1.38 (m, 2H, O-$CH_2CH_2C\underline{H_2}$$CH_3$) and 0.96 (t, 3H, J = 7.5 Hz, O-$CH_2CH_2CH_2$C$\underline{H_3}$); δ_C (100 MHz, $CDCl_3$) 176.9 (C=S), 160.0 (C=O), 158.7 (C4'''), 154.1 (C6), 138.8 (C1''a), 131.5 (C1'), 129.9 (CH, Ar), 128.7 (CH, Ar), 128.6 (CH, Ar), 128.4 (CH, Ar), 128.3 (CH, Ar), 127.8 (CH, Ar), 127.4 (C1'''a), 126.4 (CH, Ar), 119.6 (C5), 114.5 (CH, Ar), 67.8 (O-$\underline{C}$$H_2CH_2CH_2CH_3$), 32.1 (C1''), 31.4 (O-$CH_2$$\underline{C}$$H_2CH_2CH_3$), 19.3 (O-$CH_2CH_2$$\underline{C}$$H_2CH_3$) and 13.9 (O-$CH_2CH_2CH_2$$\underline{C}$$H_3$); *m/z* ($ES^+$) 478.80 [$(M+Na)^+$, 100%]; HRMS ($ES^+$) [Found: $(M+Na)^+$, 479.1760, $C_{28}H_{28}N_2O_2NaS$ requires 479.1769] (-1.9 ppm).

1-Benzyl-5-[2''-methoxynaphthyl-(1'')-methyl]-6-phenyl-2-thioxo-2,3-dihydro-1*H*-pyrimidin-4-one (149)

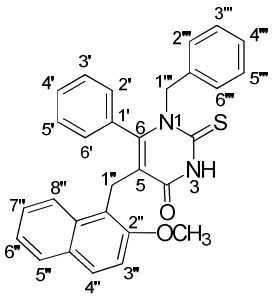

Yielded **149** (30 mg, 0.66 mmol, 23%) over 2 steps from **115** (100 mg, 0.33mmol) as a white microcrystalline powder after column chromatography (Hexane/EtOAc, 90:10 to 80:20). Mp 211-214 °C; ν_{max} cm^{-1} (KBr): 3172, 3071 (CONH), 2952 (CH_2), 2831 (C-O-CH_2), 1655 (C=O), 1592 (NH), 1493 (CSNH), 1251 (C=S), 1172 (C=S); δ_H (400 MHz, $CDCl_3$) 9.77 (brs, 1H, NH), 7.64 (dd, 1H, ^2J = 8.4 Hz, ^3J = 1.1 Hz, H-5''), 7.55 (d, 1H, J = 8.9 Hz, H-4''), 7.49 (d, 1H, J = 8.3 Hz, H-6''), 7.35-7.20 (m, 2H, H-7'' + 1 × ArH), 7.18-7.08 (m, 3 H-8'' + 2 × ArH), 6.98 (dt, 1H, ^2J = 7.5 Hz, ^3J = 1.0 Hz, ArH), 6.84 (d, 1H, J = 8.9 Hz, ArH), 6.82-6.71 (m, 2H, H-3'' + 1 × ArH), 6.68 (dd, 2H, ^2J = 7.8 Hz, ^3J = 1.8 Hz, ArH), 6.26 (brs, 2H, ArH), 4.07 (s, 2H, H-1'') and 3.60 (s, 3H, O-CH_3); δ_C (100 MHz, $CDCl_3$) 176.4 (C=S), 160.1 (C=O), 154.4 (C2''), 153.1 (C6), 135.6 (C1'''a), 132.9 (C8''a), 131.1 (C1'), 128.9 (CH, Ar), 128.8 (C4''a), 128.4 (CH, Ar), 128.3 (CH, Ar), 128.2 (C4''), 127.9 (C5''), 127.6 (CH, Ar), 127.4 (CH, Ar), 126.4 (C4'''), 126.1 (C8''), 123.2 (C6''), 123.0 (C7''), 120.9 (C1''a), 120.1 (C5), 112.4 (C3''), 55.8 (O-CH_3) and 21.5 (C1''); *m/z* (ES^+) 486.79 [$(M+Na)^+$, 100%]; HRMS (ES^+) [Found: $(M+Na)^+$, 487.1447, $C_{29}H_{24}N_2O_2NaS$ requires 487.1456] (-1.9 ppm).

1-(4'''-Methoxybenzyl)-5-[2''-benzyloxynaphthyl-(1'')-methyl]-6-phenyl-2-thioxo-2,3-dihydro-1*H*-pyrimidin-4-one (158)

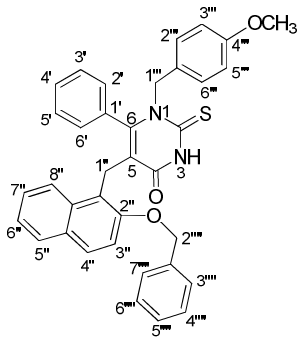

Yielded **158** (131 mg, 0.23 mmol, 25%) over 2 steps from ketoester **118** (400 mg, 1.06 mmol) as a white microcrystalline powder after column chromatography (Hexane/EtOAc, 90:10 to 80:20). Mp 100 °C (decomposes); ν_{max} cm^{-1} (KBr): 3420 (CONH), 2933 (CH_2), 1663 (C=O), 1594 (NH), 1513, 1431 (CSNH), 1248 (C=S), 1176 (C=S), 1084; δ_H (300 MHz, $CDCl_3$) 9.74 (brs, 1H, NH), 7.64 (dd, 1H, *J'* = 8.0 Hz, *J''* = 1.0 Hz, H-5''), 7.56-7.44 (m, 2H, H-4'' + 1 × ArH), 7.46-7.21 (m, 7H, H-6'', H-7'' + 5 × ArH), 7.00-6.87 (m, 2H, H-3'' + 1 × ArH), 6.76-6.66 (m, 2H, H-2' + 1 × ArH), 6.65-6.52 (m, 4H, H-2''', H-3''', H-5''', H-6'''), 6.30-6.09 (m, 2H, ArH), 4.85 (s, 2H, H-2''''), 4.12 (s, 2H, H-1'') and 3.75 (s, 3H, O-CH_3); δ_C (100 MHz, $CDCl_3$) 176.3 (C=S), 160.1 (C=O), 158.8 (C4'''), 153.5 (C2''), 152.9 (C6), 137.1 (C2''''a), 132.9 (C8''a), 131.1 (C1'), 129.1 (C4''a), 128.7 (CH, Ar × 2), 128.3 (C5''), 128.2 (CH, Ar), 128.1 (CH, Ar), 127.9 (CH, Ar), 127.6 (CH, Ar), 127.5 (CH, Ar), 126.3 (C7''), 123.3 (C8''), 123.2 (C6''), 120.7 (C1''a), 120.5 (C5), 113.7 (C3''', C5'''), 113.5 (C3''), 70.4 (C2''''), 55.3 (O-CH_3) and 21.7 (C1''); *m/z* (ES^+) 592.99 [$(M+Na)^+$, 100%].

1-Benzyl-5-[2''-benzyloxynaphthyl-(1'')-methyl]-6-phenyl-2-thioxo-2,3-dihydro-1*H*-pyrimidin-4-one (157)

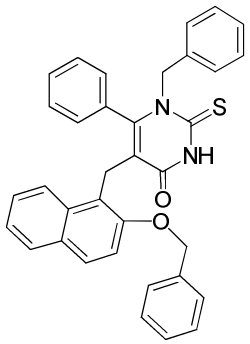

Yielded **157** (313 mg, 0.57 mmol, 31%) over 2 steps from **118** (820 mg, 2.1 mmol) as a white microcrystalline powder after column chromatography (Hexane/EtOAc, 90:10 to 80:20). Mp 189-191 °C; ν_{max} cm^{-1} (KBr): 3062 (CONH), 1593 (NH), 1646 (C=O), 1495 (CSNH), 1249

(C=S), 1171 (C=S); δ_H (400 MHz, $CDCl_3$) 10.43 (brs, 1H, NH), 7.53 (d, 1H, *J* = 8.1 Hz, H-5''), 7.42 (t, 2H, *J* = 9.8 Hz, H-6'' + 1 × ArH), 7.35-7.07 (m, 8H, ArH), 7.04-6.96 (m, 3H, ArH), 6.84 (t, 1H, *J* = 7.6 Hz, ArH), 6.78 (d, 1H, *J* = 9.0 Hz, H-3''), 6.62-6.49 (m, 3H, ArH), 6.06 (brs, 2H, ArH), 4.73 (s, 2H, H-2''') and 4.03 (s, 2H, H-1'');δ_C (100 MHz, $CDCl_3$) 176.3 (C=S), 160.5 (C=O), 153.5 (C2''), 153.1 (C6), 137.1 (C2''''a), 135.6 (C1'''a), 132.8 (C8''a), 131.1 (C1'), 129.0 (C4''a), 128.6 (CH, Ar), 128.3 (C5''), 128.0 (CH, Ar × 2), 127.7 (C4''), 127.5 (CH, Ar × 2), 127.4 (CH, Ar), 127.2 (CH, Ar), 127.1 (CH, Ar), 126.3 (CH, Ar), 126.1 (C7''), 123.3 (C6''), 123.1 (C8''), 120.6 (C1''a), 120.4 (C5), 113.3 (C3''), 70.3 (C2'''') and 21.6 (C1''); *m/z* (ES^+) 562.77 [$(M+Na)^+$, 100%].

1-(4'''-Methoxybenzyl)-5-[2''-methoxynaphtyl-(1'')-methyl]-6-phenyl-2-thioxo-2,3-dihydro-1*H*-pyrimidin-4-one (150)

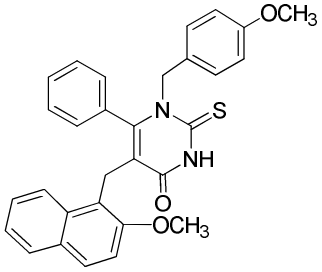

Yielded **150** (90 mg, 0.18 mmol, 33%) over 2 steps from **115** (200 mg, 0.67 mmol) as a white microcrystalline powder after column chromatography (Hexane/EtOAc, 80:20). Mp 159-161 °C; ν_{max} cm^{-1} (KBr): 3446 (CONH), 3058 (CONH), 2937 (CH_2), 1651 (C=O), 1591 (NH), 1486 (CSNH), 1251 (C=S), 1165 (C=S); δ_H (400 MHz, $CDCl_3$) 9.76 (brs, 1H, NH), 7.64 (dd, 1H, ^2J = 7.7 Hz, ^3J = 1.5 Hz, H-5''), 7.54 (d, 1H, *J* = 9.0 Hz, H-4''), 7.48 (d, 1H, *J* = 8.4 Hz, H-6''), 7.35-7.17 (m, 2 H, ArH), 7.00 (dt, 1H, ^2J = 7.5 Hz, ^3J = 1.0 Hz, ArH), 6.90-6.70 (m, 3H, H-3' + 2 × ArH), 6.70-6.55 (m, 4H, H-2'', H-3'', H-5'', H-6''), 6.26 (brs, 2H, ArH), 4.06 (s, 2H, H-1''), 3.74 (s, 3H, O-CH_3) and 3.60 (s, 3H, O-CH_3); δ_C (100 MHz, $CDCl_3$) 176.4 (C=S), 160.2 (C=O), 158.9 (C4'''), 154.0 (C2''), 153.0 (C6), 132.9 (C8''a), 131.1 (C1'), 129.0 (C4''a), 128.8 (C1'''a), 128.8 (C4''), 128.3 (C5''), 128.2 (CH, ArH 127.9 (C2''', C6'''), 127.6 (CH, ArH), 127.5 (CH, ArH), 126.3 (C7''), 123.2 (C6''), 123.1 (C8''), 120.8 (C1''a), 120.1 (C5), 113.8 (C3''', C5'''), 112.4 (C3''), 55.8 (O-CH_3), 55.3 (O-CH_3) and 21.4 (C1''); *m/z* (ES^+) 516.81 [$(M+Na)^+$, 100%]; HRMS (ES^+) [Found: $(M+Na)^+$, 517.1550, $C_{30}H_{26}N_2O_3NaS$ requires 517.1562] (-2.4 ppm).

1-(4'''-Ethoxybenzyl)-5-[2''-methoxynaphthyl-(1'')-methyl]-6-phenyl-2-thioxo-2,3-dihydro-1*H*-pyrimidin-4-one (151)

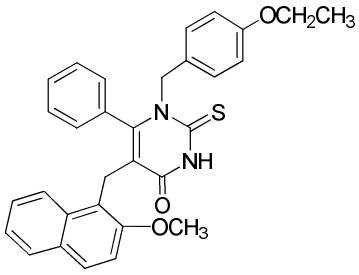

Yielded **151** (79 mg, 0.15 mmol, 26%) over 2 steps from **115** (220 mg, 0.73 mmol) as a white microcrystalline powder after column chromatography (Hexane/EtOAc, 90:10 to 80:20). Mp 112-115 °C; ν_{max} cm^{-1} (KBr): 3059 (CONH), 2934 (CH_2), 1659 (C=O), 1593 (NH), 1475 (CSNH), 1250 (C=S), 1165 (C=S); δ_H (400 MHz, $CDCl_3$) 10.01 (brs, 1H, NH), 7.54 (d, 1H, *J* = 7.9 Hz, H-5''), 7.44 (d, 1H, *J* = 9.0 Hz, H-4''), 7.39 (d, 1H, *J* = 8.4 Hz, H-8''), 7.26-7.09 (m, 2H, H-6'', H-7''), 6.89 (t, 1H, *J* = 7.6 Hz, H-4'), 6.74 (d, 1H, *J* = 9.0 Hz, H-3''), 6.69 (brs, 2H, H-3', H-5'), 6.55 (d, 2H, *J* = 8.9 Hz, AA'BB', H-3''', H-5'''), 6.48 (d, 2H, *J* = 8.9 Hz, AA'BB', H-2''', H-6'''), 6.16 (brs, 2H, H-2', H-6'), 3.97 (s, 2H, H-1''), 3.84 (q, 2H, *J* = 6.9 Hz, O-C$\underline{H_2}$$CH_3$), 3.49 (s, 3H, O-$CH_3$) and 1.27 (t, 3H, *J* = 6.9 Hz, O-CH_2C$\underline{H_3}$) δ_C (100 MHz, $CDCl_3$) 176.4 (C=S), 160.3 (C=O), 158.2 (C4'''), 154.4 (C2''), 153.1 (C6), 132.8 (C8''a), 131.1 (C1'), 128.9 (C4''a), 128.8 (C4'), 128.3 (C5''), 128.1 (C4''), 127.9 (C2', C6'), 127.6 (C1'''a), 127.5 (C3', C5'), 127.2 (C2''', C6'''), 126.3 (C7''), 123.2 (C6''), 123.0 (C8''), 120.8 (C1''a), 120.0 (C5), 114.3 (C3''', C5'''), 112.4 (C3''), 63.5 (O-$\underline{C}H_2CH_3$), 55.8 (O-CH_3), 21.4 (C1'') and 14.9 (O-$CH_2\underline{C}H_3$); *m/z* (ES^+) 530.78 [$(M+Na)^+$, 100%]; HRMS (ES^+) [Found: $(M+Na)^+$, 531.1728, $C_{31}H_{28}N_2O_3NaS$ requires 531.1718] (+1.8 ppm).

1-(4'''-Butoxybenzyl)-5-[2''-methoxynaphthyl-(1'')-methyl]-6-phenyl-2-thioxo-2,3-dihydro-1*H*-pyrimidin-4-one (153)

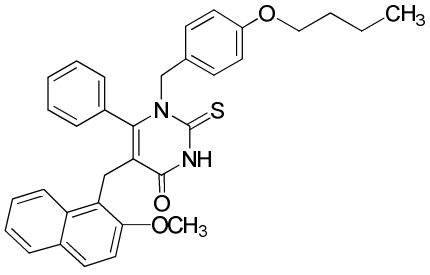

Yielded **153** (94 mg, 0.17 mmol, 20%) over 2 steps from **115** (325 mg, 1.08 mmol) as a white microcrystalline powder after column chromatography (Hexane/EtOAc, 90:10 to 80:20). Mp 95 °C (decomposes); ν_{max} cm^{-1} (KBr): 3426 (CONH), 2958 (CH_2), 1679 (C=O), 1613 (NH), 1512, 1473 (CSNH), 1176 (C=S); δ_H (400 MHz, $CDCl_3$) 9.82 (brs,1H, NH), 7.64 (d, 1H,

J = 7.9 Hz, H-5''), 7.55 (d, 1H, *J* = 9.0 Hz, H-4''), 7.47 (d, 1H, *J* = 8.5 Hz, H-6''), 7.33-7.17 (m, 2H, H-7'', H-8''), 6.99 (m, 1H, ArH), 6.90-6.73 (m, 3H, H-3'' + 2 × ArH), 6.66-6.54 (m, 4H, H-2'', H-3'', H-5'', H-6''), 6.28 (brs, 2H, ArH), 4.06 (s, 2H, H-1''), 3.87 (t, 2H, *J* = 6.5 Hz, O-C$\underline{H_2}$CH$_2$CH$_2$CH$_3$), 3.60 (s, 3H, O-CH$_3$), 1.79-1.65 (m, 2H, O-CH$_2$C$\underline{H_2}$CH$_2$CH$_3$), 1.53-1.40 (m, 2H, O-CH$_2$CH$_2$C$\underline{H_2}$CH$_3$) and 0.96 (t, 3H, *J* = 7.4 Hz, O-CH$_2$CH$_2$CH$_2$C$\underline{H_3}$); δ_C (100 MHz, CDCl$_3$) 176.6 (C=S), 160.4 (C=O), 158.7 (C4'''), 154.6 (C2''), 153.3 (C6), 133.1 (C8''a), 131.3 (C1'), 129.1 (C4''a), 129.0 (CH, Ar), 128.5 (CH, Ar), 128.4 (CH, Ar), 127.8 (CH, Ar), 127.7 (CH, Ar), 127.6 (C1'''a), 126.5 (C7''), 123.4 (C6''), 123.2 (C8''), 120.7 (C1''a), 119.9 (C5), 114.6 (CH, ArH), 112.6 (C3''), 68.0 (O-$\underline{C}$H$_2$CH$_2$CH$_2$CH$_3$), 56.0 (O-CH$_3$), 31.6 (O-CH$_2$$\underline{C}H_2CH_2CH_3$), 21.7 (C1''), 19.5 (O-CH$_2$CH$_2$$\underline{C}H_2CH_3$) and 14.2 (O-CH$_2CH_2CH_2$$\underline{C}H_3$); *m/z* (ES$^+$) 558.77 [(M+Na)$^+$, 100%]; HRMS (ES$^+$) [Found: (M+Na)$^+$, 559.2036, $C_{33}H_{32}N_2O_3NaS$ requires 559.2031] (+0.9 ppm).

1-Methyl -5-[2''-methoxynaphthyl-(1'')-methyl]-6-phenyl-2-thioxo-2,3-dihydro-1*H*-pyrimidin-4-one (154)

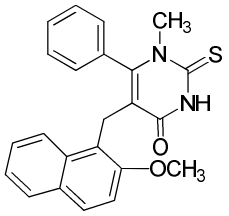

Yielded **154** (100 mg, 0.25 mmol, 24%) over 2 steps from **115** (400 mg, 1.34 mmol) as a white microcrystalline powder after column chromatography (Hexane/EtOAc, 90:10 to 80:20). Mp 235-237 °C; ν_{max} cm^{-1} (KBr): 1650 (C=O), 1267 (C=S), 1140 (C=S); δ_H (400 MHz, DMSO-d$_6$) 12.78 (brs, 1H, NH), 7.74 (d, 1H, *J* = 7.7 Hz, H-5''), 7.66 (d, 1H, *J* = 9.0 Hz, H-4''), 7.62 (d, 1H, *J* = 8.5 Hz, H-6''), 7.33 (dt, 1H, ^2J = 7.6 Hz, ^3J = 1.6 Hz, H-7''), 7.29-7.17 (m, 2H, H-8'', H-4'), 7.13 (t, 2H, *J* = 7.8 Hz, H-3', H-5'), 7.01 (d, 1H, *J* = 9.0 Hz, H-3''), 6.80 (d, 2H, *J* = 6.9 Hz, H-2', H-6'), 3.92 (s, 2H, H-1''), 3.54 (s, 3H, O-CH$_3$) and 3.10 (s, 3H, N-CH$_3$); δ_C (100 MHz, DMSO-d$_6$) 175.3 (C=S), 160.5 (C=O), 154.1 (C2''), 152.3 (C6), 132.4 (C8''a), 132.1 (C1'), 128.7 (C5''), 128.3 (C4''a), 128.2 (C4''), 128.1 (CH, Ar), 127.8 (CH, Ar), 127.5 (CH, Ar), 125.9 (C7''), 123.1 (C6''), 122.7 (C8''), 119.5 (C1''a), 118.5 (C5), 112.7 (C3''), 55.6 (O-CH$_3$), 40.1 (N-CH$_3$) and 20.9 (C1''); *m/z* (ES$^+$) 410.78 [(M+Na)$^+$, 100%]; HRMS (ES$^+$) [Found: (M+Na)$^+$, 411.1140, $C_{23}H_{20}N_2O_2NaS$ requires 411.1143] (-0.7 ppm).

1-Butyl-6-(4'-chlorophenyl)-5-[2-methoxynaphthyl-(1'')-methyl)-2-thioxo-2,3-dihydro-1*H*-pyrimidin-4-one (155)

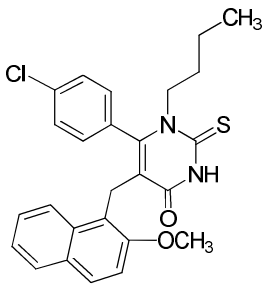

Yielded **155** (84 mg, 0.18 mmol, 33%) over 2 steps from **116** (215 mg, 0.64 mmol) as a white microcrystalline powder after column chromatography (Hexane/EtOAc, 90:10 to 80:20). Mp 172-174 °C; ν_{max} cm^{-1} (KBr): 3399 (CONH), 3069 (CONH), 2958 (CH_2), 1656 (C=O), 1594 (NH), 1488 (CSNH), 1252 (C=S); δ_H (400 MHz, $CDCl_3$) 9.71 (brs, 1H, NH), 7.69 (d, 1H, *J* = 7.7 Hz, H-5''), 7.62 (d, 1H, *J* = 8.9 Hz, H-4''), 7.46 (d, 1H, *J* = 8.5 Hz, H-8''), 7.34-7.22 (m, 2H, H-6'', H-7''), 6.95-6.84 (m, 3H, H-3'', H-3', H-5'), 6.42 (d, 2H, *J* = 8.4 Hz, AA'BB', H-2', H-6'), 4.10 (s, 2H, H-1''), 3.70 (brs, 2H, N-C$\underline{H_2}$$CH_2CH_2CH_3$), 3.64 (s, 3H, O-$CH_3$), 1.60 (brs, 2H, N-$CH_2C\underline{H_2}$$CH_2CH_3$), 1.40 (brs, 2H, br, 2H, N-CH_2CH_2C$\underline{H_2}$$CH_3$) and 0.60 (t, 3H, *J* = 7.3 Hz, N-$CH_2CH_2CH_2$C$\underline{H_3}$); δ_C (100 MHz, $CDCl_3$) 174.9 (C=S), 160.1 (C=O), 154.2 (C2''), 151.8 (C6), 135.3 (C4'), 132.8 (C8''a), 129.7 (C1'), 129.1 (CH, Ar), 128.8 (C4''a), 128.4 (CH, Ar), 128.3 (CH, Ar), 128.1 (CH, Ar), 126.7 (C7''), 123.3 (C8''), 123.1 (C6''), 120.7 (C5), 120.0 (C1''a), 112.1 (C3''), 55.7 (O-CH_3), 51.6 (N-$\underline{C}H_2CH_2CH_2CH_3$), 29.3 (N-$CH_2\underline{C}H_2CH_2CH_3$), 20.7 (N-$CH_2CH_2\underline{C}H_2CH_3$), 19.6 (C1'') and 13.2 (N-$CH_2CH_2CH_2\underline{C}H_3$); *m/z* ($ES^+$) 486.74 [$(M+Na)^+$, 100%]; HRMS ($ES^+$) [Found: $(M+Na)^+$, 487.1223, $C_{26}H_{25}N_2O_2NaSCl$ requires 487.1231] (+1.7 ppm).

1-Butyl-5-[2''-methoxynaphthyl-(1'')-methyl]-2-thioxo-6-(*o*-tolyl)-2,3-dihydro-1*H*-pyrimidin-4-one (156)

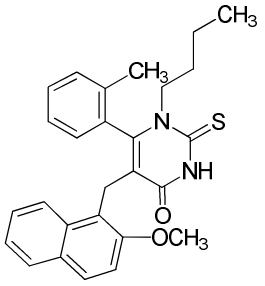

Yielded **156** (117 mg, 0.26 mmol, 31%) over 2 steps from **117** (320 mg, 1.0 mmol) as a white microcrystalline powder after column chromatography (Hexane/EtOAc, 90:10 to 80:20). Mp 176-178 °C; ν_{max} cm^{-1} (KBr): 2954 (CH_2), 1659 (C=O), 1493 (CSNH), 1252 (C=S); δ_H

(400 MHz, $CDCl_3$) 9.78 (brs, 1H, NH), 7.66 (dd, 1H, ^2J = 7.7 Hz, ^3J = 1.7 Hz, H-5''), 7.56 (d, 1H, J = 9.0 Hz, H-4''), 7.51 (d, 1H, J = 8.4 Hz, H-6''), 7.34-7.18 (m, 2H, H-7'', H-8''), 7.04 (dt, 1H, ^2J = 7.6 Hz, ^3J = 1.2 Hz, ArH), 6.87-6.74 (m, 3H, H-3'', ArH), 6.50 (d, 1H, J = 7.3 Hz, ArH), 4.28-4.02 (m, 3H, H1'', N-C$\underline{H_2}$$CH_2CH_2CH_3$), 3.56 (s, 3H, O-$CH_3$), 3.10 (m, 1H, N-C$\underline{H_2}$$CH_2CH_2CH_3$), 1.58 (m, 1H, N-$CH_2C\underline{H_2}$$CH_2CH_3$), 1.07 (m, 1H, N-$CH_2C\underline{H_2}$$CH_2CH_3$), 0.87-0.69 (m, 2H, N-$CH_2CH_2C\underline{H_2}$$CH_3$) and 0.54 (t, 3H, J = 7.4 Hz, N-$CH_2CH_2CH_2$C$\underline{H_3}$); δ_C (100 MHz, $CDCl_3$) 175.1 (C=S), 160.4 (C=O), 153.0 (C2''), 152 (C6), 135.8 (C2'), 133.1 (C8''a), 130.9 (C1'), 129.7 (CH, ArH), 129.5 (CH, ArH), 128.8 (C4''a), 128.4 (CH, Ar), 128.3 (CH, Ar), 128.0 (CH, Ar), 126.5 (C7''), 125.4 (CH, Ar), 123.2 (C6''), 123.0 (C8''), 120.0 (C1''a), 119.7 (C5), 112.1 (C3''), 55.6 (O-CH_3), 51.2 (N-$\underline{C}H_2CH_2CH_2CH_3$), 28.9 (N-$CH_2\underline{C}H_2CH_2CH_3$), 19.6 (N-$CH_2CH_2\underline{C}H_2CH_3$), 18.7 ($CH_3$) and 13.1 (N-$CH_2CH_2CH_2\underline{C}H_3$); *m/z* ($ES^+$) 466.84 [$(M+Na)^+$, 100%]; HRMS ($ES^+$) [Found: $(M+Na)^+$, 467.1755, $C_{27}H_{28}N_2O_2NaS$ requires 467.1769] (-3.0 ppm).

1-(4'''-Propoxybenzyl)-5-[2''-methoxynaphthyl-(1'')-methyl]-6-phenyl-2-thioxo-2,3-dihydro-1*H*-pyrimidin-4-one (152)

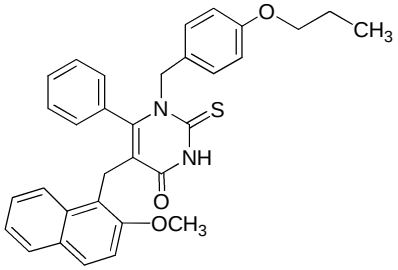

Yielded **152** (181 mg, 0.34 mmol, 39%) over 2 steps from **115** (325mg, 1.0 mmol) as a white microcrystalline powder after column chromatography (Hexane/EtOAc, 90:10 to 80:20). ν_{max} cm^{-1} (KBr): 3420 (CONH), 2963 (CH_2), 1656 (C=O), 1512 (NH), 1474 (CSNH), 1251 (C=S), 1175 (C=S); δ_H (400 MHz, $CDCl_3$) 10.04 (brs, 1H, NH), 7.64 (d, 1H, J = 8.0 Hz, H-5''), 7.54 (d, 1H, J = 9.1 Hz, H-4''), 7.48 (d, 1H, J = 8.4 Hz, H-8''), 7.32-7.19 (m, 2H, H-6'', H-7''), 7.14 (d, 1H, J = 8.5 Hz, ArH), 6.99 (dt, 1H, ^2J = 7.5 Hz, ^3J = 1.1 Hz, ArH), 6.88-6.74 (m, 2H, H-3'' + 1 × ArH), 6.67-6.55 (m, 4H, H-2''', H-3''', H-5''', H-6'''), 6.27 (brs, 2H, ArH), 4.05 (s, 2H, H-1''), 3.85 (t, 2H, J = 6.6 Hz, O-C$\underline{H_2}$$CH_2CH_3$), 3.60 (s, 3H, O-$CH_3$), 1.85-1.69 (m, 2H, O-$CH_2C\underline{H_2}$$CH_3$) and 1.01 (t, 3H, J = 5.3 Hz, O-CH_2CH_2C$\underline{H_3}$); δ_C (100 MHz, $CDCl_3$) 176.4 (C=S), 160.3 (C=O), 158.4 (C4'''a), 154.4 (C2''), 153.1 (C6), 132.9 (C8''a), 131.1 (C1'), 129.0 (CH, Ar), 128.8 (CH, ArH), 128.7 (C1'''a), 128.3 (CH, Ar), 128.1 (CH, Ar), 128.0 (CH, Ar), 127.5 (C2''', C6'''), 126.3 (C7''), 123.2 (C6''), 123.0 (C8''), 120.8 (C1''a), 120.0 (C5), 114.9 (C3''', C5'''), 112.4 (C3''), 69.6 (O-$\underline{C}H_2CH_2CH_3$), 55.8 (O-CH_3), 22.6 (O-$CH_2\underline{C}H_2CH_3$), 21.4 (C1'') and 10.6 (O-$CH_2CH_2\underline{C}H_3$);

m/z (ES^+) 544.78 [$(M+Na)^+$, 100%]; HRMS (ES^+) [Found: $(M+Na)^+$, 545.1879, $C_{32}H_{30}N_2O_3NaS$ requires 545.1875] (+ 0.7 ppm).

1-(4'''-Ethoxybenzyl)-5-[2''-benzyloxynaphthyl-(1'')-methyl]-6-phenyl-2-thioxo-2,3-dihydro-1*H*-pyrimidin-4-one (159)

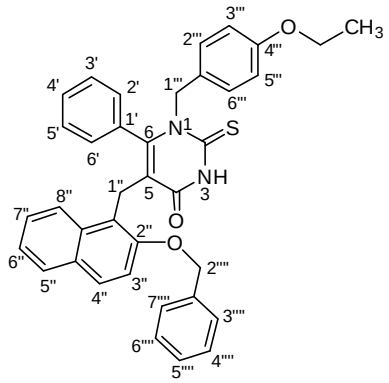

Yielded **159** (80 mg, 0.13 mmol, 39%) over 2 steps from **118** (442 mg, 1.18 mmol) as a white microcrystalline powder after column chromatography (Hexane/EtOAc, 90:10 to 80:20). Mp 85-90 °C (decomposes); ν_{max} cm^{-1} (KBr): 3446 (CONH), 1655 (C=O), 1513 (CSNH), 1177 (C=S); δ_H (400 MHz, $CDCl_3$) 9.58 (brs, 1H, NH), 7.64 (d, 1H, *J* = 7.8 Hz, ArH), 7.58-7.46 (m, 2H, ArH), 7.46-7-19 (m, 7H, ArH), 6.99-6.87 (m, 2H, ArH), 6.71 (brs, 2H, ArH), 6.61 (d, 2H, *J* = 8.7 Hz, ArH), 6.55 (d, 2H, *J* = 8.7 Hz, ArH), 6.19 (brs, 2H, ArH), 4.85 (s, 2H, H-2''''), 4.11 (s, 2H, H-1"), 3.94 (q, 2H, *J* = 7.0 Hz, O-C$\underline{H_2}$$CH_3$) and 1.37 (t, 3H, *J* = 7.0 Hz, O-CH_2C$\underline{H_3}$); δ_C (100 MHz, $CDCl_3$) 176.3 (C=S), 160.0 (C=O), 158.2 (C4'''), 153.5 (C2"), 152.9 (C6), 137.1 (C2''''a), 132.9 (C8"a), 131.1 (C1'), 130.1 (C4"a), 128.7 (CH, Ar), 128.6 (CH, Ar), 128.4 (CH, Ar), 128.1 (CH, Ar), 128.0 (CH, Ar), 127.8 (CH, Ar), 127.7 (CH, ArH), 127.6 (CH, Ar), 127.5 (CH, Ar), 127.5 (C1'"a), 126.3 (CH, Ar), 123.3 (CH, Ar), 123.2 (CH, Ar), 120.8 (C1"a), 120.5 (C5), 114.3 (CH, Ar), 113.4 (CH, Ar), 70.5 ($\underline{C}H_2$-Ph), 63.5 (O-$\underline{C}H_2CH_3$), 21.7 (C1") and 14.9 (O-$CH_2\underline{C}H_3$); *m/z* (ES^+) 585.07 [$(M+H)^+$, 100%].

1-(4'''-Propoxybenzyl)-5-[2''-benzyloxynaphthyl-(1'')-methyl]-6-phenyl-2-thioxo-2,3-dihydro-1*H*-pyrimidin-4-one (160)

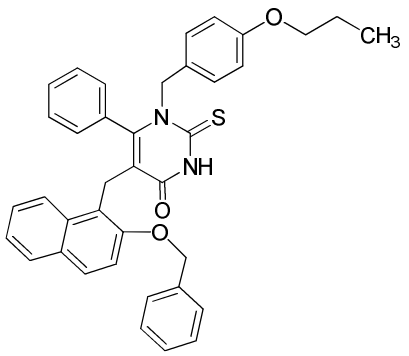

Yielded **160** (90 mg, 0.15 mmol, 21%) over 2 steps from **118** (246 mg, 0.65 mmol) as a white microcrystalline powder after column chromatography (Hexane/EtOAc, 90:10 to 80:20). Mp 85-90 °C (decomposes); ν_{max} cm^{-1} (KBr): 3420, 2963 (CH_2), 1678 (C=O), 1594 (CONH), 1512 (NH), 1474 (CSNH), 1274 (C=S), 1176 (C=S); δ_H (400 MHz, $CDCl_3$) 9.75 (brs, 1H, NH), 7.64 (d, 1H, *J* = 7.6 Hz, ArH), 7.52 (t, 2H, *J* = 9.3 Hz, ArH), 7.47-7.20 (m, 7H, ArH), 7.00-6.88 (m, 2H, ArH), 6.71 (brs, 2H, ArH), 6.62 (d, 2H, *J* = 8.7 Hz, ArH), 6.55 (d, 2H, *J* = 8.7 Hz, ArH), 6.20 (brs, 2H, ArH), 4.86 (s, 2H, H-2''''), 4.12 (s, 2H, H-1''), 3.82 (t, 2H, *J* = 6.6 Hz, O-C$\underline{H_2}$$CH_2CH_3$), 1.80-1.72 (m, 2H, O-$CH_2C\underline{H_2}$$CH_3$) and 1.04 (t, 3H, *J* = 7.5 Hz, O-CH_2CH_2C$\underline{H_3}$); δ_C (100 MHz, $CDCl_3$) 176.3 (C=S), 160.1 (C=O), 158.5 (C4'''), 153.5 (C2''), 152.9 (C6), 137.1 (C2''''a), 132.9 (C8''a), 131.1 (C1'), 129.0 (CH, Ar), 128.7 (CH, Ar), 128.3 (CH, Ar), 128.1 (CH, Ar), 128.0 (CH, Ar), 127.9 (CH, Ar), 127.6 (CH, Ar), 127.5 (CH, Ar × 2), 127.4 (C1'''a), 126.3 (CH, Ar), 123.3 (CH, Ar), 123.2 (CH, Ar), 120.7 (C1''a), 120.5 (C5), 114.3 (CH, Ar), 113.5 (CH, Ar), 70.4 ($\underline{C}H_2$-Ph), 69.6 (O-$\underline{C}H_2CH_2CH_3$), 22.6 (O-$CH_2\underline{C}H_2CH_3$), 21.7 (C1'') and 10.6 (O-$CH_2CH_2\underline{C}$H3); *m/z* (ES^+) 620.74 [$(M+Na)^+$, 100%]; HRMS (ES^+) [Found: $(M+Na)^+$, 621.2180, $C_{38}H_{34}N_2O_3NaS$ requires 621.2188] (-1.2 ppm).

6.4 1.4 General Procedure for Deprotection of the Naphtholic OH

To a stirring solution of **157-160** (1 eq) in DCM (4 mL) at -78 °C was added *n*Bu_4NI (1.1 eq.) and the resulting solution stirred for 5 min at -78 °C. BCl_3 (1.0 M in heptane, 2.5 eq.) was added dropwise and the reaction stirred for 5 min at the same temperature. After warming to 0 °C, the reaction mixture was stirred for further 2 h. After this time, an ice-water mixture was added, DCM removed at reduced pressure and the aqueous layer extracted with diethyl ether (3 × 5 mL). The organic layers were collected, washed with brine, dried ($MgSO_4$) and

concentrated at reduced pressure. The product was obtained as a white microcrystalline powder after purification by column chromatography (Hexane/EtOAc, 85:15).

1-Benzyl-5-[2''-hydroxynaphthyl-(1'')-methyl]-6-phenyl-2-thioxo-2,3-dihydro-1*H*-pyrimidin-4-one (93)

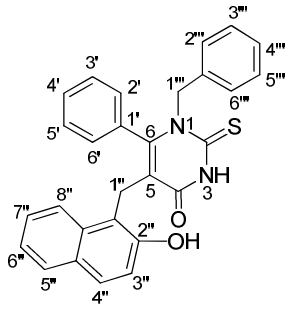

Yielded **93** (15 mg, 0.03 mmol, 53%) from **157** (41 mg, 0.07 mmol) as a white microcrystalline powder after column chromatography (Hexane/EtOAc, 85:15 to 80:20). Mp 94 °C (decomposes); ν_{max} cm^{-1} (KBr): 3420 (CONH or OH), 1655 (C=O), 1482 (CSNH), 1166 (C=S); δ_H (400 MHz, $CDCl_3$) 8.69 (brs, 1H, OH), 7.64 (d, 1H, J = 7.8 Hz, H-5"), 7.59 (d, 1H, J = 8.7 Hz, H-4"), 7.44-7.36 (m, 1H, H-4'), 7.31-7.09 (m, 8H, H-3", H-6" + 6 × ArH), 6.98 (dt, 2H, ^2J = 7.7 Hz, ^3J = 1.1 Hz, ArH), 6.91 (brs, 1H, ArH), 6.76 (dd, 1H, ^2J = 7.8 Hz, ^3J = 1.8 Hz, ArH), 6.71 (d, 1H, J = 8.8 Hz, ArH) and 3.90 (s, 2H, H-1"); δ_C (100 MHz, $CDCl_3$) 176.2 (C=S), 162.7 (C=O), 155.5 (C2"), 153.8 (C6), 135.2 (C1'"a), 133.2 (C1'), 131.2 (C8"a), 130.6 (CH, Ar), 129.3 (C4"a), 129.2 (CH, Ar), 129.0 (CH, Ar), 128.9 (CH, Ar), 128.6 (C4"), 128.5 (C5"), 127.7 (CH, Ar), 126.2 (CH, Ar), 125.7 (C7"), 122.5 (C6"), 122.4 (C8"), 120.5 (C3"), 118.2 (C1"a), 116.3 (C5) and 23.1 (C1"); *m/z* (ES^+) 472.81 [$(M+Na)^+$, 100%]; *m/z* (ES^-) 448.78 [$(M-H)^-$, 100%]; HRMS (ES^-) [Found: $(M-H)^-$, 449.1323, $C_{28}H_{21}N_2O_2S$ requires 449.1324] (-0.2 ppm).

1-(4'''-Methoxybenzyl)-5-[2''-hydroxynaphthyl-(1'')-methyl]-6-phenyl-2-thioxo-2,3-dihydro-1*H*-pyrimidin-4-one (92)

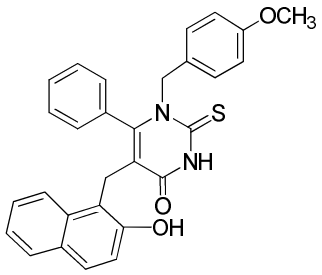

Yielded **92** (25 mg, 0.05 mmol, 46%) from **158** (65 mg, 0.11 mmol) as a white microcrystalline powder after column chromatography (Hexane/EtOAc, 85:15 to 80:20). Mp 90 °C

(decomposes); ν_{max} cm^{-1} (KBr): 3201 (CONH or OH), 1655 (C=O), 1513 (NH), 1176 (C=S); δ_H (400 MHz, $CDCl_3$) 10.15 (brs, 1H, NH), 8.70 (s, 1H, OH), 7.64 (d, 1H, *J* = 8.0 Hz, H-5''), 7.59 (d, 1H, *J* = 8.8 Hz, H-4''), 7.43 (t, 1H, *J* = 7.4 Hz, H-4'), 7.28 (brs, 2H, ArH), 7.21-7.07 (m, 2H, H-6'' + 1 × ArH), 7.04-6.84 (m, 3H, H-3'', H-7'' + 1 × ArH), 6.73-6.65 (m, 5H, H-2''', H-3''', H-5''', H-6''', H-8''), 3.89 (s, 2H, H-1'') and 3.75 (s, 3H, O-CH_3); δ_C (100 MHz, $CDCl_3$) 176.2 (C=S), 162.7 (C=O), 159.2 (C4'''), 155.6 (C2''), 153.8 (C6), 133.2 (C8''a), 131.2 (C1'), 130.6 (CH, Ar), 129.3 (CH, Ar), 129.3 (C4''a), 129.0 (C4''), 128.9 (C2''', C6'''), 128.5 (C5''), 127.8 (CH, Ar), 127.2 (C1'''a), 125.3 (C7''), 122.6 (C6''), 122.5 (C8''), 120.5 (C3''), 118.3 (C1''a), 116.4 (C5), 113.9 (C3''', C5'''), 55.4 (O-CH_3) and 23.2 (H-1''); *m/z* (ES^-) 478.84 [$(M-H)^-$, 100%]; HRMS (ES^+) [Found: $(M-H)^-$, 479.1439, $C_{29}H_{23}N_2O_3S$ requires 479.1429] (+1.9 ppm).

1-(4'''-Ethoxybenzyl)-5-[2''-hydroxynaphthyl-(1'')-methyl]-6-phenyl-2-thioxo-2,3-dihydro-1*H*-pyrimidin-4-one (94)

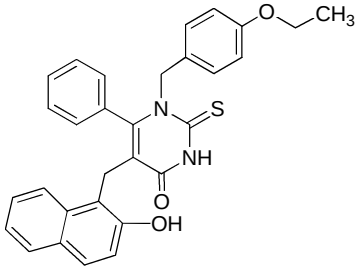

Yielded **94** (10 mg, 0.02 mmol, 22%) from **159** (54 mg, 0.09 mmol) as a white microcrystalline powder after column chromatography (Hexane/EtOAc, 85:15). Mp 185 °C (decomposes); δ_H (400 MHz, $CDCl_3$) 9.87 (brs, 1H, NH), 8.72 (brs, 1H, OH), 7.64 (d, 1H, *J* = 7.8 Hz, H-5''), 7.59 (d, 1H, *J* = 8.8 Hz, H-4''), 7.44 (t, 1H, *J* = 7.5 Hz, H-4'), 7.34-7.22 (m, 2H, H-6'', H-7''), 7.19-7.10 (m, 2H, ArH), 7.02-6.83 (m, 3H, ArH), 6.73-6.60 (m, 5H, H-2''', H-3''', H-5''', H-6''', H-8''), 3.89 (s, 2H, H-1''), 3.97 (q, 2H, *J* = 7.0 Hz, O-C$\underline{H_2}$$CH_3$) and 1.39 (t, 3H, *J* = 7.0 Hz, O-CH_2C$\underline{H_3}$); δ_C (100 MHz, $CDCl_3$) 176.0 (C=S), 162.7 (C=O), 158.4 (C4'''), 155.4 (C2''), 153.7 (C6), 133.1 (C8''a), 131.1 (C1'), 130.5 (CH, Ar), 129.3 (CH, Ar), 129.0 (CH, Ar), 128.8 (CH, ArH), 128.4 (CH, Ar), 127.7 (CH, Ar) , 126.9 (C), 125.7 (C7''), 122.4 (C8''), 122.3 (C6''), 120.4 (C3''), 118.2 (C1''a), 116.2 (C5), 114.4 (C3''', C5'''), 67.7 (O-$\underline{C}H_2CH_3$), 23.3 (C1''), 14.8 (O-$CH_2\underline{C}H_3$); *m/z* (ES^-) 493.11 [$(M-H)^-$, 100%]; *m/z* (ES^+) 517.12 [$(M+Na)^+$, 100%]; HRMS (ES^-) [Found: $(M-H)^-$, 493.1581, $C_{30}H_{25}N_2O_3S$ requires 493.1586] (-1.0 ppm).

1-(4'''-Propoxybenzyl)-5-[2''-hydroxynaphthyl-(1'')-methyl]-6-phenyl2-thioxo-2,3-dihydro-1*H*-pyrimidin-4-one (95)

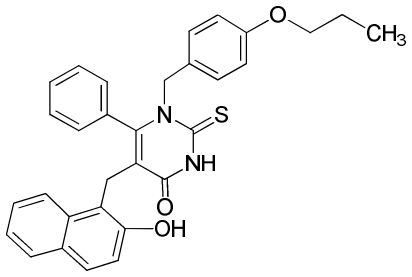

Yielded **95** (14 mg, 0.02 mmol, 25%) from **160** (67 mg, 0. 11 mmol) as a white microcrystalline powder after column chromatography (Hexane/EtOAc, 85:15). Mp 185 °C (decomposes); δ_H (400 MHz, $CDCl_3$) 9.75 (brs, 1H, NH), 8.72 (brs, 1H, OH), 7.64 (d, 1H, *J* = 7.9 Hz, H-5''), 7.59 (d, 1H, *J* = 8.9 Hz, H-4''), 7.46-7.39 (m, 1H, H-4'), 7.34-7.22 (m, 2H, H-6'', H-7''), 7.19-7.10 (m, 2H, ArH), 7.02-6.85 (m, 3H, ArH), 6.73-6.59 (m, 5H, H-2''', H-3''', H-5''', H-6''', H-8''), 3.89 (s, 2H, H-1''), 3.85 (t, 2H, *J* = 6.5 Hz, O-C$\underline{H_2}$$CH_2CH_3$), 1.84-1.71 (m, 2H, O-$CH_2C\underline{H_2}CH_3$) and 1.02 (t, 3H, *J* = 7.6 Hz, O-$CH_2CH_2C\underline{H_3}$); δ_C (100 MHz, $CDCl_3$) 174.5 (C=S), 162.5 (C=O), 158.7 (C4'''), 156.2 (C2''), 153.8 (C6), 133.3 (C8''a), 131.1 (C1'), 130.6 (CH, Ar), 129.3 (CH, Ar), 129.0 (C4''), 128.8 (CH, Ar), 128.5 (C5''), 128.4 (C4''a), 127.8 (CH, Ar), 127.4 (C1'''a), 125.7 (C7''), 122.5 × 2 (C6'', C8''), 120.4 (C3''), 118.3 (C1''a), 116.1 (C5), 114.5 (C3''', C5'''), 69.6 (O-$\underline{C}H_2CH_2CH_3$), 29.8 (O-$CH_2\underline{C}H_2CH_3$), 22.6 (C1'') and 10.7 (O-$CH_2CH_2\underline{C}H_3$). *m/z* (ES^-) 507.07 [$(M-H)^-$, 100%]; *m/z* (ES^+) 531.07 [$(M+Na)^+$, 100%]; HRMS (ES^-) [Found: $(M-H)^-$, 531.1720, $C_{31}H_{28}N_2O_3SNa$ requires 531.1718] (0.3 ppm).

6.5 PART I-III: Computational and Biological Procedures

6.5.1 Molecular Docking and Molecula Dynamics Simulations

The SIRT2 structure (PDB ID: 1J8F, chain-A residues 57-356) was used for the molecular docking studies which were performed using the program GOLD.[109] A homology model of SIRT1 was generated using the PHYRE server. All visualisation and analysis were performed using Pymol.[139] Hydrogen atoms were added to the protein structure using the program Reduc and small molecule structures were generated using the PRODRG server.[140] The neighbouring residues around the C pocket were identified from the previously reported work and these residues were used to define sphere (15 Å) in flexible docking.[34] The selected residues were also allowed to be flexible during docking. Top ten poses were saved for each ligand after docking and 100 steps of rigid body minimization followed by simulated annealing. Each of the 10 poses saved after docking were re-scored with the best score for each molecule being retained and subsequently used for further molecular dynamics study.

The top 2 poses were selected for the subsequent molecular dynamics study for Sirtuin2. Molecular dynamics simulations were performed with the SANDER module of the AMBER9 package employing the all-atom Cornell force field.[126] Simulations were carried out for the complexes of ligand-SIRT2 and ligand-SIRT1. In addition, simulations were also carried out for the uncomplexed proteins separately. Each system was solvated with a TIP3P water box whose sides are at a minimum distance of 8 Å to any protein atom.[141] Initially, the whole system was minimized for 4,000 steps, to remove any unfavourable interactions. Subsequently, the systems were each heated to 300 K for 75 ps under NPT conditions. After this, each system was simulated for 20 ns at constant temperature (300 K) and pressure (1 atm) and structures were stored every 1 ps. The free energy of binding (ΔGbind) of the peptides to MDM2 was computed using the MM-GBSA (molecular mechanics/Generalized Born surface area) method using the GB module in Amber while the non-polar component was estimated from the solvent accessible surface area using MOLSURF.[142,143] Each energy term was averaged over frames taken every 50 ps from the simulation. Vibrational entropy was estimated using normal mode analysis (Nmode module of Amber) and averaged over 500 ps intervals.[144]

6.5.2 *In Vitro* SIRT1 and SIRT2 Inhibition Assay

Compounds were tested for inhibition of SIRT1 and SIRT2 using the human recombinant SIRT1 and SIRT2 enzymes provided with the Fluor de Lys^{TM} fluorescent-based assay kit (AK555, AK556, BIOMOL, Plymouth Meeting, U.S.A.).[105] All the other required reagents were provided with the kit. All kit components were stored at -78 °C to ensure the highest stability. Positive controls were provided by the known SIRT1/T2 inhibitors tenovin-6 (**38**), cambinol (**39**) and analogues **46** and **47**.[11,18,103]

Fresh dilutions of cambinol analogues were prepared in DMSO (Aldrich), added to the assay buffer and pipetted (10 μL) into a white 96 well white microplate. Enzyme (15 μL, 0.02 U/μL for SIRT1, 0.1 U/μL for SIRT2) and Fluor de Lys SIRT1 or SIRT2 (15 µM) plus NAD^+ (1 mM) in assay buffer were added. After incubating for 1 h at 37 °C, a developer solution (250 μL developer and 50 μL nicotinamide in 950 μL of buffer) was added (50 μL) to each well and the microplate incubated for a further 45 min at room temperature. Plates were read in a microplate Spectra max Gemini XS$^{(TM)}$ fluorimeter with an excitation wavelength of 355 nm and an emission wavelength of 460 nm.

6.5.3 Cell Culture and Western Blotting

Human cancer cell lines MCF-7 were cultured in Dulbecco's modified Eagle's medium (DMEM, Invitrogen, UK), while H1299 cells were cultured in RPMI. Both were supplemented with 10% fetal calf serum (FCS, Hyclone, UK) and gentamycin (complete medium). Cells were seeded at a concentration of 2×10^5 (MCF-7) and 6×10^4 (H1299) in 6 well collagen pre-coated plates (TPP, Helena Biosciences, UK) and incubated in a humidified atmosphere containing 5% CO_2:95% air at 37 °C for 42 h (MCF-7) and 24 h (H1299). A range of concentrations of the target compounds in DMSO were added to MCF-7 and they were incubated for a further 6 h. A range of concentrations of the target compounds in DMSO were also added to H1299 cells with 40 nM thrichostatin (TSA) also being added, and the mixture incubated for a further 24 h. After lysing the cells with 1 × LDS sample buffer (100 µL per well for MCF-7s and 200 µL for H1299) (Invitrogen, UK), the protein concentration was assessed with a BCA protein assay kit (Pierce, UK) and the concentration of proteins equalised with 1 × LDS sample buffer. Proteins were separated with 4-12% bis-tris gels (Invitrogen, USA) and electrophoretically transferred to PVDF transfer membranes (Millipore, UK). Membranes were blocked with Marvel non-fat

milk (45 min, 5% solution in PBS/0.1% tween) and immunoblotted using a rabbit polyclonal antibody against p53 acetylated at K382 (Biolegend, UK) and DO.1 (anti total p53, in-house produced) for the MCF-7 membranes. PC-10 mouse monoclonal antibody (in house produced) was used to detect PCNA as a loading control. Anti-K40 acetylated tubulin (SIGMA) and anti α-tubulin (SIGMA) were used for the H1299 membranes. All the primary antibodies were diluted in Marvel non-fat milk (5% solution in PBS/0.1% tween). The secondary antibody used against anti-acetylated p53 was a HRP-tagged polyclonal swine anti-rabbit IgG (DAKO, UK). The secondary antibody used against the remaining primary antibodies was a HRP-tagged polyclonal rabbit anti-mouse IgG (DAKO, UK). After incubation with primary (1 h) and secondary antibodies (45 min), bound antibody was visualized with enhanced chemiluminescence (ECL) western blotting developer (Amersham, UK) in a darkroom.

Part I, References

(1) *Cancer Research UK home page. http://www.cancerresearchuk.org. (Accessed July 2010)*

(2) Landis, S. H.; Murray, T.; Bolden, S.; Wingo, P. A. *Canc. J. Clinic.* **1998**, *48*, 6-29.

(3) Willis, R. A. *The Spread of Tumours in the Human Body* **1952**, *London, Butterworth & Co.*

(4) Cotran, R. S.; Collins, T. *Pathologic Basis of Disease, VI edition*, Elsevier.

(5) Lane, D. P.; Crawford, L. V. *Nature* **1979**, *278*, 261-263.

(6) Koshland, D. E. *Science* **1993**, *262*, 1953.

(7) Gallagher, W. M.; Brown, R. *Ann. Onc.* **1999**, *10*, 139-150.

(8) Lain, S.; Lane, D. P. *Eur. J. Cancer* **2003**, *39*, 1053-1060.

(9) Vousden, K. H.; Lane, D. P. *Nat. Rev. Mol. Cell Biol.* **2007**, *8*, 275-283.

(10) Berkson, R. G.; Hollick, J. J.; Westwood, N. J.; Woods, J. A.; Lane, D. P.; Lain, S. *Int. J. Cancer* **2005**, *115*, 701-710.

(11) Lain, S.; Hollick, J. J.; Campbell, J.; Staples, O. D.; Higgins, M.; Aoubala, M.; McCarthy, A.; Appleyard, V.; Murray, K. E.; Baker, L.; Thompson, A.; Mathers, J.; Holland, S. J.; Stark, M. J. R.; Pass, G.; Woods, J.; Lane, D. P.; Westwood, N. J. *Cancer Cell* **2008**, *13*, 454-463.

(12) Lane, D. P.; Lain, S. *Trends Mol. Med.* **2002**, *8*, S38-S42.

(13) Brooks, C. L.; Gu, W. *Mol. Cell* **2006**, *21*, 307-315.

(14) Smith, J. S. *TRENDS in Cell Biology* **2002**, *12*, 404-406.

(15) Sauve, A. A., Wolberger, C., Schramm, V. L., Boeke, J. D. *Annual Review of Biochemistry* **2006**, *75*, 453-465.

(16) Ford, J.; Jiang, M.; Milner, J. *Cancer Res.* **2005**, *65*, 10457-10463.

(17) Cho, Y.; Gorina, S.; Jeffrey, P. D.; Pavletich, N. P. *Science* **1994**, *265*, 346-355.

(18) Heltweg, B.; Gatbonton, T.; Schuler, A. D.; Posakony, J.; Li, H.; Goehle, S.; Kollipara, R.; DePinho, R. A.; Gu, Y.; Simon, J. A.; Bedalov, A. *Cancer Res.* **2006**, *66*, 4368-4377.

(19) Sterner, D. E.; Berger, S. L. *Microbiol. Mol. Rev.* **2000**, *64*, 435-459.

(20) Itoh, Y.; Takayoshi, S.; Naoki, M. *Curr. Pharm. Des.* **2008**, *14*, 529-544.

(21) Lin, H. *Org. Biomol. Chem.* **2007**, *5*, 2541-2554.

(22) Michan, S.; Sinclair, D. *Biochem. J.* **2007**, *404*, 1-13.

(23) Haigis, M. C.; Guarente, L. P. *Genes Dev.* **2006**, *20*, 2913-2921.

(24) Sauve, A. A.; Celic, I.; Avalos, J.; Deng, H. T.; Boeke, J. D.; Schramm, V. L. *Biochemistry* **2001**, *40*, 15456-15463.

(25) Jackson, A. D.; Denu, J. M. *J. Biol. Chem.* **2002**, *277*, 18535-18544.

(26) Tong, L.; Denu, J. M. *Biochim. Biophys. Acta - Proteins and Proteomics* **2010**, *1804*, 1617-1625.

(27) Sauve, A. A. *Biochim. Biophys. Acta - Proteins and Proteomics* **2010**, *1804*, 1591-1603.

(28) Smith, B. C.; Denu, J. M. *Biochemistry* **2006**, *45*, 272-282.

(29) Anderson, R. M.; Bitterman, K. J.; Wood, J. G.; Medvedik, O.; Sinclair, D. A. *Nature* **2003**, *423*, 181-185.

(30) Bitterman, K. J.; Anderson, R. M.; Cohen, H. Y.; Latorre-Esteves, M.; Sinclair, D. A. *J. Biol. Chem.* **2002**, *277*, 45099-45107.

(31) Min, J. R.; Landry, J.; Sternglanz, R.; Xu, R. M. *Cell* **2001**, *105*, 269-279.

(32) Liszt, G.; Ford, E.; Kurtev, M.; Guarente, L. *J. Biol. Chem.* **2005**, *280*, 21313-21320.

(33) Haigis, M. C.; Mostoslavsky, R.; Haigis, K. M.; Fahie, K.; Christodoulou, D. C.; Murphy, A. J.; Valenzuela, D. M.; Yancopoulos, G. D.; Karow, M.; Blander, G.; Wolberger, C.; Prolla, T. A.; Weindruch, R.; Alt, F. W.; Guarente, L. *Cell* **2006**, *126*, 941-954.

(34) Avalos, J. L.; Celic, I.; Muhammad, S.; Cosgrove, M. S.; Boeke, J. D.; Wolberger, C. *Mol. Cell* **2002**, *10*, 523-535.

(35) Zhao, K. H.; Chai, X. M.; Clements, A.; Marmorstein, R. *Nat. Struct. Biol.* **2003**, *10*, 864-871.

(36) Finnin, M. S.; Donigian, J. R.; Pavletich, N. P. *Nat. Struct. Biol.* **2001**, *8*, 621-625.

(37) Jin, L.; Wei, W. T.; Jiang, Y. B.; Peng, H.; Cai, J. H.; Mao, C.; Dai, H.; Choy, W.; Bemis, J. E.; Jirousek, M. R.; Milne, J. C.; Westphal, C. H.; Perni, R. B. *J. Biol. Chem.* **2009**, *284*, 24394-24405.

(38) Antoshenko, T.; Min, J. R.; Schuetz, A.; Loppnau, P.; Edwards, A. M.; Arrowsmith, C. H.; Bochkarev, A.; Plotnikov, A. N. *PDB ID: 2B4Y, to be pubblished*.

(39) Schuetz, A.; Min, J. R.; Antoshenko, T.; Wang, C. L.; Allali-Hassani, A.; Dong, A. P.; Loppnau, P.; Vedadi, M.; Bochkarev, A.; Sternglanz, R.; Plotnikov, A. N. *Structure* **2007**, *15*, 377-389.

(40) Sanders, B. D.; Jackson, B.; Marmorstein, R. *Biochim. Biophys. Acta - Proteins and Proteomics* **2010**, *1804*, 1604-1616.

(41) Zhao, K. H.; Chai, X. M.; Marmorstein, R. *J. Mol. Biol.* **2004**, *337*, 731-741.

(42) Avalos, J. L.; Boeke, J. D.; Wolberger, C. *Mol. Cell* **2004**, *13*, 639-648.

(43) Sanders, B. D.; Zhao, K. H.; Slama, J. T.; Marmorstein, R. *Mol. Cell* **2007**, *25*, 463-472.

(44) Wolberger, C. *Mol. Cell* **2007**, *28*, 1102-1103.

(45) Zhao, K. H.; Harshaw, R.; Chai, X. M.; Marmorstein, R. *Proc. Nati. Acad. Sci. USA* **2004**, *101*, 8563-8568.

(46) Hoff, K. G.; Avalos, J. L.; Sens, K.; Wolberger, C. *Structure* **2006**, *14*, 1231-1240.

(47) Avalos, J. L.; Bever, K. M.; Wolberger, C. *Mol. Cell* **2005**, *17*, 855-868.

(48) Cosgrove, M. S.; Bever, K.; Avalos, J. L.; Muhammad, S.; Zhang, X. B.; Wolberger, C. *Biochemistry* **2006**, *45*, 7511-7521.

(49) McLaughlin, F.; La Thangue, N. B. *Biochem. Pharmacol.* **2004**, *68*, 1139-1144.

(50) Porcu, M.; Chiarugi, A. *Trends in Pharmacological Sciences* **2005**, *26*, 94-103.

(51) Vaziri, H.; Dessain, S. K.; Eagon, E. N.; Imai, S. I.; Frye, R. A.; Pandita, T. K.; Guarente, L.; Weinberg, R. A. *Cell* **2001**, *107*, 149-159.

(52) Luo, J. Y.; Nikolaev, A. Y.; Imai, S.; Chen, D. L.; Su, F.; Shiloh, A.; Guarente, L.; Gu, W. *Cell* **2001**, *107*, 137-148.

(53) Cohen, H. Y.; Lavu, S.; Bitterman, K. J.; Hekking, B.; Imahiyerobo, T. A.; Miller, C.; Frye, R.; Ploegh, H.; Kessler, B. M.; Sinclair, D. A. *Mol. Cell* **2004**, *13*, 627-638.

(54) Brunet, A.; Sweeney, L. B.; Sturgill, J. F.; Chua, K. F.; Greer, P. L.; Lin, Y. X.; Tran, H.; Ross, S. E.; Mostoslavsky, R.; Cohen, H. Y.; Hu, L. S.; Cheng, H. L.; Jedrychowski, M. P.; Gygi, S. P.; Sinclair, D. A.; Alt, F. W.; Greenberg, M. E. *Science* **2004**, *303*, 2011-2015.

(55) Bereshchenko, O. R.; Gu, W.; Dalla-Favera, R. *Nat. Genet.* **2002**, *32*, 606-613.

(56) Cheng, H. L.; Mostoslavsky, R.; Saito, S.; Manis, J. P.; Gu, Y. S.; Patel, P.; Bronson, R.; Appella, E.; Alt, F. W.; Chua, K. F. *Proc. Nati. Acad. Sci. USA* **2003**, *100*, 10794-10799.

(57) Ota, H.; Tokunaga, E.; Chang, K.; Hikasa, M.; Iijima, K.; Eto, M.; Kozaki, K.; Akishita, M.; Ouchi, Y.; Kaneki, M. *Oncogene* **2006**, *25*, 176-185.

(58) Kim, J. E.; Chen, J. J.; Lou, Z. K. *Nature* **2008**, *451*, 583-U10.

(59) Bradbury, C.; Khanim, F.; Hayden, R.; Bunce, C. M.; White, D. A.; Drayson, M. T.; Craddock, C.; Turner, B. M. *Leukemia* **2005**, *19*, 1751-1759.

(60) Huffman, D. M.; Grizzle, W. E.; Bamman, M. M.; Kim, J. S.; Eltoum, I. A.; Elgavish, A.; Nagy, T. R. *Cancer Res.* **2007**, *67*, 8423-8423.

(61) Stunkel, W.; Peh, B. K.; Tan, Y. C.; Nayagam, V. M.; Wang, X.; Salto-Tellez, M.; Ni, B.; Entzeroth, M.; Wood, J. *Biotechnol. J.* **2007**, *2*, 1360-8.

(62) Hida, Y.; Kubo, Y.; Murao, K.; Arase, S. *Arch. Dermatol. Res.* **2007**, *299*, 103-106.

(63) Vaquero, A.; Scher, M. B.; Lee, D. H.; Sutton, A.; Cheng, H. L.; Alt, F. W.; Serrano, L.; Sternglanz, R.; Reinberg, D. *Genes Dev.* **2006**, *20*, 1256-1261.

(64) Bae, N. S.; Swanson, M. J.; Vassilev, A.; Howard, B. H. *J. Biochem.* **2004**, *135*, 695-700.

(65) Dryden, S. C.; Nahhas, F. A.; Nowak, J. E.; Goustin, A. S.; Tainsky, M. A. *Mol. Cell. Biol.* **2003**, *23*, 3173-3185.

(66) Lavu, S.; Boss, O.; Elliott, P. J.; Lambert, P. D. *Nat. Rev. Drug Discovery* **2008**, *7*, 841-853.

(67) North, B. J.; Verdin, E. *J. Biol. Chem.* **2007**, *282*, 19546-19555.

(68) Pandithage, R.; Lilischkis, R.; Harting, K.; Wolf, A.; Jedamzik, B.; Luscher-Firzlaff, J.; Vervoorts, J.; Lasonder, E.; Kremmer, E.; Knoll, B.; Luscher, B. *J. Cell Biol.* **2008**, *180*, 915-929.

(69) North, B. J.; Marshall, B. L.; Borra, M. T.; Denu, J. M.; Verdin, E. *Mol. Cell* **2003**, *11*, 437-444.

(70) Inoue, T.; Hiratsuka, M.; Osaki, M.; Oshimura, M. *Cell Cycle* **2007**, *6*, 1011-1108.

(71) Hiratsuka, M.; Inoue, T.; Toda, T.; Kimura, N.; Shirayoshi, Y.; Kamitani, H.; Watanabe, T.; Ohama, E.; Tahimic, C. G. T.; Kurimasa, A.; Oshimura, M. *Biochem. Biophys. Res. Comm.* **2003**, *309*, 558-566.

(72) Jin, Y. H.; Kim, Y. J.; Kim, D. W.; Baek, K. H.; Kang, B. Y.; Yeo, C. Y.; Lee, K. Y. *Biochem. Biophys. Res. Comm.* **2008**, *368*, 690-695.

(73) Harting, K.; Knoll, B. *Eur. J. Cell Biol.* **2010**, *89*, 262-269.

(74) Alcain, F. J.; Villalba, J. M. *Expert Opinion on Therapeutic Patents* **2009**, *19*, 283-294.

(75) Grubisha, O.; Smith, B. C.; Denu, J. M. *Febs J.* **2005**, *272*, 4607-4616.

(76) Ouaissi, M.; Ouaissi, A. *J. Biomed. Biotechnol.* **2006**.

(77) Cen, Y. *Biochim. Biophys. Acta* **2010**, *1804*, 1635-1644.

(78) Sauve, A. A.; Schramm, V. L. *Biochemistry* **2003**, *42*, 9249-9256.

(79) Prusty, D.; Mehra, P.; Srivastava, S.; Shivange, A. V.; Gupta, A.; Roy, N.; Dhar, S. K. *Fems Microbiol Lett.* **2008**, *282*, 266-272.

(80) Suzuki, T.; Imai, K.; Nakagawa, H.; Miyata, N. *Chem. Med. Chem.* **2006**, *1*, 1059-1062.

(81) Fatkins, D. G.; Monnot, A. D.; Zheng, W. P. *Bioorg. Med. Chem. Lett.* **2006**, *16*, 3651-3656.

(82) Kiviranta, P. H.; Suuronen, T.; Wallen, E. A. A.; Leppanen, J.; Tervonen, J.; Kyrylenko, S.; Salminen, A.; Poso, A.; Jarho, E. M. *J. Med. Chem.* **2009**, *52*, 2153-2156.

(83) Grozinger, C. M.; Chao, E. D.; Blackwell, H. E.; Moazed, D.; Schreiber, S. L. *J. Biol. Chem.* **2001**, *276*, 38837-38843.

(84) Mai, A.; Massa, S.; Lavu, S.; Pezzi, R.; Simeoni, S.; Ragno, R.; Mariotti, F. R.; Chiani, F.; Camilloni, G.; Sinclair, D. A. *J. Med. Chem.* **2005**, *48*, 7789-7795.

(85) Lara, E.; Mai, A.; Calvanese, V.; Altucci, L.; Lopez-Nieva, P.; Martinez-Chantar, M. L.; Varela-Rey, M.; Rotili, D.; Nebbioso, A.; Ropero, S.; Montoya, G.; Oyarzabal, J.; Velasco, S.; Serrano, M.; Witt, M.; Villar-Garea, A.; Imhof, A.; Mato, J. M.; Esteller, M.; Fraga, M. F. *Oncogene* **2009**, *28*, 1168-1168.

(86) Napper, A. D.; Hixon, J.; McDonagh, T.; Keavey, K.; Pons, J. F.; Barker, J.; Yau, W. T.; Amouzegh, P.; Flegg, A.; Hamelin, E.; Thomas, R. J.; Kates, M.; Jones, S.; Navia, M. A.; Saunders, J.; DiStefano, P. S.; Curtis, R. *J. Med. Chem.* **2005**, *48*, 8045-8054.

(87) Kiviranta, P. H.; Leppanen, J.; Rinne, V. M.; Suuronen, T.; Kyrylenko, O.; Kyrylenko, S.; Kuusisto, E.; Tervo, A. J.; Jarvinen, T.; Salminen, A.; Poso, A.; Wallen, E. A. A. *Bioorg. Med. Chem. Lett.* **2007**, *17*, 2448-2451.

(88) Huhtiniemi, T.; Wittekindt, C.; Laitinen, T.; Leppanen, J.; Salminen, A.; Poso, A.; Lahtela-Kakkonen, M. *J. Comput. Aided Mol. Des.* **2006**, *20*, 589-599.

(89) Trapp, J.; Jochum, A.; Meier, R.; Saunders, L.; Marshall, B.; Kunick, C.; Verdin, E.; Goekjian, P.; Sippl, W.; Jung, M. *J. Med. Chem.* **2006**, *49*, 7307-7316.

(90) Hirao, M.; Posakony, J.; Nelson, M.; Hruby, H.; Jung, M. F.; Simon, J. A.; Bedalov, A. *J. Biol. Chem.* **2003**, *278*, 52773-52782.

(91) Bedalov, A.; Gatbonton, T.; Irvine, W. P.; Gottschling, D. E.; Simon, J. A. *Proc. Nati. Academ. Sci. USA* **2001**, *98*, 15113-15118.

(92) Posakony, J.; Hirao, M.; Stevens, S.; Simon, J. A.; Bedalov, A. *J. Med. Chem.* **2004**, *47*, 2635-2644.

(93) Pagans, S.; Pedal, A.; North, B. J.; Kaehlcke, K.; Marshall, B. L.; Dorr, A.; Hetzer-Egger, C.; Henklein, P.; Frye, R.; McBurney, M. W.; Hruby, H.; Jung, M.; Verdin, E.; Ott, M. *Plos Biol.* **2005**, *3*, 210-220.

(94) Neugebauer, R. C.; Uchiechowska, U.; Meier, R.; Hruby, H.; Valkov, V.; Verdin, E.; Sippl, W.; Jung, M. *J. Med. Chem.* **2008**, *51*, 1203-1213.

(95) Howitz, K. T.; Bitterman, K. J.; Cohen, H. Y.; Lamming, D. W.; Lavu, S.; Wood, J. G.; Zipkin, R. E.; Chung, P.; Kisielewski, A.; Zhang, L. L.; Scherer, B.; Sinclair, D. A. *Nature* **2003**, *425*, 191-196.

(96) Trapp, J.; Meier, R.; Hongwiset, D.; Kassack, M. U.; Sippl, W.; Jung, M. *Chem. Med. Chem.* **2007**, *2*, 1419-1431.

(97) Uciechowska, U.; Schemies, J.; Neugebauer, R. C.; Huda, E. M.; Schmitt, M. L.; Meier, R.; Verdin, E.; Jung, M.; Sippl, W. *Chem. Med. Chem.* **2008**, *3*, 1965-1976.

(98) Outeiro, T. F.; Kontopoulos, E.; Altmann, S. M.; Kufareva, I.; Strathearn, K. E.; Amore, A. M.; Volk, C. B.; Maxwell, M. M.; Rochet, J. C.; McLean, P. J.; Young, A. B.; Abagyan, R.; Feany, M. B.; Hyman, B. T.; Kazantsev, A. G. *Science* **2007**, *317*, 516-519.

(99) Luthi-Carter, R.; Taylor, D. M.; Pallos, J.; Lambert, E.; Amore, A.; Parker, A.; Moffitt, H.; Smith, D. L.; Runne, H.; Gokce, O.; Kuhn, A.; Xiang, Z. M.; Maxwell, M. M.; Reeves, S. A.; Bates, G. P.; Neri, C.; Thompson, L. M.; Marsh, J. L.; Kazantsev, A. G. *Proc. Nati. Ac. Sci. U. S. A.*, *107*, 7927-7932.

(100) Gey, C.; Kyrylenko, S.; Hennig, L.; Nguyen, L. H. D.; Butner, A.; Pham, H. D.; Giannis, A. *Angew. Chem. Int. Ed.* **2007**, *46*, 5219-5222.

(101) Gutierrez, M.; Andrianasolo, E. H.; Shin, W. K.; Goeger, D. E.; Yokochi, A.; Schemies, J.; Jung, M.; France, D.; Cornell-Kennon, S.; Lee, E.; Gerwick, W. H. *J. Org. Chem.* **2009**, *74*, 5267-5275.

(102) Rotili, D.; Tarantino, D.; Carafa, V.; Lara, E.; Meade, S.; Botta, G.; Nebbioso, A.; Schemies, J.; Jung, M.; Kazantsev, A. G.; Esteller, M.; Fraga, M. F.; Altucci, L.; Mai, A. *Chem. Med. Chem.* **2010**, *5*, 674-677.

(103) Medda, F. *MSc by Research in Life Sciences Final Dissertation, The University of Edinburgh* **2007**.

(104) Wamhoff, H.; Korte, F. *Chem. Ber.* **1967**, *100*, 1324-1330.

(105) BIOMOL *www.biomol.com*.

(106) Medda, F.; Russell, R. J. M.; Higgins, M.; McCarthy, A. R.; Campbell, J.; Slawin, A. M. Z.; Lane, D. P.; Lain, S.; Westwood, N. J. *J. Med. Chem.* **2009**, *52*, 2673-2682.

(107) http://pubs.acs.org/journal/jcchff.

(108) Pouchet, C. J.; Behnke, J. *The Aldrich Library of 13C and 1H FT NMR Spectra* **1993**, *II*, 1063.

(109) *Cambridge Crystallographic Data Centre, Cambridge, UK, www.ccdc.cam.ac.uk*.

(110) Schuettelkopf, W.; Van Alten, D. M. F. *Acta Crystallogr.* **2004**, *D60*, 1355-1363.

(111) *PDB ID 2HJH*.

(112) Tame, J. R. H. *J. Comput. Aided Mol. Des.* **2005**, *19*, 445-451.

(113) D'Angelo, N. D.; Bellon, S. F.; Booker, S. K.; Cheng, Y.; Coxon, A.; Dominguez, C.; Fellows, I.; Hoffman, D.; Hungate, R.; Kaplan-Lefko, P.; Lee, M. R.; Li, C.; Liu, L. B.; Rainbeau, E.; Reider, P. J.; Rex, K.; Siegmund, A.; Sun, Y. X.; Tasker, A. S.; Xi, N.;

Xu, S. M.; Yang, Y. J.; Zhang, Y. H.; Burgess, T. L.; Dussault, I.; Kim, T. S. *J. Med. Chem.* **2008**, *51*, 5766-5779.

(114) Tamaru, Y.; Kagotani, M.; Yoshida, Z. I. *J. Org. Chem.* **1980**, *45*, 5221-5223.

(115) Mizutani, M.; Sanemitsu, Y.; Tamaru, Y.; Yoshida, Z. I. *J. Org. Chem.* **1985**, *50*, 764-768.

(116) Mizutani, M.; Sanemitsu, Y.; Tamaru, Y.; Yoshida, Z. *J. Org. Chem.* **1983**, *48*, 4585-4589.

(117) Tamaru, Y.; Kagotani, M.; Yoshida, Z. *Tet. Lett.* **1981**, *22*, 4245-4248.

(118) Therkelsen, F. D.; Hansen, A. L. L.; Pedersen, E. B.; Nielsen, C. *Org. Biomol. Chem.* **2003**, *1*, 2908-2918.

(119) Barger, G.; Starling, W. W. *J. Chem. Soc. Trans.* **1911**, *99*, 2030-2033.

(120) Bergeron, R. J.; Wiegand, J.; Wollenweber, M.; McManis, J. S.; Algee, S. E.; Ratliff-Thompson, K. *J. Med. Chem.* **1996**, *39*, 1575-1581.

(121) McCauley, J. A.; Rudd, M. T.; Nguyen, K. T.; McIntyre, C. J.; Romano, J. J.; Bush, K. J.; Varga, S. L.; Ross, C. W.; Carroll, S. S.; DiMuzio, J.; Stahlhut, M. W.; Olsen, D. B.; Lyle, T. A.; Vacca, J. P.; Liverton, N. J. *Angew. Chem. In. Ed.* **2008**, *47*, 9104-9107.

(122) Coxon, G. D.; Furman, B. L.; Harvey, A. L.; McTavish, J.; Mooney, M. H.; Arastoo, M.; Kennedy, A. R.; Tettey, J. M.; Waigh, R. D. *J. Med. Chem.* **2009**, *52*, 3457-3463.

(123) Kumar, V.; Nair, V. A. *Tetrahedron Lett.*, *51*, 966-969.

(124) Weissman, S. A.; Zewge, D. *Tetrahedron* **2005**, *61*, 7833-7863.

(125) Brooks, P. R.; Wirtz, M. C.; Vetelino, M. G.; Rescek, D. M.; Woodworth, G. F.; Morgan, B. P.; Coe, J. W. *J. Org. Chem.* **1999**, *64*, 9719-9721.

(126) Case, D. E. D., T. E.; Cheatham, III, C. L.; Simmerling *University of California, San Francisco* **2006**.

(127) Tervo, A. J.; Kyrylenko, S.; Niskanen, P.; Salminen, A.; Leppanen, J.; Nyronen, T. H.; Jarvinen, T.; Poso, A. *J. Med. Chem.* **2004**, *47*, 6292-6298.

(128) Blander, G.; Olejnik, J.; Olejnik, E. K.; McDonagh, T.; Haigis, M.; Yaffe, M. B.; Guarente, L. *J. Biol. Chem.* **2005**, *280*, 9780-9785.

(129) Gurard-Levin, Z.; Kilian, K., A. ; Kim, J. E.; Bahr, K.; Mrksich, M. *ACS Chem. Biol.* **2010**, *in press*.

(130) Andreichikov, Y. S.; Tokmakova, T. N. *Zh. Org. Khim.* **1987**, *23*, 880-885.

(131) Herkstroeter, W. G.; Specht, D. P.; Farid, S. *J. Photochem.* **1983**, *21*, 325-342.

(132) Wamhoff, H.; Schorn, G.; Korte, F. *Chem. Ber.* **1967**, *100*, 1296-1304.

(133) Jacobson, S.; Grosh, B. *J. Chem. Soc. Trans.* **1915**, *107*, 959-966.

(134) Lüehr, S.; Vilches-Herrera, M.; Fierro, A.; Ramsay, R. R.; Edmondson, D., E. ; Reyes-Parada, M.; Cassels, K.; Iturriaga-Vásquez, P. *Bioorg. Med. Chem. Lett.* **2010**, *18*, 1388-1395.

(135) Gibbons, L. K.; Peake, C., J.; Harnish, W. N. *USXXAM US 3983246 19760928.* **1976**.

(136) Weissflog, V. W.; Schubert, H. *Journal f. Prakt. Chem.* **1976**, *318*, 785-794.

(137) Profft, E.; Runge, F.; Jumar, A. F. *J. f. Prakt. Chem.* **1954**, *1*, 57-86.

(138) Surrey, A. R.; Lesher, J. Y. *J. Am Chem. Soc.* **1956**, *78*, 2573-2576.

(139) DeLano, W. L. *DeLano Scientific, Palo Alto, CA* **2002**.

(140) Adams, P. D.; Grosse-Kunstleve, R. W.; Hung, L.-W.; Ioerger, T. R.; McCoy, A. J.; Moriarty, N. W.; Read, R. J.; Sacchettini, J. C.; Sauter, N. K.; Terwilliger, T. C. *Acta Cryst.* **2002**, *D58*, 1948-1954.

(141) Jorgensen, W. L.; Chandrasekhar, J.; Madura, J. D.; Impey, R. W.; Klein, M. L. *J. Chem. Phys.* **1983**, *79*, 926-935.

(142) Bashford, D.; Case, D. A. *Annu. Rev. Phys. Chem.* **2000**, *51*, 129-152.

(143) Tsui, V.; Case, D. A. *J. Am. Chem. Soc.* **2000**, *122*, 2489-2498.

(144) Case, D. A. *Curr. Opin. Struct. Biol.* **1994**, *4*, 285-290.

7. INTRODUCTION

7.1 Alkaloids

Amongst the naturally occurring chemical entities used in medicine throughout history, alkaloids have always played a pivotal role.[1] They have been reported to exhibit a wide range of pharmacological properties, such as anaesthetic (cocaine), stimulant (cocaine, caffeine), analgesic (morphine) and antimalarial activities (quinine).[2] Anticancer activity has also been described for some alkaloids, such as vinblastine and vincristine.[3]

The large number and variety of compounds classified under this name often complicates a clear and unambiguous definition of the alkaloid family. They are usually defined as naturally occurring compounds incorporating one or more nitrogen atoms into their structures. Over and above carbon, hydrogen and nitrogen, other elements, such as phosphorus, oxygen and halogens can be found in their structure. [4]

In the past, alkaloids were mainly used as therapeutic agents in their crude form extracted from a broad range of organisms (plants, fungi, animals and bacteria). However, nowadays the dramatic development of synthetic organic chemistry and spectroscopic techniques has made it possible not only to precisely determine their structures, but also to access multigram quantities of pure and biologically active alkaloids. This can be achieved either by chemical extraction and purification from the natural source or by total synthesis of the desired compound.

Alkaloids are usually divided into different classes, according to their chemical structure.[4] Amongst these classes, compounds characterised by an indole ring system have received growing interest due to their biological properties.[5] For example, the above mentioned anticancer agents vinblastine and vincristine belong to this category. Other indole-based alkaloids, such as the *calycanthaceous* alkaloids, have recently been isolated and the anticancer activity of a number of these determined.[6-8]

7.2 Calycanthaceous alkaloids

The *calycanthaceous* alkaloids were first isolated from the plant genus *Calycanthus*.[9] Their structure is characterised by a common carbon skeleton which differs only in the aminal connectivity amongst the different members of the family (**Figure 7.2**). The first member to be isolated was (+)-calycanthine (**174**). Its structure was first determined by Robinson (1954) and Woodward (1960) with confirmation of the proposed structure provided by means of crystallographic analysis by Hamor and Robertson in 1960.[10-12]

It was suggested that **174** was one of the possible structural isomers which could be derived through aminal construction from the hypothetical intermediate **175**. Compound **175** itself was proposed to derive from the hydrolysis of indolenine (**176**), which can be produced by oxidative dimerisation of *N*-methyltryptamine (**177**) (**Figure 7.2**).[11]

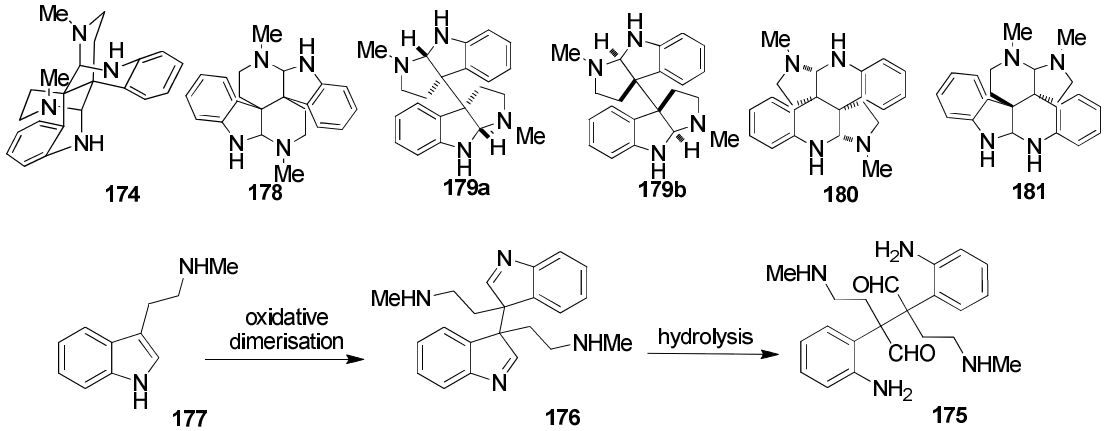

Figure 7.2 – Proposed biosynthetic pathway for the calycanthaceous alkaloids and structure of isomers **174** and **178**-**181** which can be obtained from **175** through aminal construction. As compound **178** has not been isolated yet, its stereochemistry is not known.

In the same period, the structure of (-)-chimonanthine (isomer **179a**) was determined by X-ray analysis after isolation from *Chimocanthus fragans*.[13] More recently, (-)-calycanthyne, *meso*-chimonanthine (isomer **179b**) and *iso*-calycanthine (isomer **180**) were extracted from *Psychotria forsteriana* (**Figure 7.2**).[14] Until 1993, structural arrangements **178** and **181** had not been reported in the literature.

7.3 Perophoramidine: Structure and Biological Activity

Perophoramidine (**182**, **Figure 7.3.1**) was isolated from the Philippine marine ascidian *Perophora namei* in 2002 by Ireland and co-workers.[6] It was characterised by an unusual heterocyclic structure consisting of six rings (named A-F) and exhibited the following architecturally intriguing aspects:

1. The presence of two amidine functionalities;

2. The presence of halogen substituents at the C-8, C-15 and C-17 positions on aromatic rings F and C. The presence of these halogens was proven by dehalogenation of the natural product by ammonium formate catalysed hydrogenation; [6]

3. The relative stereochemistry of the quaternary carbon atoms at C-4 and C-20 is *trans*, as determined by means of NMR experiments.[6] Although an optical rotation has been observed for **182**, the absolute stereochemistry of the naturally occurring perophoramidine **182** has not been determined as yet.

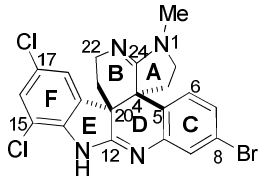

Figure 7.3.1 – Structure of perophoramidine **182**. The numbering system shown is the same as that reported by Ireland and co workers in the original publication.[6]

In terms of anti-cancer activity, perophoramidine **182** showed a moderate cytotoxicity against a HCT116 colon carcinoma cell line, with an IC_{50} of 60 μM. Interestingly, **182** was shown to induce apoptosis *via* PARP cleavage.[6]

Perophoramidine **182** exhibits structural similarities with the communesin family of natural products. The first compounds to be isolated from this family, communesins A and B (**183** and **184**, **Figure 7.3.2**), were isolated by Numata and co-workers in 1993 from a *penicillium* fungus found attached to the marine alga *Enteromorpha intestinalis*.[8] More recently, a further six related compounds (communesins C-G) were isolated and characterised.[15-18] This class of

compounds displays a variety of biological activities, including anti-cancer activity (communesins A and B) and insecticidal activity (communesins A, B, D, E and F).[8,16,18-20]

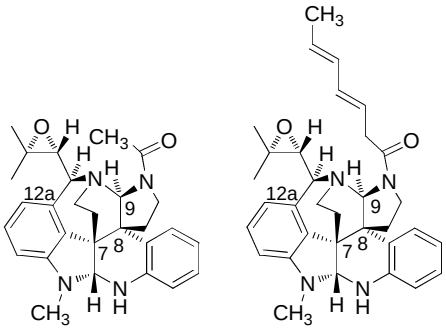

Figure 7.3.2 – Structure of communesins A (**183**) and B (**184**).[8]

7.4 Approaches to the Total Synthesis of Perophoramidine (182)

Since its discovery in 1992, perophoramidine **182** has been an attractive target for synthetic chemists. Amongst its interesting structural features, construction of the two vicinal chiral quaternary carbon centres on C-4 and C-20 in an asymmetric manner appeared to be the most challenging aspect. In general, the establishment of vicinal quaternary centres in an asymmetric manner is still, to date, considered one of the biggest challenges in synthetic organic chemistry.[21-23]

Many studies towards the total synthesis of perophoramidine **182** and its structurally related analogues communesins A-G have been reported. It is not our aim to describe all the reported syntheses, but for a general overview, the reader can consult a recently published literature review.[24] We wish to highlight here the efforts and achievements related to the total synthesis of **182** in which, for simplicity, only the key steps of each synthetic pathway will be described.

Based on a biomimetic approach, racemic perophoramidine (**182**) was synthesised for the first time by Funk and co-workers (10% over 12 steps).[25] The key step of this preparation was the coupling of protected alcohol **185** with azide **186** in order to afford lactam **187** (**Scheme 7.4.1**). After reduction of the azide moiety of **187**, a sequence of cascade reactions culminated in the isolation of **188**. The F-ring of **188** was then selectively chlorinated in the positions *ortho* and *para* to the indolic nitrogen to afford advanced intermediate **189**. The total synthesis of racemic **182** was then completed after a further eight steps.

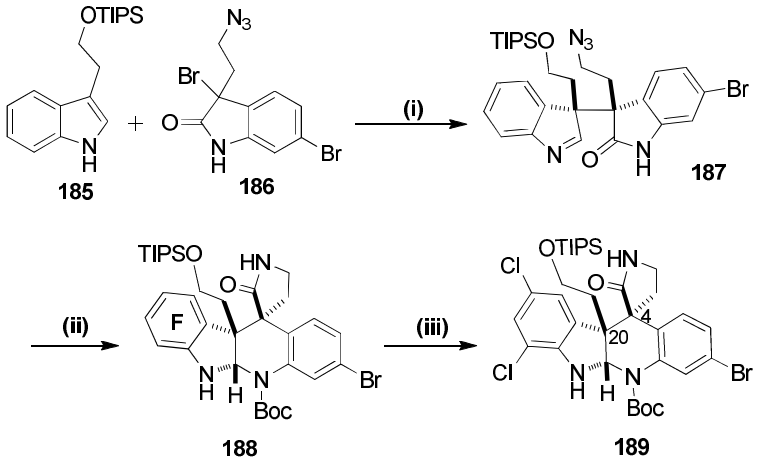

Scheme 7.4.1 – Key steps in the total synthesis of racemic perophoramidine **182** reported by Funk and co-workers.[25] *Reagents and Conditions:* (i) Cs_2CO_3, DCM, rt, 48 h, 89%; (ii) a) NaH, Boc_2O, THF, 92%; b) PPh_3, THF, H_2O, 89%; (iii) NCS, AcOH, 86%.

In another biomimetic approach towards the total synthesis of perophoramidine (**182**), Quin and co-workers synthesised advanced intermediate **190** (**Scheme 7.4.2**).[26] The key reaction was an intramolecular cyclopropanation which afforded the indolo[2,3-*b*]quinoline core of **190**. More specifically, intermediate **191** underwent diazo decomposition with copper triflate to afford cyclopropane intermediate **192**. Once again, reduction of the azide with sodium borohydride generated the corresponding amine, which attacked the iminium derived from opening of the cyclopropane ring, giving **190** as a mixture of diastereoisomers.

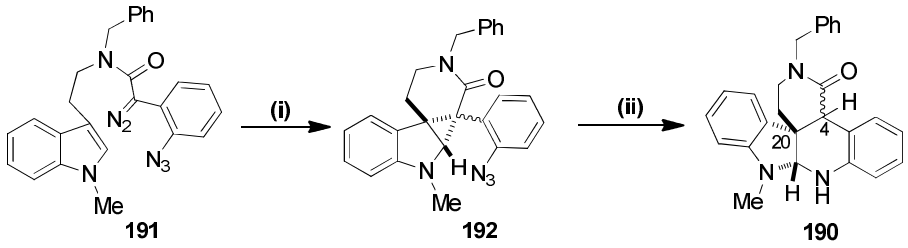

Scheme 7.4.2 - Key step for the model studies of Quin and co-workers directed towards the total synthesis of perophoramidine **182**.[26] *Reagents and Conditions:* (i) CuOTf, DCM, 58%; (ii) $NaBH_4$, THF, 91%.

Racemic dehaloperophoramidine **193** (**Figure 7.4.1**) was prepared by Rainer and co-workers in eighteen steps and with an overall yield of 11%.[27]

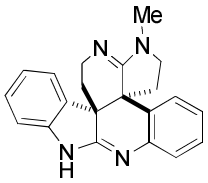

Figure 7.4.1 - Structure of dehaloperophoramidine **193**.

This approach was based on intermediate **194**, which is similar in structure to **189** (**Scheme 7.4.3**). Treatment of **195** and **196** with benzenesulphenyl chloride yielded **197**, which was subsequently reduced to alcohol **198**. **198** underwent spontaneous cyclisation to afford **199** as a diastereomeric mixture (1:1). The indolo[2,3-*b*]quinoline system of **200** was obtained as a single diastereoisomer after treatment of **199** with base. Finally, **194** was obtained after deprotonation of the acidic C-4 proton of **200** and treatment with allyl iodide. X-ray analysis established that **194** had the same relative stereochemistry of perophoramidine **182**. The desired dehaloperophoramidine **193** was then isolated after a further twelve steps.

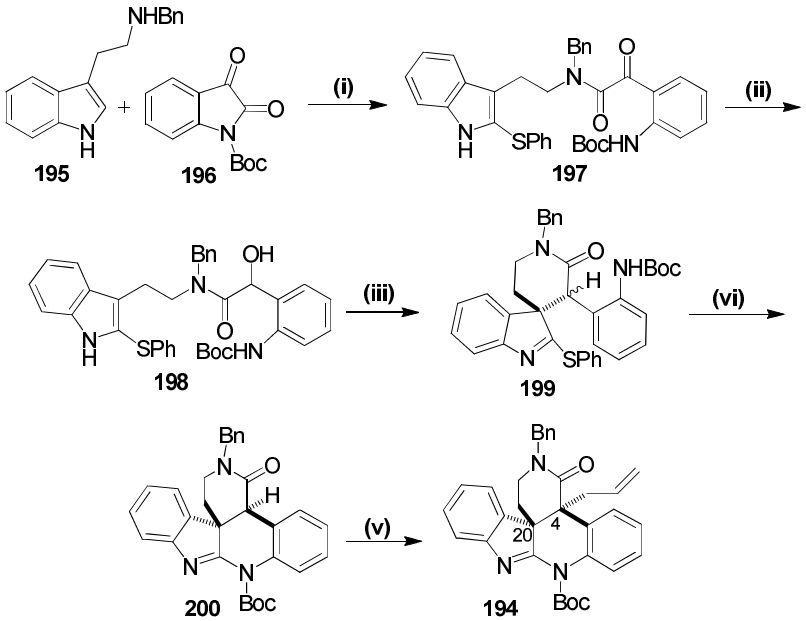

Scheme 7.4.3 - Key steps in the total synthesis of dehaloperophoramidine **182**.[27] *Reagents and Conditions:* (i) a) THF, rt; b) PhSCl, DCM, 0 °C to rt, 90%; (ii) $NaBH_4$, MeOH; (iii) MsCl, pyridine, 0 °C; (iv) DBU, DCM, 0 °C to rt, 79% (3 steps); (v) KO*t*Bu, allyl iodide, THF, 89%.

Weinreb and co-workers developed a new methodology based on a halogen-selective tandem Heck/carbonylation sequence.[28] Initially, a series of model studies were carried out. It was envisaged that this reaction would selectively occur at the iodine atom of **202** in the presence of two chlorine atoms (**Scheme 7.4.4**). Indeed, when the reaction was attempted, this was found to

be the case, with a high degree of halogen selectivity observed and **203** being isolated as a single diastereomer (88%). Subsequently, lactone **204** was obtained as a single diastereoisomer after deprotection of the alcohol in **203** and heating under acidic conditions. Finally, the second quaternary centre in **205** was installed after treatment of **204** with base and allylation of the corresponding enolate. In the absence of a crystal structure for **205**, the relative stereochemistry was established by means of nOe experiments, with the enhancement observed between H-18 and H-1' aiding in the stereochemical assignment.

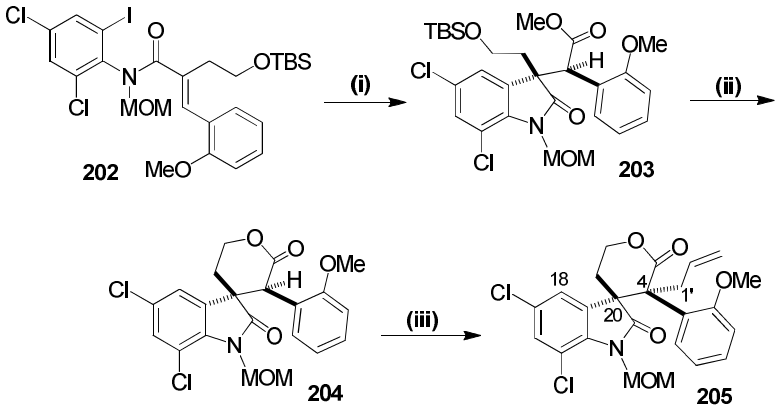

Scheme 7.4.4 – Key steps in the model studies conducted by Weinreb and co-workers directed towards the synthesis of perophoramidine **182**.[28] *Reagents and Conditions:* i) $Pd(OAc)_2$, P(*o*-Tol)$_3$, Et_3N, Bu_4NBr, CO, DMA, MeOH, 85 °C, 12 h (88%); ii) a) HCl, MeOH; b) TsOH, PhH, (79%); iii) NaH, allyl bromide, 70 °C (65%).

Based on this model study, the total synthesis of perophoramidine (**182**) was attempted by the same group.[29] Intermediate **206** (**Figure 7.4.2**) was prepared following the same synthetic protocol outlined in **Scheme 7.4.4**. Surprisingly, X-ray analysis showed that **206** had the same relative stereochemistry as the communesin family of natural products at the C-4 and C-20 centres.[29]

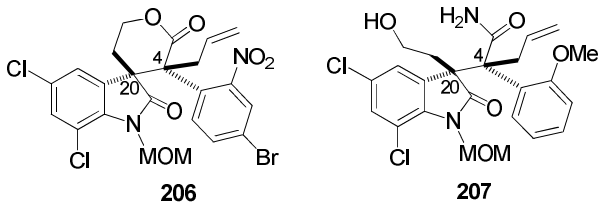

Figure 7.4.2 – Structure of intermediate **206**, prepared in an analogous way to **205** during the attempted total synthesis of **182**. The stereochemistry of **206** was established by means of X-ray crystallographic analysis. Structure **207** was found to display the same relative stereochemistry as the communesin family of natural products (determined by X-ray crystallographic analysis).[29]

This surprising result led to a re-examination of the stereochemistry of intermediate **205**. Conversion of **205** to the corresponding amide **207** (**Figure 7.4.2**) afforded crystals which were suitable for X-ray crystallographic analysis.[29] The crystal structures obtained unambiguously established that the two quaternary carbons at C-4 and C-20 displayed the same relative stereochemistry as the communesin family, and that the previous assignment was therefore incorrect. Thus the total synthesis of perophoramidine using this approach was temporarily abandoned.

Only recently, the same group has reported a modified substrate for the tandem Heck-carbonylation reaction whose elaboration affords intermediate **208**, which was found to display the correct stereochemistry for the development of the asymmetric synthesis of perophoramidine **182** (**208**, **Figure 7.4.3**).[30]

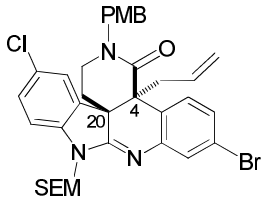

Figure 7.4.3 - Structure of the advanced intermediate **208** recently developed by Weinreb in new model studies towards the total synthesis of perophoramidine **182**.[30]

The first step in this route involved the mono-chloro intermediate **209** undergoing an intramolecular Heck-carbonylation reaction to afford the desired product **210** after deprotection of the hydroxyl group (**Scheme 7.4.5**). Subsequent oxidation of alcohol **210** with Dess-Martin reagent gave aldehyde **211**, which was converted into the corresponding aminoester under reductive amination conditions. Subsequent thermal cyclisation with toluene afforded δ-lactam diastereoisomers **212** and **213** (1:1.66 mixture). Of importance for the continuation of the synthesis, isomers **212** and **213** could be equilibrated by treatment with K_2CO_3 in DMF to afford a mixture where the desired *cis* isomer **213** was the main component (1:2 ratio).

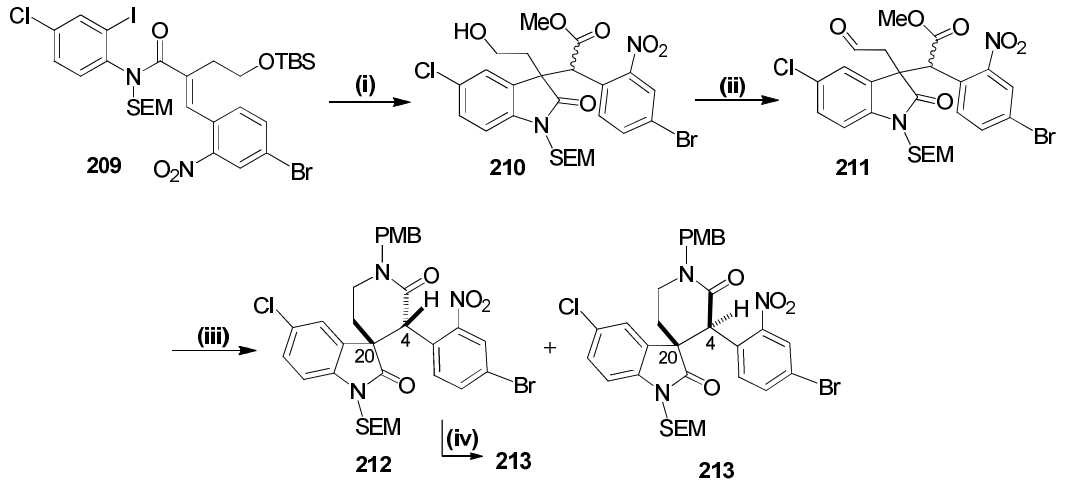

Scheme 7.4.5 – An improved synthetic approach towards the total synthesis of perophoramidine **182**.[30] *Reagents and Conditions:* i) a) $Pd(dba)_3$, $P(o\text{-}Tol)_3$, TEA, Bu_4NBr, CO, 5:1 DMA: MeOH, 85 °C, 48 h; b) TBAF, THF, rt, (45%, two steps); ii) Dess-Martin reagent, DCM; iii) a) $PMBNH_2$, DCM; b) $NaBH_4$; c) PhMe, 110 °C (85%); iv) K_2CO_3, DMF, rt.

δ-Lactam **213** was then converted into intermediate **208** after a further three steps. Insertion of the third halogen, the C-6 chlorine, was planned for later in the synthesis.[30]

7.5 A Novel Approach to the Synthesis of Perophoramidine: Previous Model Studies in the Westwood Group

Studies towards the total synthesis of racemic dehaloperophoramidine were previously developed by Dr Nicholas Voute during his doctoral studies in the Westwood group.[31,32] The retrosynthetic analysis resulted in the development of a novel synthetic route as shown in **Scheme 7.5.1**. More specifically, construction of the second amidine unit of **182** required a precursor bearing two *trans* C-2 units, such as those present in compound **214**. The two allyl groups at C-4 and C-20 in **215** can be considered as protected C-2 units, suitable for further functionalisation. The configuration shown for **215** could be obtained by a highly stereoselective alkylation at the C-4 position in **216**. Through manipulation of ketone **217** it was envisaged that aldehyde **216**, with an acidic proton in the 4-position, could be obtained. At an earlier point in the synthetic route, introduction of the first quaternary carbon centre at C-20 was planned *via* a Claisen rearrangement on allyl ether **218**. Ether **218** was previously obtained from indolo[2,3-b]quinolone **219**.

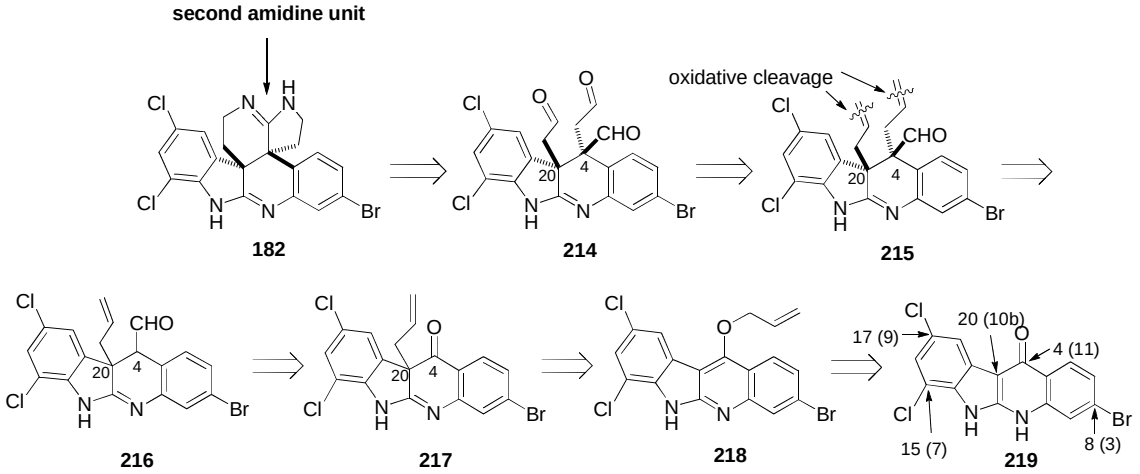

Scheme 7.5.1 - Retrosynthetic analysis for the new total synthesis of racemic perophoramidine **182** in the Westwood group.[31,32] Compound **219** shows the indolo[2,3-*b*]quinoline numbering system used in the following discussion.

Thus far, the numbering system adopted has been based upon that reported for perophoramidine **182**.[6] As the following model studies will describe the synthesis of relatively simple indolo[2,3-*b*]quinoline based substrates, the atoms will be now numbered according to the numbering system conventionally adopted for this ring system. In particular, the two all-carbon quaternary centres C-4 and C-20 of **182** will be now referred as C-10b and C-11 respectively.

Based on this retrosynthetic analysis, a series of model studies were carried out. For simplicity, halogens were omitted from the synthesis at this early stage of the research, with dehaloperophoramidine **193** becoming the main target. The synthesis of intermediates **220** and **221**, suitable for the total synthesis of racemic dehaloperophoramidine **193** (**Figure 7.5**) was successful.[31]

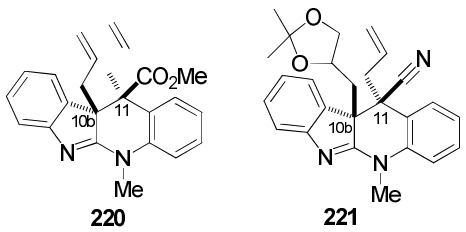

Figure 7.5 - Advanced racemic intermediates **220** and **221** previously synthesized in the Westwood group during model studies directed towards the total synthesis of racemic **193**.[31]

While **220** was synthesized *via* an analogous route to that of **215** (**Scheme 7.5.1**), compound **221** was obtained after protection of the allylic double bond on C-10b and manipulation of the

ketone at C-11 with TosMIC reagent to give the corresponding nitrile. Allylation at C-10b afforded intermediate **221**.

In a second generation study, intermediate **222**, characterized by a crotyl chain at C-10b, was prepared. Due to the presence of a bromine substituent at the C-10 position, **222** was considered to be a suitable intermediate for the asymmetric total synthesis of members of the communesin family of natural products. Furthermore, using enantiomerically enriched 3-buten-2-ol instead of allylic alcohol allowed the introduction of the new C-10b with the desired stereochemistry.[31]

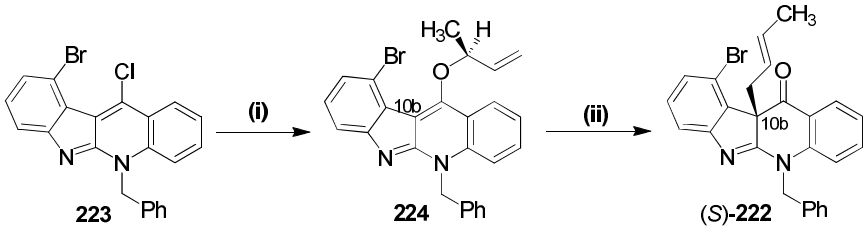

Scheme 7.5.2 – **Scheme 8.1.2.2 –** Synthesis of the enantiomerically enriched intermediate (*S*)-**222** *via* ether **224**. *Reagents and Conditions:* (i) Na (3 eq.), (*S*)-2-buten-3-ol (1 eq.), THF, rt, 1.5 h; (ii) THF, reflux, 6 h, (74%, 3 steps), 93:7 enantiomeric ratio. [31]

7.6 Aims of this Study

After the successful preparation of both **220** and **222**, the main aim of this study was to synthesise ester **223** (**Figure 7.6**) by means of the same synthetic approach previously developed in the group for **220** and **222**.

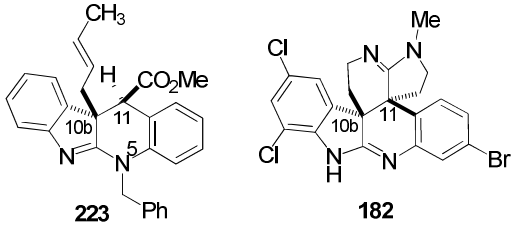

Figure 7.6 – New target ester **223** and perophoramidine **182**.[6,31]

Target compound **223** was considered to be a suitable substrate for second generation model studies aimed at the introduction of the second quaternary carbon centre at C-11 and for the

construction of the second amidine moiety of perophoramidine **182**. Two main advantages can be envisaged in the synthesis of this re-designed model substrate:

1. The crotyl group, installed through a Claisen rearrangement, will allow chirality transfer with asymmetric formation of the C-10b centre, something which was not possible in the preparation of **217** using allyl alcohol. Although at this point the asymmetric synthesis of perophoramidine **182** was not a priority, to the best of our knowledge no current asymmetric synthesis of **182** has been reported. The preparation of racemic **223** would, however, allow us to carry out further model studies towards the construction of the second amidine motif in perophoramidine **182**;

2. The benzyl moiety at *N*-5 can be envisaged as a cleavable protecting group which will allow deprotection of this position at a later stage in the synthesis, something which was not considered to be achieved easily with the methyl group in **220**.

The synthetic route followed was the same used for the synthesis of **220**. Particular efforts were put into the optimisation of the low yielding steps previously observed during the synthesis of **220**. The efforts directed towards the synthesis of **223** will be reported in **Chapter 8**.

8. SYNTHESIS OF A REDESIGNED MODEL SYSTEM

This chapter describes the synthesis of target ester **223** (**Figure 8.1**). The synthetic approach followed was the same as that previously developed in our group for the synthesis of model compound **220** (**Figure 8.1**).[31] The major differences between **223** and **220** are the replacement of the allyl substituent at C-10b with a crotyl chain and the presence, on *N*-5, of a benzyl protecting group instead of a methyl group.

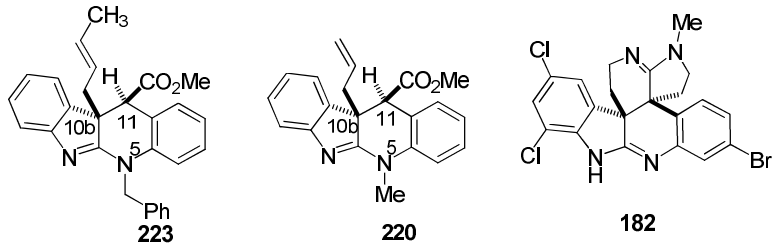

Figure 8.1 – New target ester **223** and model intermediate **220** previously synthesised in the Westwood group.[6,31]

As two of the last steps of the synthesis of **220** were characterised by a low yield, studies have been conducted towards its optimisation. Efforts aimed at understanding the possible causes of the low yields led us to a re-designed model system, the synthesis of which is described in **Section 8.3**. Spectroscopic data for the compounds described in this section are reported in **Chapter 9**.

8.1 Synthesis of Target Compound 223

8.1.1 Synthesis of 11-chloro-5-benzyl-5*H*-indolo[2,3-b]quinoline (224)

Chloride **224** was prepared according to a synthetic route previously reported by our group (**Scheme 8.1.1**).[31,32] Indole-3-carboxylic acid methyl ester (**225**) was coupled with *N*-benzyl aniline in order to afford 2-aminoindole **226** in high yield after recrystallisation from a mixture of dichloromethane and hexane. Treatment of **226** with diphenyl ether at reflux afforded cyclised compound **227** in high yield as colourless crystals after cooling the reaction mixture to room temperature. Finally, treatment of **227** with neat $POCl_3$ at reflux gave chloride **224** after basic work-up. This synthesis was carried out on a multigram scale. Furthermore, the use of column chromatography was avoided, with purification carried out only by recrystallisation

(**226** and **227**). In the case of compound **224**, analysis of the ^{1}H NMR spectrum of the crude material suggested a high level of purity and therefore further purification was avoided. All analytical data obtained for **224**, **226** and **227** were in agreement with the literature.[31]

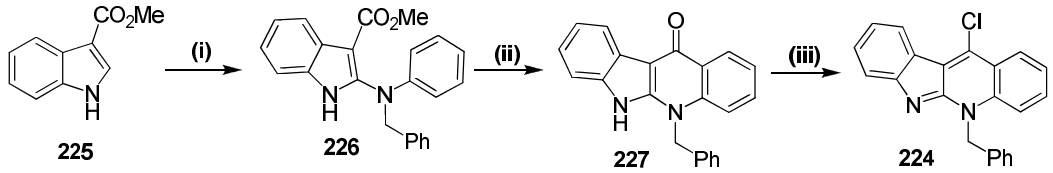

Scheme 8.1.1 – Preparation of 11-chloro-5-benzyl-5*H*-indolo[2,3-b]quinoline **224** according to a reported procedure.[31] *Reagents and conditions:* (i) DMP (0.5 eq.), NCS (1.1 eq.), DCM, 2 h, 0 °C; PhNHBn (2 eq.), TCA (0.2 eq.), 2 h, rt (65%); (ii) Ph_2O, 3 h, reflux (85%); (iii) $POCl_3$, 3 h, reflux (86%); DMP = *N'*,*N*-dimethylpiperazine, NCS = *N*-chlorosuccinimide, TCA = trichloroacetic acid.

8.1.2 Formation of the C-10b Quaternary Centre using a Claisen Rearrangement

With chloride **224** in hand, the next step was the formation of the new quaternary centre at the C-10b position. Formation of a quaternary centre at the same carbon atom on model substrate **228** was previously achieved in our group (**Scheme 8.1.2.1**).[31] After the preparation of **224**, Claisen rearrangement of the allyl group on C-10b was observed upon heating of **229** in toluene at reflux. The migration of the allyl group to C-10b (**228**) was unambiguously established by means of [^{1}H-^{13}C] HMBC analysis and crystal structure determination.

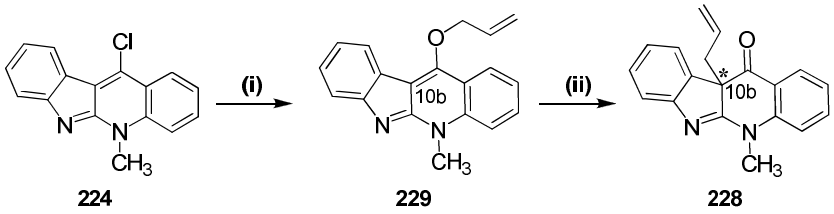

Scheme 8.1.2.1 – Previous preparation of **228** *via* **229** using allyl alcohol. *Reagents and Conditions:* (i) allyl alcohol (35 eq.), Na (5 eq.), THF, rt, 18 h; (ii) PhMe, reflux, 5 h (83% over two steps).[31]

The same methodology was also applied in our group to the modified substrate **223** using enantiomerically enriched (*S*)-3-buten-2-ol (see **Introduction, Scheme 7.5.2**).[31] The advantage of employing this alcohol instead of allyl alcohol was that it would enable the transfer of the chiral information embedded in the chiral centre of **224** into the new stereogenic centre C-10b of **222**.

Upon treatment of chloride **224** with racemic 3-buten-2-ol in the presence of sodium, ether **230** was obtained (**Scheme 8.1.2.2**). However, the crude reaction mixture was contaminated by variable amounts of rearranged product **231**. The presence of **231** was confirmed by the presence in the ^{1}H NMR spectrum of two doublets at 5.92 and 5.10 ppm, each integrating for one proton, assignable to the diastereotopic benzylic protons adjacent to *N*-5. In the absence of the C-10b chiral centre, the same protons appeared as a singlet in **224** and **230**. All signals derived from the protons of the new crotyl chain at C-10b were clearly detectable in the crude ^{1}H NMR. Due to contamination of crude ether **230** with variable amounts of **231**, full characterisation of **230** was not carried out and it was decided to heat crude **230** in THF in order to complete the Claisen rearrangement. After 5 hours heating at reflux, rearranged compound **231** was obtained in an overall yield of 60% over two steps (**Scheme 8.1.2.2**). Compound **231** was fully characterised and the position of the crotyl substituent unequivocally established by means of [^{1}H-^{13}C] HMBC spectroscopy and X-ray crystal structure determination (**Figure 8.1.2**).

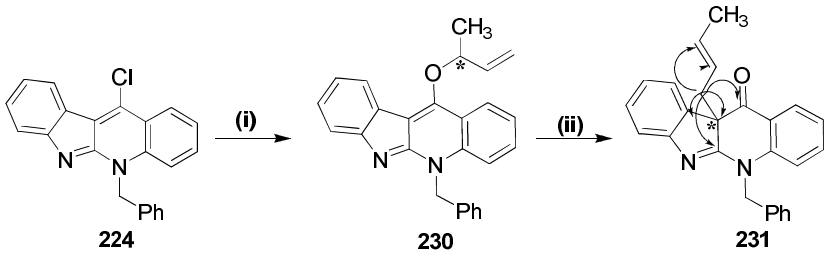

Scheme 8.1.2.2 – Preparation of **231** from **223** using racemic 3-buten-2-ol. *Reagents and Conditions:* (i) Na, 3-buten-2-ol, THF, 18 h; (ii) THF, 5 h, reflux (60% over two steps). Curly arrows show the diagnostic interactions observed in the [^{1}H-^{13}C] HMBC spectrum of **59** between the methylene protons of the crotyl chain at C-10b and the neighbouring carbon atoms. These interactions enabled us to establish the regiochemistry of the Claisen rearrangement.

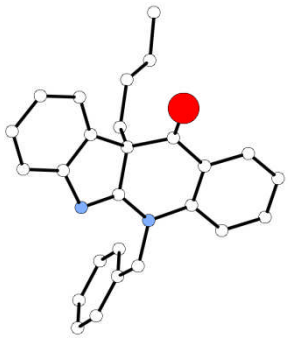

Figure 8.1.2 – Crystal structure of **231.**

The moderate yield observed for **231** is partially rationalised by the formation of side product **232** (**Scheme 8.1.2**). Indeed, after purification by silica-gel column chromatography, a less

polar compound was eluted and fully characterised by means of ^{1}H NMR, ^{13}C NMR, 2D [^{1}H-^{1}H] COSY, [^{1}H-^{13}C] HSQC and [^{1}H-^{13}C] HMBC spectroscopy. All data suggested the formation of **232**. An analogous product was previously observed when **228** was treated with methanol.[31] In our case, it may be possible that traces of moisture in the reaction led to nucleophilic attack of water at the C-11 ketone functionality of **231** and subsequent formation of **232** through intermediates **233** and **234** according to the mechanism proposed in **Scheme 8.1.2.4**

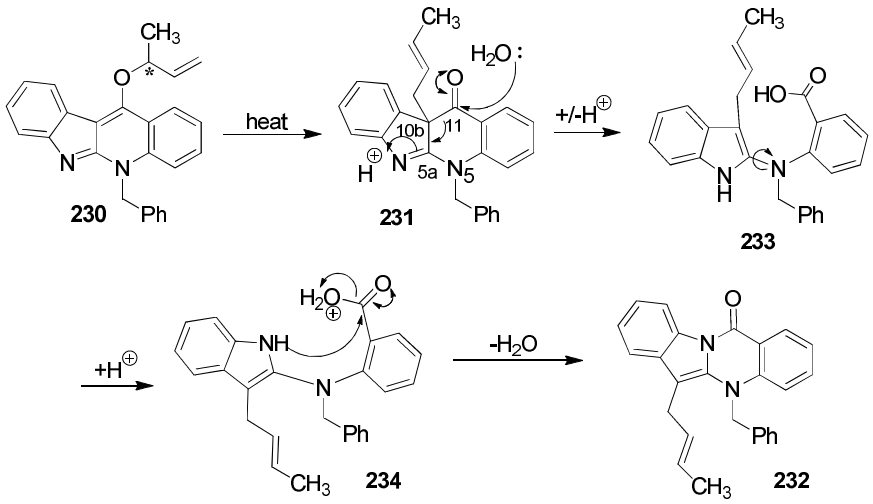

Scheme 8.1.2.4 – Proposed mechanism for the formation of side product **232** during the two step synthesis of **231** from **224**.

8.1.3 Synthesis of Epoxide 235

With compound **231** in hand, formation of epoxide **235** was attempted according to a reported methodology previously applied in our group to the synthesis of **236** (**Scheme 8.1.3.2**).[31] Compound **236** was previously obtained in high yields after treatment of **237** with ICH_2Cl and MeLi-LiBr (**Scheme 8.1.3.1**). The stereochemistry of the new quaternary centre at C-10 was established by means by X-ray crystallographic analysis.

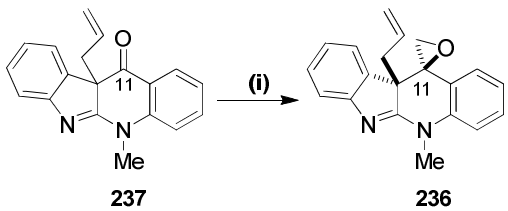

Scheme 8.1.3.1 – Preparation of epoxide **236** from **237**. *Reagents and Conditions*: (i) ICH_2Cl (1.3 eq.), MeLi-LiBr (1.2 eq.), THF, -78 °C (0.5 h) to rt, 18 h (88%). [31]

When intermediate **231** was treated with the same reagents, the new epoxide **235** was obtained in high yields and good purity after recrystallisation from diethyl ether (**Scheme 8.1.3.2**). The proton atoms of the new methylene group next to the epoxide oxygen appeared in the ^{1}H NMR spectrum as two doublets at 3.07 and 2.53 ppm. In the absence of a crystal structure for **235**, it was assumed that the stereochemistry of the chiral C-11 centre was the same as that previously observed for **236** (**Scheme 8.1.3.1**).

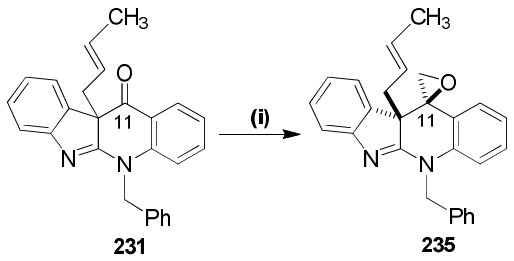

231 **235**

Scheme 8.1.3.2 – Preparation of new epoxide **235** from **231**. *Reagents and Conditions*: (i) ICH_2Cl (1.3 eq.), MeLi-LiBr (1.2 eq.), THF, -78 °C (0.5 h) to rt, 18 h (90%).

8.1.4 Reductive Opening of Epoxide 235: Synthesis of Alcohol 238

With epoxide **235** in hand, the next step involved its reductive opening in order to afford the new alcohol **238** (**Scheme 8.1.4.2**). Reductive opening of epoxide **236** was previously performed in our group in modest yields (**239**, **Scheme 8.1.4.1**, 35%). Due to its polar nature, purification of **239** by silica gel column chromatography proved difficult, with **239** often being co-eluted with unidentified side products.[31] Furthermore, in order to minimise the formation of unwanted side products, the reaction temperature and time were always kept low and short respectively, which resulted in incomplete consumption of starting material **236**.

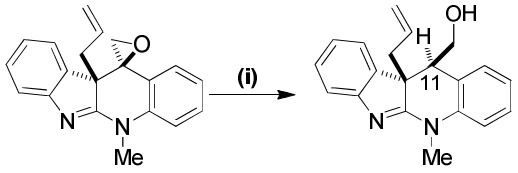

236 **239**

Scheme 8.1.4.1 – Low yield synthesis of alcohol **239**. *Reagents and Conditions:* BF_3OEt_2 (2.7 eq.), $NaBH_3CN$ (2.5 eq.), THF, -10 °C, 3 h (35%).[31]

When new epoxide **235** was treated with $BF_3.OEt_2$ and $NaBH_3CN$ using the same conditions reported for **236**, alcohol **238** was obtained in low yields after purification by column chromatography (32%, **Figure 8.1.4.2**). Formation of the desired product was confirmed by the

presence of a new doublet at 3.15 ppm in the ^{1}H NMR spectrum, which was assigned to the proton at C-11. The two protons adjacent to the hydroxyl group appeared as a multiplet at 4.76-4.58 ppm. Structure determination by means of X-ray crystallography indicated that **236** had the relative opposite configuration at C-10b and C-11 as perophoramidine **182**. Thus, the reductive opening of **235** had occurred with inversion of configuration, as previously observed for **236 (Figure 8.1.4)**.

Being still at an early stage of our studies, it was envisaged that this yield was too low for the continuation of our synthesis. Thus, it was decided to perform a series of optimisation studies.

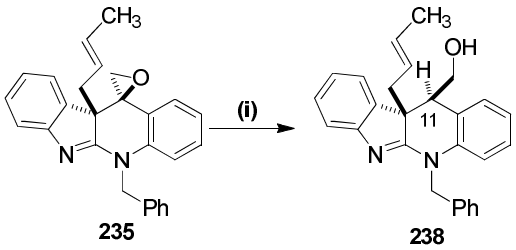

Scheme 8.1.4.2 – Synthesis of new alcohol **238** from **235**. *Reagents and Conditions:* $BF_3.OEt_2$ (4 eq.), $NaBH_4CN$ (2.5 eq.), THF, -78 °C to rt, 3 h (64%).

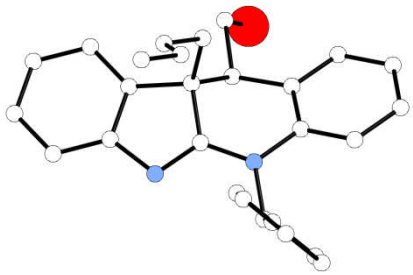

Figure 8.1.4 – Crystal structure of primary alcohol **238.**

It was envisaged that longer reaction times, along with higher temperatures would possibly lead to higher yields. When the reaction temperature was increased to room temperature, full consumption of the starting material **235** was observed after 18 h. Analysis of the ^{1}H NMR spectrum of the crude material suggested that the expected alcohol **238** had formed in good yields. The ^{1}H NMR spectrum of the crude material was cleaner when 4 equivalents of $BF_3.OEt_2$ were used instead of 2.7 equivalents. After purification by column chromatography, **238** was isolated in a good 57% yield. However, isolation of **238** by column chromatography still led to some difficulties, with a conspicuous amount of **238** still remaining on the column

and only being eluted using polar eluents (EtOAc 100%). Furthermore, co-elution of newly formed side-products was observed by ^{1}H NMR analysis of the collected fractions. These observations together suggested that silica gel column chromatography was not the optimal method for the purification of this type of alcohol.

In our group, blebbistatin precursor **240** and analogue **241** were previously synthesised (**Scheme 8.1.4.3**).[33] Interestingly, when purified using basic silica column chromatography (obtained by treating commercially available silica with NH_4OH) the yields for these compounds were significantly higher than those observed when the purification was run on acidic silica gel. **240** and **241** exhibit structural similarities with our substrates **238** and **239**, such as the amidine and the alcohol moieties. Thus, it was decided to purify crude **238** using basic silica as the solid phase in the column chromatography. This approach led to slightly higher yields (64%) and alcohol **238** was now eluted in a pure form without contamination from undesired side-products or product being left on the column.

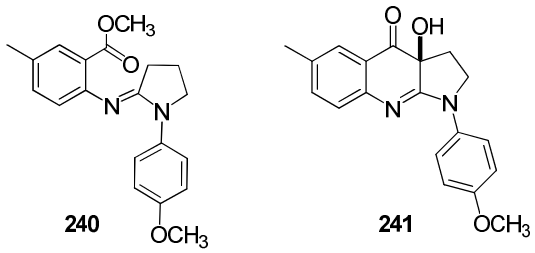

Scheme 8.1.4.3 – Structure of compounds **240** and **241** previously synthesised in the Westwood group and purified by means of basic silica gel chromatography. [33]

8.1.5 Synthesis of Target Ester 223

Previously in our group alcohol **239** was converted to ester **220** in moderate yields according to a two step synthetic methodology (**Scheme 8.1.5.1**).

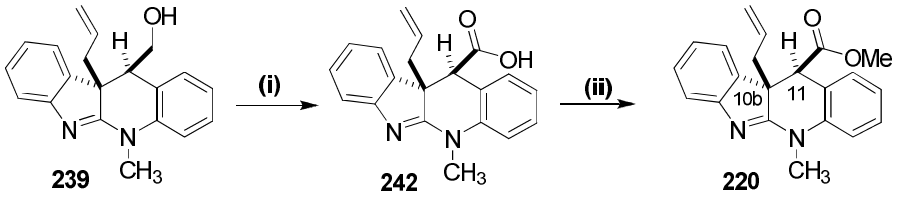

Scheme 8.1.5.1 – Two step preparation of ester **220** from alcohol **239**.[31] *Reagents and Conditions:* (i) CrO_3 (5 eq.), H_2SO_4 (1.5 M), acetone, 5 h, rt; (ii) $TMSCH_2N_2$ (2 eq.), MeOH, 0.5 h, rt (54% over two steps).

Having improved the yields for the reductive opening of epoxide **235**, the next step was conversion of primary alcohol **238** into the corresponding methyl ester **223** (**Scheme 8.1.5.2**).

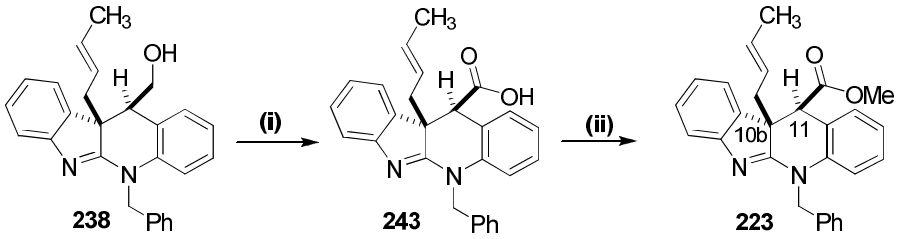

Scheme 8.1.5.2 – Two step preparation of ester **223** from alcohol **238** *via* acid **243**. *Reagents and Conditions:* (i) CrO_3 (5 eq.), H_2SO_4 (1.5 M), acetone, 5 h, rt; (ii) $TMSCH_2N_2$ (2 eq.), MeOH, 0.5 h, rt (25% over two steps).

The same synthetic methodology as described in **Scheme 8.1.5.1** was applied to substrate **238** (**Scheme 8.1.5.2**). Treatment of **238** with CrO_3 in the presence of 1.5M H_2SO_4 (Jones conditions) afforded acid **243**. No attempt to purify or fully characterise this acid was made as it was expected that purification would be troublesome and could be carried out more easily on the subsequent methyl ester **223**. Consistent with the formation of **243**, in the ^{1}H NMR spectrum, the singlet assigned to the acidic α-proton at C-11 was observed at 4.05 ppm. In the ^{13}C NMR spectrum, the signal at 174.2 ppm was assigned to the carbon of the acid carbonyl. Furthermore, the high resolution mass spectrometry analysis showed the expected peak at *m/z* 409.1927 $(M+H)^+$. Disappointingly, the mass of product recovered after the oxidation of **238** was always lower than expected, with an average of 60% recovery. This can be partially explained with the zwitterionic nature of acid **71**, which would render this molecule extremely soluble in the aqueous phase during work-up.

Thus, **243** was reacted directly in the following step with $TMSCH_2N_2$ in methanol. Ester **223** was obtained after column chromatography in a modest 25% overall yield after two steps (**Scheme 8.1.5.2**). In the ^{1}H NMR spectrum, the singlet assigned to the protons of the ester methyl group was detected at 3.94 ppm.

Despite the successful synthesis of target ester **223**, the low yield observed in the last two steps (oxidation plus esterification) was not suitable for the continuation of our model studies. Thus it was decided to optimise these steps before conducting any further study towards the formation of the C-11 quaternary centre and the construction of the new amidine motif in **182**.

8.2 Empirical Optimisation of the Oxidation of 238 to 243

Having previously improved the synthesis for the reductive opening of **235**, alcohol **238** could now be synthesised in multigram scale and used for optimisation studies of its oxidation to the corresponding acid **243**. Three strategies were adopted in attempting to optimise this transformation:

1. Optimisation of the low yielding Jones oxidation;
2. Direct oxidation to **238** using alternative reported methodologies;
3. Oxidation of alcohol **238** to the corresponding aldehyde **244**, with isolation of the aldehyde **244** and further oxidation to **243**.

The results of these three strategies will now be described.

8.2.1 Attempted Optimisation of Jones Oxidation

Encouraged by the acceptable yield of crude acid **243** isolated after the Jones oxidation of **238**, it was decided to attempt optimisation of this methodology. Several parameters could be varied, such as the reaction time, the temperature and the amount of oxidant employed. Another parameter commonly varied in this type of oxidation is the acid utilised in the reaction.

Unfortunately, the ^{1}H NMR spectra of the crude reaction mixtures often exhibited poor resolution and lack of the signal multiplicity, due to the presence of residual amounts of chromium in the NMR tube. This aspect often limited the interpretation of the results, in particular the calculation of percentage conversion to product.

Initially, it was decided to study the influence of time on the reaction at room temperature (**Table 8.2.1**, **Entries 1-3**). As this oxidation was difficult to follow by TLC, it was decided to set up three reactions in parallel and quench them at different times. In the presence of 5 equivalents of oxidant, it was necessary to allow the reaction to run for 4 hours in order to reach completion (**Entry 3**). Unfortunately, in all cases the crude mass recovered after work-up was always modest (61-53%).

Attempts to speed up the reaction by addition of further equivalents of CrO_3 led to low amounts of mass recovery after work-up (**Table 8.2.1, Entries 4-5**). Furthermore, the ^{1}H NMR spectra of the crude materials displayed poor resolution and the multiplicity of the signals could not be easily observed. This may be due to increased residual amounts of chromium present in the crude sample after work-up. Filtering the crude reaction mixture several times on celite or stirring it in the presence of charcoal did not improve the quality of the NMR spectrum.

From these results it is clear that increasing the number of equivalents of oxidant does not have a beneficial effect on the reaction. Therefore, having established that 5 equivalents of CrO_3 and 4 hours at room temperature were necessary for reaching completion, it was then decided to study the influence of temperature on the reaction. To the best of our knowledge, Jones oxidations at temperatures higher than 25°C have not been previously described in the literature. Thus we focused on the use of lower temperatures for the purpose of these studies (**Table 8.2.1, Entries 6-11**). Disappointingly, the use of low temperatures always led to poor progression of the reaction, as assessed by ^{1}H NMR analysis (**Entries 6-8**). Attempts to balance the negative effect of the low temperatures with increasing amounts of oxidant (**Entries 9-10**) resulted once again in low amounts of material recovered and low resolution of the corresponding ^{1}H NMR spectrum. However, when the reaction time was extended to 24 h, completion was achieved even at 0 °C (**Entry 11**). These data suggested to us that at this point, our original conditions (4 h, rt, 5 eq. of CrO_3) were still the most successful for the oxidation of **238** to **243**.

Table 8.2.1 – Influence of the different parameters on the oxidation of **238** to **243**. For entries **1-11** and **14**, a solution of **238** was prepared in acetone and added dropwise to a solution of CrO_3 in 1.5M H_2SO_4. Reactions were quenched by the addition of *i*-PrOH and worked-up as reported in the experimental section for the synthesis of **243**. For entries **12** and **13**, literature protocols were followed (see also supplementary material). Mass recovered refers to the amount of material recovered after work-up, but does not reflect the percentage yield, as variable amounts of product **243** had dissolved in the aqueous layer. Key: h = time (hours); rt = room temperature, ~25 °C; -* Interpretation of the crude ^{1}H NMR spectrum was not possible due to the lack of multiplicity of the signals or formation of various side products. – not calculated.

Entry	CrO_3 (eq.)	Acid	Conditions	Mass recovered	Outcome
1	5	1.5 M H_2SO_4	0.5 h, rt	61%	mainly **238**
2	5	1.5 M H_2SO_4	2.5 h, rt	58%	mixture **238**-**243**
3	5	1.5 M H_2SO_4	4 h, rt	53%	mainly **243**
4	7.5	1.5 M H_2SO_4	4 h. rt	46%	-*
5	10	1.5 M H_2SO_4	4 h, rt	43%	-*
6	5	1.5 M H_2SO_4	4 h, 0° C	61%	mainly **238**
7	5	1.5 M H_2SO_4	4 h, 5° C	58%	mainly **238**
8	5	1.5 M H_2SO_4	4h, 10° C	57%	mainly **238**
9	7	1.5M H_2SO_4	4h, 0° C	< 30%	-*
10	10	1.5M H_2SO_4	4h, 0° C	< 30%	-*
11	5	1.5M H_2SO_4	24h, 0° C	69%	mainly **243**
12	5	H_5IO_6	0.5h, 5° C	-	-*
13	5	CH_3COOH	10 h, rt	-	-*
14	5	0.15M H_2SO_4	4h, rt	-	-*

We therefore sought to investigate the effects of a range of other acids and solvents employed in the reaction (**Table 8.2.1, Entries 12-14**). Jones oxidations were previously reported to be successful using a combination of CrO_3-H_5IO_6 in wet CH_3CN and CrO_3-CH_3COOH in water.[34,35] Dilute sulfuric acid (0.15 M) was also employed in one experiment (**Entry 14**). These modified conditions were subsequently applied to our system and the results are summarised in **Table 8.2.1**. Once again, it was disappointing to notice that the progression of all the reactions was difficult to follow by TLC. Furthermore, the ^{1}H NMR spectra of the crude mixtures always suggested the formation of unidentified side products and the diagnostic resonances of the product **243** could not be found.

These problems prompted us to temporarily abandon this approach and focus on other methodologies for the conversion of primary alcohols to acids.

8.2.2 Attempted Alternative Direct Oxidation of Alcohol 238 to Acid 243

As the attempted optimisation of the Jones oxidation did not lead to an improvement in yields or conversions, it was decided to use alternative available methods for the direct oxidation of primary alcohols to acids (**Table 8.2.2**).

Treatment of primary alcohols with PDC in the presence of DMF as solvent has been reported to result in conversion to the corresponding acid.[36] However, treatment of our alcohol **238** with different amounts of PDC in DMF under a range of conditions did not result in the expected transformation (**Table 8.2.2, Entries 1-3**).

Table 8.2.2 - Summary of the conditions used in the attempted direct oxidation of alcohol **238** to acid **243** using different reported methodologies. Key: h = time (hours); rt = room temperature, ~25 °C. For experimental procedures see supplementary material.

Entry	Oxidant (eq.)	Solvent	Conditions
1	PDC (1.2)	DMF	24 h, rt
2	PDC (3.5)	DMF	24 h, rt
3	PDC (8.0)	DMF	24 h, rt
4	$RuCl_3.H_2O$ $NaIO_4$, (cat)	CCl_4-H_2O-CH_3CN	12 h, rt
5	$KMnO_4$ (1.2)	*t*BuOH	0.5 M NaOH, 18 h, rt
6	TEMPO-BAIB (4, 10)	DCM:H_2O	2h, rt

A number of problems were encountered during the investigation of these conditions. Firstly, the progression of these reactions was difficult to follow by TLC. Furthermore, the mass of material recovered after work-up was disappointingly lower than that expected (average 25%). This was particularly true when a high number of equivalents of PDC was employed (**entry 3**). For lower amounts of oxidising agents, traces of starting material **238** were observed in the ^{1}H NMR spectrum of the crude mixture (**entry 1**). Despite full consumption of **238** being achieved when 8 equivalents of PDC were utilised, the ^{1}H NMR spectra associated with these reactions were always characterised by a lack of the diagnostic peaks for acid **243** and by the presence of further unidentified side products.

The combination of $RuCl_3.H_2O$ and $NaIO_4$ in the presence of a mixture of carbon tetrachloride, water and acetonitrile as solvent has been reported to oxidise primary alcohols directly to the corresponding acid.[37] When these conditions were attempted on our alcohol **238** (**Table 8.2.2, Entry 4**), although the mass recovered from the reaction was higher than in previous cases

(94% mass recovered), ^{1}H NMR analysis of the crude mixture once again suggested the formation of a mixture of products. Due to time constraints and the complexity of these mixtures, attempts to isolate and characterise the products were not carried out. It cannot be ruled out that this combination of reagents has led to preferential dihydroxylation of the crotyl double bond of **238**, with the formation of a mixture of diastereoisomers. Due to this potential competing reaction, this methodology was abandoned.

Another oxidant commonly used for the direct oxidation of alcohols to acids is $KMnO_4$ (1.0 M in water).[38] When this methodology was applied to our substrate (**Table 8.2.2, Entry 5**), the expected transformation was not detected by TLC. Analysis of the ^{1}H NMR spectrum of the crude material suggested formation of a complex mixture which did not allow identification of the decomposition products obtained.

Finally, we attempted the use of a methodology based on the combination of TEMPO/BAIB in DCM:H_2O (**Table 8.2.2, Entry 6**).[39] Analysis of the crude reaction mixture by ^{1}H NMR suggested the formation of different side products than those obtained in previous reactions. However, the diagnostic signals for the desired acid **243** were not detected.

It could therefore be concluded from the above results that none of the attempted direct oxidations of **238** to **243** had led to better results to those observed when the reaction was run using the Jones conditions.

8.2.3 Attempted Oxidation *via* Aldehyde 244

As the majority of methodologies previously employed for the direct conversion of alcohol **238** to acid **243** were unsuccessful, it was decided to attempt the same transformation *via* aldehyde **244** (**Figure 8.2.3**). Although **244** may have indeed formed as an intermediate during the reported direct oxidations, it was now planned to perform the conversion in two steps by isolating the aldehyde **244** and subsequently oxidising it further to the corresponding acid.

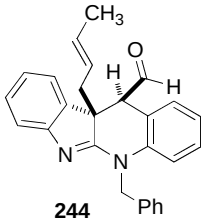

244

Figure 8.2.3 – Structure of aldehyde **244**.

A large variety of reagents have been described for the oxidation of primary alcohols to aldehydes. For the purposes of this study, only those reagents most commonly used in organic synthesis have been attempted. For an overview of the subject, specialised reviews can be consulted.[40-42] From our investigation of the subject, it appeared that TPAP/NMO, IBX-DMSO, and Dess-Martin periodinane were the most commonly used reagents.[43,44 45] Unfortunately, when applied to our substrate, the results were quite disappointing in all cases and the clean aldehyde was not obtained (**Table 8.2.3.1**).

Table 8.2.3.1. - Summary of the oxidising agents and conditions used for the oxidation of alcohol **238** to aldehyde **244**. Key: h = time (hours); rt = room temperature, ~25 °C. For experimental procedures see supplementary material.

Conditions	Oxidant (eq.)	Solvent	Conditions	Detection
TPAP-NMO	cat, 3	DCM	1 h, rt	TLC
IBX-DMSO	1.2	DMSO	1 h, rt	TLC
Dess-Martin	1.2	DCM	1 h, rt	TLC

When both the Dess-Martin periodinane and TPAP-NMO conditions were employed, analysis of the ^{1}H NMR spectrum of the crude material suggested the formation of the desired aldehyde. However, no purification by silica gel chromatography was attempted due to the complexity of the crude reaction mixtures which were recovered.

As the ^{1}H NMR spectrum of the crude material of the oxidation carried out using Dess-Martin periodinane conditions resulted in the formation of fewer side products, it was decided to study this reaction more carefully. As this oxidation can be performed in chloroform, we utilised deuterated chloroform ($CDCl_3$) and the progression of the reaction was followed by ^{1}H NMR spectroscopy. After addition of the oxidising agent, aliquots of reaction mixtures were analysed by ^{1}H NMR at regular intervals. Consumption of the starting material **238** was observed after

30 min with the new aldehyde having been formed cleanly. Amongst the diagnostic signals, the one deriving from the aldehyde proton was observed at 10.2 ppm.

Encouraged by the successful synthesis of aldehyde **244**, it was decided to attempt its conversion to the corresponding acid by means of the Pinnick oxidation.[46] This methodology has often been applied to the conversion of aldehydes to their corresponding acids and employs the use of $NaClO_4$ and $Na_2HPO_4.H_2O$. The results of these studies on aldehyde **244** are summarised in **Table 8.2.3.2.**

Table 8.2.3.2 – Overview of the attempted oxidation of aldehyde **238** to acid **244** under Pinnick conditions. Key: h = time (hours); rt = room temperature, ~25 °C; sm = starting material.

Entry	Dess-Martin Conditions	Dess-Martin Work-up	Pinnick Conditions	Outcome
1	rt, 0.5 h	removal of solvent	rt, 1 h	No acid
2	rt, 0.5 h	removal of solvent	0 °C, 1 h	No acid
3	rt, 1 h	pinnick added	rt, 1 h	sm
4	0 °C, 1 h	pinnick added	0 °C, 1 h	sm

Four oxidation attempts of alcohol **238** to aldehyde **244** were run in parallel under different conditions using Dess-Martin periodinane. While for entries **1** and **2**, the Pinnick reagents were added after removal of the chloroform solvent, for entries **3** and **4**, the reagents were added directly to the previous oxidation reaction. Disappointingly, the results were poor in all cases and only complex mixtures of products could be observed by ^{1}H NMR analysis of the crude mixtures.

8.2.4 Stability of Aldehyde 244

Attempted isolation of the aldehyde *via* basic aqueous work-up and further analysis of the product by ^{1}H NMR spectroscopy revealed that **244** was unstable to this type of isolation, with the ^{1}H NMR spectrum now characterised by the presence of many unidentified decomposition products which were not observed previously. This prompted us to further investigate the stability of **244**.

After the oxidation of **238** to **244** had reached completion (from ^{1}H NMR analysis) further aliquots of solution were taken from the reaction flask and analysed by means of ^{1}H NMR

spectroscopy. From these experiments it was clear that aldehyde **244** underwent decomposition in $CDCl_3$. After one hour the ^1H NMR spectrum was characterised by the presence of a range of unidentified side products. This led us to conclude that **244** is intrinsically unstable and undergoes rapid decomposition not only in the aqueous media of the work up, but also in the organic media which we have utilised in this stability study.

It seems likely that the observed instability of **244** contributes to the modest yields observed during the direct oxidation of **238** to **243** under Jones conditions. Consistent with this, the instability of a similar aldehyde **245** had previously been observed and reported in our group (**Figure 8.2.4**). [31] Indeed, oxidations of primary alcohols to the corresponding acids under Jones conditions are reported to proceed *via* the corresponding aldehyde. Therefore, once formed, aldehyde **244** may undergo partial decomposition before being further oxidised to the acid **243**.

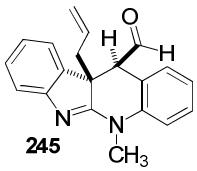

245

Figure 8.2.4 – Structure of aldehyde **245**.[31]

Having determined the intrinsic instability of aldehyde **244** as a partial explanation for the low yields observed in this oxidation reaction, it was decided to further study this oxidation by means of HPLC and LC-MS analysis.

8.2.5 Further Analysis of the Jones Oxidation

In an attempt to further understand the causes of the low yields of the above mentioned oxidation, it was decided to follow its progression by LC-MS. This method was considered better than monitoring the reaction by ^1H NMR spectroscopy as it avoided long work-up procedures and the intrinsic poor resolution of the ^1H NMR spectra, due to residual amounts of chromium present in the crude mixture.

Under the conditions used for the LC-MS analysis, alcohol **238** exhibited a retention time of 5.30 min and *m/z* 394.99 $(M+H)^+$ (**Figure 8.2.5.1**).

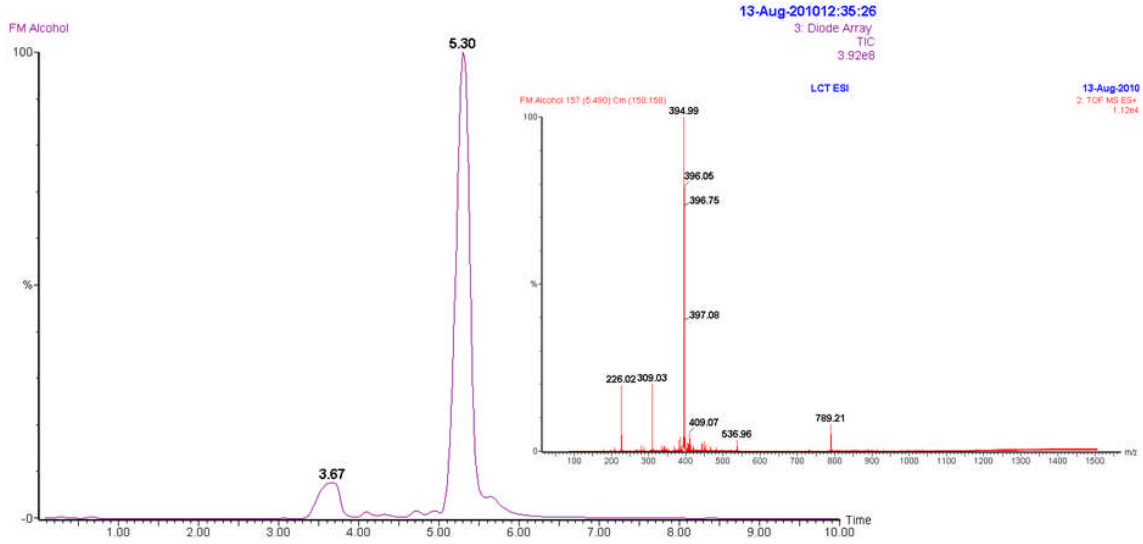

Figure 8.2.5.1 – LCMS peak of the alcohol starting material **238** (5.30 min, purple) and the corresponding LR-MS spectrum [*m/z* 394.99 $(M+H)^+$, red]. The other small peak at 3.67 min. derived from small impurities and their mass was not determined. For experimental conditions and ionisation method see experimental, **Chapter 9**, **Method B**.

We observed that 5 minutes after the addition of the oxidising agent, a series of new peaks had already formed (**Figure 8.2.5.2, A**). After one hour, their intensity had increased significantly (**Figure 8.2.5.2, B**). Amongst these new peaks, the acid **243** was detected at 5.05 min [*m/z* 409.00 $(M+H)^+$] (**Figure 8.2.5.2, D**). The signal corresponding to the aldehyde **244** was not observed as it was overlapping with the co-running alcohol and acid peaks (5.30 min and 5.05 min, respectively). However, on a more positive note, the mass assignable to the aldehyde could be observed at *m/z* 393.06 $(M+H)^+$ (**Figure 8.2.5.2, D**). Importantly, a new signal was observed at 2.82 min with *m/z* 352.96 (**Figure 8.2.5.2, A, B and C**).

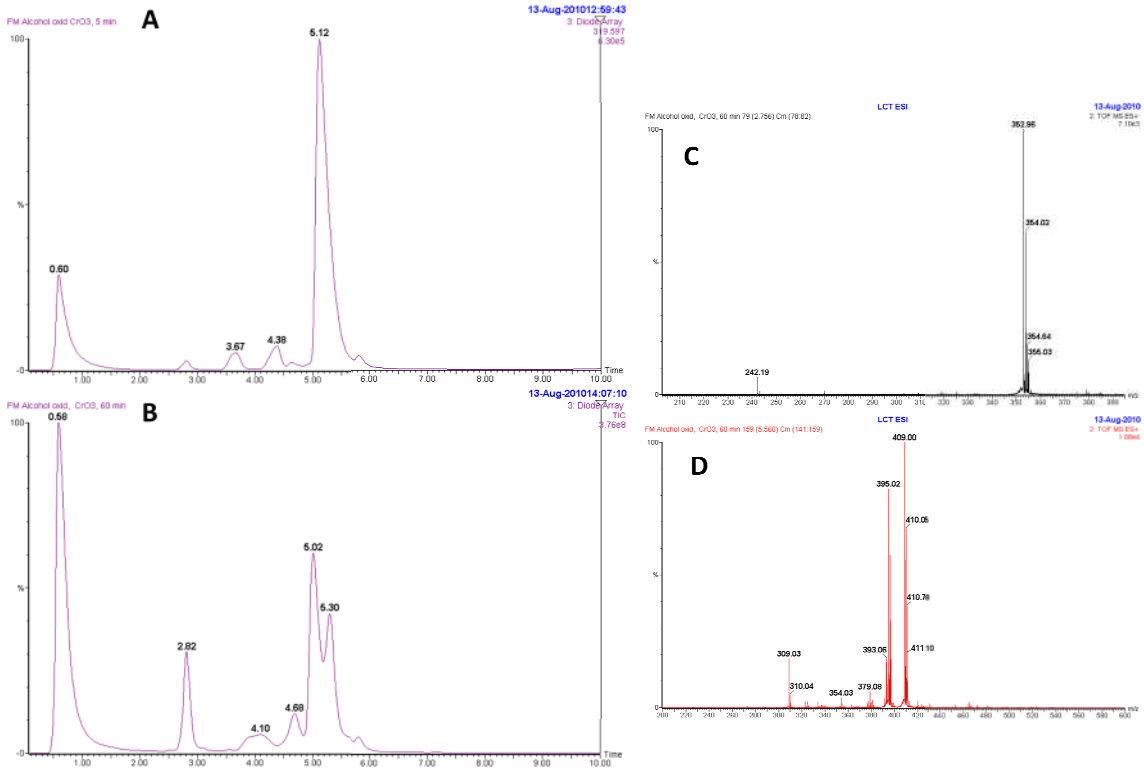

Figure 8.2.5.2 – **A**: progression of the reaction after 5 min; **B**: progression of the reaction after 1 h; **C**: LR-MS of the new peak at 2.82 min (*m/z* 352.96); **D**: LR-MS of the peaks at 5.02 min (**243**) and 5.30 min (**238**). Peaks at 0.60 (**A**) and 0.58 min (**B**) were due to the injection of the sample and no significant mass was found for them. For experimental conditions and ionisation method see experimental, **Chapter 9**, **Method B**.

After 2 hours, the acid **243** (5.05 min) and the unidentified product at 2.77 min were the main constituents of the reaction, with some starting material **238** still remaining (**Figure 8.2.5.3, A**). The reaction apparently reached completion after 4 hours at room temperature (**Figure 8.2.5.3, B**). Along with that of the acid **243** (**Figure 8.2.5.3, D)**, the signal at 2.77 min was observed as the other main component of the crude reaction mixture (**Figure 8.2.5.3, B** and **C**). This clearly suggests that a side-product had formed during the oxidation of **238** to **243**.

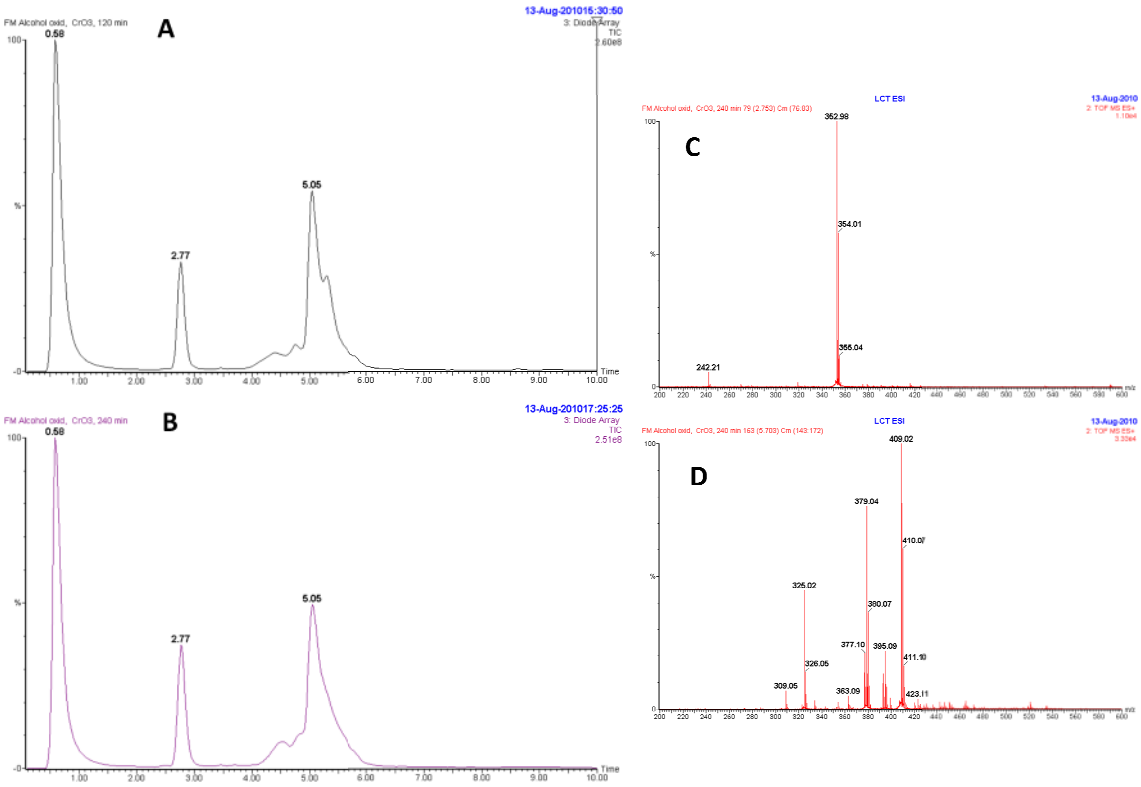

Figure 8.5.3 – **A**: progression of the reaction after 2 h; **B**: progression of the reaction after 4 h; **C**: LR-MS of the new peak at 2.77 min (*m/z* 352.96); **D**: LRMS of the peaks at 5.05 min (acid **243**, *m/z* 409.02). Peak at 0.58 (**A** and **B**) was due to the injection of the sample and no significant mass was found for them. For experimental conditions and ionisation method see experimental, **Chapter 9**, **Method B**.

In a second experiment, we planned to establish the structure of the polar side-product (**246**) corresponding to the peak at 2.77 min. After repeating the oxidation, the above mentioned compound was isolated by means of semi-preparative RP-HPLC. ^{1}H NMR analysis proved difficult, as **246** showed high polarity and very low solubility even in DMSO-d_6. A clear spectrum could be obtained only in the solvent suppression mode and this limited the complete characterisation of this compound. This led us to carry out only a "tentative assignment" of the spectrum of this compound. In the aromatic region, as expected, the ^{1}H NMR was characterised by a series of signals assignable to the 13 aromatic protons. A singlet at 6.18 ppm, integrating as two protons, was assigned to the benzylic methylene protons. These data suggest that the crotyl chain was no longer present. In the absence of other factors, and consistent with the observed mass of *m/z* 352.98, we proposed the structure for **246** as shown in **Scheme 8.2.5.1.**

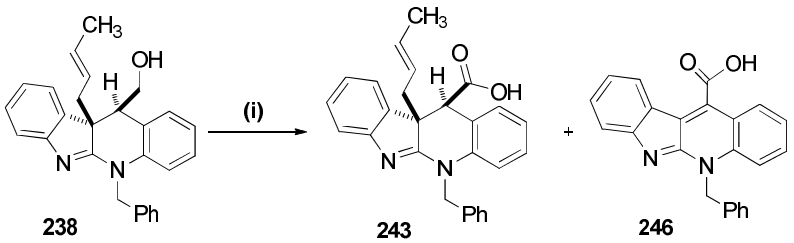

Scheme 8.2.5.1 – Proposed structure for side-product **246** isolated after the oxidation of **238** to **243** under Jones conditions.

A possible mechanism for the formation of side product **246** is outlined in **Scheme 8.2.5.2.** After protonation of the amidine nitrogen of **243** to give **247**, enolisation of the carboxylic acid (**247**) is proposed to occur under the acidic conditions of the Jones oxidation to give **248**. **248** subsequently rearranges into intermediate **249** after release of the crotyl chain. Finally **246** is formed through loss of a proton into the media.

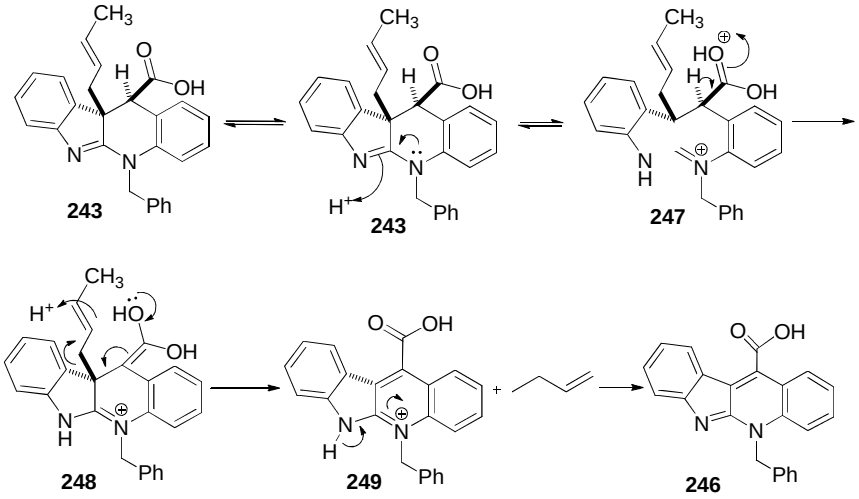

Scheme 8.2.5.2 – Proposed mechanism for the formation of side product **246** from acid **243**.

This decomposition is proposed to occur after oxidation of **238** to **243** and is not thought to take place solely due to the acidic reaction conditions. This is supported by the fact that when alcohol **238** was stirred for 5 hours at room temperature with 1.5M H_2SO_4 and acetone in the absence of the oxidising agent, it appeared to be stable and no decomposition had occurred. The analysis was carried out using the LC-MS conditions previously described.

These studies led us to conclude that there were three possible causes for the observed low yields of oxidation of **238** to **271**:

1. The zwitterionic nature of **243**, with a variable amount of **243** lost in water during work up;
2. Instability of the intermediate aldehyde **244** during the conditions used for the Jones oxidation;
3. Decomposition of **243** to side product **246**, as suggested by LC-MS and ^{1}H NMR analysis.

While no obvious solution could be envisaged for the first two problems, it was proposed that functionalisation of the crotyl chain to a saturated chain could solve the third problem. In order to test this hypothesis, the synthesis of a re-designed model substrate was planned. This work will be described in the next section.

8.3 Functionalisation of the Crotyl Chain of 231

Manipulation of the crotyl chain at C-10b is ultimately required for the construction of the second amidine moiety of perophoramidine (**182**). Furthermore, based on the previously proposed mechanism for the decomposition of acid **243** to **246**, it was envisaged that conversion of the crotyl chain to a saturated two carbon unit should avoid this decomposition, leading to expected higher yields during the final oxidation-esterification process. Thus, synthesis of the target compound **250** was planned (**Scheme 8.3.1**). Aldehyde **251** could be obtained after dihydroxylation of the crotyl double bond of **231** and subsequent cleaveage. Reduction of **251** to **252** followed by protection of the resulting alcohol would lead to **250**.

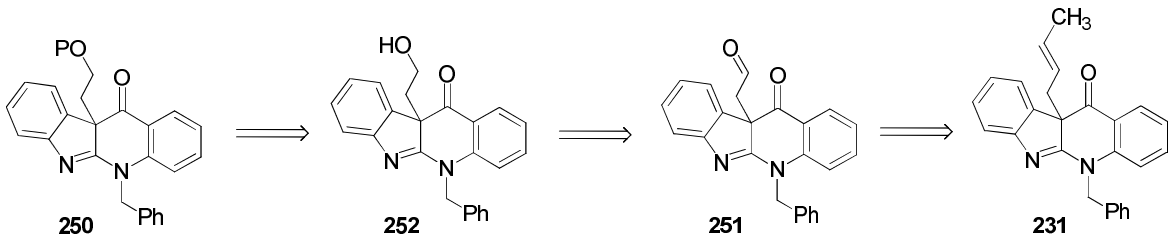

Scheme 8.3.1 – Retrosynthetic analysis for the preparation of protected alcohol **250** from ketone **231**.

With **250** in hand, functionalisation of **250** to alcohol **253** *via* epoxide **254** would then lead to the substrate required for the Jones oxidation (**253**, **Scheme 8.3.2**).

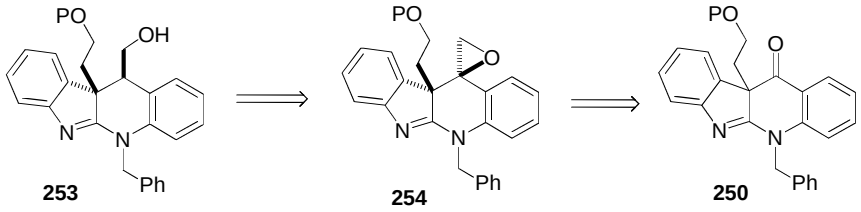

Scheme 8.3.2 – Retrosynthetic analysis for the preparation of primary alcohol **253** from ketone **250**. P = generic protecting group.

8.3.1 Conversion of the C-10b Crotyl Chain into a Saturated Protected Alcohol

Ketone **231** was treated with catalytic amounts of OsO_4 in the presence of NMO to afford the dihydroxylated product **255** as a mixture of diastereoisomers (**Scheme 8.3.1.1**). This was suggested by the presence of two distinct sets of benzylic protons which were observed as four doublets integrating as one proton each. However, due to the complexity of the ^{1}H NMR spectrum of the crude material, purification of **255** was not attempted.

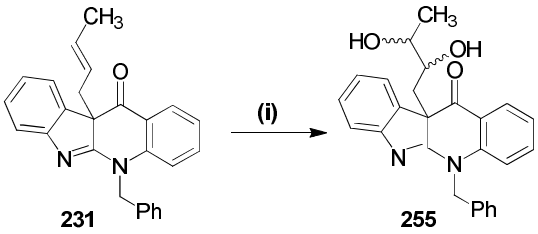

Scheme 8.3.1.1 – Synthesis of diol **255** from alkene **231**. *Reagents and Conditions:* (i) NMO (2 eq.), OsO_4 (cat.), THF:H_2O (9:1), 12 h, rt (100% conversion, determined by ^{1}H NMR spectroscopy).

Treatment of **255** with lead tetra-acetate afforded aldehyde **251** (**Scheme 8.3.1.2**). As in the case of **244**, this intermediate underwent rapid decomposition and therefore full characterisation was not possible. Consistent with the structure of **251**, the ^{1}H NMR spectrum showed a triplet at 9.17 ppm, which was assigned to the aldehyde proton. The two diastereotopic methylene protons next to the aldehyde were observed as two doublets of doublets at 3.09 ppm and 2.79 ppm respectively. LR-MS analysis also showed the expected peak corresponding to **251** [*m/z* 388.84 $(M+Na)^+$] thus confirming its successful synthesis.

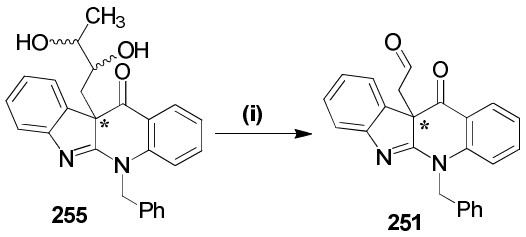

Scheme 8.3.1.2 – Cleavage of diol **255** to aldehyde **251**. *Reagents and Conditions:* $Pb(AcO)_4$ (2 eq.), DCM, 0.5 h, rt (100% conversion, determined by ^1H NMR spectroscopy).

Indeed, aldehyde **251** is of great value for the future total synthesis of perophoramidine **182**. It was envisaged that reductive amination of **251** with an appropriate protected amine would afford analogue **256**, which is a suitable starting point for progression towards the construction of the second amidine unit of **182** (**Scheme 8.3.1.3**).

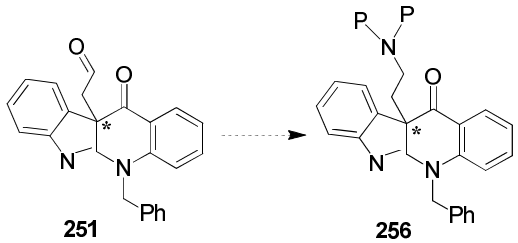

Scheme 8.3.1.3 – Proposed conversion of aldehyde **251** to protected amine **256** *via* reductive amination. P = generic protecting group.

Due to the rapid decomposition of aldehyde **251**, it was decided to carry out an immediate reduction to the corresponding alcohol **252**. Treatment of **251** with $NaBH(AcO)_3$ (1.1 eq.) afforded alcohol **252** (**Scheme 8.3.1.4**). Formation of a single product was observed by ^1H NMR analysis, therefore suggesting that the reduction occurred selectively at the most electrophilic aldehyde over the C-11 ketone or the amidine group.

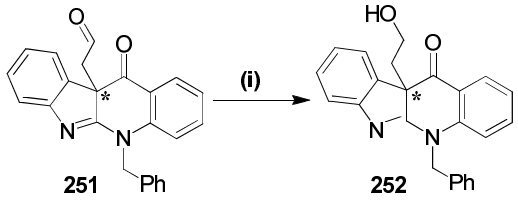

Scheme 8.3.1.4 – Synthesis of alcohol **252**. *Reagents and Conditions*: (i) $NaBH(AcO)_3$ (1.1 eq.), THF, 18 h, rt.

The ^{1}H NMR spectrum of the crude material of **252** was characterised by the disappearance of the triplet previously assigned to the aldehyde proton. Furthermore, the four diasterotopic protons of the two methylene groups now appeared as two multiplets at 3.49 and 2.45 ppm, integrating as two protons each. The LR-MS analysis showed a peak with the expected molecular weight at *m/z* 390.85 $(M+Na)^{+}$. Purification of alcohol **252** appeared difficult by silica gel column chromatography, probably due to its high polarity. Therefore, a full characterisation of **252** was not carried out at this stage. It was envisaged that protection of the hydroxyl functionality of **252** would reduce the polarity and allow for a more efficient purification of **250**.

Therefore, **252** was treated with TBDMSCl in the presence of imidazole to afford target compound **250** (**Scheme 8.3.1.5**). As previously carried out for **238**, **250** was purified using basic silica gel column chromagraphy. Protected alcohol **250** was obtained in 49% yield over four steps, including the final purification.

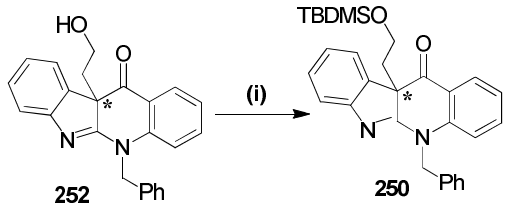

Scheme 8.3.1.5 – TBDMS protection of **252** to give **250**. *Reagents and Conditions*: (i) TBDMSCl (1.1 eq.), imidazole (2.2 eq.), DCM, 12 h, rt (49% after four steps).

The protons of the TBDMS protecting group appeared as one singlet integrating for nine protons (0.75 ppm) and two singlets (-0.12 and -0.14 ppm) integrating for three protons each, confirming that protection of the hydroxyl group was successful.

Due to time constraints, **250** is the only protected alcohol synthesised in this study. Protection of the alcohol functionality of **252** with other protecting groups, particularly acid resistant groups, was not attempted. With **250** in hand, the next step was functionalisation of the C-11 ketone to the corresponding primary alcohol. This would allow us to test the feasibility of the previously developed reactions (epoxidation and reductive opening) in the presence of the new saturated substituent at C-10b.

8.3.2 Synthesis of Alcohol 253

Intermediate **250** was converted into target alcohol **253** according to the two step procedure previously described in **Sections 8.1.3** and **8.1.4**. Ketone **250** was treated with ICH_2Cl and MeLi-LiBr to afford epoxide **254** in good yield (75%, **Scheme 8.3.2.1**).

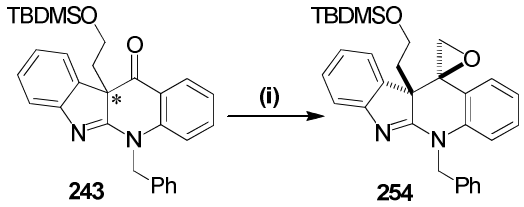

Scheme 8.3.2.1 – Synthesis of epoxide **243** from ketone **250**. *Reagents and Conditions:* (i) ICH_2Cl (1.3 eq.), MeLi-LiBr (1.2 eq.), THF, -78 °C (0.5 h) to rt, 18 h (75%).

Finally, epoxide **254** underwent reductive opening to afford **253** after treatment with $BF_3.OEt_2$ and $NaBH_3CN$ (**Scheme 8.3.2.2**).

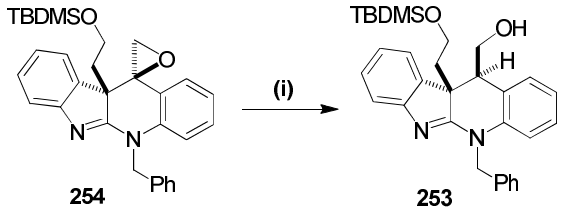

Scheme 8.3.2.2 – Preparation of alcohol **253** from epoxide **254**. *Reagents and Conditions:* (i) $BF_3.OEt_2$ (4 eq.), $NaBH_3CN$ (2.5 eq.), THF, -78 °C to rt, 3 h (45%).

The successful preparation of final compound **253** suggests that manipulation of the crotyl chain at C-10b can therefore be carried out before conversion of the C-11 ketone to a primary alcohol.

With alcohol **253** in hand, oxidation to the corresponding acid **257** was attempted. As the TBDMS protecting group was not considered stable enough under the acidic conditions of the Jones oxidation, this methodology was not employed. PDC in DMF were used instead (**Scheme 8.3.2.3**).

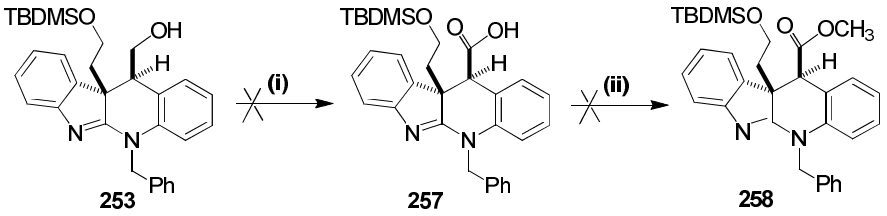

Scheme 8.3.2.3 - Attempted conversion of alcohol **253** to the corresponding ester **258** *via* **257**. *Reagents and Conditions*: (i) PDC (3 eq.), DMF, 24h , rt; (ii) $TMSCH_2N_2$ (2 eq.), MeOH, O.5h, rt

After 24 h stirring at room temperature, consumption of **253** was observed by TLC. Disappointingly, once again analysis of the crude reaction by ^{1}H NMR showed the presence of a complex mixture of products. A singlet ~4.00 ppm was observed and tentatively assigned to the acidic α-proton at C-11 of the newly formed acid **257**. Therefore, esterification of this complex mixture was attempted using $TMSCH_2N_2$ in methanol. Unfortunately, the ^{1}H NMR spectrum of the crude esterification reaction product was difficult to interpret and the diagnostic peak of the protons of the new ester methyl group of **258** could not be detected. Due to time constraints, these studies were abandoned and no further oxidation was attempted on **253**.

8.4 Conclusions

The successful synthesis of target model substrate **223** (**Figure 8.4.1**) has been described. Despite the fact that **223** does not bear the required halogens of perophoramidine **182**, it can be considered to be a suitable substrate for continuing the model studies aimed at the construction of the second amidine motif of perophoramidine **182**, and also to the installment of the quaternary centre at C-11.

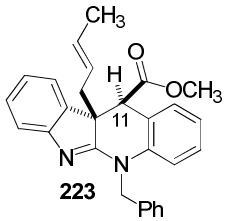

Figure 8.4.1 – Structure of target ester **223.**

Despite the successful optimisation of the reductive opening of **235**, the final steps of the synthesis of **223** were poor in terms of yield. This still represents a limitation, as a multigram synthesis of **223** is required for the continuation of the synthesis. Despite the numerous

attempts at optimisation, no improved yields were observed for the oxidation of **238** to acid **243** and subsequent esterification to **223**. Three possible causes for the observed low yields of **243** were proposed. In particular, it was considered that during the oxidation, formation of side product **246** would have been avoided through saturation of the crotyl chain at C-10b. This consideration inspired the synthesis of model substrate **253** (**Figure 8.4.2**).

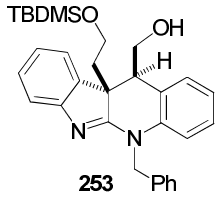

253

Figure 8.4.2 – Structure of the new primary alcohol **253.**

Although optimal conditions for the oxidation of **253** to the corresponding acid were not obtained during our studies, the presence of the TBDMS group on **253** proved that manipulation of the C-11 ketone can be carried out after functionalisation of the C-10b crotyl chain.

Significantly, the preparation of aldehyde **251** (**Figure 8.4.3**) was successful. This intermediate is of great synthetic utility, as it can be used for further reductive amination reactions aimed towards the preparation of a suitable amine required for the construction of the second amidine motif of **182**.

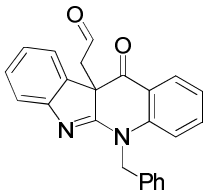

Figure 8.4.3 – Structure of aldehyde **251**.

8.5 Future Work

Based on the results discussed in this chapter, the model studies towards the total synthesis of perophoramidine **182** can be continued as follows:

1. Installment of the second quaternary carbon centre at the C-11 position of **223**. After deprotonation of the acidic α-proton on C-11, the resulting anion would be quenched with the required electrophile to give **259** (**Figure 8.5.1**).

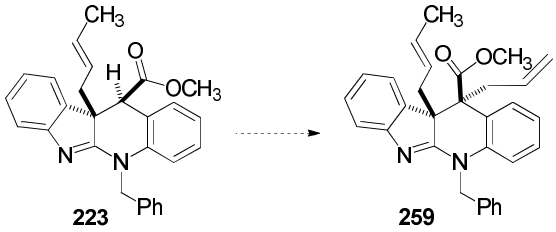

Figure 8.5.1 – Proposed alkylation at the C-11 position after treatment of **223** with base.

2. Synthesis of **260**, where the new benzyl protecting group on the C-10b substituent is resistant to the acidic conditions of the Jones oxidation (**Figure 8.5.2**).

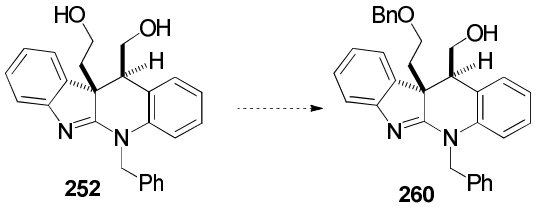

Figure 8.5.2 – Proposed new protecting group for the alcoholic function on C-10b of **252**.

3. With aldehyde **251** in hand, reductive amination aimed at installing the required amino moiety is proposed. This will allow further construction of the second amidine motif of perophoramidine **182** (**Figure 8.5.3**).

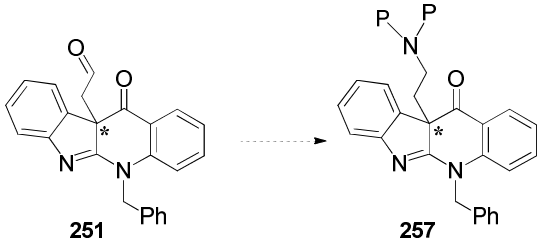

Figure 8.5.3 – Proposed reductive amination of **251** to afford intermediate **257**.

9. EXPERIMENTAL

9.1 Instrumentation and General Techniques

All chemicals and solvents were purchased from Sigma Aldrich (UK) or Alfa-Aesar and used without further purification. All reactions were carried out under a positive pressure of nitrogen or argon in flame or oven-dried glassware. DCM and THF were purified and dried according to reported procedures.[47]

Thin layer chromatography (TLC) analysis was performed on silica pre-coated SIL G-25 UV_{254} sheets (layer: 0.25 mm silica gel with fluorescent indicator UV_{254}, Alugram, UK). Compounds were visualized by UV light (UV lamp, model UVGL-58, Mineralight LAMP, Multiband UV-254/365 nm) and stained with potassium permanganate. Flash column chromatography was carried out on silica gel (40-63 μm, Fluorochem, UK). Where stated, basic silica gel was obtained upon treatment of commercially available silica with saturated aqueous NH_4OH solution according to a reported procedure.[33]

Melting points were measured with an Electrothermal 9100 capillary melting point apparatus and are uncorrected.

Fourier Transform infra-red spectra (FT-IR) were acquired on a Perkin Elmer paragon 1000 FT spectrometer. Absorption maxima are reported in wavenumbers (cm^{-1}).

Unless otherwise stated, ^1H NMR spectra were measured at room temperature (298 K) on a Bruker DPX 400 (^1H = 400 MHz) and Bruker Avance 300 (^1H = 300.1 MHz) instruments. Deuterated solvents were used and ^1H NMR chemical shifts were internally referenced to $CHCl_3$ (7.26 ppm) in chloroform-d_1 solution, to $CD_2HSO_2CHD_2$ (2.50 ppm) in dimethylsulfoxide-d_6 solution. Chemical shifts are expressed as δ in unit of ppm.

^{13}C NMR spectra were recorded in the same conditions and in the same solvents using the PENDANT sequence mode on a Bruker DPX 400 (^{13}C = 100 MHz). Data processing was carried out using TOPSPIN 2 NMR version (Bruker UK, Ltd). In ^1H NMR assignment the multiplicity used is indicated by the following abbreviations: s = singlet, d = doublet, dd = doublet of doublets, t = triplet, q = quartet, m = multiplet, brs = broad singlet. Signals of protons and carbons were assigned, as far as possible, by using the following two-dimensional

NMR spectroscopy techniques: [^{1}H-^{1}H] COSY, [^{1}H-^{13}C] HSQC (Heteronuclear Single Quantum Coherence) and long range [^{1}H-^{13}C] HMBC (Heteronuclear Multiple Bond Connectivity).

Mass spectrometry analysis (electrospray mode, ES; chemical ionization mode, CI) were performed by Ms Caroline Hosburgh and were recorded on a high performance orthogonal acceleration reflecting TOF mass spectrometer operating in positive and negative mode, coupled to a Waters 2975 HPLC.

HPLC analyses were performed on a GILSON UV-VIS 155 HPLC system under gradient conditions (**Table 9, Method A**) using a reverse phase (RP) Gemini 5µ C18 110A column (250 mm × 4.6 mm, 5 micron, Phenomenex). The concentration of the compounds were *ca.* 4 mmol, injection volumes were 20 µL, flow rate was 1 mL/min and detection was acquired with UV (254 nm).

LCMS analyses were carried out under gradient conditions (**Table 9, Method B**) on a WATERS 2795 separation module connected to a MICROMASS LCT under gradient conditions (Table 9) using a reverse phase (RP) WATERS XTerra SP18 5 µM, 3.0 × 50 mm column. The flow rate was 1mL/min, whereas detection was acquired with UV (254 nm).

Table 9. HPLC and LCMS Elution Methods.

Method A (RP)			**Method B (RP)**		
Time (min)	**% H_2O[a]**	**% CH_3CN**	**Time (min)**	**% H_2O**	**% CH_3CN**
0	80	20	0	98	2
20	20	80	7	2	98
24	20	80	10	2	98
27	80	20	11	98	2
30	80	20	-	-	-

[a] With 0.1% TFA

9.2 General Experimental Procedures

2-(Benzylphenylamino)-1*H*-indole-3-carboxylic acid methyl ester (226)[31]

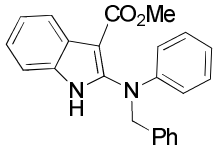

To a stirring solution of indole-3-carboxylic acid methyl ester (**225**) (24.8 g, 142 mmol, 1 eq.) in DCM (400 ml) at 0 °C, were added *N*-chlorosuccinimide (20.8 g, 156 mmol, 1.1 eq.) and *N,'N*-dimethylpiperazine (7.50 mL, 77.6 mmol, 0.5 eq.) and the reaction mixture stirred for 2 h at 0 °C. After this time, a solution of trichloroacetic acid (6.36 g, 38.9 mmol, 0.27 eq.) and *N*-benzylaniline (51.9 g, 283 mmol, 2 eq.) in DCM (400 mL) was added and the reaction mixture allowed to warm to room temperature and stirred for further 2 h. The reaction mixture was sequentially washed with aqueous $NaHCO_3$ solution (10%, 400 mL), hydrochloric acid (1.0M, 400 mL) and water (400 mL). The organic layers were dried ($MgSO_4$), filtered through a pad of silica and concentrated at reduced pressure to afford the crude product which was crystallised from CH_2Cl_2/hexane to yield the desired product **226** as colourless crystals (33.0 g, 92 mmol, 65%). Mp 163-165 °C (*lit.*[31] 165-166 °C); δ_H (300 MHz, $CDCl_3$) 8.26 (brs, 1H, NH), 8.11-8.15 (m, 1H, ArH), 7.16-7.37 (m, 10H, ArH), 6.83-6.91 (m, 3H, ArH), 5.13 (s, 2H, C$\underline{H_2}$-Ph) and 3.80 (s, 3H, CH_3O); *m/z* (ES^+) 379.06 [$(M+Na)^+$, 100%]; *m/z* (ES^-) 355.04 [$(M-H)^-$, 100%]. Data are in agreement with the literature.[31]

5,6-Dihydro-5-benzylindolo[2,3-*b*]quinolin-11-one (227)[31]

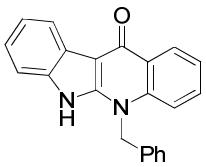

2-(Benzylphenylamino)-1*H*-indole-3-carboxylic acid methyl ester (**226**) (10 g, 28.1 mmol) was dissolved in Ph_2O (150 ml) and the reaction mixture stirred at reflux for 2 h. After cooling down to room temperature, the desired product **227** was obtained as a brown micro crystalline solid (7.80 g, 24.0 mmol, 85%). Mp *ca.* 300 °C (*lit.*[31] *ca.* 300 °C, dec.); δ_H (400 MHz, $(CD_3)_2SO$) 12.25 (s, 1H, NH), 8.41 (dd, J = 8.4, 1.3 Hz, 1H, ArH), 8.23-8.26 (m, 1H, ArH), 7.57-7.64 (m, 2H, ArH), 7.43-7.46 (m, 1H, ArH), 7.16-7.46 (m, 8H, ArH) and 5.81 (s, 2H, C$\underline{H_2}$-Ph); *m/z* (ES^+) 347.09 [$(M+Na)^+$, 100%]; *m/z* (ES^-) 323.06 [$(M-H)^-$, 100%]. Data are in agreement with the literature.[31]

11-Chloro-5-benzyl-5*H*-indolo[2,3-*b*]quinoline (224)[31]

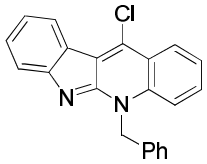

A solution of 5,6-dihydro-6-benzylindolo[2,3-*b*]quinolin-11-one (**227**) (7.80 g, 24.1 mmol) in $POCl_3$ (100 ml) was stirred at reflux for 1 h. After cooling to room temperature, the $POCl_3$ was partially removed at reduced pressure. The residue was added to a crushed ice-water mixture and basified by the addition of saturated aqueous $NaHCO_3$ solution. The yellow residue became an orange colour, after which time the aqueous phase was extracted with DCM (3 × 100 mL), the organic phase combined, dried ($MgSO_4$) and the solvent removed at reduced pressure. The desired product was obtained as bright orange solid (6.80 g, 20.9 mmol, 86%). Mp 219-221 (*lit*.[31] 220-222 °C); δ_H (400 MHz, $CDCl_3$) 8.48 (d, *J* = 7.7 Hz, 1H, ArH), 8.41 (d, *J* = 8.3 Hz, 1H, ArH), 7.73 (d, *J* = 8.0 Hz, 1H, ArH), 7.56-7.64 (m, 3H, ArH), 7.41-7.46 (m, 1H, ArH), 7.17-7.32 (m, 6H, ArH) and 6.15 (s, 2H, C$\underline{H_2}$Ph); *m/z* (ES^+) 365.01 [$(M+Na)^+$, 100%]. Data are in agreement with the literature.[31]

5,10b-Dihydro-10b-crotyl-5-benzyl-10b*H*-indolo[2,3-*b*]quinolin-11-one (231)

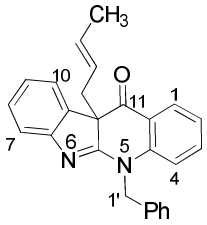

A solution of alkoxide was prepared by the careful addition of sodium (1.72 g, 75 mmol, 2 eq.) to 3-buten-2-ol (21.0 g, 243 mmol, 3.2 eq.) in THF (5 mL). This solution was added to a stirring solution of 11-chloro-5-benzyl-5*H*-indolo[2,3-*b*]quinoline **(224)** (10 g, 37.5 mmol, 1 eq.) in THF (200 mL). The resulting reaction mixture was stirred at room temperature for 18 h. Saturated aqueous NH_4Cl was then added (100 mL) and the solvent removed at reduced pressure. The resulting residue was suspended in water (100 mL) and extracted with DCM (3 × 100 mL). The combined organic extracts were dried ($MgSO_4$) and the solvent removed at reduced pressure to afford the crude ether **230**. **230** was dissolved in THF (150 mL) and stirred at reflux for 5 h. After cooling to room temperature, the residue was purified by column chromatography (Hexane/EtOAc, 95:5 to 90:10) to afford the desired product **231** as a yellow microcrystalline powder (8.50 g, 22.5 mmol, 60%). Mp 148-150 °C; ν_{max} cm^{-1} (KBr) 1697 (C=O), 1558 (Ar), 1469 (CH_3, CH); δ_H (300 MHz, $CDCl_3$) 7.95 (dd, 1H, ^2J = 7.7 Hz, ^3J = 1.6 Hz, H-1), 7.70 (dd, 1H, ^2J = 7.7 Hz, ^3J = 0.6 Hz, H-10), 7.53-7.21 (m, 8H, ArH), 7.20-

6.97 (m, 3H, ArH), 5.92 (d, 1H, *J* = 16.5 Hz, C*H*$_2$-Ph), 5.35-5.19 (m, 1H, CH$_3$C*H*=CH), 5.11-4.96 (m, 2H, C*H*$_2$-Ph, CH=C*H*CH$_2$), 2.87 (dd, 1H, ^2J = 13.3 Hz, ^3J = 6.5 Hz, CH=CHC*H*$_2$), 2.46 (dd, 1H, ^2J = 13.3 Hz, ^3J = 8.0 Hz, CH=CHC*H*$_2$) and 1.53 (dd, 3H, ^2J = 6.2 Hz, ^3J = 0.6 Hz, C*H*$_3$CH=CH); δ_C (100 MHz, $CDCl_3$) 192.9 (C=O), 172.3 (C5a), 153.5 (C6a), 144.8 (C4a), 136.9 (C1'a), 133.6 (C10a), 131.6 (CH$_3$*C*H=CH), 129.0 (CH, Ar), 128.7 (CH, Ar), 128.4 (CH, Ar), 127.8 (CH, Ar), 127.6 (CH, Ar), 126.7 (C2', C6'), 124.8 (CH, Ar), 123.1 (CH, Ar), 122.6 (CH, Ar), 122.5 (CH$_3$CH=*C*H), 119.3 (C11a), 118.7 (CH, Ar), 115.5 (CH, Ar), 66.5 (C10b), 49.6 (*C*H$_2$-Ph), 44.3 (CH=CH*C*H$_2$) and 17.9 (*C*H$_3$CH=CH); *m/z* (ES$^+$) 401.09 [(M+Na)$^+$, 100%]; HRMS (ES$^+$) [Found: (M+Na)$^+$, 401.1614, $C_{23}H_{20}O_4Na$ requires 401.1630] (-3.9 ppm). Crystals suitable for X-ray analysis were grown by slow evaporation from Hexane/EtOAc (1:1).

6-Crotyl-5-benzyl-5*H*-indolo[2,1-b]quinazolin-12-one (232)

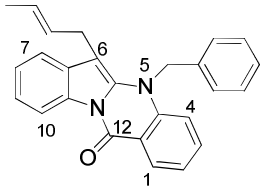

Compound **232** was obtained as a side product during the synthesis of **231** and subsequent analysis carried out. Yellow powder (3.11 g, 8.25 mmol, 22% over two steps). Mp 188-191 °C; ν_{max} cm^{-1} (KBr) 1683 (C=O), 1613 (C=O), 784 (CH), 638 (CH); δ_H ($CDCl_3$, 400 MHz) 8.83 (dd, 1H, ^2J = 7.7 Hz, ^3J = 1.5 Hz, ArH), 8.44 (dd, 1H, ^2J = 7.9 Hz, ^3J = 1.5 Hz, H-1), 7.58-7.23 (m, 9H, ArH), 7.17 (t, 1H, *J* = 7.9 Hz, ArH), 6.97 (d, 1H, *J* = 8.5 Hz, ArH), 5.71-5.57 (m, 1H, CH$_3$C*H*=CH), 5.46 (s, 2H, CH$_2$-Ph), 5.40-5.25 (m, 1H, CH$_3$CH=C*H*), 3.36-3.28 (m, 2H, CH=CHC*H*$_2$) and 1.62 (dd, 3H, ^2J = 6.4 Hz, ^3J = 1.6 Hz, C*H*$_3$CH=CH); δ_c ($CDCl_3$, 100 MHz) 159.6 (C=O), 142.5 (C4a), 137.2 (C12a), 135.3 (C1'a), 135.1 (CH, Ar), 131.5 (C6a), 130.l (CH, Ar), 129.6 (CH$_3$*C*H=CH), 129.l (CH, Ar), 128.0 (CH, Ar), 126.4 (CH, Ar), 125.7 (CH=*C*HCH$_2$), 124.6 (CH, Ar), 122.0 (CH, Ar), 121.0 (CH, Ar), 116.8 (CH, Ar), 116.6 (CH, Ar), 114.3 (C10a), 113.4 (CH, Ar), 94.0 (C6), 52.7 (*C*H$_2$Ph), 27.1 (CH=CH*C*H$_2$) and 18.2 (*C*H$_3$CH=CH); *m/z* (ES$^+$) 379.12 [(M+Na)$^+$, 100%].

rac-(10b*S*,11*S*)-10b-Crotyl-5-benzyl-5,11-dihydro-10b*H*-indolo[2,5-*b*]quinolin-11-spiro-2'-oxirane (235)

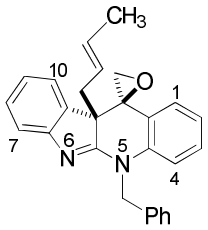

To a mixture of 5,10b-dihydro-10b-crotyl-5-benzyl-10b-*H*-indolo[2,3-*b*]quinolin-11-one (**231**) (4.90 g, 12.9 mmol, 1 eq.) in THF (50 mL) at -78 °C was added slowly MeLi-LiBr (12.2 mL of a 1.5 M solution, 19.4 mmol, 1.5 eq) over a period of 20 minutes. Chloroiodomethane (1.22 mL, 19.4 mmol, 1.5 eq.) was added and the reaction mixture stirred for 30 min at -78 °C before allowing to warm to room temperature. After stirring for 18 h at room temperature, saturated aqueous NH_4Cl solution (50 mL) was added and the solvent removed at reduced pressure. Water (50 mL) and Et_2O (50 ml) were added, the organic phase was separated and the aqueous phase further extracted with Et_2O (3 x 50 mL). The combined organic extracts were dried ($MgSO_4$) and filtered through a plug of silica. The resulting organic solution was left to slowly evaporate at ambient temperature until nearly dry (*ca*. 10 mL of Et_2O remaining). The desired product **235** was obtained as large colourless crystals (4.45 g, 11.35 mmol, 88%). Mp 138-141 °C ; ν_{max} cm^{-1} (KBr) 3029 (CH=CH), 2938 (N-CH_2), 1813, 1689 (CH=CH), 1558 (Ar), 1491 (CH_3, CH); δ_H (400 MHz, $CDCl_3$) 7.43-7.16 (m, 10H, ArH), 7.07-6.97 (m, 2H, ArH), 6.91 (dd, 1H, ^2J = 8.2 Hz, ^3J = 0.6 Hz, ArH), 5.91 (d, 1H, J = 16.5 Hz, C$\underline{H_2}$-Ph), 5.33-5.21 (m, 1H, $CH_3C\underline{H}$=CH), 4.97-4.83 (m, 2H, C$\underline{H_2}$-Ph, CH=C$\underline{H}CH_2$), 3.07 (d, 1H, J = 5.7 Hz, C$\underline{H_2}$-O), 2.81 (dd, 1H, ^2J = 14.0 Hz, ^3J = 5.8Hz, HC=CHC$\underline{H_2}$), 2.62 (dd, 1H, ^2J = 13.8 Hz, ^3J = 8.4 Hz HC=CHC$\underline{H_2}$), 2.53 (d, 1H, J = 5.6 Hz, C$\underline{H_2}$-O) and 1.45 (d, 3H, J = 6.0 Hz, C$\underline{H_3}$CH=CH); δ_C (100 MHz, $CDCl_3$) 172.6 (C5a), 155.5 (C6a), 141.5 (C10a), 137.0 (C1'a), 134.6 (C4a), 129.7 (CH, Ar), 129.4 ($CH_3\underline{C}$H=CH), 128.9 (CH, Ar), 128.8 (CH, Ar), 127.4 (CH, Ar), 126.6 (CH, C2', C6'), 124.2 (CH, Ar), 123.8 (CH_3CH=$\underline{C}$H), 123.5 (C11a), 123.3 (CH, Ar), 122.8 (CH, Ar), 122.8 (CH, Ar), 118.0 (CH, Ar), 115.1 (CH, Ar), 60.2 ($\underline{C}H_2$-O), 55.3 (C10b), 53.6 (C11), 49.9 (C$\underline{H_2}$Ph), 37.3 (CH=CH$\underline{C}H_2$) and 17.9 ($\underline{C}H_3$CH=CH); *m/z* (ES^+) 415.02 [$(M+Na)^+$, 100%]; HRMS (ES^+) [Found: $(M+H)^+$, 393.1956, $C_{27}H_{25}N_2O$ requires 393.1967] (-2.6 ppm).

rac-(10b*R*,11*S*)-10b-Crotyl-11-hydroxymethyl-5-benzyl-5,11-dihydro-10b*H*-indolo[2,5-*b*]quinoline (238)

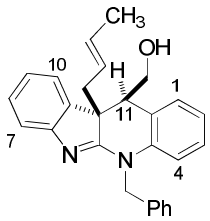

To a stirring solution of rac-(10b*S*, 11*S*)-10b-crotyl-5-benzyl-5,11-dihydro-10b*H*-indolo[2,5-*b*]quinolin-11-spiro-2'-oxirane (**235**) (5.30 g, 13.5 mmol, 1 eq.) in THF (150 mL) at -78 °C was added $NaBH_3CN$ (2.12 g, 33.7 mmol, 2.5 eq.). A solution of $BF_3.OEt_2$ (6.78 mL, 54.0 mmol, 4 eq.) was then added over a period of 20 min and the resulting reaction mixture allowed to warm to room temperature. After stirring for 18 h at room temperature, the reaction was quenched by the addition of water (50 mL) and the aqueous solution extracted with DCM (4 x 50 mL). The combined organic extracts were washed with brine (50 mL), dried ($MgSO_4$), and the solvent removed at reduced pressure to afford the crude product. Purification by basic silica gel column chromatography (Hexane/EtOAc, 80:20) afforded the desired product **238** as a yellow oily solid (3.49 g, 8.64 mmol, 64%). Mp 130-133 °C; ν_{max} cm^{-1} (KBr) 3375 (OH), 3029 (CH=CH), 2931 (N-CH_2), 1615, 1558 (Ar), 1494 (CH_3, CH), 1454, 1408 (OH), 1326 (OH), 1214 (OH) and 1026 (OH); δ_H (300 MHz, $CDCl_3$) 7.68-7.62 (d, 1H, J = 7.62 Hz, ArH), 7.42-7.16 (m, 9H, ArH), 7.11-6.98 (m, 2H, ArH), 6.93 (dd, 1H, ^2J = 8.0 Hz, ^3J = 1.1 Hz, ArH), 5.79 (d, 1H, J = 16.4 Hz, C$\underline{H_2}$-Ph), 5.25-5.09 (m, 1H, $CH_3C\underline{H}$=CH), 4.86 (d, 1H, J = 16.4 Hz, C$\underline{H_2}$-Ph), 4.76-4.58 (m, 2H, C$\underline{H_2}$OH), 4.52-4.35 (m, 1H, CH_3CH=C$\underline{H}$), 3.15 (d, 1H, J = 5.2 Hz, H-11), 2.40 (d, 2H, J = 7.0 Hz, CH=CHC$\underline{H_2}$), 1.94 (brs, 1H, OH) and 1.38 (dd, 3H, ^2J = 6.5 Hz, ^3J = 1.5 Hz, C$\underline{H_3}$CH=CH); δ_C (100 MHz, $CDCl_3$) 173.6 (C5a), 153.2 (C6a), 140.6 (C4a), 136.2 (C1'a), 135.9 (C10a), 129.8 (CH, Ar), 129.0 (CH, Ar), 128.9 (CH, Ar), 128.4 (CH, Ar), 127.6 (CH, Ar), 127.3 (CH, Ar), 126.7 (CH, Ar), 125.7 (C11a), 124.5 (CH, Ar), 124.2 (CH, Ar), 124.0 (CH, Ar), 123.1 (CH, Ar), 116.9 (CH, Ar), 116.0 (CH, Ar), 61.4 ($\underline{C}H_2$OH), 54.9 ($\underline{C}H_2$-Ph), 51.1 (C10b), 44.0 (C11), 33.9 (CH=CH$\underline{C}H_2$) and 17.8 ($\underline{C}H_3$CH=CH); *m/z* (ES^+) 417.10 [$(M+Na)^+$, 100%]; HRMS (ES^+) [Found: $(M+Na)^+$, 417.1939 , $C_{27}H_{26}N_2ONa$ requires 419.1943] (-0.8 ppm). Crystals suitable for X-ray analysis were obtained by slow evaporation from methanol.

rac-(10b*R*,11*S*)-10b-Crotyl-5-benzyl-5,11-dihydro-10b*H*-indolo[2,5-*b*]quinoline-11-carboxylic acid methyl ester (223)

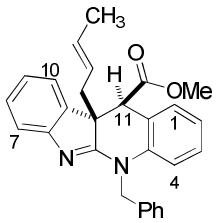

To a stirring mixture of CrO_3 (630 mg, 6.3 mmol, 5 eq.) and celite (2 g) in 1.5M H_2SO_4 (10 mL) was added in one portion a solution of rac-(10b*R*,11*S*)-10b-crotyl-11-hydroxymethyl-5-benzyl-5,11-dihydro-10b*H*-indolo[2,5-*b*]quinoline (**239**) (500 mg, 1.18 mmol, 1 eq.) in acetone (20 mL). After stirring for 5 h at room temperature, *i*-PrOH (10 mL) was added and the reaction stirred for further 30 min. The mixture was then filtered through celite and the celite washed with additional EtOAc (10 mL). After adding brine (10 mL) to the filtrate, and the pH of the aqueous layer adjusted to pH 7 by addition of saturated aqueous $NaHCO_3$ solution. The organic phase was separated and the aqueous phase further extracted with EtOAc (4 x 10 mL). The combined organic extracts were dried ($MgSO_4$) and the solvent removed at reduced pressure to afford the crude acid **243**. The acid was then dissolved in MeOH (20 mL) and Me_3SiCHN_2 (1.25 mL of a 2.0M solution in Et_2O, 2.36 mmol) was added. After stirring for 30 min at room temperature, AcOH (0.5 mL) was added and the reaction mixture stirred for a further 30 min. After this time the solvent was removed at reduced pressure and the residue partitioned between layers of saturated aqueous $NaHCO_3$ solution (10 mL) and DCM (10 mL). The organic phase was separated and the aqueous phase further extracted with DCM (3 x 10 mL). The combined extracts were dried ($MgSO_4$) and the solvent removed at reduced pressure. The crude product was purified by flash column chromatography (Hexane/EtOAc, 95:5 to 90:10) to afford the desired product **223** as a colourless crystalline solid (124 mg, 0.29 mmol, 25% over two steps). Mp 145-147 ° C; ν_{max} cm^{-1} (KBr) 3453, 3026 (CH=CH), 2953 (N-CH_2), 2850 (O-CH_3), 1735 (C=O), 1558 (Ar), 1493 (CH_3, CH); δ_H (400 MHz, $CDCl_3$) 7.41-7.14 (m, 8H, ArH), 7.10 (d, 1H, ArH), 7.06-6.93 (m, 4H, ArH), 5.76 (d, 1H, J = 16.5 Hz, C$\underline{H_2}$-Ph), 5.27-5.14 (m, 1H, $CH_3C\underline{H}$=CH), 4.94 (d, 1H, J = 16.5 Hz, C$\underline{H_2}$-Ph), 4.73-4.60 (m, 1H, HC=C$\underline{H}CH_2$), 4.14 (s, 1H, H-11), 3.94 (s, 3H, C$\underline{H_3}$O), 2.91 (dd, 1H, ^2J = 14.2 Hz, ^3J = 6.0 Hz, CH=CHC$\underline{H_2}$), 2.62 (dd, 1H, ^2J = 14.3 Hz, ^3J = 8.0 Hz , CH=CHC$\underline{H_2}$) and 1.37 (dd, 3H, ^2J = 6.5 Hz, ^3J = 0.6 Hz, C$\underline{H_3}$CH=CH); δ_C (100 MHz, $CDCl_3$) 172.9 (C=O), 171.9 (C5a), 155.9 (C6a), 140.7 (C4a), 137.0 (C10a), 136.8 (C1'a), 129.1 ($CH_3\underline{C}$H=CH), 128.9 (CH, Ar), 128.8 × 2 (CH, Ar), 127.4 (CH, Ar), 127.3 (CH, Ar), 126.9 (CH, Ar), 124.5 (CH_3CH=$\underline{C}$H), 123.1 (CH, Ar), 122.7 (CH, Ar), 122.3 (CH, Ar), 121.5 (C11a), 117.7 (CH, Ar), 115.8 (CH, Ar), 53.6 (C10b), 52.1 ($\underline{C}H_3O$), 50.2 ($\underline{C}H_2$-Ph), 49.4 (C11), 33.4 (CH=CH$\underline{C}H_2$) and 17.9 ($\underline{C}H_3CH$=CH); *m/z* (ES^+)

445.10 [$(M+Na)^+$, 100%]; HRMS (ES^+) [Found: $(M+Na)^+$, 423.2071, $C_{28}H_{27}N_2O_2$ requires 423.2073] (-0.4 ppm).

5-Benzyl-5*H*-indolo[2,3-*b*]quinoline-11-carboxylic acid (246)

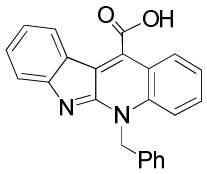

Obtained as a side product during the synthesis of **243** and isolated as a colourless oil after semi-preparative HPLC according to METHOD A (2.77 min). δ_H (400 MHz, $CDCl_3$) 8.22 (dd, 2H, ^2J = 16.7 Hz, ^3J = 7.7 Hz, ArH), 8.02 (d, 1H, J = 8.7 Hz, ArH), 7.89 (t, 1H, J = 7.0 Hz, ArH), 7.72-7.52 (m, 3H, ArH), 7.44-7.15 (m, 6H, ArH), 6.22 (s, 2H, C$\underline{H_2}$-Ph); *m/z* (ES^+) 352.98 $(M+Na)^+$, 100%.

5,10b-Dihydro-10b-(2-((*tert*-butyldimethylsilyl)oxy)ethyl)-5-benzyl-10b*H*-indolo[2,3-*b*]quinolin-11-one (250)

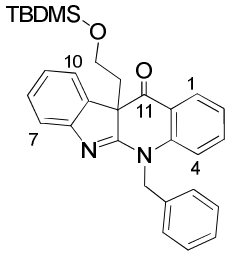

To a stirring solution of 5,10b-dihydro-10b-crotyl-5-benzyl-10b*H*-indolo[2,3-*b*]quinolin-11-one **231** (50 mg, 0.13 mmol, 1 eq.) in THF:H_2O (9:1, 2.5 mL) were added osmium tetroxide (2.5M solution in *t*-BuOH, 82 µL, cat.) and NMO (169 mg, 2.0 mmol, 2 eq.) and the reaction mixture stirred at room temperature for 18 h. After this time, saturated Na_2SO_3 solution (5 mL) was added and the resulting mixture stirred for 30 min. Brine (5 mL) was then added and the mixture extracted with DCM (3 × 5 mL), the organic layer collected, dried ($MgSO_4$) and the solvent removed at reduced pressure to afford the crude product **255** as a mixture of diastereoisomers (79 mg). Diol **255** was used in the following reaction without further purification.

To a stirring solution of the crude diol **255** (50 mg, 0.12 mmol, 1 eq.) in DCM (2.5 mL) was added lead tetraacetate (107 mg, 2 mmol, 2 eq.) reaction mixture stirred at room temperature for 45 min. After filtration through a celite column, the solvent was removed at reduced pressure to afford the crude aldehyde **251** as a yellow oil which was used in the following reaction without

further purification. δ_H (400 MHz, $CDCl_3$) 9.17 (t, 1H, J = 2.5 Hz, CHO), 7.95 (dd, 1H, ^2J = 7.8 Hz, ^3J = 1.6 Hz, ArH), 7.79 (dd, 1H, ^2J = 7.4 Hz, ^3J = 0.6 Hz, ArH), 7.55-7.17 (m, 8H, ArH), 7.15-7.03 (m, 3H, ArH), 5.91 (d, 1H, J = 16.5 Hz, C$\underline{H_2}$Ph), 5.14 (d, 1H, J = 16.5 Hz, C$\underline{H_2}$Ph), 3.10 (dd, 1H, ^2J = 15.2 Hz, ^3J = 2.5 Hz, C$\underline{H_2}$CHO) and 2.80 (dd, 1H, ^2J = 15.2 Hz, ^3J = 2.5 Hz, CH_2CHO); *m/z* (ES^+) 388.84 $(M+Na)^+$, 100%].

To a stirring solution of the crude aldehyde **251** (2.24 g, 6.1 mmol, 1 eq.) in THF (10 mL) was added sodium triacetoxyborohydride (1.3 g, 6.1 mmol, 1.1 eq.) and the reaction mixture stirred at room temperature for 18 h. Water (2 mL) was added and the mixture extracted with DCM (3 × 5 mL). The resulting organic layer was dried ($MgSO_4$) and the solvent removed at reduced pressure to give the crude product **252** as a yellow oil. ν_{max} cm^{-1} (KBr) 3200 (OH), 1695 (C=O), 1468 (CH_2), 799 (CH) and 755 (CH); δ_H ($CDCl_3$, 400 MHz) 7.95 (dd, 1H, ^2J = 7.7 Hz, ^3J = 1.6 Hz, ArH), 7.76 (dd, 1H, ^2J = 7.4 Hz, ^3J = 0.5 Hz, ArH), 7.51-6.92 (m, 11H, ArH), 5.85 (d, 1H, J = 16.7 Hz, C$\underline{H_2}$Ph), 5.15 (d, 1H, J = 16.7 Hz, C$\underline{H_2}$Ph), 2.54-2.40 (m, 2H, CH_2-C$\underline{H_2}$-OH) and 2.21-2.07 (m, 2H, C$\underline{H_2}$-CH_2); *m/z* (ES^+) 391.05 [$(M+Na)^+$, 100%]; HRMS (ES^+) [Found: $(M+Na)^+$, 369.1609, $C_{24}H_{21}N_2O_2$ requires 369.1603] (+ 1.5 ppm).

To a stirring solution of alcohol **252** (650 mg, 1.76 mmol, 1 eq.) in DCM (40 mL) were added TBDMSCl (289 mg, 1.93 mmol, 1.1 eq.) and imidazole (270 mg, 3.87 mmol, 2.2 eq.) and the resulting reaction was stirred at room temperature for 18 h. After this time saturated $NaHCO_3$ solution (20 mL) was added and the resulting mixture extracted with DCM (3 × 10 mL). The resulting organic layer was dried over $MgSO_4$ and the solvent removed at reduced pressure. The product was purified by silica gel chromatography (Hexane/EtOAc, 90:10 to 70:30) to give the desired product **250** as a yellow oil (600 mg, 49% over four steps). ν_{max} cm^{-1} (KBr) 1659 (C=O), 1212 ($SiMe_2$), 1150 (SiO), 799 (CH) and 639 (CH); δ_H ($CDCl_3$, 400 MHz) 7.93 (dd, 1H, ^2J = 7.7 Hz, ^3J = 1.6 Hz, ArH), 7.74 (dd, 1H, ^2J = 7.3 Hz, ^3J = 0.5 Hz, ArH), 7.51-7.21 (m, 8H, ArH), 7.17 (dt, 1H, ^2J = 7.4 Hz, ^3J = 1.3 Hz, ArH), 7.08 (dt, 1H, ^2J = 7.8 Hz, ^3J = 0.4 Hz, ArH), 7.00 (d, 1H, J = 8.4 Hz, ArH), 5.84 (d, 1H, J = 16.6 Hz, C$\underline{H_2}$-Ph), 5.16 (d, 1H, J = 16.6 Hz, C$\underline{H_2}$-Ph), 3.56-3.34 (m, 2H, O-C$\underline{H_2}$-CH_2), 2.50-2.37 (m, 1H, O-CH_2-C$\underline{H_2}$), 2.17-2.03 (m, 1H, O-CH_2-C$\underline{H_2}$), 0.76 (s, 9H, (C$\underline{H_3}$)$_3$C) and -0.12 (s, 6H, (C$\underline{H_3}$)$_2$Si); δ_C ($CDCl_3$, 100 MHz) 193.2 (C=O), 172.0 (C5a), 152.0 (C6a), 144.9 (C4a), 136.5 (C1'a), 135.9 (CH, Ar), 133.5 (C10a), 129.3 (CH, Ar), 129.2 (CH, Ar), 128.7 (CH, Ar), 127.8 (CH, Ar), 126.9 (CH, C2', C6'), 125.0 (CH, Ar), 123.6 (CH, Ar), 122.7 (CH, Ar), 119.6 (C11a), 119.2 (CH, Ar), 115.8 (CH, Ar), 65.0 (C10b), 59.3 (O-$\underline{C}H_2$-CH_2), 50.0 ($\underline{C}H_2$-Ph), 42.9 (O-CH_2-$\underline{C}H_2$), 27.0 ((CH_3)$_3\underline{C}$), 26.2 (($\underline{C}H_3$)$_3$C), and -5.3 (($\underline{C}H_3$)$_2$Si); *m/z* (ES^+) 483.37 [$(M+H)^+$, 100%].

rac-(10b*S*,11*S*)-(2-((*Tert*-butyldimethylsilyl)oxy)ethyl)-5-benzyl-5,11-dihydro-10b*H*-indolo[2,5-*b*]quinolin-11-spiro-2'-oxirane (254)

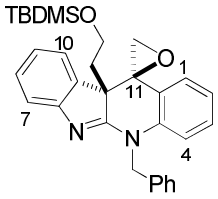

From **250** (62 mg, 0.13 mmol), prepared in an analogous way to **235**. The desired product **254** was obtained after recrystallisation from ether as colourless crystals (50 mg, 0.10 mmol, 75%). δ_H (400 MHz, $CDCl_3$) 7.64-7.34 (m, 10H, ArH), 7.25 (t, 2H, *J* = 7.4 Hz, ArH), 7.14 (d, 1H, *J* = 8.1 Hz, ArH), 6.00 (d, 1H, *J* = 16.5 Hz, C$\underline{H_2}$-Ph), 5.28 (d, 1H, *J* = 16.5 Hz, C$\underline{H_2}$-Ph), 3.72-3.62 (m, 1H, CH_2-C$\underline{H_2}$-O), 3.59-3.45 (m, 1H, CH_2-C$\underline{H_2}$-O), 3.27 (d, 1H, *J* = 5.6 Hz, C$\underline{H_2}$O), 2.75 (d, 1H, *J* = 5.6 Hz, C$\underline{H_2}$O), 2.63-2.53 (m, 1H, CH_2-C$\underline{H_2}$-O), 2.50-2.38 (m, 1H, CH_2-C$\underline{H_2}$-O), 0.97 (s, 9H, (C$\underline{H_3}$)$_3$C), -0.04 (s, 3H, (C$\underline{H_3}$)$_2$Si); δ_C (100 MHz, $CDCl_3$) 172.8 (C5a), 155.6 (C6a), 143.4 (C4a), 141.2 (C10a), 136.9 (C1'a), 129.4 (CH, Ar), 129.0 (CH, Ar), 128.9 (CH, Ar), 127.4 (CH, Ar), 126.6 (CH, Ar), 123.8 (CH, Ar), 123.4 (C11a), 123.3 (CH, Ar), 122.9 (CH, Ar), 122.8 (CH, Ar), 118.4 (CH, Ar), 115.2 (CH, Ar), 60.6 (C11), 59.4 (O-$\underline{C}H_2$-CH_2), 53.6 ($\underline{C}H_2$O), 53.2 (C10b), 49.6 ($\underline{C}H_2$-Ph), 36.6 (O-CH_2-$\underline{C}H_2$), 29.8 ((CH_3)$_3\underline{C}$), 25.0 (($\underline{C}H_3$)$_3$Si), -5.4 (($\underline{C}H_3$)$_2$Si) and -5.5 (($\underline{C}H_3$)$_2$Si); *m/z* (ES^+) 497.38 [$(M+H)^+$, 100%].

rac-(10b*R*,11*S*)-10b-)-(2-((*Tert*-butyldimethylsilyl)oxy)ethyl)-11-hydroxymethyl-5-benzyl-5,11-dihydro-10b*H*-indolo[2,5-*b*]quinoline (253)

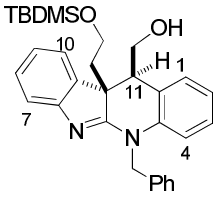

From **254** (50 mg, 0.10 mmol), prepared in an analogous way to **238.** The desired product **253** was obtained as a colourless oil after basic alumina column chromatography (Hexane/EtOAc, 90:10) (22.4 mg, 0.45 mmol, 45%). δ_H (300 MHz, $CDCl_3$) 7.65 (d, 1H, *J* = 7.5 Hz, ArH), 7.42-7.10 (m, 8H, ArH), 7.08-6.89 (m, 2H, ArH), 5.61 (d, 1H, *J* = 16.4 Hz, C$\underline{H_2}$-Ph), 5.10 (d, 1H, *J* = 16.4 Hz, C$\underline{H_2}$-Ph), 4.65 (dd, 1H, ^2J = 11.3 Hz, ^3J = 2.4 Hz, C$\underline{H_2}$OH), 4.51-4.37 (m, 1H, C$\underline{H_2}$OH), 3.29-3.15 (m, 1H, O-C$\underline{H_2}$-CH_2), 3.09 (d, 1H, *J* = 6.0 Hz, H-11), 2.94-2.82 (m, 1H, O-C$\underline{H_2}$-CH_2), 2.12-1.84 (m, 2H, O-CH_2-C$\underline{H_2}$), 0.70 (s, 9H, (C$\underline{H_3}$)$_3$C) and -0.21 (s, 6H, Si(C$\underline{H_3}$)$_2$); δ_C (75.5 MHz, $CDCl_3$) 174.3 (C5a), 156.1 (C6a), 140.9 (C4a), 137.1 (C10a), 136.7 (C1'a), 129.9 (CH, Ar), 129.1 (CH, Ar), 128.8 (CH, Ar), 127.3 (CH, Ar), 126.8 (CH, Ar), 125.5 (C11a), 123.7 (CH, Ar), 123.4 (CH, Ar), 122.7 (CH, Ar), 122.4 (CH, Ar), 117.8 (CH, Ar), 115.6 (CH, Ar),

61.7 (CH_2, $\underline{C}H_2OH$), 59.6 (CH_2, O-$\underline{C}H_2$-CH_2), 52.4 (C10b), 49.9 ($\underline{C}H_2$-Ph), 44.9 (C11), 33.1 (CH_2, O-CH_2-$\underline{C}H_2$), 29.8 ((CH_3)$_3\underline{C}$), 26.1 (($\underline{C}H_3$)$_3$C) and -5.4 (($\underline{C}H_3$)$_2$Si; *m/z* (ES^+) 499.19 [$(M+Na)^+$, 100%].

PART II, References

(1) Pelletier, S. W. *Chemistry of Alkaloids. Van Nostard Reinhold Company* **1970**.

(2) Rhoades, D. F.; Rosenthal, G. A.; Janzen, D. H. *Herbivores: Their Interaction with Secondary Plant Metabolites. New York: Academic Press.* **1979**, 41.

(3) Johnson, I. S.; Armstrong, J. G.; Gorman, M.; Burnett, J. P. *Cancer Res.* **1963**, *8*, 1390-1427.

(4) Manske, R. H. F. *The Alkaloids. Chemistry and Physiology, New York Academic Press* **1965**, *VIII*, 673.

(5) Neuss, N. *Chapter 9 in ref 1*.

(6) Verbitski, S. M.; Mayne, C. L.; Davis, R. A.; Concepcion, G. P.; Ireland, C. M. *J. Org. Chem.* **2002**, *67*, 7124-7126.

(7) Verotta, L.; Pilati, T.; Tato, M.; Elisabetsky, E.; Amador, T. A.; Nunes, D. S. *J. Nat. Prod.* **1998**, *61*, 392-396.

(8) Numata, A.; Takahashi, C.; Ito, Y.; Takada, T.; Kawai, K.; Usami, Y.; Matsumura, E.; Imachi, M.; Ito, T.; Hasegawa, T. *Tetrahedron Lett.* **1993**, *34*, 2355-2358.

(9) Hendrickson, J. B.; Rees, R.; Goschke *Proc. Chem. Soc., London* **1962**, 383.

(10) Robinson, R.; Teuber, H. J. *Chem. Ind.* **1954**, 783-784.

(11) Woodward, R. B.; Yang, N. C.; Katz, T. J.; Clark, V. M.; Harley-Mason, J.; Ingleby, R. F.; Shepard, N. *Proc. Chem. Soc., London* **1960**, 465-466.

(12) Hamor, T. A.; Robertson, J. M.; Shrivastave, H. N.; Silverton, J. V. *Proc. Chem. Soc., London* **1960**, 78.

(13) Hodson, H. F.; Robinson, B.; Smith, G. F. *Proc. Chem. Soc., London* **1961**, 465-466

(14) Adjibade, Y.; Weniger, B.; Quirion, J. C.; Kuballa, B.; Cabalion, P.; Anton, R. *Phytochemistry* **1992**, *31*, 317-319.

(15) Jadulco, R.; Edrada, R. A.; Ebel, R.; Berg, A.; Schaumann, K.; Wray, V.; Steube, K.; Proksch, P. *J. Nat. Prod.* **2004**, *67*, 78-81.

(16) Hayashi, H.; Matsumoto, H.; Akiyama, K. *Biosci. Biotechnol. Biochem.* **2004**, *68*, 753-756.

(17) Andersen, B.; Smedsgaard, J.; Frisvad, J. C. *Journal. Agric. Food Chem.* **2004**, *52*, 2421-2428.

(18) Dalsgaard, P. W.; Blunt, J. W.; Munro, M. H. G.; Frisvad, J. C.; Christophersen, C. *J. Nat. Prod.* **2005**, *68*, 258-261.

(19) Cooper, J. A. *J. of Cell Biol.* **1987**, *105*, 1473-1478.

(20) Ratnayake, A. S.; Yoshida, W. Y.; Mooberry, S. L.; Hemscheidt, T. K. *J. Org. Chem.* **2001**, *66*, 8717-8721.

(21) Fuji, K. *Chem. Rev.* **1993**, *105*, 1473-1478.

(22) Christoffers, J.; Mann, A. *Angew. Chem. Int. Ed.* **2001**, *40*, 4591-4597.

(23) Denissova, I.; Barriault, L. *Tetrahedron* **2003**, *59*, 10105-10146.

(24) Siengalewicz, P.; Gaich, T.; Mulzer, J. *Angew. Chem. Int. Ed.* **2008**, *47*, 8170-8176.

(25) Fuchs, J. R.; Funk, R. L. *J. Am. Chem. Soc.* **2004**, *126*, 5068-5069.

(26) Yang, J.; Song, H.; Xiao, X.; Wang, J.; Qin, Y. *Org. Lett.* **2006**, *8*, 2187-2190.

(27) Sabahi, A.; Novikov, A.; Rainier, J. D. *Angew. Chem. Int. Ed.* **2006**, *45*, 4317-4320.

(28) Artman, G. D.; Weinreb, S. M. *Org. Lett.* **2003**, *5*, 1523-1526.

(29) Seo, J. H.; Artman, G. D.; Weinreb, S. M. *J. Org. Chem.* **2006**, *71*, 8891-8900.

(30) Evans, M. A.; Sacher, J. R.; Weinreb, S. M. *Tetrahedron* **2009**, *65*, 6712-6719.

(31) Voute, N. *PhD Thesis, The University of St Andrews* **2007**.

(32) Voute, N.; Philp, D.; Slawin, A. M. Z.; Westwood, N. J. *Org. Biomol. Chem.* **2010**, *8*, 442-450.

(33) Lawson, C. *PhD Thesis, The University of St Andrews* **2010**.

(34) Bonnaud, B.; Mariet, N.; Vacher, B. *Eur. J. Org. Chem.* **2006**, 246-256.

(35) Avery, M. A.; Mehrotra, S.; Bonk, J. D.; Vroman, J. A.; Goins, D. K.; Miller, R. *J. Med. Chem.* **1996**, *39*, 2900-2906.

(36) Corey, E. J.; Schmidt, G. *Tetrahedron Lett.* **1979**, *5*, 399-402.

(37) Overman, L. E.; Ricca, D. J.; Tran, V. D. *J. Am. Chem. Soc.* **1997**, *119*, 12031-12040.

(38) Chu, Y. J.; Lynch, V.; Iverson, B. L. *Tetrahedron* **2006**, *62*, 5536-5548.

(39) Vesely, J.; Rydner, L.; Oscarson, S. *Carbohydr. Res.* **2008**, *343*, 2200-2208.

(40) March, J. *Adavanced Organic Chemistry, John Wiley and Sons: New York* **1992**, 1158-1238.

(41) Carey, F. A.; Sundberg, R. J. *Advanced Organic Chemistry, Part B, Plenum Press: New York* **1990**, 615-664.

(42) Carruthers, W. *Some Modern Methods of Organic Synthesis, 3rd Edition, Cambridge University Press: Cambridge, UK* **1987**, 344-410.

(43) Frigerio, M.; Santagostino, M. *Tetrahedron Lett.* **1994**, *35*, 8019-8022.

(44) Dess, D. B.; Martin, J. C. *J. Org. Chem.* **1983**, *48*, 4155-4156.

(45) Ley, S. V.; Norman, J.; Griffith, W. P.; Marsden, S. P. *Synthesis* **1994**, 639-666.

(46) Bal, B. S.; Childers, W. E.; Pinnick, H. W. *Tetrahedron* **1981**, *37*, 2091-2096.

(47) Armarego, W. L. F.; Chai, C. L. L. *Purification of Laboratory Chemicals, Fift Edition, Elsevier* **2003**.